

GEOPHYSICAL DATA ANALYSIS

To apply the maxim “Look here, look there, compare, and interrelate” to time series, then, we very often need to work in terms of frequency descriptions of these series, rather than in terms of time observations, and to introduce ideas and techniques that are closely related to some corresponding sort of spectrum analysis. . . . Given two time series, and wishing to learn about the existence and nature of their interrelationship, it is all too easy to place a plot of y against t above a plot of x against t and then to sit and stare. Too easy – and too misleading.

JOHN W. TUKEY “Data Analysis and the Frontiers of Geophysics”,
based on a talk given at the dedication of the La Jolla Laboratories of
the Institute of Geophysics and Planetary Physics of the University of
California, 26 February 1964.

GEOPHYSICAL DATA ANALYSIS: FOURIER METHODS

DUNCAN CARR AGNEW

ROBERT L. PARKER

CATHERINE CONSTABLE

SIO 223B CLASS NOTES, WINTER 2022

© 2022 Duncan Carr Agnew

Contents

Contents	i
1 Introduction	1
1.1 Introduction	1
1.2 Kinds of Ordered Data	4
1.3 Some History and Terminology	9
1.4 Topics to be Discussed	10
2 Orthogonal Functions and Linear Systems	12
2.1 Introduction	12
2.2 Orthogonality	13
2.3 Orthogonality of Sines and Cosines	17
2.4 Representing a Function: Fourier Series	18
2.5 Linear Time-Invariant Systems	24
2.6 Convolution	28
3 Fourier Transforms	31
3.1 The Fourier Transform	31
3.2 Three Transform Pairs	33
3.3 Fourier Theorems I: Similarity and Shift	35
3.4 Generalized Functions	37
3.5 Fourier Transforms of Generalized Functions	39
3.6 Fourier Theorems II: Derivatives and Differentiability	41
3.7 Fourier Theorems III: Combinations of Two Functions	44
3.8 Summary of Theorems	51
4 The Fourier Transform in Many Dimensions	53
4.1 Introduction	53
4.2 The Fourier Transform for Cartesian Coordinates	53
4.3 Circular Symmetry: The Hankel Transform	57
5 Fourier Theory for Discrete Time	60
5.1 Introduction	60
5.2 Discrete-Time Sequences and Operations	61
5.3 Fourier Transforms for Infinite Sequences	62
5.4 The Dirichlet, Fejér, and Other Kernels	65

5.5	Discrete Fourier Transform	68
5.6	Fourier Theorems for the DFT	71
5.7	Computing the DFT: the Fast Fourier Transform	78
6	Sampling Theory for Time-Series	82
6.1	Introduction: Sampling Data	82
6.2	The Sampling Problem	83
6.3	The Nyquist Theorem	86
6.4	Aliasing	88
6.5	Decimation	91
6.6	Violating the Nyquist Criterion	92
6.7	The Poisson Sum Formula	92
6.8	Quantization Error	93
7	Digital Filters I: Frequency-Selective Filters	95
7.1	Introduction: Some General Digital Filters	95
7.2	FIR Filters for Frequency Selection	98
8	Digital Filters II: Simulating Linear Systems	108
8.1	Introduction	108
8.2	Lumped-Parameter Systems	108
8.3	The Laplace Transform: Poles and Zeros	112
8.4	The z -transform for Digital Filters	115
8.5	Recursive Digital Filters	118
9	Digital Filters III: Specialized FIR Filters	125
9.1	FIR Filters: Other Applications	125
9.2	Differentiators and Digital Hilbert Transformers	125
9.3	Least-squares Fits as Filters	128
9.4	Minimum-Phase Filters	130
10	Stochastic Processes	135
10.1	Ordered Random Data	135
10.2	Stationary Processes	137
10.3	Some Examples	146
11	Spectra of Stochastic Processes	152
11.1	Introduction	152
11.2	Allocating Variance by Frequency	153
11.3	Two Definitions of the Power Spectrum	155
11.4	Some Properties of the PSD	159
11.5	Power Spectral Density for Discrete Processes	161
11.6	Some PSD Examples	164

<i>Contents</i>	iii
11.7 Appendix: Proof of Equation (11.18)	168
12 Estimating Power Spectra: Theory and Challenges	170
12.1 Introduction	170
12.2 Statistical Estimation	171
12.3 The Periodogram	172
13 Estimating Power Spectra: Multitapers	186
13.1 Introduction	186
13.2 The Minimum-Leakage Tapers	187
13.3 Multitaper Spectral Estimation with Slepian Functions	190
13.4 Local Bias Minimization	196
13.5 An Adaptive Multitaper Estimate	197
14 Estimating Power Spectra: Prewhitening	201
14.1 Introduction	201
14.2 Prewhitening with Prediction-Error Filters	202
14.3 A Prewhitening Example	204
14.4 Spectrum Estimation: Summary and Suggestions	207
15 Multivariate Spectra	209
15.1 Introduction	209
15.2 Pairs of Random Sinusoids	210
15.3 Pairs of Stationary Signals	214
15.4 Estimating Cross Spectra	215
15.5 An Example: Seismometer Calibration	218
16 Multidimensional Spectra	222
16.1 Introduction	222
16.2 Stationary Processes in the Plane	222
16.3 An Example: Magnetics over the Ocean	225
16.4 Stationary Processes on a Sphere	228
A Notation and Symbols	232
B Complex Variables and Complex Sinusoids	235
B.1 Complex Variables	235
B.2 Sinusoids	236
B.3 Conventions	238
B.4 Complex Representation of Two-Dimensional Vectors	238
C Probability and Statistics	240
C.1 Introduction	240

C.2	Probability	240
C.3	Single Random Variables	241
C.4	Estimation	247
C.5	Multiple Random Variables: Covariance and Correlation	251
D	Times and Dates	261
D.1	Introduction	261
D.2	Time	261
D.3	Dates	262
D.4	Best Practices	264
E	Estimating Power Spectra: Other Methods	268
E.1	Introduction	268
E.2	The Blackman-Tukey Method	268
E.3	Parametric Methods	269
E.4	Singular Spectrum Analysis	270
E.5	Least-squares Spectrum	270
F	Computing the Discrete Fourier Transform	271
F.1	Introduction	271
F.2	The Basis of the Fast Fourier Transform	271
F.3	Computing DFT's of Real Series	273
F.4	Computing the Fourier Transform for a Few Frequencies	274
G	Tapers for Spectrum Estimation: The Details	277
G.1	Slepian Tapers	277
H	The Durbin-Levinson Algorithm	281
I	Other Reading	283
I.1	Introduction	283
I.2	Linear Systems and Fourier Analysis	283
I.3	Digital Signal Processing	284
I.4	Probability and Statistics	284
I.5	Time Series and Spectral Estimation	285
I.6	History	286
Bibliography		287
Index		294

CHAPTER 1

INTRODUCTION

The leading idea which is present in all our researches, and which accompanies every fresh observation, the sound of which to the ear of the student of Nature seems echoed from every part of her works, is—Time!—Time!—Time!

G. P. SCROPE (1827), page 165

1.1 Introduction

Most of the data that geophysicists analyze depend on time or location: to be useful each data value has to have a label describing when or where (or both) it is. Often these labels allow us to create an **ordered sequence**: we cannot take them in any order without destroying the information they provide. This is most obvious for a **time series**, with data ordered in time, but applies just as well to data ordered in space, (a **data profile**), whether along a path on the Earth’s surface or one below it. In all these cases the data ordering is in one dimension, which will be the main focus of the course, though with some discussion of data in two dimensions.

To introduce some concepts, and to illustrate the different processes that appear at different timescales, we look at measurements of sea level at the end of the pier of the Scripps Institution of Oceanography (SIO) in La Jolla, California. Figure 1.1 shows this sea level, month by month, over about a century. Clearly, rearranging these values would lose much information.

The two most obvious features of this time series are a periodic variation and a long-term rise. The periodic variation turns out to be largely **annual**, which is to say a frequency of one cycle per year, though this variation is more properly termed **seasonal** since it also includes fluctuations at two, three, ... cycles per year.

Sea level, like many other geophysical variables, is a continuous function of time, $x(t)$. But any actual data will be samples from this at some set of times t_j where j is an index, increasing with time. In this particular case the spacing between the t_j ’s is one month, so there are twelve samples per year. We can describe the seasonal and long-term changes by writing an equation that describes each

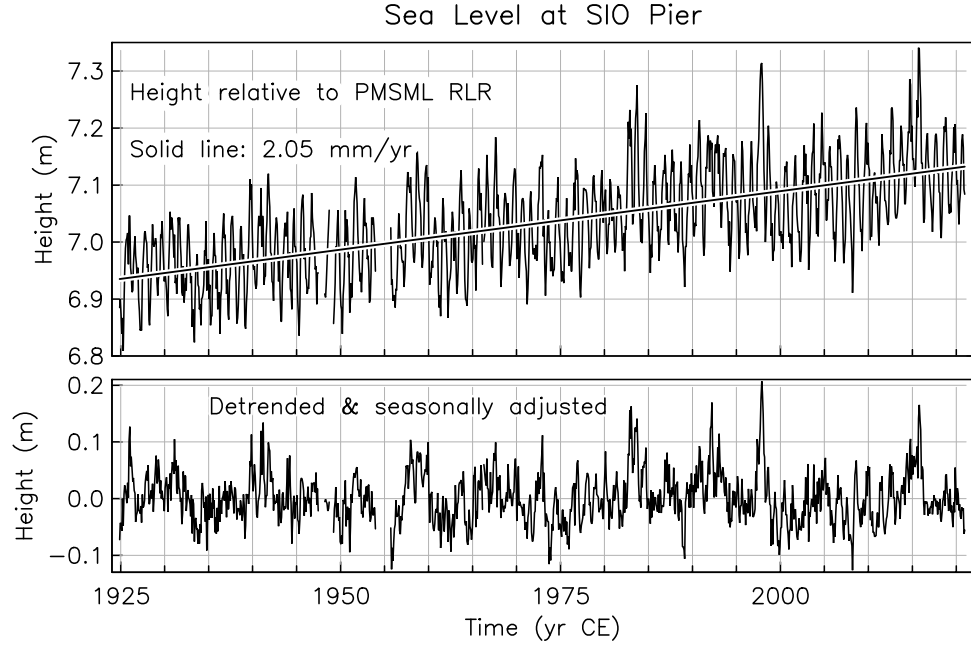


Figure 1.1: The top panel shows monthly mean sea level measured at the end of the SIO pier. The reference level (RLR) is chosen (by the Permanent Service for Mean Sea Level, PSMSL) to be well below the lowest water level; in this case it is defined to be 17.221 m below benchmark TIDAL 7 1958, which puts it about 7 m below mean sea level. The bottom panel shows the residual after removing the long-term trend (shown in the top panel) and the seasonal variation.

value x_j :

$$x_j \stackrel{\text{def}}{=} x(t_j) = a_1 + a_2 t_j + \sum_{m=1}^M [b_m \sin(2m\pi t_j) + c_m \cos(2m\pi t_j)] + r_j \quad (1.1)$$

where the times t_j are in years¹ and M is the number of annual, six-month, four-month, three-month, ... sinusoidal variations we choose to describe the seasonal changes. We can use least-squares methods to estimate the parameters in equation (1.1); doing this, and subtracting the result from the data, gives the residuals r_j , also plotted in Figure 1.1. These residuals certainly cannot be called “error;” rather, these are irregular fluctuations in sea level, presumably caused by changes in the ocean and atmosphere.

¹Years from when? (In calendrical terminology (Appendix D) from what era?). It doesn’t really matter, since the choice only affects the value of a_1 ; numerically it is best to have t be zero in the middle of the series (Section 9.8).

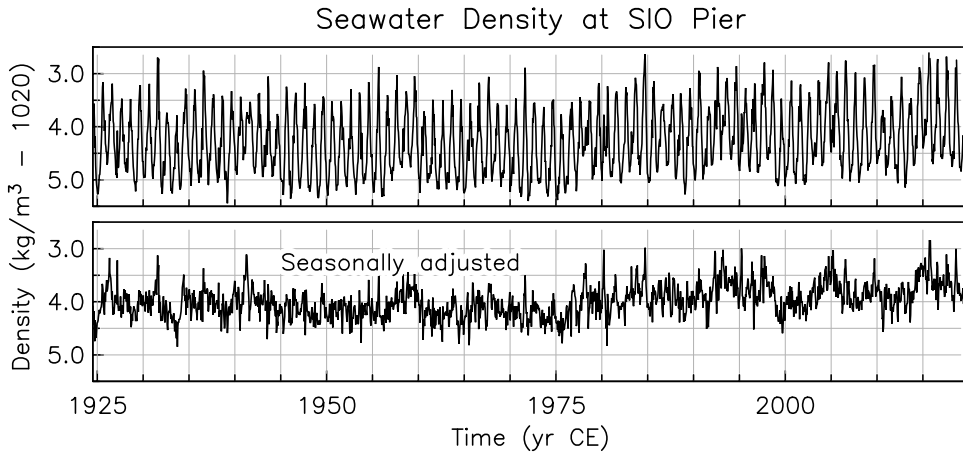


Figure 1.2: The top panel shows monthly mean seawater density, based on daily shallow temperature and salinity data collected at the end of the SIO pier. The bottom panel shows the residual after removing the seasonal variation. Because they cause higher sea levels, Lower densities are plotted at the top.

The seasonal cycle in sea level is mostly caused by changes in seawater density. Figure 1.2 shows these, which are mostly caused by changes in shallow-water temperature. Warmer water expands, causing apparent sea level rise, a phenomenon known as the “steric effect”.

The question naturally arises, how much of the irregular sea-level changes shown in the bottom panel of Figure 1.1 are caused by the irregular density changes shown in the bottom panel of Figure 1.2? This comparison of two (or more) time series is often needed, and one aim of this course is to show you how to do it: as stated in the quotation opposite the title page, it is not best done by looking at the two time series.

Figure 1.3 shows the same quantity, sea level, over a much shorter time: one of the months that is a single value in Figure 1.1. The largest variations are now those from the tides, which were smoothed out by the averaging used to produce the data in Figure 1.1. As we did for the long-term sea-level changes, we can construct a mathematical model for these changes, representing the sea level by

$$x_j \stackrel{\text{def}}{=} x(t_j) = a_1 + \sum_{m=1}^M [b_m \sin(2\pi t_j/T_m) + c_m \cos(2\pi t_j/T_m)] + r_j \quad (1.2)$$

where M is now the number of tidal sinusoids we choose; the values T_m are the periods of these sinusoids, which are determined from gravitational theory and the known motions of the Moon and Sun. We may again use least-squares to determine a_1 and the b 's and c 's, and subtract the result (in this case plotting

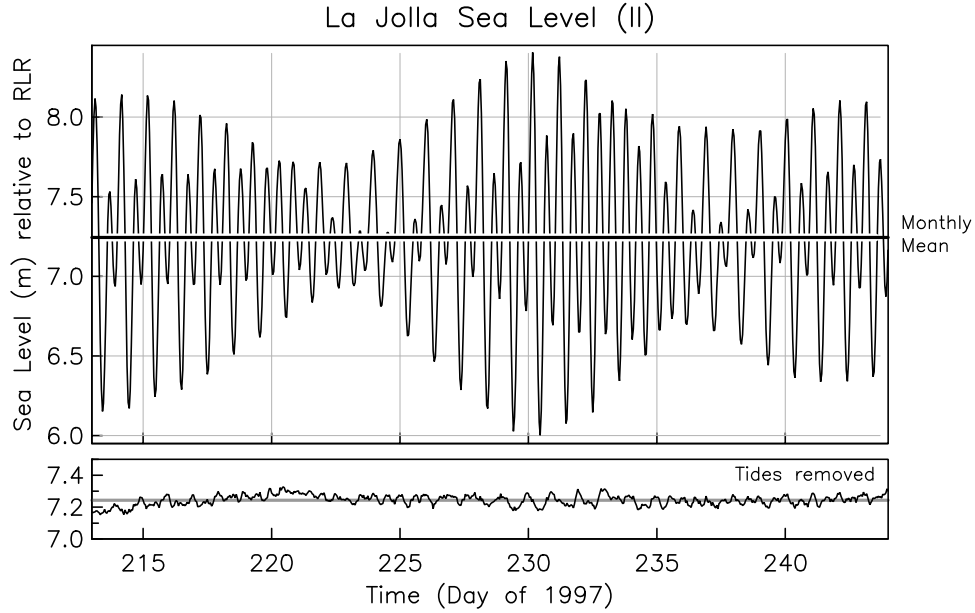


Figure 1.3: The top panel shows hourly sea level at the end of the SIO pier, again relative to the RLR. The bottom panel shows the residual after removing the tides. The black line in the top panel (in gray in the bottom) is the monthly mean plotted in Figure 1.1.

$a_1 + r_j$) to produce another residual series, shown in the lower panel of Figure 1.3: again, a series of irregular fluctuations.

Looking at even smaller sections of the data in Figure 1.3, we have the data in Figure 1.4, collected every second, and showing variations averaged out when creating the data in Figure 1.3. In both panels of this plot the main variation is an oscillation with amplitude about 15 cm and period about 10 seconds: this is ocean waves. But these variations are so irregular that it is difficult to say any more: the behavior is too irregular for a simple sinusoidal variation to be useful.

1.2 Kinds of Ordered Data

In both equation (1.1) and equation (1.2) there are two kinds of behavior present. Here the a 's, b 's, and c 's are unknown variables, called parameters, that set the size of specified functions of time: such functions produce what is called **deterministic** behavior, in the sense that the form of the time variation is completely determined. Finding the “best values” of these parameters, usually using least-squares methods, is called **estimation**; Section C.4 discusses some general aspects of this, though not such procedures as least squares.

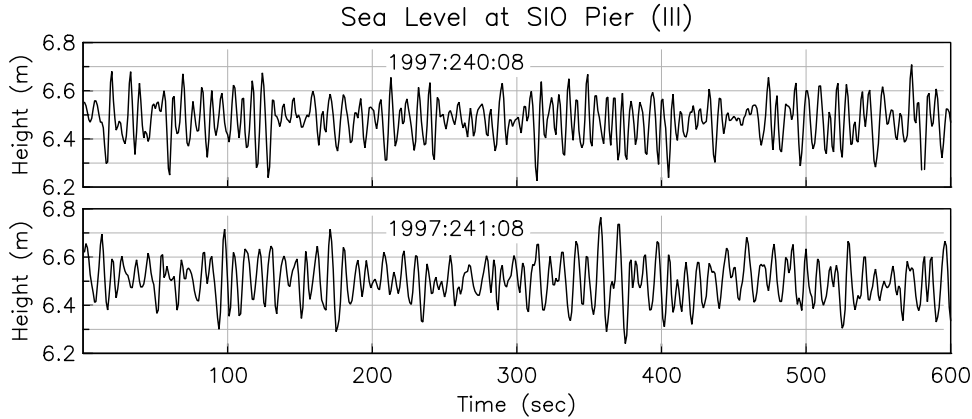


Figure 1.4: Sea level measured at the end of the SIO pier. Both panels show 10 minutes of data, the top one starting at 1997:240:08:00:00 and the bottom one day later.

But there is in addition what is left over, the the **residual** series $\{r_j\}$, which in both cases seems much less, if at all, predictable, and not something to be modeled by any function. So we will model this using random variables² the name for such a model being a **stochastic process**, something we turn to in Chapter 10. It is however important to remember that the division between stochastic and deterministic behavior is often more a matter of convenience than of strict separation. After all, if we had 10^5 years of sea level data, this linear trend over a century would be viewed as a small part of a stochastic process. Sometimes the distinction is justified by different physics for the two components; for example, changes in atmospheric pressure occur for very different reasons than the reason that the pressure is not zero. But often it mostly comes down to a choice of how best to model data.

For the data shown in Figure 1.4 it seems like there is nothing but irregularity, so the relevant equation would be $x_i = r_i$: the residual, or stochastic process is all there is. In Chapters 11 through 16 we will describe what we believe is one of the most useful ways to analyze such processes, namely, computing their **power spectral density**, or psd, also called the **power spectrum**. Chapters 12 through 14 will describe the best ways to compute the psd.

The simplest way to describe the power spectrum is that it shows how much of the variation in the time series occurs at different frequencies. Even this simple description of the spectrum may seem abstract, but it is part of what our ears and brain do with sound waves, namely create sensations that describe variability at different frequencies. The power spectrum of a sound is how we decide if it is

²Appendix C discusses such variables and concepts related to them.

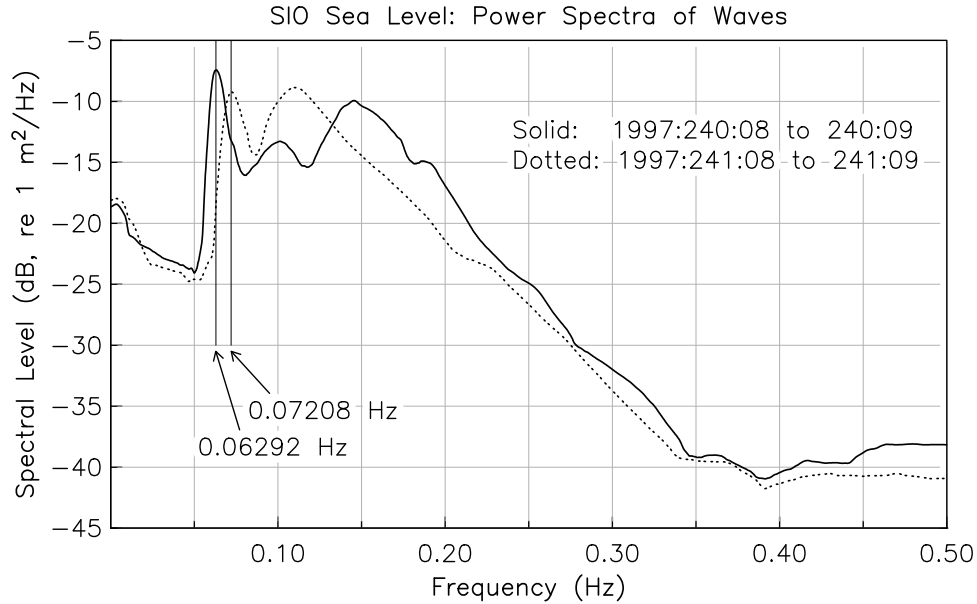


Figure 1.5: Power spectrum of the wave data in Figure 1.4 (actually, of a full hour beginning at the times shown in that figure). The frequency values of the lowest-frequency peak are given, and correspond to periods of 15.9 and 13.9 s.

high-pitched or low-pitched, frequency being just the physicist's word for pitch.

Figure 1.5 shows the power spectrum estimated from an hour of wave measurements on the two days chosen for Figure 1.4. As we would expect from the plotted time series, the power spectrum is largest for frequencies of 0.06 to 0.12 Hz, (periods of 8 to 15 seconds). But we can see more than this: the spectrum increases abruptly from 0.05 to 0.06 Hz, and decreases at a very steady rate from 0.15 to 0.35 Hz. Neither result is obvious from the time series; both of these behaviors provide information about how ocean waves are created. Looking at finer details, we can see a narrow peak on both days, but with a frequency 0.01 Hz higher on day 241 than on day 240.

We can estimate many power spectra at different times and use them to make a contour plot (Figure 1.5) of the power spectral value as a function of time and frequency. This plot shows a “ridge line” of high values, with the frequency shifting linearly with time. This ridge line appears because swell waves in deep water are dispersive: the longer the period the faster they travel. A storm in one place will produce waves over a broad range of frequencies but the lower-frequency energy travels faster; as time passes, higher-frequency energy arrives. This ridge line thus corresponds to waves from a distant storm.³ Given how rapidly the frequency

³For much more on this subject, based on an ocean-spanning data set, see the classic paper by

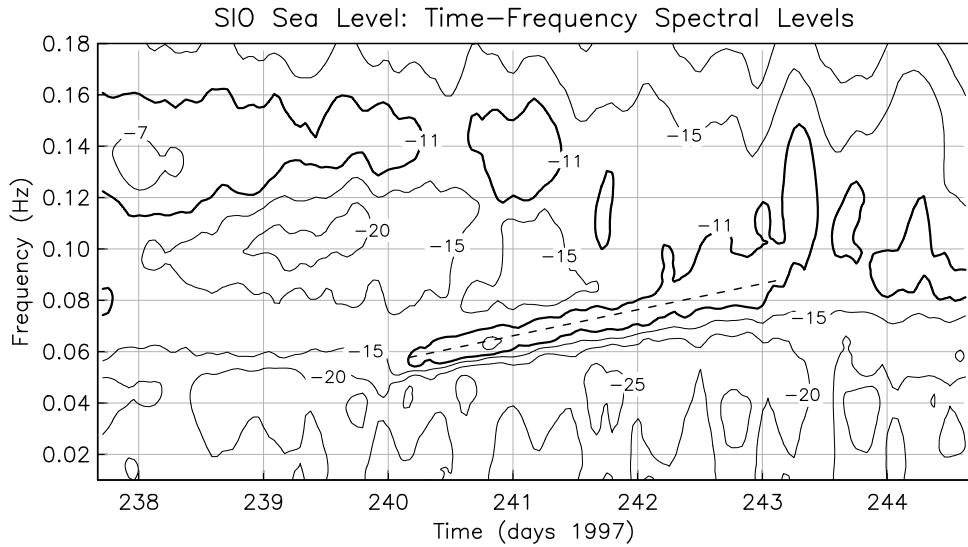


Figure 1.6: Power spectral density as a function of time for sea level at the end of the SIO pier. Contours are in dB relative to $1 \text{ m}^2/\text{Hz}$. The dashed line shows a (rough) fit to the “ridge line” outlined by the heavy contour: swell from this single storm arrives over a three-day time period, which took six days to travel to La Jolla from a storm about 60° away.

shifts with time, and the known physics of water waves, we can find the distance to the source and when the waves began.

This example illustrates something we will see many times over: the power spectrum of a time series often shows features of the data that are not at all obvious when the data are simply viewed as a function of time. A major aim of this course is to teach you to understand what a power spectrum is, to know how to estimate it from the data, and to know how to decide which of the bumps on the plotted spectrum mean something and which do not.

Figure 1.7 shows an even more extreme example of the value of finding a power spectrum. We do not show the time series (of earth motion measured by a seismometer) because it looks like purely random variations with no interesting features at all. But the power spectrum shows that there is much extra variability in a very narrow frequency range. This variability is from the lowest-order dilatational free oscillation of the Earth, ${}_0S_0$, which had been excited by the magnitude 8.3 Sumbawa earthquake 25 days earlier, 15 days before the seismometer was even installed. This spectral peak was quite unexpected. Later studies with more data (Riedesel *et al.*, 1980; Rosat *et al.*, 2007) show that the ${}_0S_0$ mode decays by a factor of two every 17 days, so after 25 days it was still one-third of its initial amplitude.

Snodgrass *et al.* (1966); Arduin *et al.* (2009) is a more recent summary, using data from satellites.

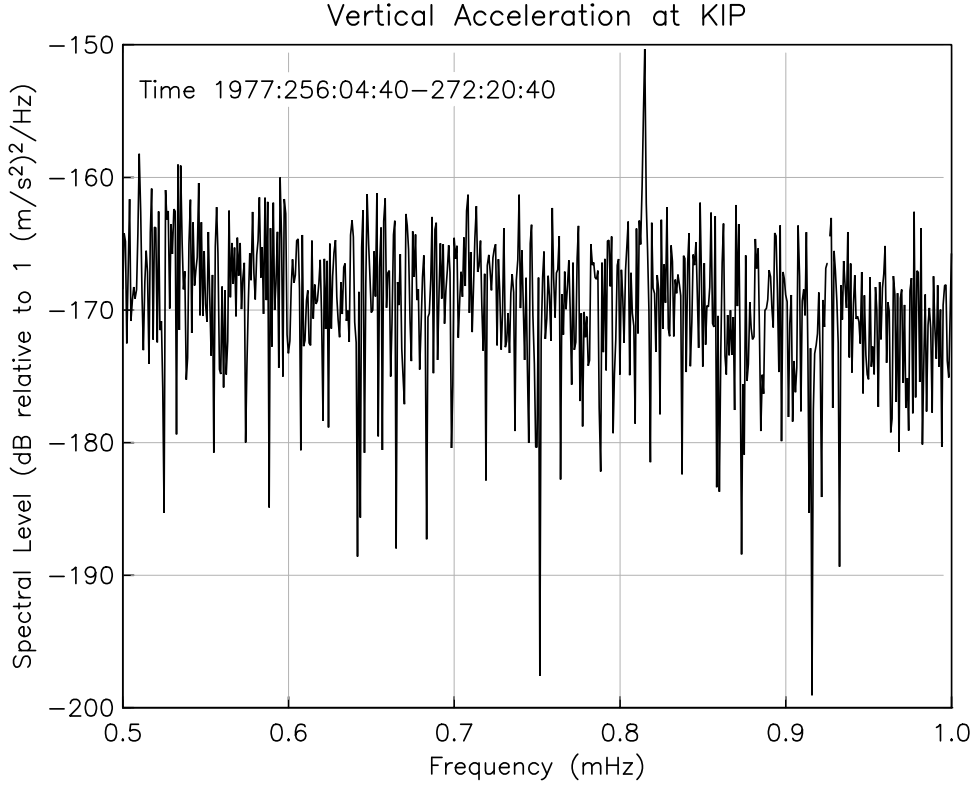


Figure 1.7: Portion of a periodogram estimate (Section 12.3) of the power spectrum of vertical acceleration, recorded by the Project IDA gravimeter at Kipapa, Hawaii (station KIP); the data analyzed were from 24.9 to 41.6 days after the earthquake.

1.2.1 A Digression on Decibels

Figures 1.5, 1.6, and 1.7 all plot the amplitude of the spectrum in units that may be new to you: **decibels (dB)**. These are a way of creating a logarithmic scale that you should become familiar with. The term comes, via acoustics, from telephony: hence the name, Bel, which refers to Alexander Graham Bell. The original definition is that the signal level in decibels is $10\log_{10}(P/P_0)$, where P is the signal power (think loudness), and P_0 some reference power. The logarithm is used for two reasons. One is that it converts very large changes into a small range of numbers, while the other is that the sensation of loudness (like many other sensations) is roughly proportional to the logarithm of the power, a rule of psychophysics known as Fechner's law.

In time series analysis we take the reference power level to be unity, in whatever units we are using. If we have something with amplitude A , then by defini-

tion its value in dB is $10\log_{10}(A^2) = 20\log_{10} A$. The amplitude is squared because squared quantities usually relate to power (see Section 3.7.2). Thus a factor of two in amplitude is very nearly equal to a 6 dB difference in power level, a factor of four to 12 dB, and a factor of eight to 18 dB. Conversely, if signal A is half as large as signal B, we would say “A is 6 dB below B”; if A had a value of one half, with the reference level being one, we would say that “A has a level of –6 dB”. And after a little practice, you will learn to say this too.

1.3 Some History and Terminology

There is not a single name for the methods described in this course because they were developed in several different fields with distinct methods and names; we give a summary history to introduce these names, which often serve as a labeling device in book and journal titles.

Music is the oldest science that used a frequency description for a time series: both the pitches and the timing of the notes matter. Much music theory was developed for a single vibrating string in tension; eighteenth century discussions of the physics of this gave the first examples of representing a function by a sum of sines and cosines. Such a representation was extended to other problems by Fourier, giving rise to the mathematical field of *Fourier analysis*: how well sums of trigonometric functions could represent arbitrary functions. As we will see in Chapter 2, the answers are not simple. Generalizations of Fourier analysis to include other sets of functions are the mathematical field of *harmonic analysis*, which provides a mathematically rigorous foundation for the whole field. The vibrating-string problem, and Fourier’s analysis, also showed how useful such sets of functions were in solving differential equations – a topic we do not discuss.

The Fourier representation of functions, describing them in terms of frequency, became even more important after the invention of ways to transmit sound electrically over wires (telephony) or through space (radio), or to record it for subsequent replaying. In the twentieth century all these technologies became the province of electrical engineers, who found behavior at different frequencies to be crucial to improving performance. From the engineering standpoint, what was to be transmitted or replayed was a signal, so methods for creating or modifying signals became an electrical engineering subfield known as *signal processing*. The electrical engineering community also developed the *linear system* concept, an important generalization we will make much use of. Much of the relevant theory and methodology was developed at the Bell Telephone Laboratories, one of the great research centers in the United States from the 1920’s through the 1980’s.

Somewhat distinct from this engineering development was the theory of random time series, which was mostly developed in two other fields. In mathematics, random time series are in the subfield of probability theory known as *stochastic*

processes: the theory and properties of sequences or functions that are ordered but need probability to be properly described. The mathematics of doing this rigorously can be quite subtle, and this subfield was almost entirely developed in the twentieth century.

The statistical treatment of ordered data began, not unusually, before there were rigorous models for such data. In the nineteenth century the increasing availability of time series in meteorology and economics led to attempts to discern patterns, most often periodic ones, and to look for connections between such things as sunspots and the price of wheat. Much of this early work was purely graphical and devoid of probabilistic reasoning. Putting such procedures on a sounder mathematical basis gave rise to the twentieth century subfield of statistics known as *time series analysis*. As with signal processing, practical problems drove many of these developments: one of the most important works in the field [Wiener \(1949\)](#) was classified during World War II because of its applicability to anti-aircraft artillery.

Two more developments made the power spectrum a broadly useful tool. One was high-speed computation: the speed of doing arithmetic has increased by a factor of at least 10^8 over the last 70 years. The other, more specific, was the algorithm known as the Fast Fourier Transform, or FFT. Finding the power spectrum requires finding Fourier transforms, and from 1966 on the FFT made the computation of the Fourier transform much faster than before.⁴ These two developments revolutionized the engineering problem of processing signals by making it possible to do on a computer, very flexibly, what had previously required careful electronic design: signal processing became *digital signal processing*, or DSP. This field now includes a huge range of methods, particularly for signals from waves, whether over telephone lines or through the Earth: signal processing is a crucial element of exploration geophysics.

In statistics *spectral analysis* is the name for the subfield of time series analysis that examines random series in terms of their frequency distribution. We have already given examples of how informative this method can be.

1.4 Topics to be Discussed

Roughly speaking, this book is divided between the two areas of nonrandom and random time series. Chapters 2 and 3 are about harmonic analysis of nonrandom functions using the Fourier series and the Fourier transform. Chapter 4 (optional) extends this discussion to more than one dimension. Chapters 5 through 9 cover the basics of digital signal processing, including the effects of going from continuous time to sampled data, and methods for doing the most common kinds

⁴Actually, Gauss developed the first FFT algorithm in 1805, but it was only published posthumously in 1866, and not noticed even then ([Heideman et al., 1985](#)).

of processing, namely removing frequencies (Chapter 7) and simulating physical systems, such as seismometers (Chapter 8). Chapter 9 (optional) looks at some other topics in signal processing.

We next discuss time series of random variables: Chapter 10 introduces some basic ideas about how to describe random time series, while Chapter 11 introduces the power spectrum as the commonest description of how random data vary with frequency. As with any probabilistic descriptions, we need statistical procedures to make the best estimate of the parameters of the descriptions from the data we have. Chapters 12 through 14 are about this, first showing a common method that is simple, popular, inadequate, and obsolete. We then introduce the procedures (multitaper estimates with prewhitening) that we believe give the best estimates. Chapter 15 introduces the theory and estimation procedures for comparing two or more series as a function of frequency. Chapter 16 (optional) extends all this to more than one dimension, including the common geophysical case in which we have to make estimates for something that is in two or three dimensions, but for which we have measurements along a track, and so only in one dimension.

CHAPTER 2

ORTHOGONAL FUNCTIONS AND LINEAR SYSTEMS

Lord Ronald said nothing; he flung himself from the room, flung himself upon his horse, and rode madly off in all directions.

STEPHEN LEACOCK, *Gertrude the Governess, or Simple Seventeen*
(1911).

All happy families are alike; each unhappy family is unhappy in its own way.

LEO TOLSTOY, *Anna Karenina* (1877).

2.1 Introduction

We begin our mathematical treatment of time series by discussing how to represent some function of time, $x(t)$, by other functions. We focus on sets of functions called **orthogonal functions** because some of these are very useful in analyzing time-series data, and others will be used in estimating the power spectrum.

Out of the many sets of orthogonal functions, we will focus on sines and cosines because they are well suited to the analysis of linear, time-invariant systems. In Section 2.5 we will discuss the properties of such systems, and show how they interact with sines and cosines. This discussion will lead us to the Fourier transform, which is ubiquitous in our study of time series.

You are probably familiar with one collection of functions that can be used to represent an arbitrary function $x(t)$, namely the powers of t : $1, t, t^2, t^3, \dots$, which appear in the **Taylor series** expression for $x(t)$:

$$x(t) = x(0) + x'(0)t + x''(0)\frac{t^2}{2} + x'''(0)\frac{t^3}{6} + \dots \quad (2.1)$$

If you are ever tempted to use this representation for anything other than theoretical derivations, by making a **polynomial fit** think again.¹ Despite the simplicity of the functions this procedure has nothing to recommend it. Because

¹Except for fitting just a constant and a linear trend to data, as we did to the sea-level data in Figure 1.1.

the powers of t increase in magnitude very rapidly away from zero, it is difficult to use this series to represent a function far from the origin. Also, for actual data the derivatives of x are never available.

2.2 Orthogonality

Instead of using powers of t to model data, we use sets of orthogonal functions. But what do we mean by saying that functions are orthogonal? The adjective “orthogonal” comes from geometry, where it refers to lines at right angles; how this gets extended to functions is a good example of mathematical generalization.

The first step is to consider the lines as vectors, and look at the **dot product**, which for two vectors \mathbf{x} and \mathbf{y} is $\mathbf{x} \cdot \mathbf{y} = |\mathbf{x}| |\mathbf{y}| \cos \theta$, where θ is the angle between the two vectors and $|\mathbf{x}|$ and $|\mathbf{y}|$ are the lengths of \mathbf{x} and \mathbf{y} . If the vectors are at right angles ($\theta = \pi/2$) the dot product is zero. In terms of the Cartesian components x_j and y_j of these vectors the dot product is:

$$\mathbf{x} \cdot \mathbf{y} = \sum_{j=1}^3 x_j y_j \quad (2.2)$$

An immediate generalization of this is to vectors in N dimensions, each represented by arrays of N numbers. Such vectors are orthogonal if

$$\mathbf{x} \cdot \mathbf{y} = \sum_{j=1}^N x_j y_j = 0 \quad (2.3)$$

where now the sum, not some expression with angles, defines the dot product.

We can go from collections of numbers to collections of functions on the real line by replacing each N -tuple of numbers by a function, and the sum by an integral: something we will do repeatedly. By doing this, we define the dot product of two functions $x(u)$ and $y(u)$ as

$$(x, y) \stackrel{\text{def}}{=} x(u) \cdot y(u) = \int_a^b x(u) y(u) du \quad (2.4)$$

where the expression (x, y) is another common notation, usually associated with another name: the **inner product**. The interval $[a, b]$ is the domain over which we evaluate the functions: it can be finite or infinite.

We have also changed the argument from t to u . Of course it does not matter what letter we use in these expressions, but later on it will be useful to distinguish between a physical quantity that has a dimension and units (such as time or distance); and a purely numerical and dimensionless quantity u . Only the latter can be used as the argument of a function.

Orthogonality for a pair of functions $x(u)$ and $y(u)$ therefore means:

$$(x, y) = \int_a^b x(u)y(u)du = 0 \quad (2.5)$$

Actually, equation 2.5 has something left out; to see what, we go back to vectors in three dimensions, and consider the dot product of a vector with itself:

$$\mathbf{x} \cdot \mathbf{x} = |\mathbf{x}|^2 = \sum_{j=1}^3 x_j^2 \quad (2.6)$$

which gives us the definition of the length in terms of the vector components: the square root of the sum of their squares. We can, again, generalize this. First, for N -dimensional vectors:

$$||\mathbf{x}||_2 = \sqrt{\sum_{j=1}^N x_j^2} \quad (2.7)$$

where we have introduced the notation $||\cdot||_2$ for the length, which is more properly referred to as the **norm** of the vector; the subscript 2 is used to show that this is the “two-norm”, involving squares of the components.

The definition of the two-norm for a function should be then be obvious, namely the inner product of the function with itself:

$$||x||_2 = \sqrt{(x, x)} = \sqrt{\int_a^b x(u)^2 du} \quad (2.8)$$

This is one way to define the “length” of the function; it is always non-negative, but might be zero (for example if the function is zero over the interval) or infinite (if the function is not integrable). We rule out functions with an infinite norm as being unacceptable; a zero-valued function, like the zero vector, will have an inner product of zero with everything else, but this does not make it orthogonal to them. So the complete specification of orthogonality for functions with a finite norm is

$$(x, y) = 0 \quad \text{for } ||x||_2 > 0 \quad \text{and} \quad ||y||_2 > 0 \quad (2.9)$$

Our definition of the inner product means that, for any constant c ,

$$||cx||_2 = \sqrt{(cx, cx)} = \sqrt{\int_a^b |c|^2 x(u)^2 du} = c||x||_2 \quad (2.10)$$

so the value of the norm scales with the function. It is often advantageous to make the norm of each function in a collection equal to unity, in which case the

functions are called **orthonormal**. A collection of orthonormal functions thus has the properties:

$$(x_n, x_m) = \delta_{nm} \quad (2.11)$$

where x_n and x_m are any two functions in the collection, and δ_{nm} is the Kronecker delta, which is one when n equals m and zero otherwise.

But again, we have left something out: our definition of the inner product (equation 2.4) and hence of the norm (equation 2.8) assume that the functions are real-valued; complex-valued functions could have complex norms. Since we will want to work with complex-valued functions, we use complex conjugates to redefine the inner product as:

$$(x, y) \stackrel{\text{def}}{=} \int_a^b x(u)y^*(u)du \quad (2.12)$$

which makes the norm into

$$\|x\|_2 = \sqrt{(x, x)} = \sqrt{\int_a^b x(u)x^*(u)du} \quad (2.13)$$

This is, as we would wish, always real and non-negative.

Finally, we note that the most general definition of the inner product includes a weighting function $w(u)$, which must be positive everywhere, and makes the inner product

$$(x, y) = \int_a^b w(u)x(u)y^*(u)du$$

though except for a couple of cases in the next section we will assume $w = 1$, and not include it.

2.2.1 Some Examples

The most obvious example of an orthonormal collection of vectors is the three unit vectors that give the directions of a Cartesian coordinate system: $(0, 0, 1)$, $(0, 1, 0)$, and $(1, 0, 0)$. For N -dimensional vectors we can extend this to the N vectors starting with $(0, 0, \dots, 1)$ and ending with $(1, 0, \dots, 0)$, though any other set of N orthogonal directions would do as well.

Once we move to sets of functions, (to use the more formal term for a collection) we have much more generality. A full discussion of orthonormal functions is well beyond the scope and purpose of this course, but to give you the idea, Figure 2.1 shows some examples of such sets. For each set we can associate an integer value with each member of the set; this integer is usually called the **order**.

The first set, the **Legendre polynomials**, are of interest through their connection with spherical harmonics, perhaps the most ubiquitous functions in geophysics. The Legendre polynomials form just one example of orthonormal functions created from powers of t ; they are what we get if the weight function $w(t)$

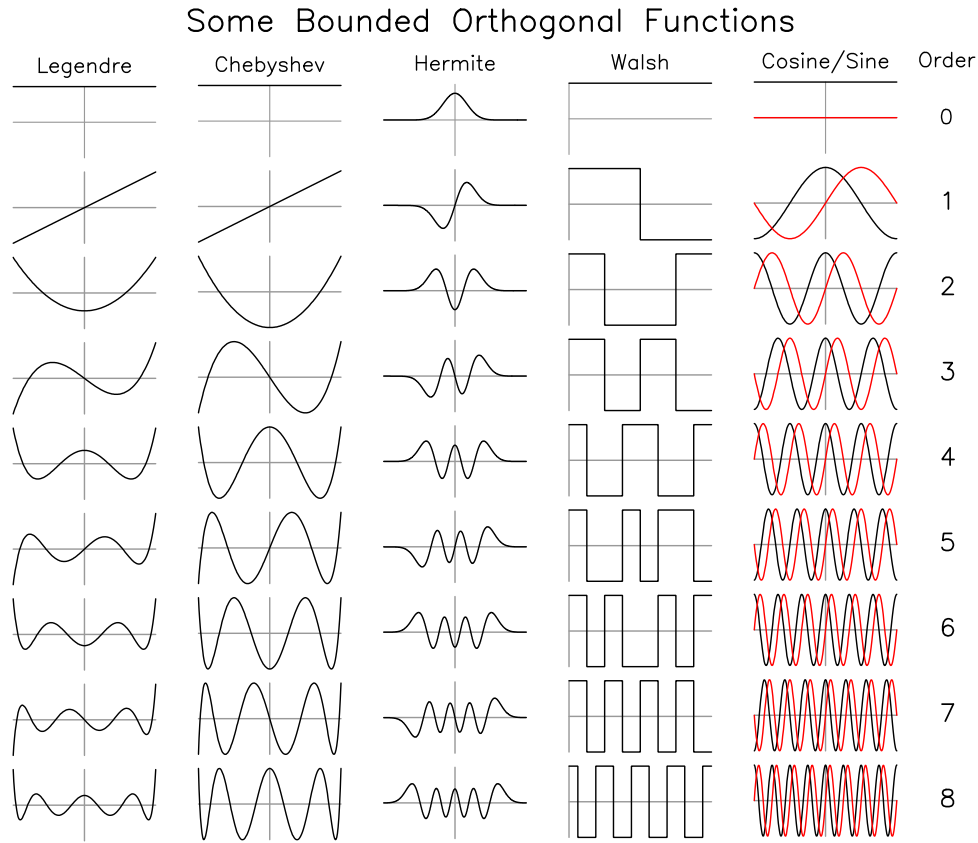


Figure 2.1: The first nine elements of different sets of orthogonal functions. In the last column, cosines are in black and sines in red. The order for each element is shown on the function.

is constant – as it is for all the examples here except the **Chebyshev polynomials**, for which $w(u) = 1/\sqrt{1-u^2}$. For both Legendre and Chebyshev polynomials the domain is $[-1, 1]$. For the next set, the **Hermite functions**, the domain is $[-\infty, \infty]$ – while we can show only the region around the origin, these functions decay exponentially outside a small interval, so the plot is not misleading.

Nothing in our definitions of products and norms requires the functions to be continuous, and Figure 2.1 also shows the first members of a set of functions that are not: the **Walsh functions**. Finally, we have the sine and cosine functions – which, if they had not already been named, might well have been called the Fourier functions.

2.3 Orthogonality of Sines and Cosines

We next look in some detail at the set of sine and cosine functions:

$$s_m(u) = \sin(2\pi mu) \quad m = 0, 1, 2, \dots \quad c_n(u) = \cos(2\pi nu) \quad n = 0, 1, 2, \dots \quad (2.14)$$

where n and m are the two integer orders; the interval is $[-\frac{1}{2}, \frac{1}{2}]$. As explained in Appendix B, it is actually better to turn these into a set of functions with a single indexing integer by using the complex exponentials:

$$e^{2\pi i n u} = c_n(u) + i s_n(u) \quad \text{for } n = -\infty, \dots, -2, -1, 0, 1, 2, \dots \infty \quad (2.15)$$

which for positive n is the functions shown in the right-hand column of Figure 2.1 if we take the black to be the real part and the red the imaginary part. The functions for negative n are the same, though with the sign of the red functions flipped.

The sines and cosines, and the complex exponentials, both have a very important trait, common to most sets of orthogonal functions: there are an infinite number of members, or to use the correct term, **elements**. This is very different from the finite dimensionality of an N -dimensional vector, and leads to some interesting issues when we try to use orthogonal functions to represent an arbitrary function (Section 2.4.1).

We start by looking at the orthogonality of the sine and cosine functions. Since the cosine functions c_n are all **even functions** ($c_n(-u) = c_n(u)$) and the sine functions s_n are all **odd functions** ($s_n(-u) = -s_n(u)$), the product of any sine and cosine function must be odd. The integral of any odd function over an interval symmetric about zero must be zero. Since this integral is our measure of orthogonality, this result means that the sines and cosines are all mutually orthogonal.

What about cosines or sines with different indexes? The easiest way to show orthogonality is to use the complex exponential to represent them:

$$\begin{aligned} \int_{-\frac{1}{2}}^{\frac{1}{2}} \cos(2m\pi u) \cos(2n\pi u) du &= \int_{-\frac{1}{2}}^{\frac{1}{2}} \frac{1}{2} [e^{2\pi i n u} + e^{-2\pi i n u}] \frac{1}{2} [e^{2\pi i m u} + e^{-2\pi i m u}] du \\ &= \frac{1}{4} \int_{-\frac{1}{2}}^{\frac{1}{2}} [e^{2\pi i (n+m)u} + e^{2\pi i (n-m)u} + e^{2\pi i (m-n)u} + e^{-2\pi i (m+n)u}] du \end{aligned} \quad (2.16)$$

For any nonzero integer k ,

$$\int_{-\frac{1}{2}}^{\frac{1}{2}} e^{2\pi i k u} du = \frac{e^{2\pi i k}}{ik} \Big|_{-\frac{1}{2}}^{\frac{1}{2}} = \frac{e^{\pi i k} - e^{-\pi i k}}{ik} = \frac{(-1)^k - (-1)^{-k}}{ik} = 0 \quad (2.17)$$

which shows that the complex exponentials are orthogonal, since the product of any two with different indices will be $e^{2\pi i k}$. Our definition (equation 2.12) of the

norm for complex functions shows that the norm for the complex exponentials is unity, so these are orthonormal.

Combining (2.16) and 2.17 gives the orthogonality relation for cosines with different indexes; a very similar development gives the same result for the sines. Since for $k = 0$, $e^{2\pi i k} = 1$, using equation (2.16) with $n = m$ gives the result that

$$\int_{-\frac{1}{2}}^{\frac{1}{2}} \cos(2n\pi u) \cos(2m\pi u) du = \frac{1}{2} \quad (2.18)$$

So if we take the sinusoidal functions defined by equation (2.14), and scale them by $\sqrt{2}$, they form an orthonormal set.

2.4 Representing a Function: Fourier Series

Given a set of orthonormal functions, it appears very straightforward to represent some arbitrary function $x(u)$ as a sum of these functions. We write such a sum as

$$x(u) = \sum_{n=0}^{\infty} \tilde{x}_n z_n(u) \quad (2.19)$$

where the \tilde{x}_n 's are numbers and the z_n 's are the orthonormal functions. The series coefficients are then given by

$$(z_n, x) \stackrel{\text{def}}{=} \int_a^b w(u) z_n(u) x(u) du = \sum_{m=0}^{\infty} \tilde{x}_n (z_n, z_m) = \tilde{x}_n \quad (2.20)$$

where the last step makes use of the orthonormality of the z 's (equation 2.11).

This is a bit abstract and general; to make it concrete we use the sines and cosines as our functions, in which case our sum becomes a **Fourier series**:

$$x(u) = \frac{a_0}{2} + \sum_{n=1}^{\infty} a_n \cos(2\pi n u) + \sum_{n=1}^{\infty} b_n \sin(2\pi n u) \quad (2.21)$$

where the coefficients are given by

$$a_n = 2 \int_{-\frac{1}{2}}^{\frac{1}{2}} x(u) \cos(2\pi n u) du \quad b_n = 2 \int_{-\frac{1}{2}}^{\frac{1}{2}} x(u) \sin(2\pi n u) du \quad n = 1, 2, \dots \quad (2.22)$$

The various factors of two are present because the sine and cosine functions, while orthogonal, are not orthonormal.

If instead we used the complex exponentials, the Fourier series expressions become simpler:

$$x(u) = \sum_{n=-\infty}^{\infty} \tilde{x}_n e^{2\pi i n u} \quad (2.23)$$

with coefficients given by

$$\tilde{x}_n = \int_{-\frac{1}{2}}^{\frac{1}{2}} x(u) e^{-2\pi i n u} du \quad \text{for } n = -\infty, -2, -1, 0, 1, 2, \dots \infty \quad (2.24)$$

Symmetries in Fourier Series

The Fourier coefficients in equations (2.23) and (2.24) have special behaviors when the function $x(u)$ has particular properties. Suppose $x(u)$ is real, and symmetric about $u = 0$, then $x(-u) = x(u)$ and the function is even. Then the sine term of the exponential in equation (2.24), being odd, will vanish when the integral is done, making the integrand $x(u)\cos -2\pi nu$. This means that the \tilde{x}_n 's are real, and also that $\tilde{x}_n = \tilde{x}_{-n}$, so these are also even. If the function is real and odd, the same reasoning shows that \tilde{x}_n is purely imaginary, and $\tilde{x}_n = -\tilde{x}_{-n}$: odd. Since any real function is the sum of an even and an odd part, this means that the Fourier coefficients for such a function will have the property $\tilde{x}_n = -\tilde{x}_{-n}^*$; we say that the coefficients are **Hermitian**, and completely specified by \tilde{x}_n for non-negative values of n . This result shows how we can apply complex exponentials to represent real-valued functions: a good thing, since data are almost always real-valued. Another approach to representing real-valued series with complex exponentials is to simply take the real part; Appendix B has a full discussion of using the real parts of complex exponentials instead of sines and cosines.

2.4.1 Convergence and Gibbs' Phenomenon

We now have a recipe for finding the coefficients of a series that will express any function as a sum, possibly an infinite sum, of a collection of orthonormal functions. Still, we have left something out – we have simply assumed that we *can* express our function by such a sum, but do not know if this is always true. More precisely the question is, will the sum (2.19) using the \tilde{x}_n 's produced by equation (2.20) be the same as the function $x(u)$, or not? And in particular, what if the sum is the Fourier series defined by equations (2.23) and (2.24)? The answer is that there are $x(u)$'s for which a Fourier series, even with an infinite number of terms, does not match the function. This mismatch occurs only in a limited sense, though one that has effects that we will encounter repeatedly.

We can make our question more precise by imposing on $x(u)$ the requirement that its norm, as defined by equation (2.8), is finite. The set of all functions that satisfy this is said to make up an infinite-dimensional **linear vector space**; the particular space for the norm we have chosen is called L_2 .² Though the mathematics of linear vector spaces are important in, for example, inverse theory, we do not discuss them here. But introducing the idea helps to make our question more precise: it becomes the question of whether there are functions in L_2 which cannot be represented by the infinite sum of equation (2.19) when the functions in the sum are complex exponentials (or sines and cosines).

²Actually, there are lots of L_2 spaces, depending on the interval we choose for the norm. And there are technical complications involving functions that differ only on sets of zero measure – you need not worry if you do not know what this means,

This question should actually be phrased in terms of **convergence**. Consider a finite sum of N exponentials

$$s_N(u) = \sum_{n=1}^N \tilde{x}_n z_n(u) \quad (2.25)$$

Then the question is, will $s_N(u)$ converge to $x(u)$ as N becomes arbitrarily large, convergence being defined as the difference $x(u) - s_N(u)$ approaching zero. Finding the precise conditions under which a Fourier series converges, and in what way, was an important mathematical topic in the nineteenth century. We state with a general result: if the set of functions z_n form an orthogonal basis (meaning that the set is **complete**) then

$$\lim_{N \rightarrow \infty} \|x(u) - S_N(u)\| = 0 \quad (2.26)$$

That is, if we define the “distance” between functions by the two-norm, the distance between the partial sums and the original function will always shrink to zero: this is usually stated by saying that we have “convergence in the sense of the L_2 norm.

But this does not mean the two functions are equal. Because the two-norm is based on an inner product (equation 2.4) that depends on an integral, it does not “see” differences if they occur at isolated points.³ In fact, examples can be devised in which $S_N(u)$ and $x(u)$ differ at an *infinite* number of points, yet satisfy equation (2.26).

Measures of Convergence

Are there other measures of convergence that take these differences into account? One natural-seeming measure is *pointwise* convergence, where we examine the difference at every point. For Fourier series we have pointwise convergence only if $x(u)$ is in the L_2 vector space, and also satisfies the **Dirichlet conditions**, which are that $x(u)$ has continuous first derivatives on the interval, except possibly at a finite number of points; at these there may be a jump, but left and right derivatives must exist. Then the Fourier series of h converges to $\frac{1}{2}(x(u^+) + x(u^-))$ for every point in the open interval $(-\frac{1}{2}, \frac{1}{2})$ ($u^+ > u$ and $u^- < u$ but the difference between them can be arbitrarily small). At $t = \pm\frac{1}{2}$ the series converges to $\frac{1}{2}(x(-\frac{1}{2}^+) + x(\frac{1}{2}^-))$. So the series always converges pointwise, and to the correct value except at the discontinuities. This kind of convergence is called **convergence in the mean**.

Another form of convergence is **uniform convergence**, for which the measure that must approach zero is the maximum of $|x(u) - S_N(u)|$. This maximum

³Remember that if a function $x(u)$ is zero for all nonzero u but one for u equal to zero, its integral will be zero.

is another kind of norm, called the **uniform norm**,⁴ symbolized by $\|\cdot\|_\infty$. Then uniform convergence occurs if

$$\lim_{N \rightarrow \infty} \|x(u) - s_N(u)\|_\infty = 0 \quad (2.27)$$

Uniform convergence implies pointwise convergence, but not the reverse.

Gibbs' phenomenon

Perhaps the best-known example of the failure of partial sums s_N to converge uniformly to $x(u)$ is also very relevant to this course; this is what is called **Gibbs' phenomenon** (Hewitt and Hewitt, 1979). Figure 2.2 shows that if we use a Fourier series to try to represent a function with a discontinuity, this series will always differ from the function close to that discontinuity. The region over which the difference is large gets narrower and narrower as we add more terms, but Gibbs' phenomenon is that the maximum difference away from the discontinuity does not decrease: it stays at 0.0894 of the size of the step. So a Fourier series has pointwise convergence (as it should – this function satisfies the Dirichlet conditions), but not uniform convergence. The bottom panel shows how the coefficients of the Fourier series vary with N , in this case as N^{-1} : this dependence on N appears over and over in Fourier expressions for discontinuous functions.

This figure shows something else that we will see many times. There is a pair of “Gibbs overshoots” not just around the discontinuity, but at the ends of the interval – which might not seem a logical place for them. But looked at properly, their presence becomes more obvious. The plots in Figure 2.2 suggest that these two ends are just the extremes of an interval – and so they are, *until* we try to use a Fourier series to represent a function. We define this representation over a finite interval, but the Fourier series, equation (2.23), can be evaluated for any value of u , using the fact that

$$e^{2\pi i n u} = e^{2\pi i n (u+m)} \quad (2.28)$$

for m any integer. So to find the Fourier sum for any real value of u , we simply evaluate it at

$$u' = u - \text{int}(u + \frac{1}{2}\text{sgn}(u)) \quad (2.29)$$

where the $\text{int}(u)$ rounds to the integer closer to zero, and $\text{sgn}(u)$ is the sign of u ; u' always falls within the interval for the Fourier series.

Figure 2.3 shows two ways of looking at this. The first one is to use the periodicity implied by equations (2.28) and (2.29) to define the series over the whole real line rather than just a finite interval. It is then clear that what is adjacent to the series for u just less than $u = \frac{1}{2}$ is the values of the series for u just greater

⁴or the **sup norm**, for supremum, the mathematical way of defining a maximum for discontinuous functions.

Fourier-Series Approximations to a Step Function

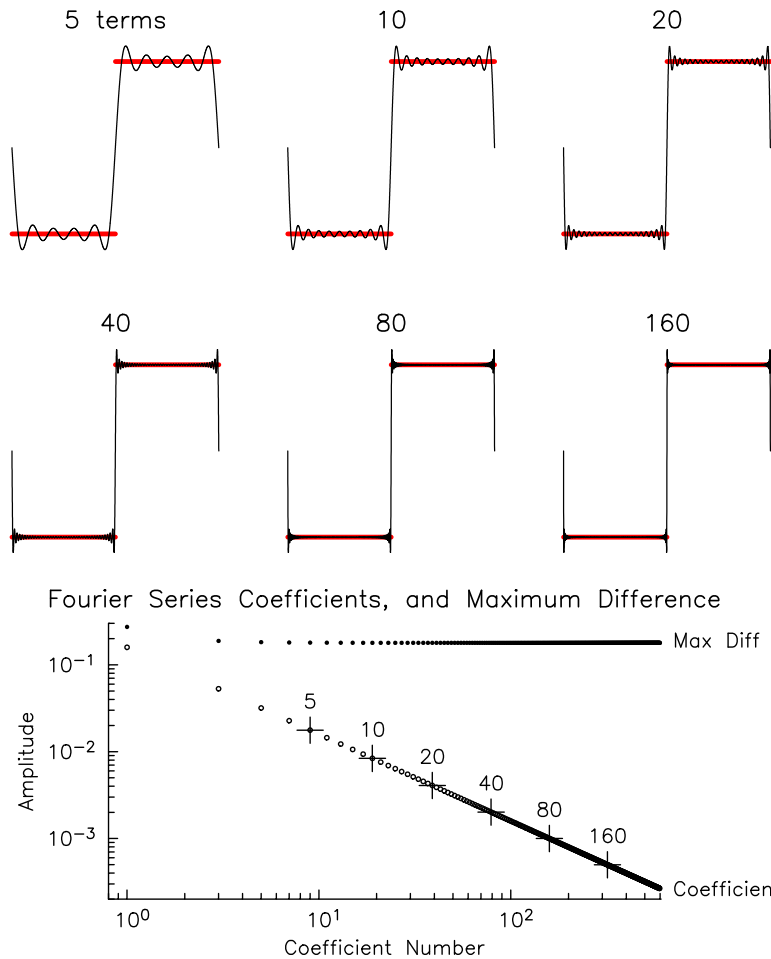


Figure 2.2: Partial sums of the Fourier-series representation of a “square-wave” function, with a discontinuity in the middle of the interval. The function is in red, and the partial sums in black. Gibbs’ phenomenon, the overshoot near the discontinuities, is visible even for very large N . The bottom panel shows how the coefficients of the Fourier series diminish with increasing order, and that the maximum difference does not.

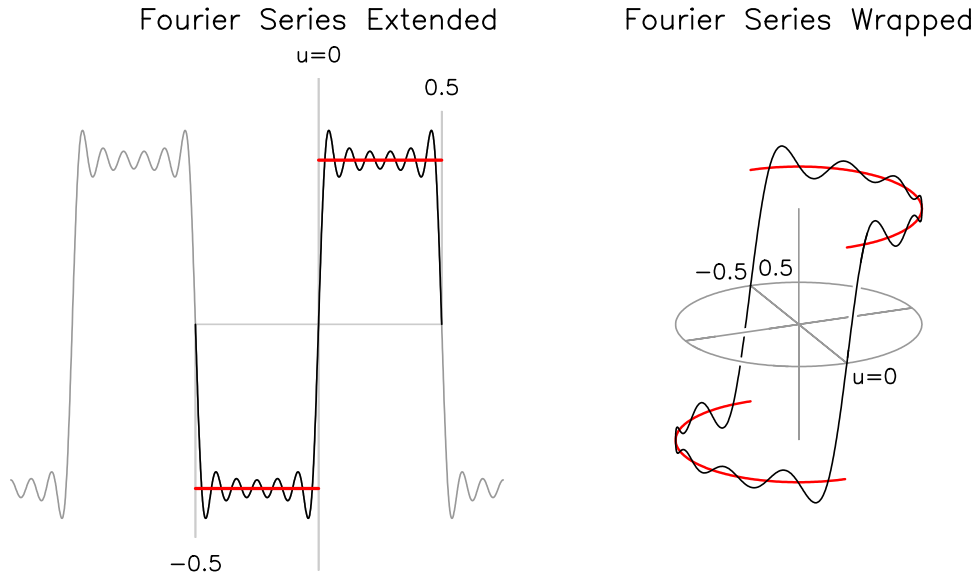


Figure 2.3: The partial sums of the Fourier-series representation of a “square-wave” function for $N = 11$. The function is in red, and the partial sums in black. On the left the Fourier series has been extended (in gray) from its original interval to the entire real line; on the right (a perspective plot) the original interval has been wrapped into a circle.

than this; but these values are the same as the values for u just greater than $-1/2$. Another way to look at this is to imagine the interval $[-1/2, 1/2]$ wrapped into a circle, so that one end is automatically “next to” the other – somewhat reminiscent of the image of a serpent swallowing its tail. We will see this circular representation of a finite interval fairly often; Chapters 5 and 8 will show how this mapping leads to useful ways to look at several features of time series.

2.4.2 Dimensionalizing the Fourier Series

As noted above, we have designated the argument of the function x by the variable u , rather than t , to indicate that this is dimensionless rather than a physical quantity. The repetition shown in Figure 2.3 suggests how to write the series if the argument is taken to be a dimensional one: since the Fourier series has to repeat with a period of one, we set $u = t/T$, where T is the length of time corresponding to the function $x(t)$; t is then the argument expressed in the same units as T . The Fourier series expressions (equations 2.23 and 2.24) then become

$$x(t) = \sum_{n=-\infty}^{\infty} \tilde{x}_n e^{2\pi i n t/T} \quad (2.30)$$

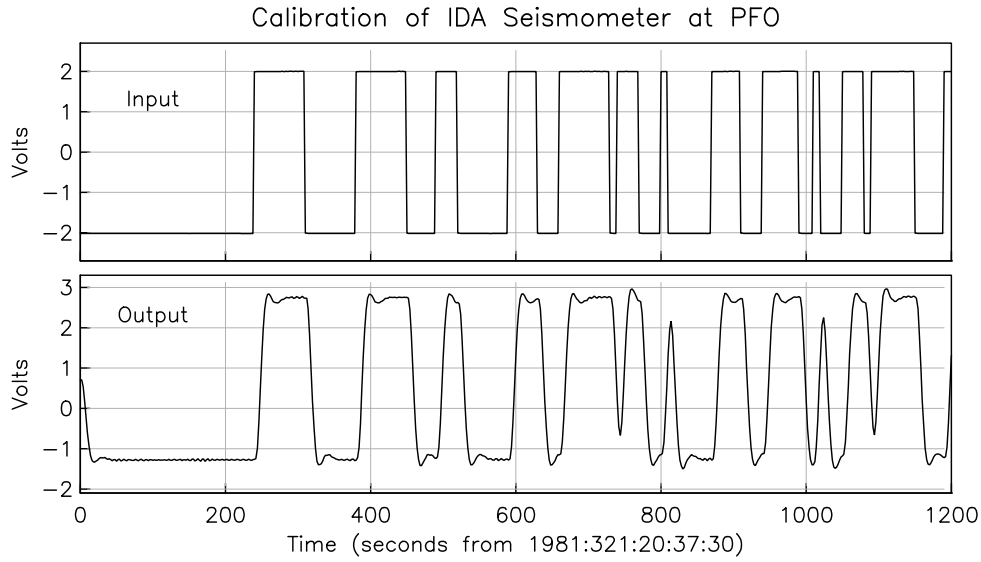


Figure 2.4: Part of the calibration of a Project IDA vertical seismometer installed at Pinyon Flat, California. The top frame shows the input signal: a **random telegraph**, switching between positive and negative values at random, at least every 10 s (Berger *et al.*, 1979). The lower frame shows the seismometer output.

and

$$\tilde{x}_n = \frac{1}{T} \int_{-T/2}^{T/2} x(t) e^{-2\pi i nt/T} dt \quad \text{for } n = -\infty, \dots, -2, -1, 0, 1, 2, \dots \infty \quad (2.31)$$

At this stage the distinction between dimensional and non-dimensional arguments may seem unnecessary, but distinguishing between dimensional and nondimensional arguments becomes less obvious (and so more important) when we discuss the Fourier transform of infinite sequences in Chapters 5 and 6.

2.5 Linear Time-Invariant Systems

Why should we choose sinusoids as our set of orthogonal functions? There are number of ways to answer this; from the standpoint of geophysical data analysis, the answer is the ubiquity of **linear time-invariant systems**, and the especially simple way in which sinusoids interact with such systems.

What do we mean by a “system”? This terminology refers to something into which we put an input $x(u)$: a function of some variable, very often time, and from which we get an output function $y(u)$; Figure 2.4 is an example: we input a voltage to a seismometer to simulate ground motion, and record both this input voltage



Figure 2.5: Block diagram showing a system with one input and one output.

and the voltage coming out. We can symbolize this input-output relationship either as a block diagram (Figure 2.5)), or with the expression $x(u) \Rightarrow y(u)$. Actual systems may well have more than one x and y , and these may be functions of more than one variable, but we avoid these complications for now.

Input	System	Output
Ground motion	Seismometer	Voltage
Magnetized sea-floor	3-4 km of water	Surface magnetics
Solar-lunar gravity	Oceans	Ocean tides
Ice loads	Upper Mantle	Postglacial rebound
Wind	Oceans	Swell
Solar radiation	Atmosphere & ocean	Weather & climate

Table 2.1: Systems, with their inputs and outputs. The first three are linear and (for most purposes) time-invariant.

Table 2.1 gives some examples of systems, listed in order of how difficult they are to model, with the easiest at the top and the most difficult at the bottom. The first three are all easy because they are all examples of systems that can be reasonably modeled as **linear** and **time-invariant**, which is the type of system we will focus on. Linear time-invariant systems (hereafter LTI systems) are basically all alike – the same mathematics applies to them all – whereas nonlinear systems can be nonlinear in many different ways.

To define a **linear** system we consider two inputs: $x_1(u)$ (which the system changes to $y_1(u)$), and $x_2(u)$ (which the system changes to $y_2(u)$). We write this symbolically as $x_1(u) \Rightarrow y_1(u)$ and $x_2(u) \Rightarrow y_2(u)$). Then the system is linear only if $x_1(u) + x_2(u) \Rightarrow y_1(u) + y_2(u)$; this is often called the **principle of superposition**. Repeated application of this definition can be used to show that for a linear system, if $x(u) \Rightarrow y(u)$, then $ax(u) \Rightarrow ay(u)$ for any value of a .

Time-invariance is a separate behavior, which is that the output from a particular input does not depend on the absolute time:

$$x(u + c) \Rightarrow y(u + c)$$

for any constant c . An example of a linear system that would not be time invariant is a pendulum whose length varies over times much longer than its period; even though a simple pendulum is linear in its response to small forces applied to the bob, gradual changes in length would keep it from being time-invariant. Time-invariance automatically holds for any system that depends only on unvarying physical laws, as in the magnetics example above; it can often be assumed as an idealization for many actual systems. For example the ocean tides will vary as the shape of the oceans changes over geologic time because of sea-level changes and continental motion (see, for example, Egbert *et al.* (2004)). From year to year we can reasonably assume time invariance.⁵ The fourth system in Table 2.1, post-glacial rebound, may or may not be linear depending on what the rheology of the mantle is; the advantages of linearity are shown by the almost-universal use of linear models of viscoelasticity for studying this problem. The last two systems in the table are definitely not linear, and as a result are vastly more difficult to model, and much less well understood.

What do these characterizations of systems have to do with Fourier methods? The answer is that sinusoids (or indeed any exponential) are unchanged “in form” by a LTI system: the output and the input have the same functional representation. One way to see this is to note that shifting an exponential e^{su} by an amount c simply multiplies it by e^{sc} , and a linear system does not change the form of the output because the amplitude of the input changes. More formally (and working with complex exponentials), we suppose that

$$x(u) = e^{2\pi i \zeta u} \Rightarrow y(u) = \tilde{g}(\zeta, u) e^{2\pi i \zeta u}$$

where ζ is the **nondimensional frequency**. Since $\tilde{g}(\zeta, u)$ is unspecified this expression allows y to be an arbitrary function of time. Then applying a time shift, and time-invariance, gives

$$x(u+c) = e^{2\pi c} e^{2\pi i \zeta u} \Rightarrow \tilde{g}(\zeta, u+c) e^{2\pi c} e^{2\pi i \zeta u}$$

for any c . Linearity allows us to cancel out the constant factor $e^{2\pi c}$ from both sides, with the result

$$e^{2\pi i \zeta u} \Rightarrow \tilde{g}(\zeta, u+c) e^{2\pi i \zeta u}$$

which implies that the unspecified function \tilde{g} has the property

$$\tilde{g}(\zeta, u+c) = \tilde{g}(\zeta, u)$$

which means that \tilde{g} can depend only on ζ . So the time-dependence of input and output have to be the same: a complex exponential, which is to say a sinusoid.

⁵Though it has recently become clear that changes in the ocean tides are more common, and less understood, than used to be thought (Haigh *et al.*, 2020); and in shallow water the ocean tides are often somewhat nonlinear.

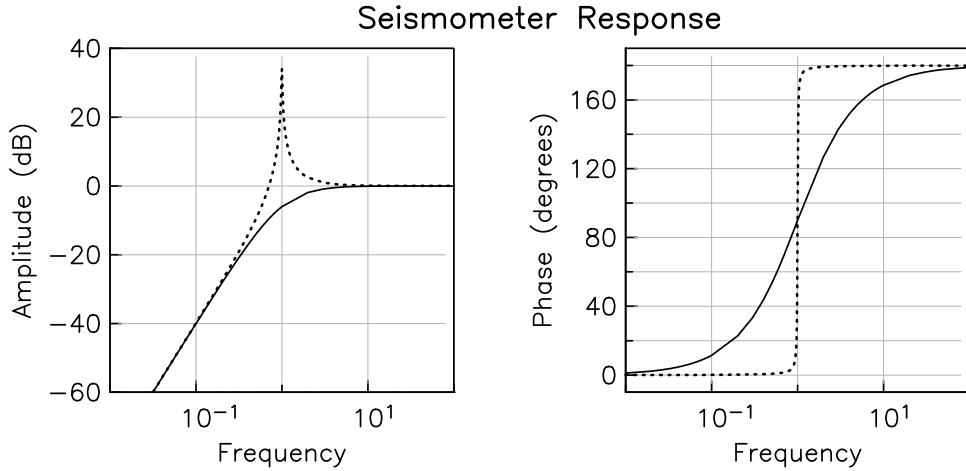


Figure 2.6: Frequency response of a seismometer to displacement. The natural frequency is $f_0 = 1$. The response is shown for $\lambda = 0.01$ (dotted), and $\lambda = 1$ (solid).

We call $\tilde{g}(\zeta)$ the **frequency response** of the system. In general $\tilde{g}(\zeta)$ will be complex (just as x and y are in our example), even though actual series are usually real. This use of complex numbers simplifies the bookkeeping; see Appendix B for a brief summary. Note that none of this argument changes if we use dimensioned time t and frequency f instead of the non-dimensional variables, since in the proof it is the product ft that appears in the exponential.

2.5.1 An Example: The Simple Harmonic Oscillator

A familiar geophysical example of a LTI system is a seismometer, the simplest form of which (such as a mass on a spring) obeys the differential equation for that favorite example of a linear system, a simple harmonic oscillator:

$$\ddot{y} + 2\pi\lambda f_0 \dot{y} + 4\pi^2 f_0^2 y = \ddot{x} \quad (2.32)$$

where y is the displacement of the mass with respect to the instrument frame, and x the displacement of that frame with respect to inertial space. The system parameters are the natural frequency f_0 , and the damping λ . If we substitute $e^{2\pi i f t}$ for $x(t)$ and $\tilde{g}(f)e^{2\pi i f t}$ for $y(t)$, we find (canceling out a lot of $4\pi^2$'s):

$$\tilde{g}(f) = \frac{f^2}{-f^2 + i\lambda f_0 f + f_0^2} \quad (2.33)$$

Figure 2.6 shows the behavior of $\tilde{g}(f)$ for two values of λ : $\lambda = 0.01$ is very under-damped, and $\lambda = 1$ is what is called **critically damped**. As is standard (and in

this context most useful) the plots show $|\tilde{g}|$ in terms of the polar representation of complex numbers as amplitude (in dB) and phase (Appendix B).

2.6 Convolution

We have shown that what a LTI system does to a sinusoid is specified by its frequency response $\tilde{g}(\zeta)$, but what about more general inputs? We shall simply state that, for any linear and time-invariant system, we can relate the output $y(u)$ to the input $x(u)$ through a **convolution integral**

$$y(u) = \int_{-\infty}^{\infty} x(v)g(u-v)dv \stackrel{\text{def}}{=} x(u) * g(u)$$

where $g(u)$ is a function characteristic of the LTI system. We say that y is the **convolution** of x and g , which we write symbolically using $*$.

It is clear that the system described by this integral is linear; to show that it is time-invariant we first show it to be commutative. Making a change of variables by letting $v' = u - v$ we see that

$$\int_{-\infty}^{\infty} x(v')g(u-v')dv' = \int_{-\infty}^{\infty} x(u-v)g(v)dv$$

which means that $x * g = g * x$. Delaying $x(u)$ by c is expressed in the convolution by $x(u-c)$, which gives

$$\int_{-\infty}^{\infty} x(u-c-v)g(v)dv = y(u-c)$$

so convolution is time-invariant.

There are many ways to look at convolutions (Bracewell, 1986). For those who think visually one way of viewing the convolution of two functions is to imagine a plot of $x(v)$, together with one of g (plotted reversed because it is $g(t-v)$). The position of g depends on the value of u ; as u increases, g moves to the right. For any value of u , we form the product gx , and the value of y is just the area under this product function. Figure 2.7 illustrates the process. To develop a better sense of how convolution works, it can be useful to practice drawing functions and sliding one past the other.

A geophysical example of a convolution (though not always so labeled) is the gravitational potential from a mass distribution. The system response is then the Green function for the potential at some point with vector coordinate \mathbf{x} from a unit point mass at \mathbf{v} , which is:

$$g(\mathbf{x}, \mathbf{v}) = \frac{G}{|\mathbf{x} - \mathbf{v}|} \quad (2.34)$$

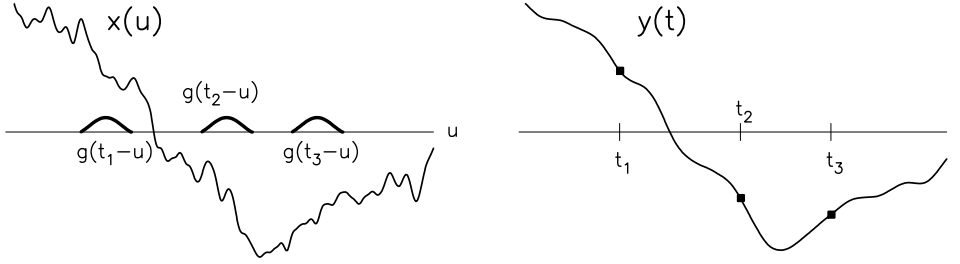


Figure 2.7: A graphical representation of convolution. The left panel shows $x(v)$, and $g(u - v)$ for three values of u . The dots in the right panel show the integral of the product gx for these three values; when this operation is performed for all values of u , we get the function $y(t)$.

where G is the gravitational constant. We get the full potential at \mathbf{x} by taking the Green function, times the source strength (mass) at each \mathbf{v} , and then summing (integrating) to get the potential $y(\mathbf{x})$:

$$y(\mathbf{x}) = \int \frac{G}{|\mathbf{x} - \mathbf{v}|} \rho(\mathbf{v}) dV \quad (2.35)$$

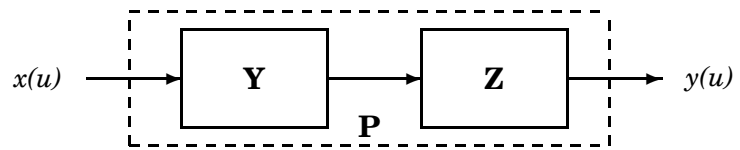
where ρ is the density and the integration is over a volume: this is just a convolution.

Convolution is associative, which we can show by writing the following series of integrals, varying the order of integration and using changes of variables. We have functions x , y , and z ; then

$$\begin{aligned} (x * y) * z &= \int_{-\infty}^{\infty} z(u - r) \int_{-\infty}^{\infty} x(v)y(r - v) dv dr \\ &= \int_{-\infty}^{\infty} x(v) \int_{-\infty}^{\infty} y(r - v)z(u - r) dr dv \\ &= \int_{-\infty}^{\infty} x(v) \int_{-\infty}^{\infty} y(w)z(u - w - v) dw dv \quad (\text{using } w = r - v) \\ &= \int_{-\infty}^{\infty} x(v) \int_{-\infty}^{\infty} y(w)z[(u - v) - w] dw dv \\ &= \int_{-\infty}^{\infty} x(v)p(u - v) dv = x * (y * z) \end{aligned}$$

where p is temporary shorthand for $y * z$.

In terms of linear systems what this means is that we can aggregate them together (or break one system into many) as we see fit, as suggested in the accompanying sketch, where the systems Y and Z can be viewed separately or as a single system P . While this result may seem a bit trivial, it is actually very important: that we can combine simple systems to make complicated ones is a major reason that the concept of linear systems is so useful.



CHAPTER 3

FOURIER TRANSFORMS

But doth suffer a sea-change
Into something rich and strange.

WILLIAM SHAKESPEARE, *The Tempest*, Act 1, Scene 2 (1611).

The Fourier integral is a most beautiful mathematical result because of the economy of means employed in obtaining a most general result. ...
The functions resulting from analysis and synthesis stand in a mutually reciprocal relation.

GEORGE A. CAMPBELL (1928)

3.1 The Fourier Transform

We are now ready to discuss the Fourier transform of a function. We have seen that exponentials $e^{2\pi ift}$ are modified in an especially simple way by linear time-invariant systems; and we have seen how to use a sum of exponentials, a Fourier series, to represent a function:

$$x(t) = \sum_n \tilde{x}_n e^{2\pi i n t / T} \quad \text{for } -T/2 \leq t < T/2 \quad (3.1)$$

where we have limited t to one period of the series. We may generalize this to a sum over complex exponentials with arbitrary frequencies f_n :

$$x(t) = \sum_n \tilde{x}_n e^{2\pi i f_n t} \quad \text{for } -\infty < t < \infty \quad (3.2)$$

In both expressions, each complex exponential is multiplied by a complex Fourier coefficient \tilde{x}_n .

As we saw in Chapter 2, the Fourier series can only represent functions with period T . So it cannot represent many functions that we want to study, in particular, a **transient**, which is any function that is nonzero only over some limited range of t . To be able to represent non-periodic functions, we need to generalize the sum in equation (3.2), which we do by changing the expression to an integral, and writing

$$x(t) = \int_{-\infty}^{\infty} \tilde{x}(f) e^{2\pi i f t} df \quad (3.3)$$

where f all the real numbers.

It can be shown that this integral holds if and only if

$$\tilde{x}(f) = \int_{-\infty}^{\infty} x(t)e^{-2\pi i f t} dt \quad (3.4)$$

which is equation (2.31) modified to have an integral over the real line and, again, complex exponentials with an argument that is real rather than derived from the integers.

Equation 3.4 defines a function $\tilde{x}(f)$ that is the **Fourier transform** of the function $x(t)$.¹ We say that equations (3.3) and (3.4) define a **transform pair**, (3.4) being the **forward** and (3.3) the **inverse** Fourier transform. We write these symbolically as

$$\mathcal{F}[x(t)] = \tilde{x}(f) \quad \text{and} \quad \mathcal{F}^{-1}[\tilde{x}(f)] = x(t)$$

Any user of canned programs or other people's formulas should be aware that the definitions (3.3) and (3.4) are common but not universal. One alternative usage writes (3.4) using angular frequency ω rather than cyclic frequency f : in units, the difference between radians/s and Hz (which is cycles/s). The transform pair is then

$$\tilde{x}(\omega) = \int_{-\infty}^{\infty} x(t)e^{-i\omega t} dt \quad x(t) = \frac{1}{2\pi} \int_{-\infty}^{\infty} \tilde{x}(\omega)e^{i\omega t} d\omega$$

or

$$\tilde{x}(\omega) = \frac{1}{2\pi} \int_{-\infty}^{\infty} x(t)e^{-i\omega t} dt \quad x(t) = \int_{-\infty}^{\infty} \tilde{x}(\omega)e^{i\omega t} d\omega$$

or

$$\tilde{x}(\omega) = \frac{1}{\sqrt{2\pi}} \int_{-\infty}^{\infty} x(t)e^{-i\omega t} dt \quad x(t) = \frac{1}{\sqrt{2\pi}} \int_{-\infty}^{\infty} \tilde{x}(\omega)e^{i\omega t} d\omega$$

all of which normalizations have been used.

A subtler difference from equation (3.4) is when the transform is defined to use a different sign for the exponential:

$$\tilde{x}(f) = \int_{-\infty}^{\infty} x(t)e^{2\pi i f t} dt \quad (3.5)$$

in which case the inverse transform must use $e^{-2\pi i f t}$. Our convention, which follows standard usage in electrical engineering, comes from our choice (in Section 2.5) of $e^{2\pi i f t}$ as a test function; using $e^{-2\pi i f t}$ instead would give the Fourier convention of equation (3.5). This alternate convention is common when dealing with

¹This notation, that the Fourier transform of $x(t)$ is $\tilde{x}(f)$ (the tilde is meant to remind you of the sinusoid), differs from Bracewell (1986), who uses regular capital letters (e.g., $X(f)$) for the transforms of functions; unfortunately, this usage, common in the literature of signal processing, conflicts with how capital and lower-case letters are used in probability and statistics. Another common notation denotes the Fourier transform of $x(t)$ by $\hat{x}(f)$ – this also conflicts with statistical notation.

waves, since if we used our convention, the test function for a traveling wave would be $e^{i(2\pi kx+2\pi ft)}$. This has a constant phase only if x decreases as t increases, so that the wave propagates “backwards” in a negative direction; to get a forward-propagating wave we need the test function to be $e^{i(2\pi kx-2\pi ft)}$.

3.2 Three Transform Pairs

When we have a pair of functions related by (3.3) or (3.4), we often say that $x(t)$ is the function viewed “**in the time domain**”, and its transform $\tilde{x}(f)$ is the same function viewed “**in the frequency domain**”. If you have not encountered this phraseology before, talking about the two domains can sound rather mysterious; but in fact we think this way all the time: music is described both by frequency (pitch) and time (rhythm). When we say “Doing A in the time domain has effect B in the frequency domain”, you should remember that this is just another way of saying, “If we modify the function in time according to A, its Fourier transform will be modified according to B”.

To some extent a familiarity with transform pairs and their behavior comes only with experience, so we begin with a simple case and explore some of the behaviors that it illustrates. We then look at $\tilde{x}(f)$ for a few more functions.

We start with the simplest kind transient function: the rectangle (really square) function also often called a boxcar²

$$\Pi(t) = \begin{cases} 1 & |t| < \frac{1}{2} \\ \frac{1}{2} & \text{for } |t| = \frac{1}{2} \\ 0 & |t| > \frac{1}{2} \end{cases} \quad (3.6)$$

This function is discontinuous; the value at $t = \frac{1}{2}$ is required in a fully rigorous definition. A more general form of Π is $a\Pi([t-b]/c)$, with amplitude a , duration c and central time b .

The Fourier transform of $\Pi(t)$ is easy to find and gives another important function:

$$\begin{aligned} \mathcal{F}[\Pi(t)] &= \int_{-\infty}^{\infty} \Pi(t) e^{-2\pi i f t} dt = \int_{-1/2}^{1/2} e^{-2\pi i f t} dt = \int_{-1/2}^{1/2} \cos 2\pi f t dt \\ &= \frac{\sin 2\pi f t}{2\pi f} \Big|_{-1/2}^{1/2} = \frac{\sin \pi f}{\pi f} \stackrel{\text{def}}{=} \text{sinc}(f) \end{aligned} \quad (3.7)$$

Figure 3.1 shows what this sinc function looks like. For f small, it approaches one; the value for $f = 0$ is this limit. For large f , the function oscillates, and its maximum amplitudes vary asymptotically as f^{-1} .

²In American usage this is a common type of railroad freight car.

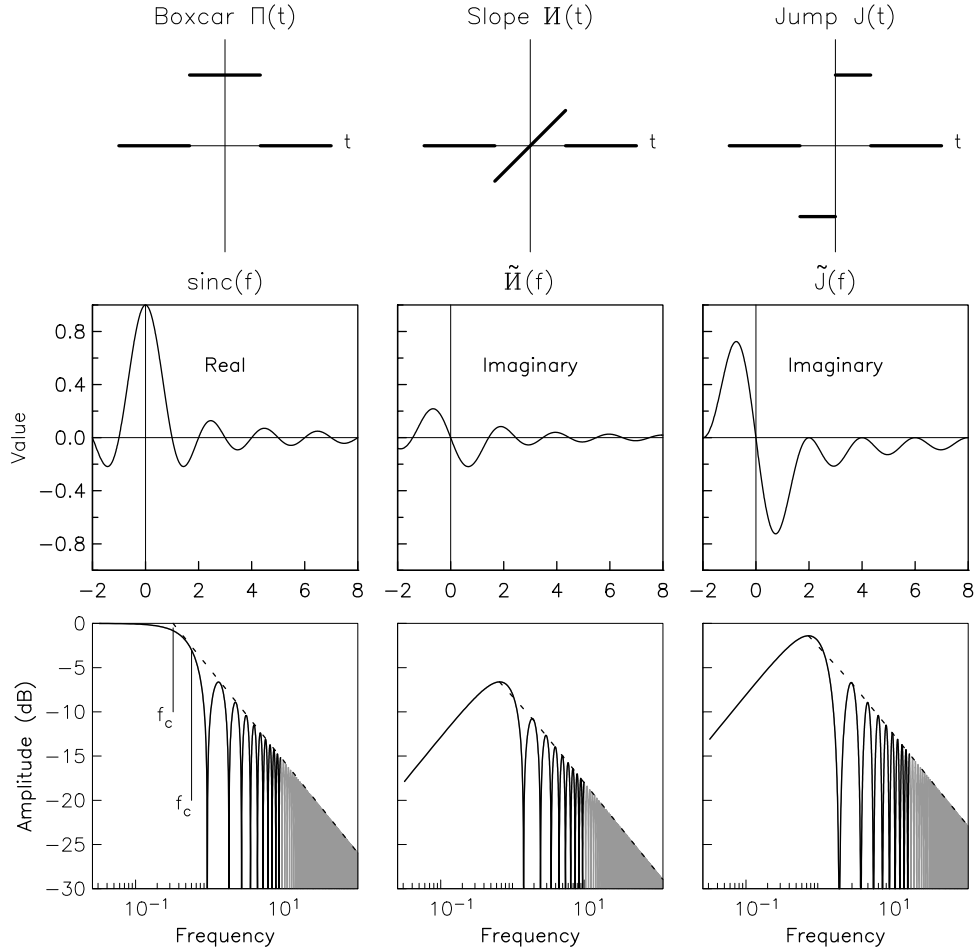


Figure 3.1: Three functions and their Fourier transforms. The top left panel shows the Π function. The two panels below it show its Fourier transform, the sinc function, plotted on a linear scale (center; note that negative frequencies are included) and its absolute value on a log-log scale (bottom); for frequencies higher what is shown in the middle panel, the function is plotted in gray. The bottom left panel also shows the “corner frequency” f_c , defined in two ways: one (right) as the frequency at which $\text{sinc}(f) = \frac{1}{2}$ (-3 dB) and the other (left) as the intersection between the high-frequency asymptote (or **envelope**): the dashed line, and the low-frequency asymptote, which is unity. The three panels in the middle column show the same three things for the slope function I , the right-hand column does the same for the jump function J . As defined in equation (3.8), $\|I\|_2$ is $1/\sqrt{12}$ as large as $\|\text{sinc}\|_2$ and $\|J\|_2$.

The inverse transform relation then gives

$$\Pi(t) = \int_{-\infty}^{\infty} \text{sinc}(f) e^{2\pi i f t} df$$

but if we interchange f and t , and substitute $-f$ for f , which is allowable because sinc is an even function, we get

$$\Pi(f) = \int_{-\infty}^{\infty} \text{sinc}(t) e^{-2\pi i f t} dt$$

another Fourier transform. We see that while $\text{sinc}(t)$ is nonzero over an infinite range, and very smooth, its distribution with frequency is $\Pi(f)$, which is nonzero only over a finite range: we say that makes $\text{sinc}(t)$ is **bandlimited** – with a Fourier transform that is anything but smooth.

Figure 3.1 shows two other functions of time that are also transients (that is, nonzero over the same range as the boxcar), but have very different transforms; perhaps not surprising since these functions are orthogonal to the boxcar (see Figure 2.1). We introduce these functions because they will be useful later in considering the frequency behavior associated with linear trends and offsets in the data.

The functions and their Fourier transforms are

$$I(t) = t \quad \text{for } |t| < \frac{1}{2} \quad \text{and} \quad \tilde{I}(f) = \frac{i}{2\pi^2 f^2} [\pi f \cos(\pi f) - \sin(\pi f)] \quad (3.8)$$

$$J(t) = \text{sgn}(t) \quad \text{for } |t| < \frac{1}{2} \quad \text{and} \quad \tilde{J}(f) = \frac{-2i}{\pi f} [\sin^2(\pi f/2)] \quad (3.9)$$

where $\text{sgn}(t) = t/|t|$ for $t \neq 0$. As Figure 3.1 shows, both of these go to zero at $f = 0$, and, like the sinc function, have maximum amplitudes that vary asymptotically as f^{-1} .

3.3 Fourier Theorems I: Similarity and Shift

Returning to the rectangle function, suppose we make it broader or narrower, so it is $\Pi(at)$. Then the transform is (defining $t' = at$):

$$\int_{-1/2a}^{1/2a} e^{-2\pi i f t} dt = \frac{1}{a} \int_{-1/2}^{1/2} e^{-2\pi i (f/a)t'} dt' = \frac{1}{a} \text{sinc}\left(\frac{f}{a}\right)$$

If a becomes large, $\Pi(at)$ becomes narrower, but its Fourier transform $\text{sinc}(f/a)$ becomes wider. This duality of width between the two domains is in fact a general result, called the **similarity theorem**; again letting $t' = at$

$$\int_{-\infty}^{\infty} x(at)e^{-2\pi i f t} dt = \frac{1}{|a|} \int_{-\infty}^{\infty} x(t')e^{-2\pi i f t'/a} dt'$$

which means that if $\mathcal{F}[x(t)] = \tilde{x}(f)$,

$$\mathcal{F}[x(at)] = \frac{1}{|a|} \tilde{x}(f/a) \quad (3.10)$$

where the $|a|$ comes from the exchange of limits for $a < 0$. Shortening in the time domain thus corresponds to broadening in the frequency domain; a generalization of the obvious case of a sine wave, for which less time between peaks means a higher frequency.

We can be more precise about this relationship between broadening and narrowing by noting that, by the definition of the transform and its inverse,

$$\tilde{x}(0) = \int_{-\infty}^{\infty} x(t) dt \quad \text{and} \quad x(0) = \int_{-\infty}^{\infty} \tilde{x}(f) df \quad (3.11)$$

which is illustrated by two of the three functions shown in Figure 3.1: both the slope and offset functions have zero area, and at zero frequency their Fourier transforms are zero. A result derived from equation (3.11) is

$$\frac{\int_{-\infty}^{\infty} x(t) dt}{x(0)} = \left[\frac{\int_{-\infty}^{\infty} \tilde{x}(f) df}{\tilde{x}(0)} \right]^{-1} \quad (3.12)$$

for $x(0)$ and $\tilde{x}(0)$ nonzero. Since $\int_{-\infty}^{\infty} x(t) dt$ is just the area under the function, $\frac{1}{x(0)} \int_{-\infty}^{\infty} x(t) dt$ is a kind of measure of the width of the function, specifically of the width of a rectangle of height $x(0)$ with the same area. This width, and the width of the transform, are thus reciprocals.

Equation 3.11 is a first example of another duality that we will see repeated: global aspects in one domain (the area) are connected to local aspects in the other (the value at zero).

We can also ask what happens to the Fourier transform if we shift a function in time. The answer, for a function $x(t)$ that has been shifted by τ , is:

$$\mathcal{F}[x(t - \tau)] = \int_{-\infty}^{\infty} x(t - \tau) e^{-2\pi i f t} dt = \int_{-\infty}^{\infty} x(t') e^{-2\pi i f(t' + \tau)} dt' = \tilde{x}(f) e^{-2\pi i f \tau} \quad (3.13)$$

Expressing $\tilde{x}(f)$ in amplitude and phase (Appendix B) means that we write it as $|\tilde{x}(f)|e^{i\phi(f)}$. Doing the same for $\tilde{x}(f)e^{-2\pi i f \tau}$, will give the same amplitude $|\tilde{x}(f)|$, but the phase $\phi(f)$ will have $-2\pi f \tau$ added to it. If we call $|\tilde{x}(f)|$ the **amplitude spectrum** we see that a time shift leaves this spectrum unaltered, but changes the **phase spectrum** $\phi(f)$, adding an amount that varies linearly with frequency: two effects that between them are called the **shift theorem**.

As noted above, our sign convention for the Fourier transform means that a time delay will cause the phase at a given frequency to be more negative. The shift theorem provides an easy check on the sign used for the exponential in computing

the Fourier transform: transform two series that are identical except that one is delayed relative to the other, and compare the phases of the output. For our convention, the phase of the delayed series will be more negative.

In any situation in which uncontrollable, or irrelevant, delays are present, the amplitude spectrum will be the useful part of the Fourier transform. For example, for seismic wave signals, the amplitude spectrum is unaffected by the time delay from the travel time, which for some analyses (such as inferring earthquake source properties) is not relevant.

3.4 Generalized Functions

So far we have proceeded as though, given a function, there would in fact be another function that is its Fourier transform. But this may easily not be true; we can easily come up with functions, for example $x(t) = \cos t$, or $x(t) = 1$, for which the transform integral (3.4) does not exist. We could limit ourselves to functions for which (3.4) does exist, but it turns out to be possible to extend the idea of what $x(t)$ can be in a way that allows a much wider class of functions to have Fourier transforms. We make this extension by introducing what are called **generalized functions**.

Adding to the kinds of entities we can consider, rather than declaring results to be meaningless, is often a fruitful approach in mathematics. For example, if we start with the integers, division of any integer by any other is possible only if we introduce rational numbers; for subtraction of any two to be possible requires introducing negative numbers; and allowing square roots requires irrational and imaginary numbers. The names of the last two show that these extensions were not easily accepted.

A full and rigorous treatment of generalized functions goes well beyond the scope of this course; [Lighthill \(1958\)](#) provides such a treatment in a compact and readable form. We follow the same strategy as found there, though without the rigor: we treat generalized functions as the limit of a sequence of ordinary functions.

To start, consider the convolution of the rectangle function with another function $x(t)$. Evaluated for $t = 0$, this is

$$x(t) * \Pi(t)|_{t=0} = \int_{-\infty}^{\infty} x(u)\Pi(-u)du = \int_{-1/2}^{1/2} x(t)dt$$

Next, do the same thing for $a\Pi(at) * x(t)$; the $t = 0$ value is

$$x(t) * a\Pi(at) = a \int_{-1/2a}^{1/2a} x(t)dt$$

What happens as $a \rightarrow \infty$, making the rectangle function higher and narrower? Provided that $x(t)$ is itself well-behaved near zero, what we get is the area under

a rectangle with height close to the average of $x(t)$, and with base a^{-1} ; we then multiply this by a . The a^{-1} and a cancel, so that this product is the average of $x(t)$ over the range from $-1/2a$ to $1/2a$. As a gets larger, this average of x approaches $x(0)$, so that

$$\lim_{a \rightarrow \infty} [a\Pi(at) * x(t)]_{t=0} = x(0)$$

If we take the limiting operation “inside” the convolution, we may define a generalized function

$$\delta(t) = \lim_{a \rightarrow \infty} [a\Pi(at)]$$

such that

$$\int_{-\infty}^{\infty} x(u)\delta(u)du = x(0)$$

This is the **Dirac delta function**, which can be pictured as an infinitely narrow, infinitely high spike (with unit area) at $x = 0$. The delta function will be our mathematical link between continuous time and sampled data.

By using a shifted version of $\Pi(t)$ we can equally well show that

$$\int_{-\infty}^{\infty} x(u)\delta(u-a)du = x(a)$$

If we replace the constant a by the variable t , we find

$$\int_{-\infty}^{\infty} x(u)\delta(u-t)du = x(t)$$

which means that convolution of $\delta(t)$ with a function reproduces the function; convolution with $\delta(t-a)$ produces a shifted version of the function, $x(t-a)$.

From the above we can conclude

$$\delta(t) = 0 \quad \text{for} \quad t \neq 0 \quad \text{but} \quad \int_{-\infty}^{\infty} \delta(t)dt = 1$$

making the delta function one that vanishes everywhere but zero, but still has a finite integral. Note that the value of $\delta(0)$ is undefined: this function (like other generalized functions) has meaningful properties only when integrated, not when standing alone.

A function closely related to the delta function (but not itself a generalized function) is the **Heaviside step function**

$$H(t) = \begin{cases} 1 & \text{for } t > 0 \\ 0 & \text{for } t < 0 \end{cases}$$

which is the mathematical way of saying, “Throw the switch.”³ If we perform the convolution $x * H$ we get

$$\int_{-\infty}^{\infty} x(u)H(t-u)du = \int_{-\infty}^t x(u)du$$

which is just the integral of x evaluated at t . Taking the derivative of this, by the theorems of calculus, gives $x(t)$ again. We may, very nonrigorously, write:

$$\frac{d}{dt}[H * x] = x$$

and applying the derivative operator to the step function (interchanging differentiation and integration) gives $H' * x = x$, which means that $H(t)' = \delta(t)$. That the derivative of H is the delta function, while graphically appealing, does considerable violence to the usual notion of derivative, but again can be made rigorous by considering sequences of functions which approach $H(t)$; if these are differentiable, it can be shown that the derivatives approach $\delta(t)$. Indeed, it is possible to keep “taking derivatives” in this fashion to get a function $\delta'(t)$, which when convolved with a function $x(t)$ produces the derivative $x'(t)$.

3.5 Fourier Transforms of Generalized Functions

So, what additional Fourier transforms can we do now? If we take Fourier transforms of the sequence of rectangle functions, $\mathcal{F}[a\Pi(at)]$, the transform is

$$a \int_{-1/2a}^{1/2a} e^{-2\pi i f t} dt = \int_{-1/2}^{1/2} e^{-2\pi(f/a)t'} dt' = \text{sinc}(f/a)$$

If we now let a go to ∞ , $f/a \rightarrow 0$ and since $\text{sinc}(0) = 1$, we have (interchanging integration and the limiting operation)

$$\mathcal{F}[\delta(t)] = 1$$

which says that the delta function contains all frequencies equally. Of course just taking the transform, and using the properties of the delta function, gives the same result:

$$\mathcal{F}[\delta(t)] = \int_{-\infty}^{\infty} \delta(t)e^{-2\pi i f t} dt = e^{-2\pi i 0} = 1$$

The inverse transform of the constant ($x(t) = 1$) then gives

$$\int_{-\infty}^{\infty} e^{2\pi i f t} df = \delta(t) \tag{3.14}$$

³Entirely appropriately, Oliver Heaviside, the inventor of this and other mathematical machinery in this field, worked as a telegrapher.

One way to “see” this is to note that for $t \neq 0$ the integrand oscillates and so gives a zero integral, but for $t = 0$ the integral is infinite. Again, in ordinary function theory this equation would be complete nonsense; the left side is nonintegrable and the right side is meaningless. The extension to generalized functions allows us to deal with such problems in a consistent way.

If we now swap f and t in equation (3.14), f becomes a parameter rather than the integrand, and if we replace f by $f - f_0$ we get

$$\int_{-\infty}^{\infty} e^{2\pi i t(f_0 - f)} dt = \delta(f_0 - f) = \delta(f - f_0)$$

Since the integral is just the Fourier transform of the complex exponential $e^{2\pi i f_0 t}$, we have $\mathcal{F}[e^{2\pi i f_0 t}] = \delta(f - f_0)$: a delta function at nonzero frequency is the Fourier transform of a complex sinusoid, the transform having, as might be expected, an “infinite” peak at frequency f_0 .

What about sines and cosines? Using the expressions for these in terms of complex exponentials, their transforms are:

$$\mathcal{F}[\cos 2\pi f_0 t] = \mathcal{F}\left[\frac{1}{2}(e^{-2\pi i f_0 t} + e^{2\pi i f_0 t})\right] = \frac{1}{2}[\delta(f - f_0) + \delta(f + f_0)]$$

which is two delta-functions at $\pm f_0$. Similarly,

$$\mathcal{F}[\sin 2\pi f_0 t] = \mathcal{F}\left[\frac{-i}{2}(e^{2\pi i f_0 t} - e^{-2\pi i f_0 t})\right] = \frac{-i}{2}[\delta(f - f_0) - \delta(f + f_0)]$$

which is purely imaginary, and also has delta functions at $\pm f_0$, though with opposite signs.

These two results are examples of some important **symmetry relations** for the Fourier transform: $\cos 2\pi f_0 t$ is real and even, and so is its transform; $\sin 2\pi f_0 t$ is odd, and its transform is purely imaginary and odd: these properties are also visible in Figure 3.1.

Since any real function can be split into even and odd parts, the transform of a real function must have a real part which is even and an odd part which is imaginary: for $x(t)$ real,

$$\mathcal{R}[\tilde{x}(f)] = \mathcal{R}[\tilde{x}(-f)] \quad \mathcal{I}[\tilde{x}(f)] = -\mathcal{I}[\tilde{x}(-f)]$$

which is to say $\tilde{x}(f) = \tilde{x}^*(-f)$. Functions with this property are called **Hermitian**. Because real functions have Hermitian transforms, the transform only needs to be specified for $f \geq 0$.⁴ Table 3.1 summarizes most of the useful symmetry relations between functions and their transforms.

Since we have just established that negative frequencies are superfluous when we are dealing with real-valued functions, and knowing that most data are real-valued, you may wonder if there is any meaning to negative frequencies. They are

⁴Or only for $f \leq 0$, but nobody does that.

Time Domain	Frequency Domain
Complex	Complex $\tilde{x}(f) \neq \tilde{x}(-f)$
Real	Hermitian $\tilde{x}(f) = \tilde{x}^*(-f)$
Real, even	Real, even $\tilde{x}(f) = \tilde{x}(-f)$
Real, odd	Imaginary, odd $\tilde{x}(f) = -\tilde{x}(-f)$
Imaginary	anti-Hermitian $\tilde{x}(f) = -\tilde{x}^*(-f)$

Table 3.1: Relationships between different properties of a function in the time domain, and its transform in the frequency domain, for the latter giving both the name and the algebraic expression.

in fact meaningful in certain cases that we describe in Appendix B.4 and apply in Section 8.2.

3.6 Fourier Theorems II: Derivatives and Differentiability

We now return to general theorems on Fourier transform pairs. We first look at what differentiation in time does to the Fourier transform. A very nonrigorous application of integration by parts gives

$$\begin{aligned}\mathcal{F}[x'(t)] &= \int_{-\infty}^{\infty} x'(t)e^{-2\pi ift} dt = \\ &\quad e^{-2\pi ift} x(t) \Big|_{-\infty}^{\infty} + 2\pi if \int_{-\infty}^{\infty} x(t)e^{-2\pi ift} dt \\ &= 2\pi if \tilde{x}(f)\end{aligned}\tag{3.15}$$

This also holds in reverse, with, $\mathcal{F}^{-1}[\tilde{x}'(f)] = -2\pi itx(t)$.

These results are the basis for using Fourier transforms to solve some classes of linear differential equations, a topic we discuss in Chapter 8 when we discuss how to design certain kinds of digital filters. Looking at the function in two domains, this result is important for showing what differentiation (or integration) in the time domain will do to the function in the frequency domain. For example, consider ground motion from an earthquake: for given displacements, the velocities (the first derivative) will have a transform scaled by f , and will thus be much richer in high frequencies (rougher), and the accelerations will be richer still, with a Fourier transform scaled by f^2 .

This result leads to other ones, which like the earlier results on widths connect local properties in one domain with global ones in another. For second derivatives

$$\mathcal{F}^{-1}[\tilde{x}''(f)] = -4\pi^2 t^2 x(t)$$

Discontinuities and Their Fourier Transform Asymptotes

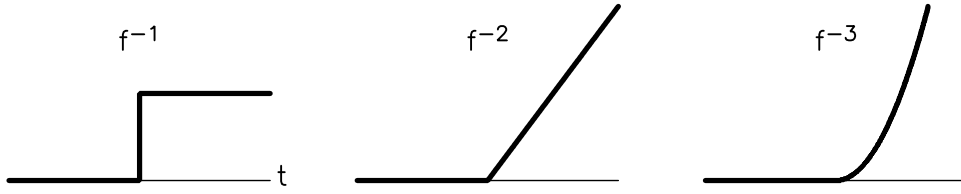


Figure 3.2: Sketches to show what level of discontinuity (left to right: in function, first derivative, and second derivative) provides what level of asymptotic decay of the Fourier transform.

Taking the transform of both sides gives

$$\int_{-\infty}^{\infty} t^2 x(t) e^{-2\pi i f t} dt = \frac{-\tilde{x}''(f)}{4\pi^2}$$

which means that the second moment of the function $x(t)$ is

$$\int_{-\infty}^{\infty} t^2 x(t) dt = \frac{-\tilde{x}''(0)}{4\pi^2} \quad (3.16)$$

that is, the second moment of the function is proportional to the second derivative of its Fourier transform, evaluated at the origin. Once again we see that a global property (the second moment) in the time domain is connected to a very local property (the second derivative at the origin) in the frequency domain.

Equation 3.16 gives an interesting behavior for the Fourier transforms of functions $x(t)$ that have infinite second moments. Then the second derivative of $\tilde{x}(f)$ does not exist at $f = 0$: the derivative there is discontinuous and the function has a “corner”. A geophysically relevant example of a transform pair can be obtained if we start with such a function: the double-sided decaying exponential $x(t) = e^{-2\pi k|t|}$. Taking just the part with $t \geq 0$, the Fourier transform is

$$\int_0^{\infty} e^{2\pi(if-k)t} dt = \frac{1}{2\pi(if-k)} e^{2\pi(if-k)t} \Big|_0^{\infty} = \frac{1}{2\pi(k-if)} \quad (3.17)$$

and the transform of the function from $-\infty$ to zero is, similarly,

$$\frac{1}{2\pi(k+if)}$$

with the sum being

$$\tilde{x}(f) = \frac{k}{4\pi(k^2+f^2)} \quad (3.18)$$

which clearly does not have a second moment.

So stated this Fourier pair might not seem that interesting; to make it so we take the function in equation (3.18) to be the one to be transformed. We replace time by distance z . Then

$$\mathcal{F}[x(z)] = \mathcal{F} \left[\frac{h}{4\pi(h^2 + z^2)} \right] = e^{-2\pi h|f|} = e^{-2\pi h/\lambda} \quad (3.19)$$

where f is spatial frequency and $\lambda = f^{-1}$ is the spatial wavelength.

Now $x(z)$ is just the expression for the gravitational attraction from a point mass located a distance h from the z axis (for example, data collected at a height h above the source). As with equations (2.34) and (2.35), we would convolve $x(z)$ with a density distribution to get the gravitational attraction along a line at elevation h . In the frequency domain we would multiply the Fourier transform of the density by the exponential function of wavelength in equation (3.19), which will reduce wavelengths of πh by a factor of $e^{-2} = 0.13$; for $\lambda = h$ the factor is 2×10^{-3} . So magnetic and gravity data taken at some distance from the source are likely to be very deficient in shorter wavelengths. In Section 10.3.2 we will see this behavior in actual data, and in Sections 12.3.3 and 13.3.1 we will see how it affects the analysis of such data.

Another example of the local/global relation between the original and the transform is how the differentiability of $x(t)$ affects the asymptotic behavior of $\tilde{x}(f)$, specifically the bounds on $|\tilde{x}(f)|$ as $f \rightarrow \infty$. Intuitively one might suppose these to be connected; the “rougher” a function is, the more high frequencies we would expect it to contain. We can motivate (not prove!) the result we seek by supposing $x(t)$ to contain steps; then $x'(t)$ (using our extended notion of differentiation) contains delta functions, and so $|\mathcal{F}[x'(t)]| \propto 1$ as f becomes large. But then we have, from equation (3.15):

$$|\mathcal{F}[x(t)]| = |\tilde{x}(f)| = \left| \frac{\mathcal{F}[x'(t)]}{2\pi i f} \right| \propto f^{-1}$$

for $f \rightarrow \infty$. Similarly, a function with steps is the derivative of one that is continuous but has corners (discontinuous derivatives) and so by the same argument the Fourier transform of such a function will be proportional to f^{-2} as $f \rightarrow \infty$. Extended, this shows that if $x(t)$ has a discontinuous n -th derivative, $|\tilde{x}(f)|$ will fall off as $f^{-(n+1)}$ at high frequencies; Figure 3.2 illustrates the first few cases.

At one extreme we have the discontinuous functions of Figure 3.1, all of which have Fourier transforms that decrease as f^{-1} for $|f|$ large. For example

$$|\mathcal{F}[\Pi(t)]| = |\text{sinc } f| < k/f \quad \text{as } f \rightarrow \infty$$

where $k = 1/\pi$. At the other extreme, suppose $x(t) = e^{-\pi t^2}$, which is infinitely differ-

entiable. For this,

$$\begin{aligned}\tilde{x}(f) &= \mathcal{F}[x(t)] = \int_{-\infty}^{\infty} e^{-(\pi t^2 + 2\pi i f t)} dt \\ &= e^{-\pi f^2} \int_{-\infty}^{\infty} e^{-\pi(t+if)^2} dt \\ &= e^{-\pi f^2} \int_{-\infty}^{\infty} e^{-\pi u^2} du = e^{-\pi f^2}\end{aligned}$$

That is, the Gaussian is its own Fourier transform, which for large f goes to zero as e^{-f^2} , much more rapidly than any power of f .

3.7 Fourier Theorems III: Combinations of Two Functions

So far, we have looked only at properties of a single function and its Fourier transform. We now consider combinations of functions. Linearity means that if we add two functions the transform of the result is the sum of the two transforms. A much more interesting result appears if we consider the function formed by the convolution or multiplication of two functions.

3.7.1 The Convolution Theorem

The key result is the **convolution theorem**, which states that

$$\mathcal{F}[x(t) * y(t)] = \mathcal{F}[x(t)] \mathcal{F}[y(t)]$$

which is to say, the transform of the function formed by convolving two functions is the product of the transform of the individual functions. This is not difficult to show; using changes of variables freely, we have:

$$\begin{aligned}\int_{-\infty}^{\infty} e^{-2\pi i f t} \int_{-\infty}^{\infty} x(u)y(t-u) du dt &= \int_{-\infty}^{\infty} x(u) \int_{-\infty}^{\infty} y(t-u)e^{-2\pi i f t} dt du \\ &= \int_{-\infty}^{\infty} x(u) \int_{-\infty}^{\infty} y(t')e^{-2\pi i f t'} e^{-2\pi i f u} dt' du \\ &= \mathcal{F}[y(t)] \int_{-\infty}^{\infty} x(u)e^{-2\pi i f u} du = \mathcal{F}[y(t)] \mathcal{F}[x(t)]\end{aligned}$$

Writing $\mathcal{F}[x] = \tilde{x}$, $\mathcal{F}[y] = \tilde{y}$, we can state this and related results compactly:

$$\mathcal{F}[x * y] = \tilde{x}\tilde{y} \quad \mathcal{F}^{-1}[\tilde{x}\tilde{y}] = x * y \quad \mathcal{F}[xy] = \tilde{x} * \tilde{y} \quad \mathcal{F}^{-1}[\tilde{x} * \tilde{y}] = xy \quad (3.20)$$

The convolution theorem is *the* main reason for our use of Fourier transforms: while the action of a linear system is a convolution in the time domain, it is a multiplication in the frequency domain – and multiplication is much easier to grasp

than convolution. While the frequency domain may initially seem less natural than the time domain, operations in it are often much simpler. In Section 2.5 we showed that a sinusoid $e^{2\pi ift}$ put into a linear time-invariant system yields another sinusoid $\tilde{g}(f)e^{2\pi ift}$; this is a special case of the convolution theorem. We write the effect of the system as $y = g * x$, which implies $\tilde{y}(f) = \tilde{g}(f)\tilde{x}(f)$, and if $\tilde{x}(f) = \delta(f - f_0)$, $\tilde{y}(f)$ will be

$$\tilde{g}(f)\delta(f - f_0) = \tilde{g}(f_0)\delta(f - f_0)$$

since $\delta(f - f_0) = 0$ for $f \neq f_0$. Again, and now perhaps more clearly than in our earlier discussion, we see that $\tilde{g}(f)$ is the frequency response of the system.

If we make the input to the system $x(t) = \delta(t)$, then the output is

$$y(t) = \int_{-\infty}^{\infty} \delta(t-u)g(u)du = g(t)$$

which is called the **impulse response** of the system; while this is less easy to produce in practice, it is still a useful characterization. Then the frequency response is seen to be $\tilde{g}(f) = \mathcal{F}[g(t)]$

A function related to the impulse response is its integral, the **step response**:

$$h(t) = \int_{-\infty}^t g(u)du$$

which is the response of the system to a Heaviside step function $H(t)$ applied at $t = 0$. For any actual system it is easier to produce step inputs than delta functions, so the step response is easier to produce than the impulse response.

As an example of a system's frequency response, consider differentiation as a linear time-invariant system – though not usually thought of as such. We have seen that $\mathcal{F}[x'(t)] = 2\pi if\tilde{x}(f)$ and so the frequency response for this system is $\tilde{g}(f) = 2\pi if$, with amplitude and phase spectra

$$|\tilde{g}(f)| = 2\pi f \quad \text{Ph}[\tilde{g}(f)] = \pi/2 = 90^\circ$$

As might be expected, the response rises with increasing frequency; the 90° phase response means that sines are turned into cosines, and vice versa.

The frequency response of a system is often much simpler to describe than its impulse response (and more indicative of the underlying physics); we will (eventually) get to ways of estimating it given $x(t)$ and $y(t)$.

3.7.2 Power Theorems

An interesting corollary of the convolution theorem relates to the total variance, also called energy.⁵ This is

$$\int_{-\infty}^{\infty} |x(t)|^2 dt$$

⁵Whether we call this energy or power turns out to depend on whether the function describes a transient or a stationary signal; we will see what “stationary” means in Section 10.2.

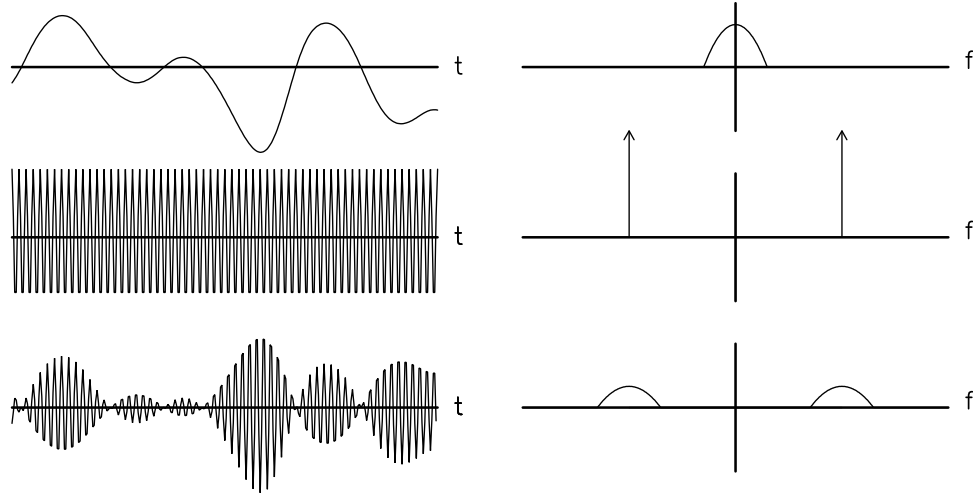


Figure 3.3: From top to bottom, the time series and spectra for a signal, a carrier wave, and the amplitude-modulated carrier. The spectra are schematic.

We first consider the Fourier transform of the conjugate of x , which is

$$\mathcal{F}[x^*(t)] = \int_{-\infty}^{\infty} x^*(t)e^{-2\pi i f t} dt = \left[\int_{-\infty}^{\infty} x(t)e^{-2\pi i (-f)t} dt \right]^* = \tilde{x}^*(-f)$$

and so, using one version of the convolution theorem,

$$\mathcal{F}[|x(t)|^2] = \mathcal{F}[xx^*] = \tilde{x}(f) * \tilde{x}^*(-f)$$

Remembering that the area under a function is the value of its Fourier transform at $f = 0$, this means that

$$\int_{-\infty}^{\infty} |x(t)|^2 dt = \tilde{x}(f) * \tilde{x}^*(-f) \Big|_{f=0} = \int_{-\infty}^{\infty} \tilde{x}(u)\tilde{x}^*(u+f) du \Big|_{f=0} = \int_{-\infty}^{\infty} |\tilde{x}(f)|^2 df \quad (3.21)$$

so that the total energy is the same in the function as in its transform.⁶ This result goes by several names; [Bracewell \(1986\)](#) calls it **Rayleigh's theorem**, but says that the name Plancherel's theorem is also in use; this result is also sometimes called **Parseval's theorem**, especially for the analogous case of discrete-time Fourier transforms that we discuss in Chapter 5.

⁶Using “energy” for the integral of the square of the function comes from electrical engineering: if a voltage V flows through a resistance R the power dissipated is V^2R ; the integral of this is the energy.

3.7.3 Modulation Theorem

The third case given in equation (3.20) simply says that the Fourier transform of the product of two functions in the time domain is the convolution of their two Fourier transforms; this is called the **modulation theorem**. Though this is nothing more than one part of the convolution theorem, it is worth looking at examples of it to get a better sense of how functions map from the time to the frequency domain.

Amplitude Modulation

The first example, which gives the theorem its name, is a sinusoid whose amplitude slowly varies with time, “slowly” meaning “at frequencies well below the frequency of the sinusoid”. We then say that the sinusoid has been **amplitude modulated**, that is, varied: one way to transmit (say) audio signals (frequencies less than 10 kHz) using radio waves (frequencies from 500 kHz to many GHz). Varying the amplitude of a sinusoid (in this context usually called a **carrier wave**). Amplitude modulation is not the only way to send low-frequency information using higher-frequency sinusoids: we might, for example, vary the frequency or phase of the sinusoid. Though these are actually better methods for communication purposes, their Fourier transforms are somewhat complicated and we do not discuss them.

Suppose the sinusoid is $\cos 2\pi f_0 t$; this has the Fourier transform

$$\mathcal{F}[\cos 2\pi f_0 t] = \frac{1}{2}[\delta(f - f_0) + \delta(f + f_0)]$$

Given a function $x(t)$, the modulated waveform is $x(t)\cos 2\pi f_0 t$. By the third expression in equation (3.20), the Fourier transform of this will be the convolution of $\tilde{x}(f)$ (the Fourier transform of $x(t)$) with the delta function that is the transform of the sinusoid. Remembering that convolution with a delta function recovers the function being convolved, we find

$$\begin{aligned}\mathcal{F}[x(t)\cos 2\pi f_0 t] &= \frac{1}{2}[\delta(f - f_0) * \tilde{x}(f) + \delta(f + f_0) * \tilde{x}(f)] \\ &= \frac{1}{2}[\tilde{x}(f - f_0) + \tilde{x}(f + f_0)]\end{aligned}$$

The effect of multiplying a function by a sine wave is thus to replicate the original transform at $\pm f_0$ (Figure 3.3); alternatively, we can say that the effect of modulating a sine wave is to spread its original delta-function transform out over a broader band, though if $x(t)$ contains only frequencies much less than f_0 (as is true in the case of radio), the band will be narrow. This spreading also occurs for other classes of modulation.

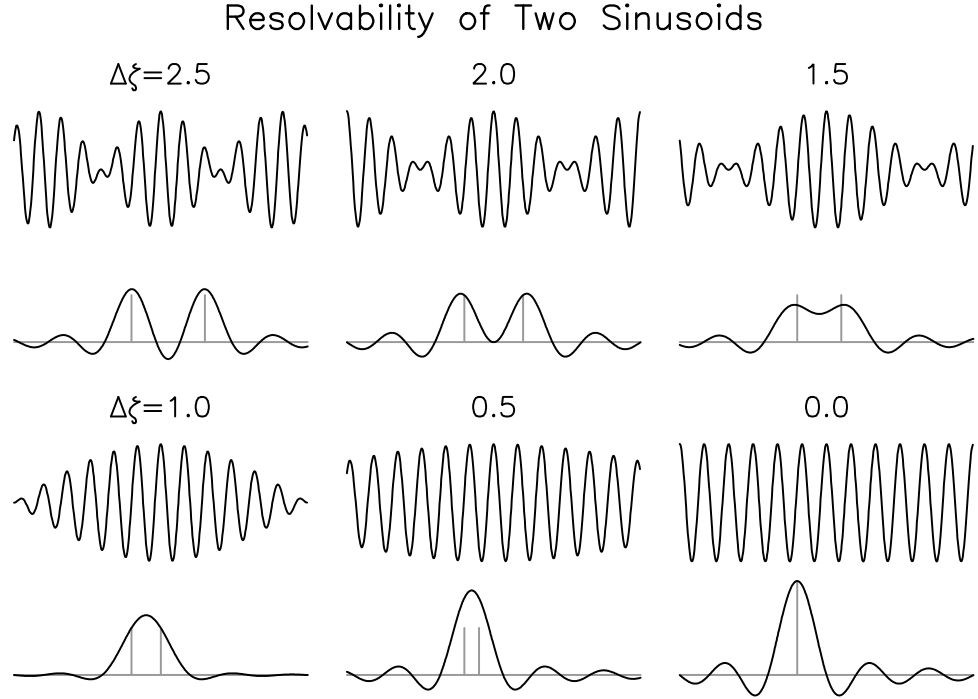


Figure 3.4: Time and frequency depictions of a function that is a sum of two sinusoids with closely spaced frequency that are nonzero over a finite time range. The short vertical lines show the frequencies of the two sinusoids; as these frequencies approach each other, the Fourier transform changes, from showing two peaks to only one.

Resolving Sinusoids

For our next application of the modulation theorem, assume that we have a function that is two sinusoids, but only over a finite range of time, say from $-T/2$ to $T/2$. That is

$$x(t) = \Pi(t/T)[\cos(2\pi f_1 t) + \cos(2\pi f_2 t)] \quad (3.22)$$

which we nondimensionalize by setting $u = t/T$, so

$$x(u) = \Pi(u)[\cos(2\pi\zeta_1 u) + \cos(2\pi\zeta_2 u)]$$

with $\zeta = f T$.

We have used cosines for this example to make the Fourier transform symmetric in frequency, so we can say that without the boxcar the Fourier transform of the sum is $\delta(\zeta - \zeta_1) + \delta(\zeta - \zeta_2)$ for $\zeta \geq 0$. Then the modulation theorem gives the Fourier transform as the convolution of a sinc function with the two delta functions, which

is the sum of two sinc functions centered on the two delta functions:

$$\tilde{x}(\zeta) = \text{sinc}(\zeta - \zeta_1) + \text{sinc}(\zeta - \zeta_2)$$

Figure 3.4 shows what this transform, and the time series, look like for different values of $\Delta\zeta = |\zeta_1 - \zeta_2|$. If $\Delta\zeta \geq 2$, the transform will have two peaks in about the right locations. But as $\Delta\zeta$ changes from 2.0 to 1.0, these peaks merge and become a single peak; for even smaller values of $\Delta\zeta$ this peak becomes larger and narrower, until for $\Delta\zeta = 0$ it is just $2\text{sinc}(\zeta)$.

Even though there is only one peak for $\Delta\zeta = 1.0$, it is clearly not a sinc function, and the time function is clearly different from a single sinusoid. But for smaller values of $\Delta\zeta$ even this is not true. So it is usually said that two peaks with separation Δf less than $1/T$ cannot be resolved separately: this is sometimes called the **Rayleigh criterion**, though as Figure (3.4) shows, actually seeing two separate peaks requires $\Delta f \geq 2/T$.

Group Delay

Next, we combine the modulation and shift theorems to introduce a property of linear systems known as **group delay**. We start with an amplitude-modulated sinusoid, but make it complex so that we only have one frequency to deal with. The time function and its Fourier transform are

$$x(t)e^{2\pi i f_0 t} \quad \text{and} \quad \tilde{x} * \delta(f - f_0) = \tilde{x}(f - f_0)$$

Now use this function as input to a linear time-invariant system. Assume the frequency response has unit amplitude and phase $e^{2\pi i \phi(f)}$, and approximate the phase in the vicinity of the carrier frequency f_0 by the first two terms of a Taylor series:

$$\phi(f) = \phi(f_0) + \frac{d\phi}{df} f \stackrel{\text{def}}{=} \phi_0 + \phi'_0 f$$

Then the Fourier transform of the output of the system will be, to this level of approximation,

$$e^{2\pi i \phi_0} [\tilde{x}(f - f_0) e^{2\pi i \phi'_0 f}] \quad (3.23)$$

The first of the two exponential terms is just a constant. The part in square brackets, by equation (3.13), has as its inverse transform the original function, shifted in time; taking the inverse transform of the expression in equation (3.23) gives

$$x(t + \phi'_0) e^{2\pi i (f_0 t + \phi_0)}$$

which is to say that the phase of the carrier is shifted by ϕ_0 and the modulating function is shifted in time by an amount depending on the derivative of the phase with frequency (note that this derivative has the dimensions of time). For our

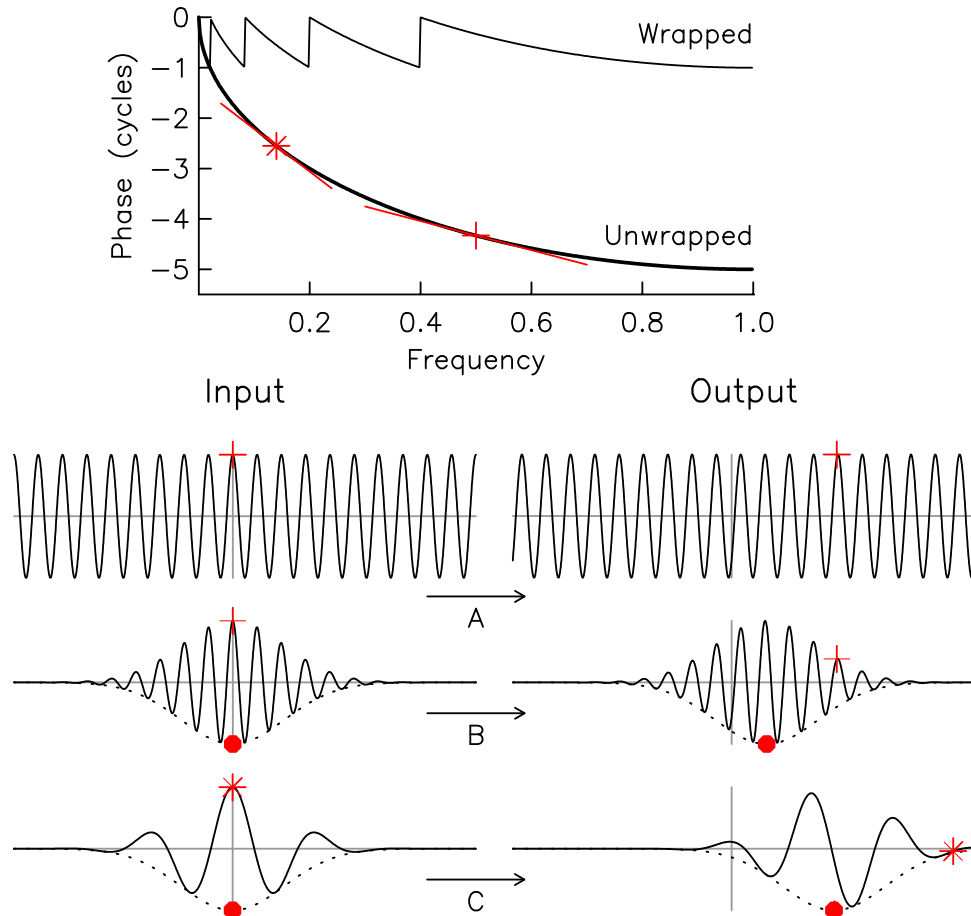


Figure 3.5: Illustration of group and phase delay. At the top is the variation of phase with frequency, shown both over the domain of 0 to 1 cycles, and with the resulting discontinuities removed, or unwrapped. The plus and asterisk show two frequencies, with their derivatives. Plot A shows what happens to a pure sinusoid at the higher frequency, which is a time shift corresponding to the phase change. Plots B and C show the input and output for the same modulating function (a Gaussian, to create a “group” of waves, or **wave packet**, for two different carrier frequencies. In both the plus (or asterisk) show the shift for the carrier, and the solid circle the shift for the group. This group delay, being the derivative of the phase with frequency, is smaller for the higher carrier frequency.

convention that a delay is equivalent to a more negative phase, ϕ' will be negative, causing a delay. This is called the group delay because it is most easily seen when the modulation isolates a particular timespan, creating a group of waves at the carrier frequency. Then the delay applies to the group as a whole, and the phase change ϕ_0 to the carrier. Figure 3.5 shows all this in cartoon form.

3.7.4 Flipping the Convolution

We can modify the convolution integral by not time-reversing one function. This is most useful when we use the same function for both parts; we will call this the flipped convolution of the function with itself.⁷ For a complex-valued x , this operation is defined as giving:

$$C(\tau) = \int_{-\infty}^{\infty} x^*(t)x(t+\tau)dt$$

The location of the conjugate part matters since in general $yz^* = (y^*z)^*$. If we conjugate the other x in the integral, we have get the complex conjugate of C :

$$\int_{-\infty}^{\infty} x(t)x^*(t+\tau)dt = \left(\int_{-\infty}^{\infty} x^*(t)x(t+\tau)dt \right)^* = C^*(\tau)$$

If we change variables we can find a symmetry property of C .

$$C(-\tau) = \int_{-\infty}^{\infty} x^*(t)x(t-\tau)dt = \int_{-\infty}^{\infty} x^*(u+\tau)x(u)du = C^*(\tau)$$

which means that C is Hermitian, meaning that its Fourier transform is always real. If $x(t)$ is real, C will also be, which means that C , and its transform, must then be even. We will encounter these properties, built on a different foundation, when we define the power spectral density in Chapter 11.

3.8 Summary of Theorems

For convenience, Table 3.8 summarizes most of the Fourier theorems we have discussed, giving both a forward- and inverse-transform version.

⁷While cumbersome, this is less confusing than the name in Bracewell (1986), which is **auto-correlation**. The usual autocorrelation (Section 10.2) refers to a different operation and a different scaling. The flipped convolution of the function with itself is more like the **autocovariance** of a random time series.

List of Fourier Theorems

Equation	Function	Transform	Transform	Function
3.4, 3.3	$x(t)$	$\tilde{x}(f)$	$\tilde{x}(f)$	$x(t)$
3.10	$x(at)$	$\frac{\tilde{x}(f/a)}{ a }$	$\tilde{x}(af)$	$\frac{x(t/a)}{ a }$
3.11	$\int_{-\infty}^{\infty} x(t) dt$	$\tilde{x}(0)$	$\int_{-\infty}^{\infty} \tilde{x}(f) df$	$x(0)$
3.13	$x(t - \tau)$	$e^{-2\pi i f \tau} \tilde{x}(f)$	$\tilde{x}(f - f_0)$	$e^{2\pi i f_0 t} x(t)$
3.15	$\frac{dx}{dt}$	$2\pi i f \tilde{x}(f)$	$\frac{d\tilde{x}}{df}$	$-2\pi i t x(t)$
3.20	$x(t) * y(t)$	$\tilde{x}(f)\tilde{y}(f)$	$\tilde{x}(f) * \tilde{y}(f)$	$x(t)y(t)$
3.21	$\int_{-\infty}^{\infty} x(t) ^2 dt$	$\int_{-\infty}^{\infty} \tilde{x}(f) ^2 df$		

Table 3.2: Summary of Fourier theorems: the first two columns are the transform pair, and the second two the inverse transform pair. The last line is Rayleigh's theorem, which is the same for the forward and inverse transform.

CHAPTER 4

THE FOURIER TRANSFORM IN MANY DIMENSIONS

For your Space is not the true Space. True Space is a Plane; but your Space is only a Line.

A SQUARE (EDWIN A. ABBOTT), *Flatland: A Romance of Many Dimensions* (1899).

4.1 Introduction

So far, we have looked at the Fourier transform of functions of a single variable, which we have usually assumed to be time. But the Fourier transform can be generalized to apply to functions of more than one variable; in this chapter we describe these generalizations, and some transforms in one variable that are derived from them. A common application of multidimensional Fourier transforms is to functions defined on a plane (and thus having two arguments) or in space (three arguments). Another use, when one of the arguments is time, and the others are spatial coordinates, is to describe phenomena that vary in time and space, such as diffusive processes and propagating waves.

4.2 The Fourier Transform for Cartesian Coordinates

We begin with two spatial dimensions, the coordinates x_1 and x_2 , and a function $a(x_1, x_2)$. The two-dimensional Fourier transform is

$$\tilde{a}(k_1, k_2) = \int_{-\infty}^{\infty} \int_{-\infty}^{\infty} a(x_1, x_2) e^{-2\pi i(k_1 x_1 + k_2 x_2)} dx_1 dx_2 \quad (4.1)$$

As a matter of convention, we use k (the **wavenumber**) rather than f (the frequency) as the Fourier variable when the argument refers to space; because of two-dimensionality, we have two wavenumbers, k_1 and k_2 . You should again be aware that our normalization of the transform is not universal. Very often the spatial transform is defined without a 2π in the exponent; the wavenumber in that case is just 2π times our wavenumber, just as the angular frequency is 2π times

the frequency we used in equation (3.4). The advantage of our normalization is again that it makes the inverse transform as similar as possible to the forward one:

$$a(x_1, x_2) = \int_{-\infty}^{\infty} \int_{-\infty}^{\infty} \tilde{a}(k_1, k_2) e^{2\pi i(k_1 x_1 + k_2 x_2)} dk_1 dk_2 \quad (4.2)$$

These expressions are easily generalized to N dimensions; we simply take the components x_1, x_2, \dots, x_N to form a vector \mathbf{x} , and the wavenumbers k_1, k_2, \dots, k_N to form another vector \mathbf{k} . Then equations (4.1) and (4.2) become N -dimensional integrals:

$$\tilde{a}(\mathbf{k}) = \int_{\Re^N} a(\mathbf{x}) e^{-2\pi i \mathbf{k} \cdot \mathbf{x}} d\mathbf{x} \quad \text{and} \quad a(\mathbf{x}) = \int_{\Re^N} \tilde{a}(\mathbf{k}) e^{2\pi i \mathbf{k} \cdot \mathbf{x}} d\mathbf{k}$$

where \Re^N means “all of N -dimensional space:” the real line \Re in N directions.

Essentially all the Fourier theorems we have discussed carry over to the multidimensional case; for example, broadening of a function in one coordinate corresponds to narrowing its transform in the corresponding wavenumber. Once again, perhaps the most important result is that the convolution of two functions corresponds to the multiplication of their Fourier transforms. That is, suppose we have two functions a and b ; their convolution is

$$a * b = \int_{-\infty}^{\infty} \int_{-\infty}^{\infty} a(x'_1, x'_2) b(x'_1 - x_1, x'_2 - x_2) dx'_1 dx'_2 \quad (4.3)$$

which gives another function $c(x_1, x_2)$. Then the Fourier transform of this new function, which we denote by $\tilde{c}(\mathbf{k})$, is the product of the Fourier transforms of the original functions:

$$\tilde{c}(k_1, k_2) = \tilde{a}(k_1, k_2) \tilde{b}(k_1, k_2)$$

We can thus apply our methods of looking at linear systems in the frequency domain to things that happen in more than one dimension: the same concepts of frequency response, impulse response, and step response all apply to multidimensional linear systems.

For a non-geophysical example of the usefulness of the frequency response, consider imaging systems such as document scanners. The only specification usually given for these is the number of pixels per inch; you should be able to see that this is no more than a statement of the density of sampling, which only partly describes what the spatial frequency response of the scanner is (Simcoe, 2009). If we want to know what an image will look like after scanning, we need the full frequency response. This particular example also illustrates different behavior for wavenumbers in different directions: the frequency response along the direction that the scanner moves can be quite different from the response perpendicular to that direction.

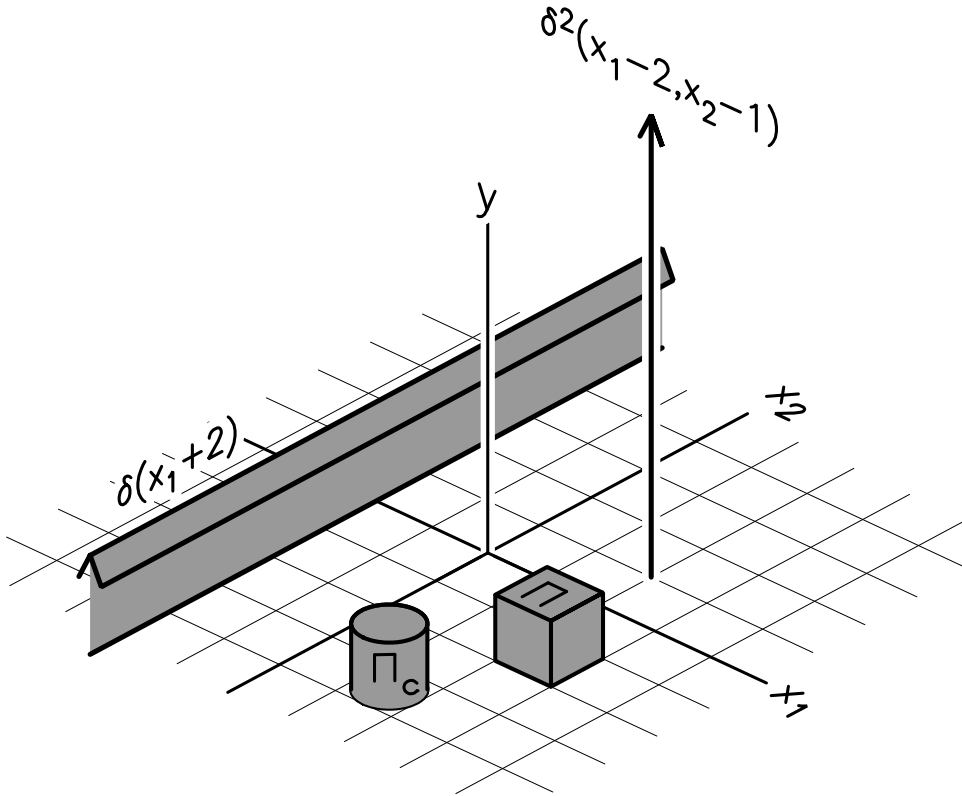


Figure 4.1: Oblique view of the $x_1 - x_2$ plane, showing two kinds of delta functions and boxcar functions. The delta functions are shown with arrowheads to indicate their “infinite” value.

4.2.1 Some Simple Functions and Their Transforms

To make this all a bit more concrete, Figure 4.1 shows a few functions that we can use as building blocks for representing phenomena of interest – though when we do so these will be more used in the \mathbf{k} plane than the \mathbf{x} plane. First of all, there are two types of delta functions. One is a delta function of only one variable, say $\delta(x_1 - x_1^0)$ where x_1^0 is a constant; we can call this a one-dimensional delta function. Such a delta function, being independent of x_2 , can be represented as a “wall”, with the integral of any path crossing it equal to one, no matter what the path is (the integral of a path along the wall is undefined). Note that the important feature of this is that the function has only one argument, which can be any combination of the two variables: $\delta(c_1 x_1 + c_2 x_2)$ defines a wall in some direction other than the axes, while a function such as $\delta(x_2 - f(x_1))$ would give a wall along the path defined by $x_2 = f(x_1)$.

A more obvious extension of the delta function to two dimensions is what we

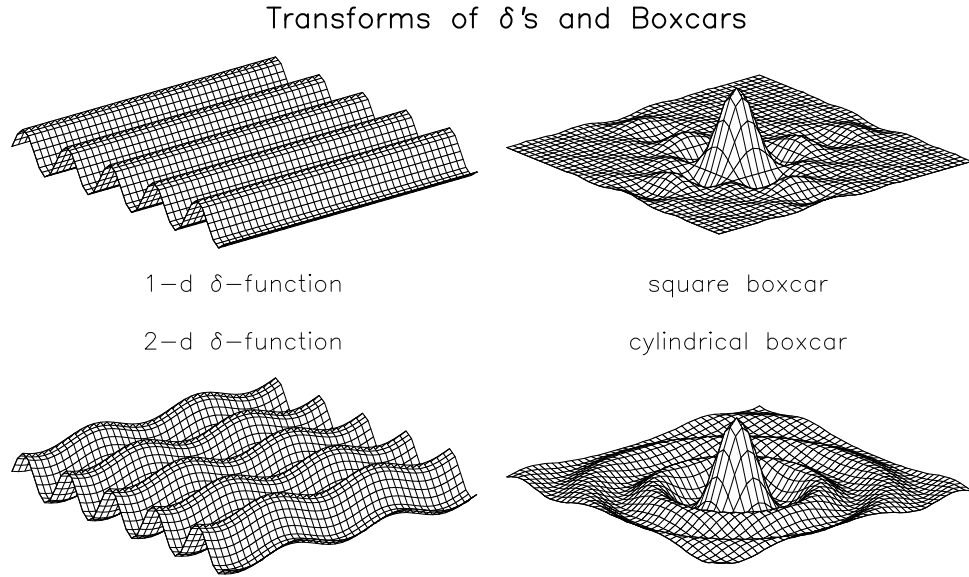


Figure 4.2: Oblique view of the $k_1 - k_2$ plane, showing the transforms of the functions in Figure 4.1.

denote as $\delta^2(x_1, x_2)$: a two-dimensional function. The integral of any path passing through the point where the function is nonzero is equal to one, while if the path does not pass through the point, the integral is zero.

Figure 4.1 also shows a pair of “boxcar” functions, analogous to the one-dimensional one. With two dimensions such a function can come in two forms. The more obvious one is the product of two one-dimensional functions along the two axes, giving a square box; of course we can always scale this to be rectangular, and for that matter rotate it so the edges are not along the two axes. Or, we can define the boxcar to be one out to some distance from its center, giving a cylindrical volume. This function looks the same in any direction, or, more formally, is invariant under rotation of the axes. One way to describe this is to say that the function has **circular symmetry**; another is to say that the function is **isotropic**. Isotropy means that we only need one dimension to describe any function, or transform, so it is often a useful idealization.

4.2.2 The Slice Theorem

Once we move into more than one dimension, there are also some new Fourier theorems. In particular, suppose there is a two-dimensional function $a(x_1, x_2)$, but all we have is its value along a line – say, $a(x_1) = a(x_1, 0)$. How does the Fourier transform of this one-dimensional function relate to $\tilde{a}(k_1, k_2)$? This question is

very relevant to geophysical data analysis, since for high-dimensional phenomena data measured along a line is often all we have.

As usual, we get the answer by writing a in terms of its inverse transform, equation (4.2). If we put $x_2 = 0$ in this expression, we find

$$\begin{aligned} a(x_1) &= \int_{-\infty}^{\infty} \int_{-\infty}^{\infty} \tilde{a}(k_1, k_2) e^{2\pi i k_1 x_1} dk_1 dk_2 \\ &= \int_{-\infty}^{\infty} \left[\int_{-\infty}^{\infty} \tilde{a}(k_1, k_2) dk_2 \right] e^{2\pi i k_1 x_1} dk_1 \\ &= \mathcal{F}^{-1}[\tilde{a}^p(k_1)] \end{aligned} \quad (4.4)$$

so the Fourier transform of a is

$$\tilde{a}^p(k_1) = \mathcal{F}[a(x_1)] = \int_{-\infty}^{\infty} \tilde{a}(k_1, k_2) dk_2$$

which is what we get when we integrate the two-dimensional function \tilde{a} with respect to k_2 only, in effect, collapsing it down onto one axis. This is usually called the **projection** of $\tilde{a}(k_1, k_2)$ onto the k_1 axis, just as $a(x_1, 0)$ is a **slice** through $a(x_1, x_2)$. So equation (4.4) is often called the **projection-slice theorem**, though we shall just use the name **slice theorem**.

4.3 Circular Symmetry: The Hankel Transform

As with the cylindrical boxcar discussed above, a two-dimensional function will sometimes have only one variable as its argument; for example, a function whose value depends only on the distance from a particular point. Putting this point at the origin, we can write the function a in terms of this distance r :

$$a(x_1, x_2) = a\left(\sqrt{x_1^2 + x_2^2}\right) \stackrel{\text{def}}{=} a(r)$$

We can then rewrite the Fourier transform as an integral over r . To see how, we turn the coordinate pairs (x_1, x_2) and (k_1, k_2) into imaginary numbers, which we then express as amplitude and phase: $x_1 + ix_2 = re^{i\theta}$ and $k_1 + ik_2 = \kappa e^{i\phi}$. The product of these two numbers is then:

$$(x_1 + ix_2)(k_1 - ik_2) = (x_1 k_1 + x_2 k_2) + i(x_1 k_2 - x_2 k_1) = r\kappa e^{i\phi - i\theta}$$

so that the product $x_1 k_1 + x_2 k_2$ used in the Fourier transform is the real part of this, or $r\kappa \cos(\phi - \theta)$. The Fourier transform (4.1) is then

$$\begin{aligned} \tilde{a}(\kappa) &= \int_0^{\infty} \int_0^{2\pi} a(r) e^{-2\pi ir\kappa \cos(\theta - \phi)} r dr d\theta \\ &= \int_0^{\infty} a(r) r \left[\int_0^{2\pi} e^{-2\pi ir\kappa \cos(\theta)} d\theta \right] r dr \end{aligned} \quad (4.5)$$

because we can, without loss of generality, set ϕ to zero.

The integral over θ is a known function. An integral relation for Bessel functions of order m is

$$J_m(x) = \frac{i^{-m}}{2\pi} \int_0^{2\pi} e^{im\theta} e^{ix\cos(\theta)} d\theta$$

which means that

$$2\pi J_0(2\pi\kappa r) = \int_0^{2\pi} e^{-2\pi i\kappa r \cos(\theta)} d\theta$$

allowing us to write equation (4.5) as

$$\tilde{a}(\kappa) = 2\pi \int_0^\infty a(r) J_0(2\pi\kappa r) r dr \stackrel{\text{def}}{=} \mathcal{H}[a(r)] \quad (4.6)$$

This is called a **Hankel transform**, and has the inverse:

$$a(r) = 2\pi \int_0^\infty \tilde{a}(\kappa) J_0(2\pi\kappa r) \kappa d\kappa$$

so the forward and inverse transforms have exactly the same form. Figure 4.2 shows the Fourier transform of a cylindrical boxcar: this is just a cylindrically symmetric function derived from the Hankel transform of a boxcar at the origin.

Hankel transforms are very commonly used when dealing with differential equations with circular symmetry, since again differentiation in the original r domain becomes multiplication in the frequency domain:

4.3.1 The Abel Transform

For some kinds of measurements, we may have only the integral along a series of profiles; this is, for example, the case in a CAT scan, in which we measure how much energy is absorbed between a source and a detector. In general we need to have measurements in many directions to reconstruct the original pattern of absorption; but if we can assume this pattern is circularly symmetric, a series of parallel profiles is sufficient. Putting the profiles parallel to the x_2 axis, we have

$$a^p(x_1) = \int_{-\infty}^\infty a(x_1, x_2) dx_2 = 2 \int_0^\infty a(x_1, x_2) dx_2 = 2 \int_{r=x_1}^\infty a(r) dx_2$$

where the single-argument function a inside the integral is the radial dependence of the function. If we now change the variable of integration from $x_2 = \sqrt{r^2 - x_1^2}$ to r , this becomes

$$a^p(x_1) = 2 \int_{x_1}^\infty a(r) \frac{r}{(r^2 - x_1^2)^{0.5}} dr \stackrel{\text{def}}{=} \mathcal{A}[a(r)] \quad (4.7)$$

which was named the **Abel transform** by [Bracewell \(1956\)](#). Since $a^p(x_1)$ is the projection of $a(x_1, x_2)$, equation (4.7) gives us a relationship between the projection

and the radial form of the function. There is an inverse transform that allows us to go from $a^P(x_1)$ to $a(r)$:

$$a(r) = \int_r^\infty \left(\frac{da^P(x)}{dx} \right) \frac{1}{\sqrt{x^2 - r^2}} dx \quad (4.8)$$

so the Abel transform is not at all symmetric.

For a function of one variable, the Fourier, Hankel, and Abel transforms actually form a chain that returns the same function:

$$\mathcal{F}[\mathcal{H}[\mathcal{A}[a(x)]]] = a(x) \quad (4.9)$$

a result we will come to use in Chapter 16, where we will also see why circularly symmetric functions might be useful: a random process that “looks the same” in any direction will have a power spectrum that does not depend on direction – that is, the spectrum will be circularly symmetric.

CHAPTER 5

FOURIER THEORY FOR DISCRETE TIME

All things began in order, so shall they end, and so shall they begin again; according to the ordainer of order and mystical Mathematicks of the City of Heaven.

SIR THOMAS BROWNE, *The Garden of Cyrus* (1658).

5.1 Introduction

We now turn from Fourier theory for functions to the same theory for ordered sets of numbers, or **sequences**: this theory is part of **digital signal processing**. As we will see, much of what has been covered in the Fourier theory discussion will have parallels here – though also significant differences, which come about because the theory of the Fourier transform assumes that the functions being transformed (and the transforms themselves) are defined on the real line (or a higher-dimensional equivalent). One term for this is that these functions are defined “in continuous time”. However, digital signals are collections of numbers, representing (usually) a continuous time signal sampled at regular intervals. Such functions are called **sampled data**¹ and are said to be defined in **discrete time**.

We begin by describing how Fourier theory is applied to two kinds of sequences:

- A discrete-time sequence defined, like that in continuous time, over an infinite range, so the sequence “goes on forever.” The Fourier transform of such a sequence turns out to be a function on the real line; but unlike the Fourier transform of a function, which is another function, the transform of an infinite sequence is a function defined on only a part of the real line. An infinite discrete-time series and its transform are very different.
- A discrete-time sequence defined over a finite range, which is what any actual time-series data is. We could treat this as an infinite series most of

¹In statistics, this terminology is commonly used for the act of getting data on a subset of some population, ideally without biasing the results of an statistical investigation. We will not deal with this topic.

which is zero, and sometimes this is useful, but more commonly we use a Fourier transform for this that produces another finite-length sequence, at discrete frequencies just as the untransformed series is at discrete times. Then, as with functions on the real line, a function and its transform are the same kind of thing.

This Fourier transform of one finite sequence into another is called (what else?) the **Discrete Fourier Transform** or **DFT**. In this chapter we describe some of the properties of the DFT, and describe ways used to compute it efficiently (the details of this are in Appendix F). In Chapter 6 we will use the theory for the DFT to discuss how to go from continuous time to discrete time without losing information, while Chapters 7 and 8 discuss some operations commonly done with discrete-time series, viewed in both the time and frequency domains.

5.2 Discrete-Time Sequences and Operations

In discrete time there are only sequences of numbers; we denote such a sequence, as a whole, by $\{x_n\}$, using $x(n)$ or x_n for the individual terms; n is always an integer-valued index. To start with we assume that we have an infinitely long sequence with n running from $-\infty$ to ∞ .

We aim for as many parallels with the continuous-time case as possible. Some things are much simpler in discrete time. For example, the distinction between generalized functions and other functions disappears: all are just sequences. The delta function is just another sequence:

$$\{\delta_n\} = \delta_{n0} = \begin{cases} 1 & n = 0 \\ 0 & n \neq 0 \end{cases} \quad (5.1)$$

where δ_{ij} is the Kronecker delta symbol. The discrete-time version of the Heaviside step function is

$$\{H_n\} = \begin{cases} 1 & n > 0 \\ 0 & n \leq 0 \end{cases}$$

so that

$$H_n = \sum_{k=-\infty}^n \delta_{k0}$$

In discrete time summation replaces integration, and we face none of the difficulties in making things rigorous that we should (but didn't) consider when dealing with functions on the real line.

Likewise, convolution is a summation rather than an integral; the convolution of two sequences (also called the **serial product**) is still written as $z = x * y$, but this now denotes

$$z_n = \sum_{k=-\infty}^{\infty} x_k y_{n-k} \quad (5.2)$$

Again, one series is reversed. This definition satisfies the requirements for convolution of being linear in x and y , and also invariant with shifts in time (here represented by sequence number); if we shift x by m terms, the convolution $x * y$ is

$$\sum_{k=-\infty}^{\infty} x_{k-m} y_{n-k} = \sum_{l=-\infty}^{\infty} x_l y_{n-m-l} = z_{n-m}$$

so z is also shifted. Note the changes of variables in the subscripts: most proofs involving discrete time make use of this.

Convolution is just as important in discrete time as in continuous time; indeed, some types of sequences are characterized by what they do in convolution. One example is that a sequence $\{g_k\}$ is **causal** if and only if $g_k = 0$ for $k < 0$; this means that if $\{x_k\}$ is causal, $g * x$ will also be: the output will not precede the input. If you are processing data in real time, or trying to emulate a system that is causal (such as an instrument, or wave propagation) only causal operations are possible; otherwise, as in data being analyzed after they are collected, causality is less important.

5.3 Fourier Transforms for Infinite Sequences

We started our discussion of Fourier theory by looking at what linear systems do to sinusoids; similarly, we will develop Fourier transforms for infinite sequences by considering the convolution of a sinusoidal sequence with the sequence of interest. In continuous time we saw that a sinusoid input into a linear system produced an output sinusoid of the same frequency, scaled by a function (the frequency response) that is the Fourier transform of the convolving function.

The same thing holds in discrete time; if we convolve $x_n = e^{2\pi i \zeta n}$ with g_n , we get, starting by commuting the series,

$$\sum_{k=-\infty}^{\infty} g_k x_{n-k} = \sum_{k=-\infty}^{\infty} g_k e^{2\pi i \zeta(n-k)} = e^{2\pi i \zeta n} \sum_{k=-\infty}^{\infty} g_k e^{-2\pi i \zeta k} \stackrel{\text{def}}{=} \tilde{g}(\zeta) e^{2\pi i \zeta n}$$

$\tilde{g}(\zeta)$ is again the frequency response, and regarding it as the Fourier transform of the sequence $\{g_k\}$ gives the definition for the Fourier transform of an infinite sequence $\{x_n\}$

$$\tilde{x}(\zeta) = \sum_{k=-\infty}^{\infty} x_k e^{-2\pi i \zeta k} \tag{5.3}$$

For this derivation we have used the variable ζ to represent a nondimensional frequency, just as in Section 2.2 we introduced u for nondimensional time. We treat the discrete sequence with each term labeled by an integer, making a dimensionless interval.

One way to create a sequence is to consider it to come from sampling a continuous-time function. We introduce the **sampled-data function** $x_s(u)$, defined by

$$x_s(u) = \sum_{k=-\infty}^{\infty} \delta(u - k)x(u) \quad (5.4)$$

While this generalized function is defined in continuous time, it is like a sequence because it contains information about the value of $x(u)$ only at integer values of u . Just as a single delta function samples x at a single time, an infinite array of them samples x at the times of the sequence $x_n = x(n)$. So the interval between samples is, like the interval between integers, unity and dimensionless. In Chapter 6 we will consider the interval between terms to have some dimension (time or length), and an arbitrary value.

If we take the continuous-time Fourier transform of the sampled-data function we obtain

$$\mathcal{F}[x_s(u)] = \int_{-\infty}^{\infty} \sum_{k=-\infty}^{\infty} \delta(u - k)x(u)e^{-2\pi i \zeta u} du = \sum_{k=-\infty}^{\infty} x(k)e^{-2\pi i \zeta k}$$

which is identical to our definition of the Fourier transform for an infinite sequence, equation (5.3).

The transform $\tilde{x}(\zeta)$ is a function of ζ , that is, a function on the real line; but it is a function that is periodic with period one:

$$\tilde{x}(\zeta + m) = \sum_{k=-\infty}^{\infty} x_k e^{-2\pi i \zeta k} e^{-2\pi i m k} = \tilde{x}(\zeta) \quad \text{for } m \text{ an integer}$$

which means that knowing $\tilde{x}(\zeta)$ only over $[-\frac{1}{2}, \frac{1}{2}]$ is sufficient. We will use this finite range from here on. (If we used, as some authors do, $\omega = 2\pi\zeta$, the interval would be $[-\pi, \pi]$.) When we discuss sampling in Chapter 6, we will see that these limits are the nondimensional version of the **Nyquist frequency**.

Equation (5.3) has exactly the form of the Fourier series expression, equation (2.23), with time and frequency swapped and with the opposite sign for the exponential. Both express a periodic function on the real line as the sum of a sequence of numbers times a complex exponential. So we can use equation (2.24), which gives the coefficients in terms of the function, to get the inverse transform that produces the sequence from integrals involving the transform function $\tilde{x}(\zeta)$:

$$x_k = \int_{-\frac{1}{2}}^{\frac{1}{2}} \tilde{x}(\zeta) e^{2\pi i \zeta k} d\zeta \quad (5.5)$$

Equations (5.3) and (5.5) are another Fourier transform pair, but with very different expressions for the transforms: one is an infinite sum and the other a definite integral. In the same way, we can regard the expressions for the Fourier

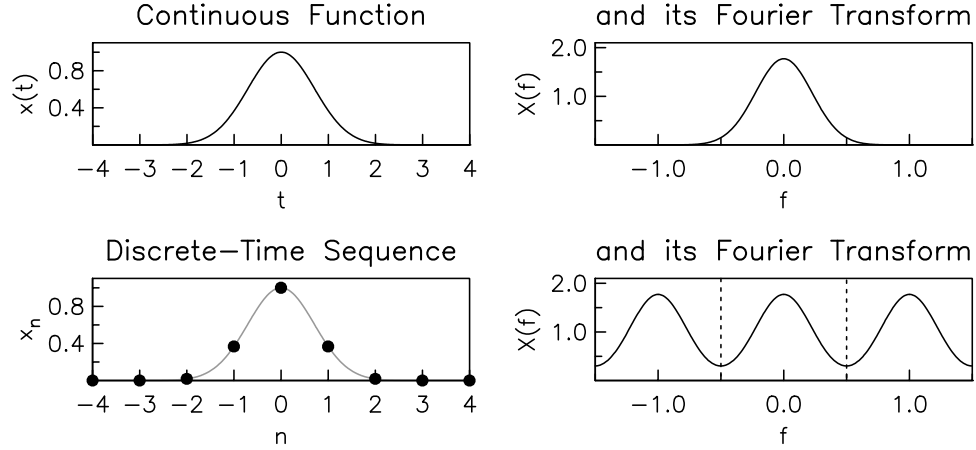


Figure 5.1: An example of the relationships between a function, a discrete-time sequence related to it, and their Fourier transforms. The function (top left) is a Gaussian, e^{-x^2} ; its Fourier transform is shown top right. The bottom left panel shows part of a discrete-time sequence that matches this (with the original function in gray). The bottom right shows the Fourier transform of the sequence; the region of f between the two dashed lines is sufficient to describe it. Note that the transform of the sequence is close to the Fourier transform of the function, except near these two lines – the effect of aliasing, which we will discuss in Chapter 6.

series and its coefficients as a transform pair between a periodic function of time, and a sequence of coefficients in frequency.

Many of the Fourier-transform theorems from Chapter 3 carry over to this new transform pair, converting to discrete time by changing integrals into sums. Looking at Table 3.8, equations (3.10) and (3.15) do not have discrete-time analogs since we can neither rescale the spacing of a sequence nor take its derivative.

But there is an analog for equation (3.11); from the forward and inverse transforms

$$\sum_{n=-\infty}^{\infty} x_n = \tilde{x}(0) \quad \text{and} \quad \int_{-1/2}^{1/2} \tilde{x}(\zeta) d\zeta = x_0 \quad (5.6)$$

and likewise the analog of equation (3.13) is

$$\mathcal{F}\{x_{n-m}\} = \tilde{x}(\zeta) e^{-2\pi i m \zeta} \quad (5.7)$$

For Rayleigh's theorem, equation (3.21), we represent the series and its complex conjugate as inverse Fourier transforms; for the complex conjugate:

$$x_k^* = \int_{-1/2}^{1/2} \tilde{x}^*(\zeta) e^{-2\pi i \zeta k} d\zeta$$

which means that

$$\begin{aligned} \sum_{n=-\infty}^{\infty} |x_n|^2 &= \sum_{n=-\infty}^{\infty} x_n x_n^* = \sum_{n=-\infty}^{\infty} x_n \int_{-1/2}^{1/2} \tilde{x}^*(\zeta) e^{-2\pi i \zeta n} d\zeta \\ &= \int_{-1/2}^{1/2} \tilde{x}^*(\zeta) \sum_{n=-\infty}^{\infty} x_n e^{-2\pi i \zeta n} d\zeta = \int_{-1/2}^{1/2} \tilde{x}^*(\zeta) \tilde{x}(\zeta) d\zeta = \int_{-1/2}^{1/2} |\tilde{x}(\zeta)|^2 d\zeta \end{aligned}$$

The convolution theorem, equation (3.20), uses sums rather than integrals: a sequence $\{z\}$ that is a convolution $\{x\} * \{y\}$ has the transform:

$$\begin{aligned} \tilde{z}(\zeta) &= \sum_{k=-\infty}^{\infty} z_k e^{-2\pi i \zeta k} = \sum_{k=-\infty}^{\infty} \sum_{l=-\infty}^{\infty} x_l y_{k-l} e^{-2\pi i \zeta k} \\ &= \sum_{l=-\infty}^{\infty} x_l \sum_{k=-\infty}^{\infty} y_{k-l} e^{-2\pi i \zeta k} = \sum_{l=-\infty}^{\infty} x_l e^{-2\pi i \zeta l} \sum_{k=-\infty}^{\infty} y_{k-l} e^{-2\pi i \zeta (k-l)} \\ &= \sum_{l=-\infty}^{\infty} x_l e^{-2\pi i \zeta l} \sum_{m=-\infty}^{\infty} y_m e^{-2\pi i \zeta m} = \tilde{x}(\zeta) \tilde{y}(\zeta) \end{aligned}$$

5.4 The Dirichlet, Fejér, and Other Kernels

We next consider the Fourier transform of the discrete-time versions of the functions we examined in Section 3.2. We start with a sequence that has the form of the rectangle (or boxcar) function; its transform is then the analog of $\text{sinc}(f)$, and is called the **Dirichlet kernel**. This gets a separate section because it plays a fundamental role in many topics in Fourier analysis and signal processing, and will serve as a bridge to the finite series we will encounter in Section 5.5.

The discrete-time version of equation (3.6) is

$$\Pi_n = \begin{cases} 1 & |n| \leq M \\ 0 & |n| > M \end{cases} \quad (5.8)$$

so that $2M + 1$ terms are nonzero. Its transform, by equation (5.3), is then the finite sum

$$\sum_{n=-M}^M e^{-2\pi i \zeta n} = e^{\pi i \zeta M} \sum_{n=0}^{2M} e^{-2\pi i \zeta n} \quad (5.9)$$

To find a closed-form expression for this, we first note that, for any variable y and number of terms N , we can write

$$\sum_{n=0}^{N-1} y^n = (1 - y^N) \sum_{n=0}^{\infty} y^n \quad \text{whence} \quad \frac{1}{(1-y)} = \sum_{n=0}^{\infty} y^n$$

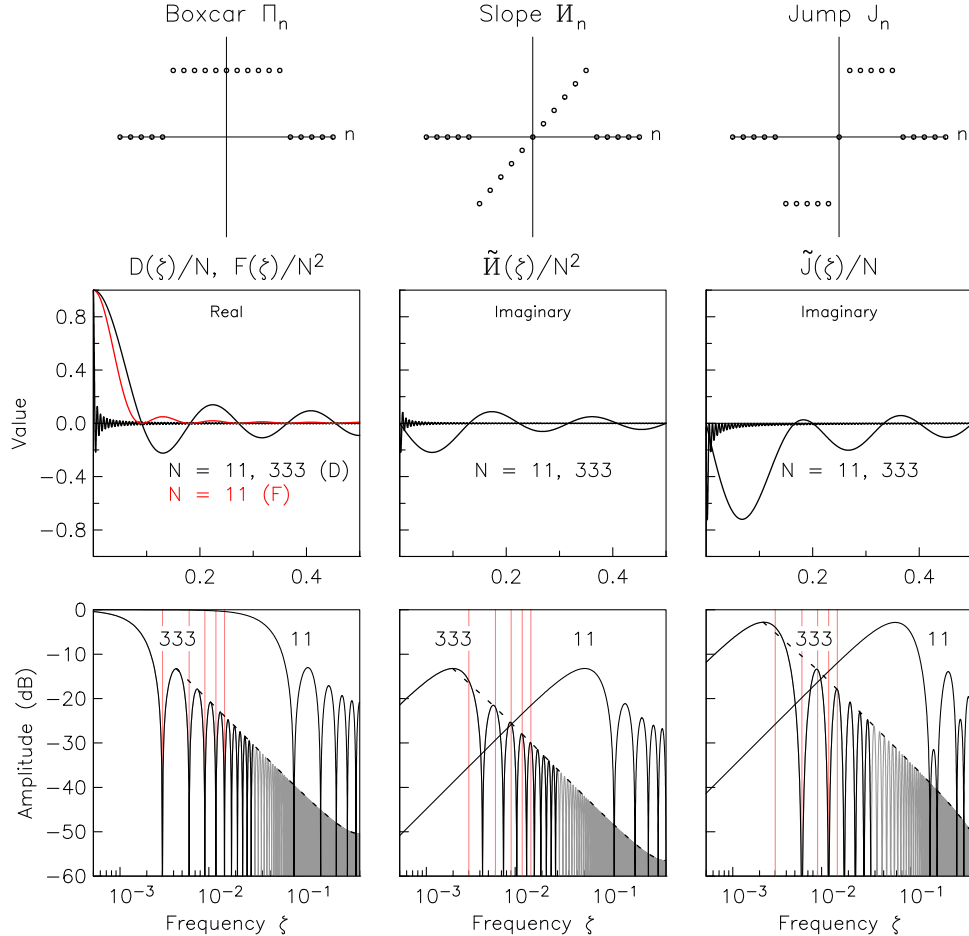


Figure 5.2: Three time-limited sequences and their Fourier transforms. The top three panels show the sequences for $N = 11$; the middle and bottom panels show the normalized transforms for $N = 11$ and $N = 333$. In the log-frequency plots of the amplitude at the bottom, as with those in Figure 3.1, a dashed line shows the falloff of amplitude with frequency, and the higher-frequency parts of the response are shown in gray. The vertical red lines in the bottom plots show the DFT frequencies $\zeta = l/N$ for l from one to five. For the boxcar sequence, the middle panel also shows the normalized Fejér kernel for $N = 11$. The bottom panel plot does not show the Fejér kernel because, being associated with power, it would be plotted as $10\log_{10}$ in dB, exactly matching the Dirichlet kernel, taken as amplitude and so plotted as $20\log_{10}$ in dB.

where the first expression can be verified through term-by-term expansion, and setting $L = 1$ in it gives the second. Combining these gives the closed-form expression for a finite sum of powers of y :

$$\sum_{n=0}^{N-1} y^n = \frac{1-y^N}{1-y} = \frac{y^{N/2} [y^{-N/2} - y^{N/2}]}{y^{1/2} [y^{-1/2} - y^{1/2}]} = y^{(N-1)/2} \frac{y^{-N/2} - y^{N/2}}{y^{-1/2} - y^{1/2}}$$

which for $y = e^{-2\pi i \zeta}$ gives

$$\sum_{n=0}^{N-1} e^{-2\pi i \zeta n} = e^{-\pi i (N-1)\zeta} \left(\frac{e^{\pi i N \zeta} - e^{-\pi i N \zeta}}{e^{-\pi i \zeta} - e^{-\pi i \zeta}} \right) = e^{-\pi i (N-1)\zeta} \left(\frac{\sin \pi N \zeta}{\sin \pi i \zeta} \right) \quad (5.10)$$

which when applied to equation (5.9) gives

$$\begin{aligned} \sum_{n=-M}^M e^{-2\pi i \zeta n} &= e^{i\pi M \zeta} e^{-i\pi M \zeta} \left(\frac{e^{\pi i \zeta (2M+1)} - e^{-\pi i \zeta (2M+1)}}{e^{\pi i \zeta} - e^{-\pi i \zeta}} \right) \\ &= \frac{\sin \pi (2M+1) \zeta}{\sin \pi \zeta} = \frac{\sin \pi N \zeta}{\sin \pi \zeta} \stackrel{\text{def}}{=} D_N(\zeta) \end{aligned} \quad (5.11)$$

This is the Dirichlet kernel for a total length N equal to $2M+1$. As with the sinc function, the value of $D_N(0) = N$ is found by taking a limit. Note that by equation (5.6), the total area under all the lobes is invariant because x_0 is. As N goes to infinity, the sidelobes become smaller and smaller, and $D_N(\zeta)$ approaches $\delta(\zeta)$. For plotting, we use $D_N(\zeta)/N$, the Fourier transform of a sequence in which all the nonzero values are N^{-1} , since then $D_N(0)/N = 1$. The zeroes of $D_N(\zeta)$ kernel are at $\zeta = \pm l/N$, with $|l|$ ranging from 1 through $N/2$. The first sidelobe peak, which is close to $\zeta = \pm 2N$, is about $-N/5$, the next extremum is about $N/7$. Away from zero $D_N(\zeta)$ thus decays rather slowly with increasing ζ .

To see the connection between the Dirichlet kernel and the sinc function, put $f = N\zeta$ and let N go to infinity while keeping f fixed: this is analogous to finer and finer sampling. Then $D_N(\zeta)/N$ behaves like

$$\frac{\sin \pi f}{N \sin \pi f / N} \rightarrow \frac{\sin \pi f}{\pi f} = \text{sinc}(f)$$

If we square the Dirichelet kernel we obtain the **Fejér kernel**:

$$F_N(\zeta) = \frac{\sin^2 \pi N \zeta}{\sin^2 \pi \zeta} \quad (5.12)$$

so that, like the Dirichlet kernel, $F_N(\zeta)$ approaches $\delta(\zeta)$ as N goes to infinity. For plotting, we use $F_N(\zeta)/N^2$, which is one at $\zeta = 0$. $F_N(\zeta)$ decays much more rapidly away from zero than $D_N(\zeta)$ does.

By the convolution theorem, the Fejér kernel is the transform of an N -length sequence with $x_n = 1$, convolved with itself:

$$F_n = \begin{cases} N - |n| & |n| \leq 2M = N - 1 \\ 0 & |n| \geq N \end{cases} \quad (5.13)$$

which is a triangle sequence with $x_0 = N = 2M + 1$.

In Section 3.2 we introduced two additional time-limited functions $I(t)$ and $J(t)$, expressing different behaviors (a slope and a jump) and both orthogonal to the boxcar. Similarly to what we have just done to produce the Dirichelet kernel, we introduce the two sequences I_n and J_n , each of which is nonzero for $-M \leq n \leq M$. In this range $I_n = n$ and $J_n = \text{sgn}(n)$, with $J_0 = 0$. The Fourier transforms of these sequences can be shown to be

$$\tilde{I}(\zeta) = -\left(\frac{i}{2}\right)\left(\frac{\sin \pi N \zeta \cos \pi \zeta - N \cos \pi N \zeta \sin \pi \zeta}{\sin^2 \pi \zeta}\right) \quad (5.14)$$

and

$$\tilde{J}(\zeta) = i\left(\frac{\cos \pi N \zeta - \cos \pi \zeta}{\sin \pi \zeta}\right) = 2i\left(\frac{\sin^2 \pi \zeta / 2 - \sin^2 N \pi \zeta / 2}{\sin \pi \zeta}\right) \quad (5.15)$$

which are purely imaginary because these are both odd functions.

As with the Dirichelet kernel and the sinc function, if $\zeta = f/N$ and we allow N to go to infinity, $\tilde{I}(\zeta)/N^2 \rightarrow \tilde{I}(f)$ and $\tilde{J}(\zeta)/N \rightarrow \tilde{J}(f)$, the functions of f defined by equations (3.8) and (3.9). So these (and the Dirichelet kernel) decay as ζ^{-1} over part of the frequency band, though the peak amplitudes flatten out close to $\zeta = \frac{1}{2}$. We will encounter $\tilde{I}(\zeta)$ again in Section 9.3 and 14.1 and $\tilde{J}(\zeta)$ again in Appendix ??.

5.5 Discrete Fourier Transform

We next consider a finite sequence $\{x_n\}$, with N terms $x_0, x_1 \dots x_{N-1}$. Since this finite sequence is identical to an infinite sequence with nonzero values only for $0 \leq n \leq N - 1$, the forward and inverse transforms defined by equations (5.3) and (5.5) remain valid. We can always use equation (5.3) to get the Fourier transform of $\{x_n\}$, which is $\tilde{x}(\zeta)$ for frequencies with $|\zeta| < \frac{1}{2}$.

But equations (5.3) and (5.5) are a transform pair between a finite sequence and a function. We instead want a transform pair which connects two finite sequences: in the time domain, $\{x_n\}$, and in the frequency domain $\tilde{x}(\zeta)$ for a finite set of frequencies that sample the function $\tilde{x}(\zeta)$. The question is how to choose the set of frequencies.

Our path to this choice will start with the general problem of fitting sinusoids to a finite sequence. We can represent such a fit as a sum of complex sinusoids plus a residual:

$$x_n = \sum_{l=0}^{L-1} C_l e^{2\pi i n \zeta_l} + \epsilon_n \quad n = 0, \dots, N-1$$

with the frequencies $\zeta_0, \zeta_1 \dots$ being specified somehow. If we have N complex exponentials we can fit the data exactly (and we will end up doing so), but for fewer exponentials we would try to choose the coefficients C_l to minimize the sum of squares of the residuals, $\sum_{n=0}^{N-1} |c_n|^2$. This is a least-squares fit; to show how this is found we first put the expressions in matrix-algebra form. The sequences become vectors of length N (for the sequence) and L (for exponentials and hence their coefficients $\{C\}$):

$$\{x^T\} = (x_0, x_1 \dots x_{N-1}) \quad \{C^T\} = (C_0, C_1 \dots C_{L-1})$$

and the exponentials (in l and n) become a $N \times L$ matrix A , which is most easily written in terms of its adjoint (the complex conjugate of the transpose) A^\dagger :

$$A^\dagger = \begin{pmatrix} 1 & e^{-2\pi i \zeta_0} & e^{-4\pi i \zeta_0} & \dots & e^{-2\pi i (N-1) \zeta_0} \\ 1 & e^{-2\pi i \zeta_1} & e^{-4\pi i \zeta_1} & \dots & e^{-2\pi i (N-1) \zeta_1} \\ \dots & \dots & \dots & \dots & \dots \\ 1 & e^{-2\pi i \zeta_{L-1}} & e^{-4\pi i \zeta_{L-1}} & \dots & e^{-2\pi i (N-1) \zeta_{L-1}} \end{pmatrix}$$

Then the standard least-squares solution is that the sum of squares of the residual is minimized if the coefficients C satisfy the expression

$$(A^\dagger A)C = A^\dagger x \quad \text{or} \quad BC = A^\dagger x$$

which is usually called the normal equations; B is an $L \times L$ matrix with elements

$$B_{pq} = \sum_{n=0}^{N-1} e^{-2\pi i n \zeta_p} \left(e^{-2\pi i n \zeta_q} \right)^* = \sum_{n=0}^{N-1} e^{-2\pi i n (\zeta_p - \zeta_q)} \quad (5.16)$$

and C is then

$$C = B^{-1}(A^\dagger x)$$

In a general least-squares problem solving for C will involve inverting B , which is an $L \times L$ matrix: a good-sized computational task if L is large.

However, we can simplify the B matrix of equation (5.16). First, we note that by applying equation (5.10) to equation (5.16), we can write the elements of B in closed form:

$$B_{pq} = e^{-i\pi(N-1)(\zeta_p - \zeta_q)} \frac{\sin \pi N(\zeta_p - \zeta_q)}{\sin \pi(\zeta_p - \zeta_q)}$$

Next, we choose the set of equispaced frequencies with the same number of terms as the sequence:

$$\zeta_l = \frac{l}{N} \quad l = 0, 1, \dots, N-1 \quad (5.17)$$

in which case the matrix elements become

$$B_{pq} = e^{-i\pi(N-1)(p-q)/N} \frac{\sin \pi(p-q)}{\sin(\pi(p-q)/N)} = \begin{cases} N & p = q \\ 0 & p \neq q \end{cases} = N \delta_{pq} \quad (5.18)$$

where we get the result for $p = q$ by treating p and q as real variables and taking the limit as $p \rightarrow q$. This relationship, as given, is only true if the integers p and q are in the range from 0 through $N - 1$, but this is exactly the range for the matrix elements. A more general expression can be gotten by setting $\zeta = l/N$ in equation (5.10) with l being any integer:

$$\sum_{n=0}^{N-1} e^{-2\pi i ln/N} = e^{-i\pi l(N-1)/N} \frac{\sin \pi l}{\sin(\pi l/N)} = \begin{cases} N & l = kN \\ 0 & \text{otherwise} \end{cases} \quad (5.19)$$

for k any integer (that is, $l = 0, \pm N, \pm 2N \dots$). We will use this result in several derivations below.

Equation (5.18) means that for this set of frequencies $B = NI$, where I is the identity matrix: so the inverse B^{-1} is just $N^{-1}I$, which means that the coefficients for our fit are

$$C = \frac{1}{N} A^\dagger x$$

which we can write out explicitly as

$$C_l = \frac{1}{N} \sum_{n=0}^{N-1} x_n e^{-2\pi i n(l/N)}$$

It is important to realize that getting B to be the identity matrix has required two conditions and a mathematical result. The first condition is that an increment in sequence number is a constant increment in the fitting function, and the second is that we choose our frequencies according to equation (5.17). Given these specifications, we can use the result that the imaginary exponentials are orthogonal in summation over the finite interval. When we discuss sampling in Chapter 6 we will assume samples equispaced in time because otherwise we lose orthogonality in the fitting functions.

We now define the **Discrete Fourier Transform (DFT)** as our fit, though with a different normalization:

$$\tilde{x}_k = \sum_{n=0}^{N-1} x_n e^{-2\pi i nk/N} \quad k = 0, \dots, N-1 \quad (5.20)$$

If we compare this expression with the definition of the Fourier transform of an infinite sequence (5.3), we see that

$$\tilde{x}_k = \tilde{x}(\zeta) \quad \text{for } \zeta = \frac{k}{N} \text{ with } k = 0, 1, \dots, N-1$$

so the DFT coefficients are, as we said above, samples of the continuous-frequency transform.

The inverse transform is

$$\frac{1}{N} \sum_{k=0}^{N-1} \tilde{x}_k e^{2\pi i nk/N} \quad (5.21)$$

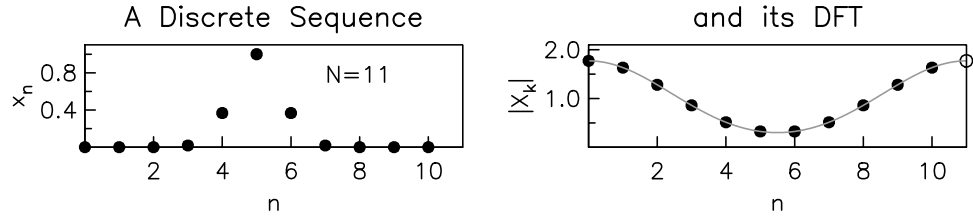


Figure 5.3: An example of a DFT pair, using a finite length of the same discrete-time sequence shown in Figure 5.1. The right side shows the DFT values (filled circles), with the gray line being the Fourier Transform of the infinite sequence; in this case these look the same because the infinite sequence is very small outside the range shown. The unfilled circle is an “extra” DFT point to show the periodicity of the DFT.

We show that this is the inverse transform by writing

$$\begin{aligned} \frac{1}{N} \sum_{k=0}^{N-1} \sum_{m=0}^{N-1} x_m e^{2\pi i (nk - mk)/N} &= \frac{1}{N} \sum_{k=0}^{N-1} \sum_{m=0}^{N-1} x_m e^{2\pi i k(n-m)/N} \\ &= \frac{1}{N} \sum_{m=0}^{N-1} x_m N \delta_{nm} = x_n \end{aligned}$$

where the next-to-last step makes use of the orthogonality relationship (5.19). So we now have a transform pair between finite-length sequences: the DFT (equation 5.20) and inverse DFT (equation 5.21).

5.6 Fourier Theorems for the DFT

While the DFT and inverse DFT are completely consistent, there are notable pitfalls in using them, mostly arising from trying to apply results in continuous and infinite time that do not carry over into the world of finite-length sequences. The basic confusion lies in supposing that our finite sequence is just a part of a longer sequence, so that we can apply continuous-time (and infinite-range) Fourier theory simply by multiplying the series by a function that is zero over most of the range, and one over some part of it. Such multiplication by a function that is nonzero only over some range is called **windowing**. It is tempting to take the view that the DFT of a finite sequence is the Fourier transform of a windowed version of an infinite series; after all, the data we analyze are usually obtained from a longer series in just this way. However, this view is *wrong*. Once we take the DFT, the process of getting the data ceases to matter: we have to regard them as a finite sequence, not part of some longer one, and use the mathematics appropriate to such sequences.

As an introductory example, suppose we compute the value of the inverse DFT of the DFT of a sequence for term numbers outside the original range from 0 to $N-1$. If we do this for the Fourier transform (equation 3.4) of a windowed function, we of course get the original function back; having been windowed, it is indeed zero except over a limited range. But this is not what happens for the DFT. From the definitions of the transforms, we can write the “recovered” series $\{x^{rec}\}$ as

$$x_n^{rec} = \sum_{m=0}^{N-1} x_m \left[\frac{1}{N} \sum_{k=0}^{N-1} e^{2\pi i k(n-m)/N} \right] \quad (5.22)$$

By equation (5.19) the part in square brackets is equal to one for $n - m$ a multiple of N , say jN where j is any integer; otherwise it is zero. Rewriting $n - m = jN$ as $n = m + jN$ gives us a relationship between n and m ; the usual way to express this is to say that “ n equals m , modulo N ”, which is written algebraically as

$$m = n \bmod N$$

Thus, the sum over k in 5.22 reduces to a single nonzero term, giving us the result

$$x_n^{rec} = x_{n \bmod N}$$

In this expression n can be any integer, but $n \bmod N$ ranges only from 0 through $N-1$, which is just the range over which we actually know the original sequence. The infinite sequence we have thus “recovered,” and which is in some sense equivalent to the finite sequence, is therefore the finite sequence replicated over and over. Because it is periodic, the extended function contains no information not in the original sequence – after all, how could it?. If we want to apply our earlier Fourier theory to an infinite sequence, it has to be to one that is periodic, not to a finite sequence surrounded by zeros on both ends.

A finite periodic sequence that is just a sinusoid ($x_n = e^{2\pi i \zeta_0 n}$, with ζ_0 real) provides another example of why finite sequences should not be viewed as part of an infinite sequence. The DFT of the finite sequence is

$$\tilde{x}_k = \sum_{n=0}^{N-1} e^{2\pi i n(\zeta_0 - k/N)} \quad k = 0 \dots N-1$$

If, but only if, $\zeta_0 = l/N$, with l an integer, we get

$$\tilde{x}_k = \begin{cases} N & k = l \\ 0 & k \neq l \end{cases}$$

so that the DFT of this finite sequence can be a discrete-frequency delta function, with only one nonzero value. But in continuous time we get a delta function as the

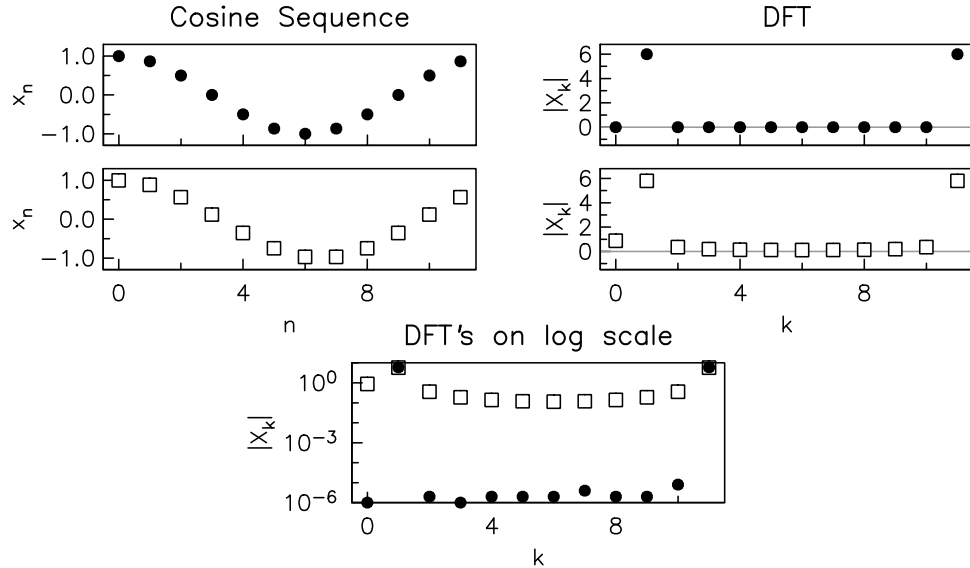


Figure 5.4: The top two pairs of plots show a 12-point sequence and its DFT, where the sequence is $x_n = \cos(2\pi\zeta n)$, with $\zeta = \frac{1}{6}$ in the top left plot and $\zeta = \frac{1}{6.5}$ in the middle left plot. These look almost identical, but compare the trough around $n = 6$. For each sequence the right-hand plot shows the amplitudes of the DFT for each sequence. Especially when plotted on a log scale (lowest plot), a very large difference is apparent. The DFT for a cosine with an integral number of cycles, is a delta sequence with roundoff error; the DFT when the number of cycles is not an integer has nonzero values between the two peaks.

transform only if the time series is an infinitely long sinusoid; the transform of a section of a windowed sinusoid is

$$\mathcal{F}[e^{2\pi i f_0 t} \Pi(t/T)] = T\delta(f - f_0) * \text{sinc}(fT) = T\text{sinc}[(f - f_0)T]$$

which is not a delta function for any choice of f_0 .

This fits with the concept of replicating the sequence over an infinite interval: $\zeta_0 = l/N$ means that exactly l cycles occur over the finite segment, and repeating the function then gives an infinite, untruncated sinusoid – with a delta function transform. But if $\zeta_0 = l/N$, the replicas of the sequence do not join smoothly, so the Fourier transform is not a delta function – and neither is the DFT. Figure 5.4 shows an example.

5.6.1 Shift Theorem

We next consider some theorems for the DFT: in this case, it is more useful to ask for the effect in the time domain (that is, the original sequence) of some operation

carried out in the frequency domain on the DFT sequence $\{\tilde{x}_n\}$. For conventional Fourier transforms, the shift theorem states that, if we take the Fourier transform of a function $x(t)$ shifted by an amount τ , we get, as stated in equation (3.13)

$$\begin{aligned}\mathcal{F}[x(t - \tau)] &= \int_{-\infty}^{\infty} x(t - \tau) e^{-2\pi i f t} dt = \int_{-\infty}^{\infty} x(t') e^{-2\pi i f (t' + \tau)} dt' \\ &= \tilde{x}(f) e^{-2\pi i f \tau}\end{aligned}$$

and so if we multiplied a Fourier transform $\tilde{x}(f)$ by $e^{-2\pi i f \tau}$, and took the inverse transform, we would get $x(t - \tau)$.

Now consider the parallel case for finite sequences. Call the DFT of $\{x_n\}$, $\{\tilde{x}_k\}$; and form $\tilde{x}_k e^{2\pi i m k / N}$. What does the inverse DFT of this produce? We use $\{x_n^s\}$ for the series whose transform is $\tilde{x}_k e^{2\pi i m k / N}$; then we write down the definitions for the DFT and inverse DFT, to get

$$\begin{aligned}x_n^s &= \frac{1}{N} \sum_{k=0}^{N-1} \tilde{x}_k e^{2\pi i m k / N} e^{2\pi i n k / N} = \frac{1}{N} \sum_{k=0}^{N-1} \sum_{l=0}^{N-1} x_l e^{-2\pi i l k / N} e^{2\pi i m k / N} e^{2\pi i n k / N} \\ &= \sum_{l=0}^{N-1} x_l \left[\frac{1}{N} \sum_{k=0}^{N-1} e^{2\pi i k(m+n-l)/N} \right]\end{aligned}$$

By equation (5.19) the sum in square brackets is again one for $n = (l - m)_{\text{mod}N}$ ($n - (l - m)$ a multiple of N) and otherwise zero. So the sum over l gives:

$$x_n^s = x_{(l-m)_{\text{mod}N}}$$

To see what this means, it helps to take a specific value for m ; if we take $m = 3$, then taking $l = 3$ gives $n = 0$, $l = 4$ gives $n = 1$, and so on:

$$x_0^s = x_3 \quad x_1^s = x_4 \quad \dots \quad x_{N-4}^s = x_{N-1}$$

This is all as we expect, but the “right end” of the back-transformed series is

$$x_{N-3}^s = x_{N_{\text{mod}N}} = x_0 \quad x_{N-2}^s = x_{N+1_{\text{mod}N}} = x_1 \quad x_{N-1}^s = x_2$$

which is to say, the start of the original series. We can look at this in two ways, both of them foreshadowed in our discussion of Fourier series (Figure 2.3). One way is to view this as a linear shift applied to a replicated, periodic sequence. The other way is to view it as a **circular shift**, where we imagine the finite sequence to be on a circle, so that any shift moves the end to the beginning.

5.6.2 Convolution Theorem for the DFT

A much more important result, with parallels to the one just given, is provided by the extension of the convolution theorem to discrete, finite-length series. If we use the time-domain definition of convolution for sequences (equation 5.2), we cannot carry out the multiplications for sequence numbers less than 0 or greater than N-1, so the output sequence has to be shorter than the longer of the two input sequences. Indeed, if we were to use this definition for two sequences of the same length, the output sequence would be just one term long.

But there is another approach. We know that the Fourier transform of the convolution of two functions is the product of the two Fourier transforms; so what is the sequence produced by multiplying two sets of DFT coefficients and taking the inverse DFT? More precisely, suppose $\{x_n\}$ and $\{y_n\}$ to have DFT's $\{\tilde{x}_k\}$ and $\{\tilde{y}_k\}$; what series $\{z_n\}$ has the DFT $\tilde{z}_k = \tilde{x}_k \tilde{y}_k$? As before, the derivation just involves writing the inverse transform, replacing \tilde{z} by the product $\tilde{x}\tilde{y}$, substituting in the DFT expressions for these, and finally collecting all the exponentials together:

$$\begin{aligned} z_n &= \frac{1}{N} \sum_{k=0}^{N-1} \tilde{z}_k e^{2\pi i n k / N} = \frac{1}{N} \sum_{k=0}^{N-1} \tilde{x}_k \tilde{y}_k e^{2\pi i n k / N} \\ &= \frac{1}{N} \sum_{k=0}^{N-1} \sum_{l=0}^{N-1} \sum_{m=0}^{N-1} x_l e^{-2\pi i l k / N} y_m e^{-2\pi i m k / N} e^{2\pi i n k / N} \\ &= \sum_{l=0}^{N-1} x_l \sum_{m=0}^{N-1} y_m \left[\frac{1}{N} \sum_{k=0}^{N-1} e^{2\pi i k (n-m-l) / N} \right] \end{aligned}$$

Once again, we need the sum over k to be nonzero; the orthogonality relation (5.19) then implies that

$$(n - m - l)_{\text{mod}N} = 0 \quad \text{or} \quad m = (n - l)_{\text{mod}N}$$

giving the final result that the sequence z is given by

$$z_n = \sum_{l=0}^{N-1} x_l y_{(n-l) \text{mod}N}$$

Again, an example may help; taking $n = 5$ gives

$$z_5 = x_0 y_5 + x_1 y_4 + \dots + x_5 y_0 + x_6 y_{N-1} + x_7 y_{N-2} + \dots + x_{N-1} y_6$$

meaning that as the convolution sum goes off the beginning of the y_n sequence it goes around to the end. One way to visualize this is to imagine both sequences mapped onto circles: a shift is then merely a rotation of one circle relative to another, and the kind of convolution described by the above equation is therefore called **circular convolution**.

The circular convolution, like the circular shift, is not intrinsic to finite sequences: these are just finite ordered collections of numbers. The circularity arises when we take the DFT of a sequence: then we must regard the sequence, and its Fourier transform, as being wrapped around a circle if we want to properly relate operations in the time and frequency domain.

For example, if we attempt to convolve two series in the time domain by multiplying their DFT's, we must be careful to ensure that no spurious effects are created by the “**wraparound**” from the circular nature of the sequence and its transform. Wraparound effects complicate such seemingly simple techniques as removing certain frequencies from data by taking the DFT, setting some of the DFT values to zero, and taking the inverse DFT: we must remember that the series we get back can show the effects of data at one end influencing data at the other, since using the DFT makes the two ends contiguous.

In practice the fastest way to convolve two sequences is often to transform them using the DFT, multiply the transforms, and find the inverse transform of the result. But to avoid wraparound effects, we must pad both series with zeroes before taking the DFT's; with enough zeros, the circularity of the convolution has no effect. Specifically, if we have an M -term series, $\{x_n\}$ and an L -term series $\{y_n\}$, we will get the correct result if we pad both out to length $M + L - 1$ before doing the DFT. The circular convolution is then

$$z_n = \sum_{l=0}^{M+L-2} x_l y_{(n-l)\bmod M+L-1} = \sum_{l=0}^{M-1} x_l y_{(n-l)\bmod M+L-1}$$

giving (as examples from the two ends of $\{z_n\}$)

$$\begin{aligned} z_0 &= x_0 y_0 + x_1 y_{M+L-2} + \dots + x_{M-1} y_{M+L-M} \\ z_{M+L-2} &= x_0 y_{M+L-2} + \dots + x_{M-2} y_{M+L-M} + x_{M-1} y_{L-1} \end{aligned}$$

For the first sum, all terms but the first are zero; for the second sum, all terms but the last, so we get the same series z_n as we would from a time-domain convolution in which both sequences were padded with infinite numbers of zeroes on both ends.

Name	Time	Frequency
Fourier transform	function $x(t)$	function $\tilde{x}(f)$
Fourier series	function $x(u)$, $ u < \frac{1}{2}$	sequence $\{\tilde{x}_n\}_\infty$
FT of infinite sequence	sequence $\{x_n\}_\infty$	function $\tilde{x}(\zeta)$, $ \zeta < \frac{1}{2}$
DFT	sequence $\{x_n\}_N$	sequence $\{\tilde{x}_n\}_N$

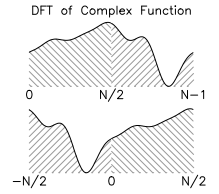
Table 5.1: The four Fourier pairs in the frequency and time domains. Sequences are expressed as $\{x_n\}_\infty$ (infinite length) or $\{x_n\}_N$ (finite length). Note that functions defined over a limited range can be regarded as periodic over an infinite one.

So far we have introduced four kinds of Fourier transforms, summarized in Table 5.6.2. We can see that the most general form is the Fourier transforms between two functions defined in continuous time. If we then limit either the time or frequency to an infinite number of discrete values, the functions in the other domain become periodic (or circular); the DFT is what we get if we have discrete sequences in both domains – and these then both have to be regarded as periodic, or circular.

5.6.3 Symmetry Relations

A common source of confusion is that the DFT output (equation 5.20) is indexed from $k = 0$ to $k = N - 1$, whereas the Fourier transform for an infinite sequence, equation (5.8), gives a transform defined for $-\frac{1}{2} \leq \zeta \leq \frac{1}{2}$. But it is easy to map the DFT results to a similar-looking range, since

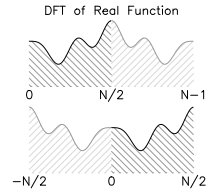
$$\tilde{x}_{N-k} = \sum_{n=0}^{N-1} x_n e^{-2\pi i n(N-k)/N} = \sum_{n=0}^{N-1} x_n e^{-2\pi i n(-k)/N} = \tilde{x}_{-k}$$



This result means that the “top half” of the DFT sequence (k from $N/2$ to $N - 1$) can also be thought of as being at negative frequencies, $k = -N/2$ to -1 .

If we map the DFT to a range about zero, then, as with the Fourier transform in continuous time, we have symmetry rules for the transforms of special classes of sequences. If the sequence $\{x_n\}$ is real, the transform sequence $\{\tilde{x}\}$ is Hermitian. Combining this with the previous result, we see that, for a real sequence, half of the DFT output coefficients \tilde{x}_k are redundant: usually we say this is the top half, which is equivalent to negative frequencies. Formally, we have that if x_n is real, then

$$\tilde{x}_{N-k} = \sum_{n=0}^{N-1} x_n e^{2\pi i n k / N} = \sum_{n=0}^{N-1} x_n^* \left(e^{-2\pi i n k / N} \right)^* = \tilde{x}_k^*$$



so the top half is just the complex conjugate of the bottom half, and is completely redundant. As indicated in the adjoining picture, we can (and should) omit this part of the DFT output.

This redundancy makes sense, since if we put in N real numbers, we expect to get N independent numbers out. We do, namely, $N/2$ independent complex DFT coefficients, though actually, for $\{x_n\}$ real, two \tilde{x} ’s are real, namely

$$\tilde{x}_0 = \sum_{n=0}^{N-1} x_n \quad \text{and} \quad \tilde{x}_{N/2} = \sum_{n=0}^{N-1} (-1)^n x_n$$

where we have assumed that N is even.

Our final theorem for the DFT is Parseval's relation:

$$\begin{aligned}\sum_{n=0}^{N-1} |x_n|^2 &= \sum_{n=0}^{N-1} x_n x_n^* = \frac{1}{N^2} \sum_{n=0}^{N-1} \sum_{k=0}^{N-1} \tilde{x}_k e^{2\pi i k n / N} \sum_{l=0}^{N-1} \tilde{x}_l^* e^{-2\pi i l n / N} \\ &= \frac{1}{N^2} \sum_{n=0}^{N-1} \sum_{k=0}^{N-1} \sum_{l=0}^{N-1} \tilde{x}_k \tilde{x}_l^* e^{2\pi i n(k-l) / N} = \frac{1}{N^2} \sum_{k=0}^{N-1} \tilde{x}_k \tilde{x}_k^* \sum_{n=0}^{N-1} 1 \\ &= \frac{1}{N} \sum_{k=0}^{N-1} |\tilde{x}_k|^2\end{aligned}$$

which is useful for checking the normalization (and accuracy) of any actual DFT algorithm.

5.7 Computing the DFT: the Fast Fourier Transform

Many methods of signal processing and data analysis require that we compute a DFT – sometimes many DFT's. This computation can be done rapidly, though this is not immediately obvious; the DFT formula, equation (5.20), appears at first sight to be the multiplication of an N -length vector (the sequence x_n) and an N -by- N matrix (the e 's) to produce another N -vector, the sequence $\{\tilde{x}_k\}$. Computing such a matrix multiplication in general requires a multiple of N^2 operations (additions and multiplications), an algorithm that we say takes **polynomial time**: the number of operations is a polynomial (of degree more than one) of the number of data. It might also appear that we have to compute N^2 sines and cosines (for the matrix of e 's), but this is not so; because of the periodicity of $e^{-2\pi i m / N}$, we have $e^{2\pi i nk / N} = e^{-2\pi i (nk)_{\text{mod } N} / N}$, so that while the matrix of e 's has N^2 elements there are only N distinct values.

In fact, the periodic nature of $e^{2\pi i nk / N}$ allows us to compute the DFT with many fewer than N^2 operations. For certain values of N we can compute all the \tilde{x}_k 's with only $N \log_2 N$ operations, so that the computation can be done $N / \log_2 N$ times faster: for example, about 100 times faster for $N = 1024$. The algorithm that does this is called the **Fast Fourier Transform**, often abbreviated as **FFT**.

Note that the FFT is just an algorithm for computing the DFT quickly, *not* a definition of the DFT. A common error is to suppose that any restrictions that apply to an FFT algorithm (notably restrictions on N) also apply to the DFT, but this is not so: the DFT is defined for any N .

The FFT algorithm is not completely obvious, as is shown by how many people failed to develop it: at the time the FFT was first announced, in 1965, many groups were computing DFT's using matrix multiplication, and it was with some amazement that they learned how much time they could save just by using a different

procedure.² But, the FFT was also obvious enough that by 1965 it had already been invented independently several times; either the inventors dismissed it as too small an improvement to be worth publishing (true for N very small), or the invention was simply ignored.

The publication and popularization of an FFT algorithm for $N = 2^M$ by [Cooley and Tukey \(1965\)](#) led to a dramatic change; developing faster Fourier (and other) transforms is its own subfield within signal processing.

The FFT is something you are very unlikely to program yourself – indeed, you shouldn't, since other people have spent much effort doing so. Appendix F gives the derivation of a simple version to provide an example of the approach used (known as divide-and-conquer).

There are two general lessons to be drawn from the FFT:

1. Considerable increases in speed can come from using a good algorithm; for whatever problem you will be doing, you should become familiar with how the time needed (the operations count) scales with problem size. There is a big difference between an algorithm, such as the FFT, whose operations count scales as $N \log N$ (not much worse than scaling as N , or as **linear time**) and one that scales as a power of N^p for $p > 1$ (**polynomial time**). For some computations the operations count scales as e^N : **exponential time**. Then computing a solution is practicable only if N is very small, which for some problems³ means that the best that can be done is an algorithm with better scaling that gives a “good enough” result.
2. A related lesson from the FFT is that the scaling with N is much more important than the details of implementation. The FFT gave at least two orders of magnitude improvement in speed for even moderate values of N . Another 35 years of effort have produced about a factor of five improvement between a general-purpose FFT from 1969 ([Singleton, 1969](#)) and the best one available in 2004.⁴

The earliest, shortest, and simplest FFT algorithms apply when N is a power of two, which seems to have established an enduring myth that sequences should be padded with zeros to reach such a length before using the FFT. The persistence of this idea is somewhat astonishing, since FFT's for more general values of N became available only a few years after the FFT was introduced. It is true that some

²For example, [Alsop and Nowroozi \(1966\)](#), computing spectra of seismic data for free oscillations, reported that their computation time shrank from 23 minutes to 2.4 seconds.

³Notably the Traveling Salesman Problem.

⁴FFTW, currently the fastest general-purpose program (hence the name: Fastest Fourier Transform in the West). For information on FFTW, and links to many other FFT programs and results, see <http://www.fftw.org>. Note that FFTW only gives its best performance if you will be doing many transforms of the same length within a single execution of the program.

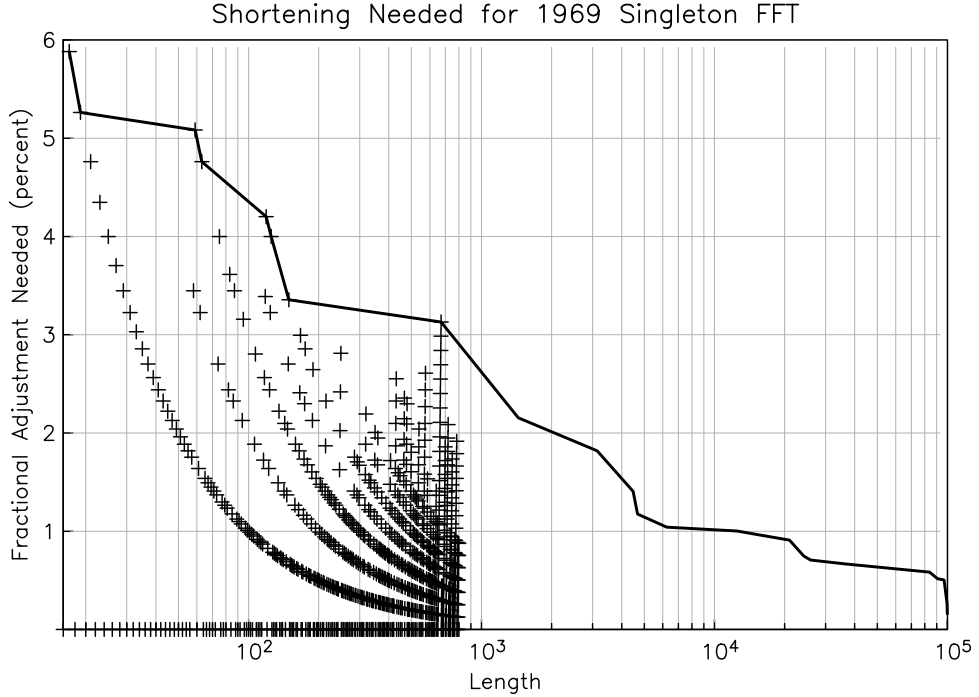


Figure 5.5: Fractional adjustment needed for a series of length N to have a highly-composite length compatible with the Singleton FFT: that is, a length having no prime factors larger than 23. The adjustment is shown for all lengths from 16 through 800; the heavy line shows the “worst-case” adjustment needed for all lengths.

lengths provide faster computations than others, but speeds close to the optimum are reached for a much larger class of N 's, namely those that are **highly composite**. This is any N that can be factored into a product of small primes. While some other special cases (for example, N being prime) also can be done quickly, you should avoid values of N whose factors include large primes; instead, find the largest highly composite number less than or equal to the length of your data, and truncate the series to this length.

Figure 5.5 shows the fractional adjustment needed as a function of length; as N increases this adjustment decreases, so that (for example) if $N > 5000$, the length never needs to be shortened by more than 1%. The maximum adjustment for an FFT restricted to powers of two would be 66%, independent of length. Some DFT programs will handle all N , but staying with highly composite lengths is a good idea unless you know that the program is designed to be fast for all N .

If, as is usually the case, your sequence $\{x_n\}$ is real, you do not need to treat it as complex with all imaginary parts zero; you can get a factor of two improve-

ment in speed by instead treating alternate terms as real and imaginary parts of a sequence of length $N/2$. The DFT result then needs some auxiliary processing, described in Appendix F.3.

Finally, if you only need the transform $\tilde{x}(\zeta)$ at a few frequencies, whether or not these are not automatically produced by the DFT relationship, there are also ways (Appendix F.4) to speed up the computation of the sum in equation (5.3).

CHAPTER 6

SAMPLING THEORY FOR TIME-SERIES

... recurring actions, made sufficiently near to each other, are perceptibly connected, and made to appear as a continued impression.

MICHAEL FARADAY On a peculiar class of optical deceptions, *J. Roy. Institut. Great Britain* 1, 205-223 (1831).

6.1 Introduction: Sampling Data

We now consider the transition from continuous time to discrete time, done by the **sampling** of a function $x(t)$ at specified times t_n to create a sequence $\{x_n\}$, with values $x_n = x(t_n)$. A bit of common jargon is to say that functions (and linear systems) defined in continuous time are **analog** functions or systems, with those in discrete time being called **digital**, as in digital signal processing. We will be using this convenient shorthand.

Almost all sequences are produced by digital dataloggers, which convert some quantity measured continuously into a sequence. Figure 6.1 shows the steps involved in such conversion, along with the corresponding time series. The first step is to remove high frequencies from the continuous function. This is done with an analog filter, called an **anti-aliasing filter** (for reasons we will see in Section 6.4); this is usually something like the RC filter we will discuss in Section 8.2. The filtered signal goes to a **sample-and-hold circuit**, which produces a continuous voltage that is held at fixed values over a sequence of time intervals specified by a clock: when the clock sends a signal to the sample and hold, its output changes to the value of the input at that time, t_n . We may call this the “stepped voltage”. This voltage is still a continuous function of time, $x(t)$, but it has the same information as, and so can be regarded as equivalent to, a sequence of values x_n . The dashed line in the block diagram indicates this change, from continuous to discrete time.

The next datalogger stage is a quantizer, or **analog-to-digital converter**, casually called “an A to D”. This device is a nonlinear system which, given an input with the real value x , produces a value \check{x} that can be represented using a finite number of digits; the reason for the sample-and-hold is to give a constant input voltage to the A-to-D for the time needed to compute its digital output. We natu-

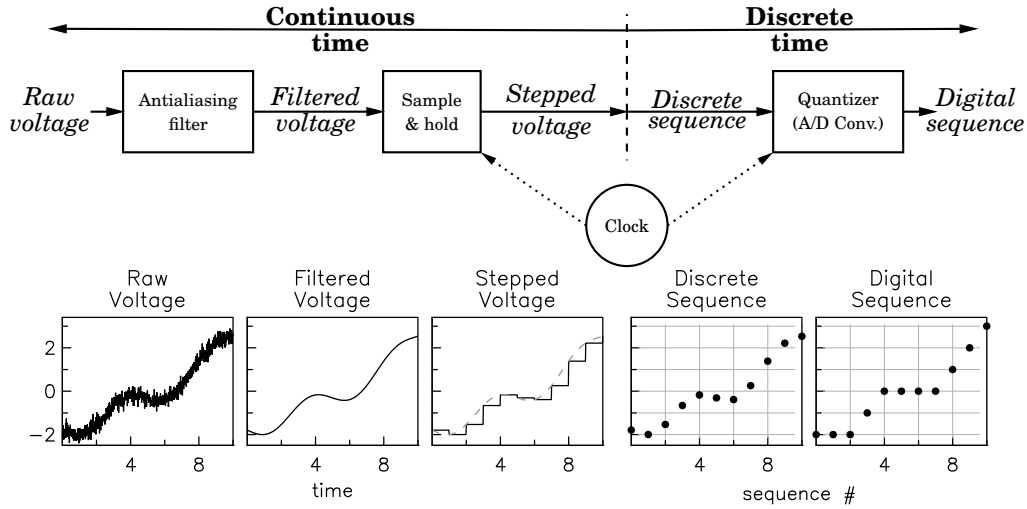


Figure 6.1: The top plot shows a block diagram of the steps involved in converting a continuous-time (analog) signal to a digital sequence; below this are cartoons of the different forms of a time series at each step.

rally want \tilde{x} to be as close to x as possible, and it can be an interesting problem is to find a representation for \tilde{x} that makes the difference $\tilde{x} - x$ unimportant. Making this difference “small enough” is usually not too difficult, as can be seen in the plots of the discrete sequence x_n and the digital sequence \tilde{x}_n , quantized by rounding to the nearest integer: these look very similar. Except in Section 6.8 we will assume that we have a real-valued sequence $\{x_n\}$.

6.2 The Sampling Problem

Most of this chapter will be about how to choose the times t_n so that, given $\{x_n\}$, we could (in principle) reconstruct $x(t)$ – and also about what errors we might incur by a poor choice of sampling times. Classical interpolation theory is one way of studying this; but a different approach, working in the frequency domain, turns out to be much more useful.

To avoid substantial complications, we assume the samples are equispaced in time, as is true for almost all dataloggers. The time spacing, or **sample interval**, is denoted by Δ , in whatever time units we are using. The sample times are then:

$$t_n = n\Delta + t_0 \quad n = -\infty, \dots, -2, -1, 0, 1, 2, \dots \infty \quad (6.1)$$

where t_0 is a reference time in whatever timescale we are using. For a single data series and time-invariant systems we can simply set $t_0 = 0$; to intercompare

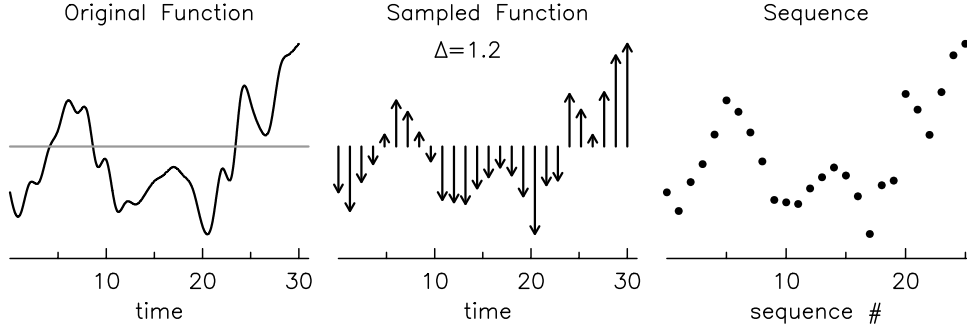


Figure 6.2: A mathematical model for sampling, shown pictorially. We start with a function, from which we create another function whose values depend only on those of the sampled data. The arrows are schematic for differently-weighted δ -functions. We can always construct the sampled-data function from the data sequence; if we can reconstruct the original function from the sampled-data function, we have lost no information by sampling. The sample interval is 1.2, so the sequence numbers do not match the times.

data with other data or phenomena we would want to set t_0 to its value in (say) Universal Time: not an easy task ([Agnew, 2020](#)).

In Chapter 2 we used nondimensional time u , only using a dimensioned quantity when we specified the period length T ; either way, the Fourier coefficients were just an ordered sequence. In the first part of Chapter 5 we considered an ordered sequence used as a time series, the Fourier transform of which used a nondimensional frequency ζ . In this chapter, as in Chapter 3, the time variable is written as t and the frequency variable as f to show that they have some dimension (that is, some units need to be attached); this dimension might be time, length, or some other variable that puts our data in order.

Slight departures of t_n from absolutely equal spacing (**sampling jitter**) do not much matter, since they can be viewed as adding some error (noise) to the data; for a timing error t_ϵ , the sample value $x(n\Delta+t_\epsilon)$ will be approximately $x(n\Delta)+t_\epsilon\dot{x}(n\Delta)$, and so long as the second term is much smaller than the first there will not be a problem. As we saw in our earlier discussion of the Discrete Fourier Transform, larger irregularities in sample interval would greatly complicate the analysis and are best avoided if at all possible. If we have equispaced data with gaps, our best course may be to fill the gaps with an estimate of what the data would have been; in statistics this is called **data imputation**.

Sampling a function gives us a sequence; to describe this process mathematically we need an intermediate step, shown in cartoon form in Figure 6.2. We start with $x(t)$, a function in continuous time; mathematically we say that it is a function on the real line, pictured in the left-hand panel of this figure. The sequence

x_n , on the other hand, is just an array of numbers, which we picture in the right-hand panel of Figure 6.2. We connect these two using delta functions $\delta(t - t_n)$; the (generalized) function

$$x(t)\delta(t - t_n)$$

is zero at $t \neq t_n$, and contains the value $x(t_n)$ in the weighting of the delta-function. This function is equivalent to the sampled value x_n : not equal to it, since one is a function and the other a number, but equivalent in the sense that either could be constructed given the other.¹

For equispaced sampling the sequence x_n is thus equivalent to the function $x_s(t)$. We defined this already in equation (5.4) for an implicit sample interval of one; for an interval Δ it is:

$$x_s(t) = x(t) \sum_{n=-\infty}^{\infty} \delta(t/\Delta - n) = \sum_{n=-\infty}^{\infty} x(n\Delta) \delta(t/\Delta - n) \quad (6.2)$$

which is shown in the middle panel of Figure 6.2, using arrows for delta-functions. We can view $x_s(t)$ as the function formed by multiplying $x(t)$ by an infinite “comb” of delta functions.

The normalized version of such a comb is called the shah function, so named by Bracewell because it uses the Cyrillic letter III, or *shah*, chosen for its pictorial similarity to the function:

$$\text{III}(u) = \sum_{n=-\infty}^{\infty} \delta(u - n)$$

Changing the spacing to Δ rescales III, so we can write the sampled-data function (equation 6.2) as

$$x_s(t) = \text{III}(t/\Delta)x(t)$$

for sample interval Δ .

The Fourier transform of $x_s(t)$ is

$$\begin{aligned} \tilde{x}_s(f) &= \int_{-\infty}^{\infty} \sum_{n=-\infty}^{\infty} x(t)\delta(t/\Delta - n)e^{-2\pi ift} dt = \sum_{n=-\infty}^{\infty} \Delta \int_{-\infty}^{\infty} x(u\Delta)\delta(u - n)e^{-2\pi ifu\Delta} du \\ &= \Delta \sum_{n=-\infty}^{\infty} x(n\Delta)e^{-2\pi ifn\Delta} \end{aligned} \quad (6.3)$$

where we have made the change of variables to $u = t/\Delta$ and back again. The final result looks, as it should, very like equation (5.3), the Fourier transform for a sequence, but with the sample interval Δ appearing in both the argument of

¹It might seem more in keeping with the action of a sampling circuit to multiply $x(t)$ by a function that is one at $t = t_n$ and zero elsewhere. But such a function on the real line integrates to zero – as would its Fourier transform.

the exponential and in front of the sum, as it must to make the dimensionality the same as for the Fourier transform of a function, equation (3.4). The inverse transform from $\tilde{x}_s(f)$ to x_n is gotten from setting ζ in equation (5.5) to $f\Delta$:

$$x_n = \int_{-1/2\Delta}^{1/2\Delta} \tilde{x}_s(f) e^{2\pi i n f \Delta} df \quad (6.4)$$

which also is dimensionally correct.

6.3 The Nyquist Theorem

We can use Fourier theory to help answer our question of reconstructing a function from its samples: how do we get (and can we get) $x(t)$ from $x_s(t)$? We approach this problem by comparing $\tilde{x}_s(f) = \mathcal{F}[x_s(t)]$ with $\tilde{x}(f) = \mathcal{F}[x(t)]$. By the convolution theorem,

$$\tilde{x}_s(f) = \mathcal{F}[x(t)\text{III}(t/\Delta)] = \tilde{x}(f) * \mathcal{F}[\text{III}(t/\Delta)] \quad (6.5)$$

To proceed further we go back to nondimensional variables and find $\mathcal{F}[\text{III}(u)]$, which is

$$\mathcal{F}[\text{III}(u)] = \int_{-\infty}^{\infty} e^{-2\pi i \zeta u} \sum_{n=-\infty}^{\infty} \delta(u - n) dt = \sum_{n=-\infty}^{\infty} e^{2\pi i \zeta n}$$

An extremely nonrigorous way to see what this infinite sum might give is to observe that for ζ an integer this is $\sum 1$, and hence infinite; while for ζ noninteger $2\pi i \zeta n$ assumes all possible values on the unit circle in the complex plane, so the sum will be zero. This suggests that

$$\mathcal{F}[\text{III}(u)] = \text{III}(\zeta)$$

making the III function is its own Fourier transform; this can be proved rigorously.

Then equation (6.5) becomes

$$\tilde{x}_s(f) = \tilde{x}(f) * \mathcal{F}[\text{III}(t/\Delta)] = \Delta \tilde{x}(f) * \text{III}(\Delta f) \quad (6.6)$$

Convolving any function with a δ -function simply recovers the original, and if we convolve with $\delta(f - f_0)$ we recover $\tilde{x}(f)$ shifted by an amount f_0 ; equation (6.6) becomes:

$$\begin{aligned} \tilde{x}_s(f) &= \Delta \tilde{x}(f) * \text{III}(\Delta f) = \Delta \sum_{n=-\infty}^{\infty} \delta(\Delta f - n) * \tilde{x}(f) \\ &= \Delta \sum_{n=-\infty}^{\infty} \tilde{x}(\Delta f - n) \end{aligned}$$

Our sampled-data series $\{x_s\}$ thus has a Fourier transform that can be gotten by replicating the transform of the original series at a frequency interval Δ^{-1} , and adding up the replicas. Figure 6.3 shows the whole process.

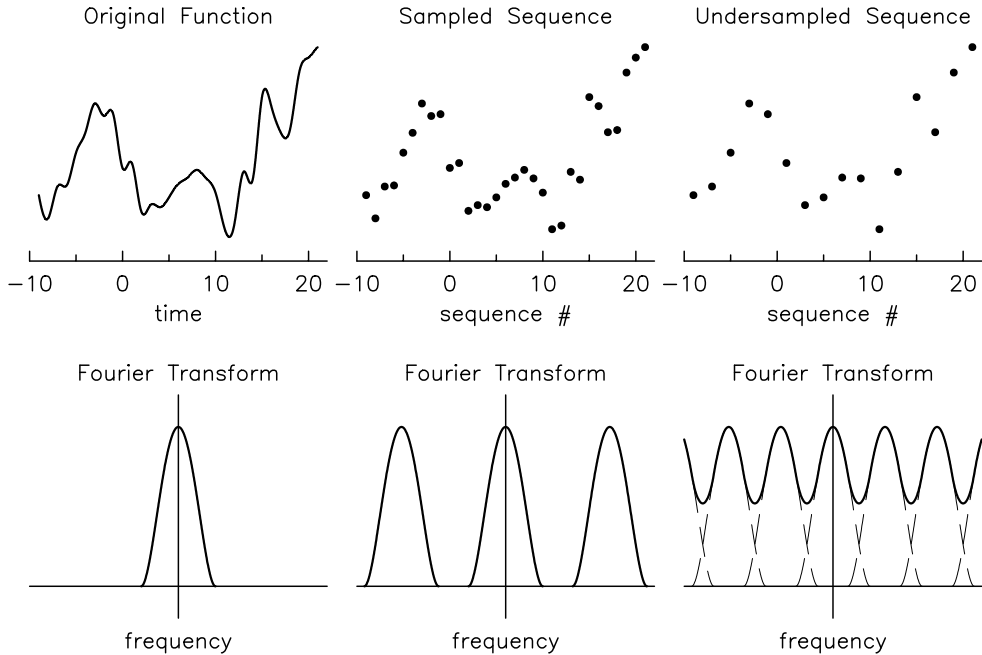


Figure 6.3: The upper panels show a function, then a sampled version of it, then a version sampled half as often. The lower panels show the corresponding Fourier transform: the original transform (this is actually a made-up function), and the replicated-and-summed version that results from sampling. In the middle, the transform replicas are separated; on the right, they are not. The right plot shows the replicas (aliases) with dashed lines.

We can now show that if \tilde{x}_s has a certain form, we can recover $x(t)$ from $x_s(t)$. The requirement for this is called the **Nyquist criterion**, and is given in the frequency domain. It states that $\tilde{x}(f)$ can be recovered from $\tilde{x}_s(f)$ and hence $x(t)$ recovered from $x_s(t)$, if and only if

$$\tilde{x}(f) = 0 \quad \text{for} \quad |f| > \frac{1}{2\Delta} \stackrel{\text{def}}{=} f_N \quad (6.7)$$

where f_N is called the **Nyquist frequency**.

This restriction on $\tilde{x}(f)$ comes from its replicated form. The replicas are spaced $1/\Delta$ apart; if the Nyquist criterion holds, each replica will remain separate, as in the lower middle panel of Figure 6.3. However, if $\tilde{x}(f)$ is nonzero above f_N , the replicas will overlap, and when summed will blend together, as in the lower right panel of Figure 6.3. There is then no way to disentangle them.

If $\tilde{x}(f) = 0$ for $|f - f_c| < f_b$, we say that $x(t)$ is **bandlimited**, with a **bandwidth** $2f_b$ and **center frequency** f_c ; we encountered one bandlimited function

in Section 3.2, the function $\text{sinc}(t)$, which had a center frequency of zero and a bandwidth of one. An amplitude-modulated sinusoid (Figure 3.3) is another such function. For the Nyquist criterion to hold, $x(t)$ must be bandlimited about zero with a bandwidth of no more than $2f_N$; when we sample data we would like Δ to have a value that makes this true.

If the Nyquist criterion holds, we also have a way of getting $\tilde{x}(f)$ from $\tilde{x}_s(f)$: we simply set all replicas but the center one to zero by multiplying $\tilde{x}_s(f)$ by a suitable boxcar function, scaled to be zero outside $|f| < f_N$:

$$\tilde{x}(f) = \frac{\tilde{x}_s(f)\Delta\Pi(f\Delta)}{\Delta}$$

Taking inverse transforms we have

$$\begin{aligned} x(t) &= x_s(t) * \text{sinc}(t/\Delta) = \text{sinc}(t/\Delta) * \sum_{n=-\infty}^{\infty} x(n\Delta)\delta(t/\Delta - n) \\ &= \sum_{n=-\infty}^{\infty} x(n\Delta)\text{sinc}(t/\Delta - n) \end{aligned} \tag{6.8}$$

The final sum is the expression for getting $x(t)$ from x_n ; note that if we put $t = m\Delta$ the zeros of the sinc function fall on all the other values than the one of interest, so we recover only one value, $x(m\Delta)$, as we should.

It is instructive to look at a pure sinusoid to see what happens at the Nyquist frequency. Suppose we have a sine (or cosine) with $f = f_N$, so there are two points per cycle, and with one sample at $t = 0$. The cosine alternates between ± 1 , but the sine is zero at all points sampled, and so cannot be recovered. In the frequency domain the sine becomes

$$\mathcal{F}[\sin(2\pi t/T)] = \frac{1}{2i} [\delta(f - 1/T) - \delta(f + 1/T)]$$

For two samples per cycle, $\Delta = T/2$, so in the frequency domain the replicas just meet. At each meeting there are opposed delta functions, one from each replica: these cancel, so $\tilde{x}_s(f) = 0$, consistent with the time-domain result. For a cosine

$$\mathcal{F}[\cos(2\pi t/T)] = \frac{1}{2} [\delta(f - 1/T) + \delta(f + 1/T)]$$

and for $\Delta = T/2$ the two delta-functions meet and reinforce, so that $\tilde{x}(f)$ and thus $x(t)$ can be recovered.

6.4 Aliasing

Having stated the Nyquist criterion, we have to ask, what if $x(t)$ is not bandlimited? For any data we collect it never is, since no transient function can be ban-

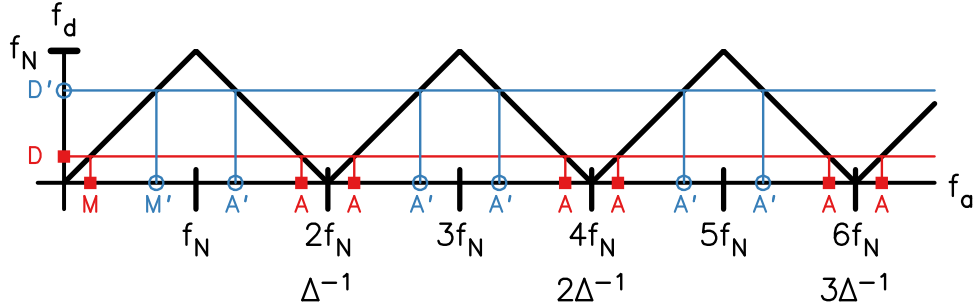


Figure 6.4: Cartoon to show how analog frequencies (on the f_a axis) map into the digital frequencies from 0 to f_N for real-valued data, as described mathematically by equation (6.10). The sawtooth function gives the mapping. As an example, the open circles on the f_a axis are all the frequencies that map (fold) into a single digital frequency on the f_d axis. The same is true for the solid squares. The main frequency M maps to the digital frequency D , as do all the frequencies marked A ; similarly, M' maps to D' , and so do all the frequencies marked A' .

dlimited.² Again, looking at replication of the Fourier transform in the frequency domain is the best way to understand the resulting errors.

For simplicity, we start by assuming that $x(t)$ is nearly bandlimited and falls to near zero at large frequency, since otherwise (with the some exceptions described in Section 6.6) we are bound to have aliasing. Suppose also that f_N is large enough that the only overlap is with the two nearest neighbors:

$$\tilde{x}_s(f) \approx \tilde{x}(f) + \tilde{x}(f - 1/\Delta) + \tilde{x}(f + 1/\Delta) \quad (6.9)$$

For frequencies near f_N , the major overlap is with $\tilde{x}(f_N - 1/\Delta) \approx \tilde{x}(-f_N)$; the other overlap is with $\tilde{x}(3f_N)$, which we assume is smaller. Thus for “large” positive frequency, the major contamination is from energy at “large” negative frequency.

We have used the term “replica” to emphasize what the convolution with III does, but usually the replicas are called **aliases** of the transform of the continuous-time function, the contaminating energy is called **aliased energy**, and the whole process is called **aliasing**. The expression (6.9) shows that for a complex-valued sequence the effect of sampling is to alias energy below the negative Nyquist frequency with positive frequencies just below the positive Nyquist frequency.

Usually $x(t)$ is real, and Table 3.1 shows that $\tilde{x}(-f) = \tilde{x}^*(f)$. We can then write the “nearest-neighbor” aliases as

$$\tilde{x}_s(f) \approx \tilde{x}(f) + \tilde{x}^*(2f_N - f) + \tilde{x}(2f_N + f)$$

²Slepian (1976) discusses the apparent paradox that no continuous function can be limited in both time and frequency, even though this is true of all signals we record. This paper thoughtfully describes how mathematical idealizations should be related to the real world.

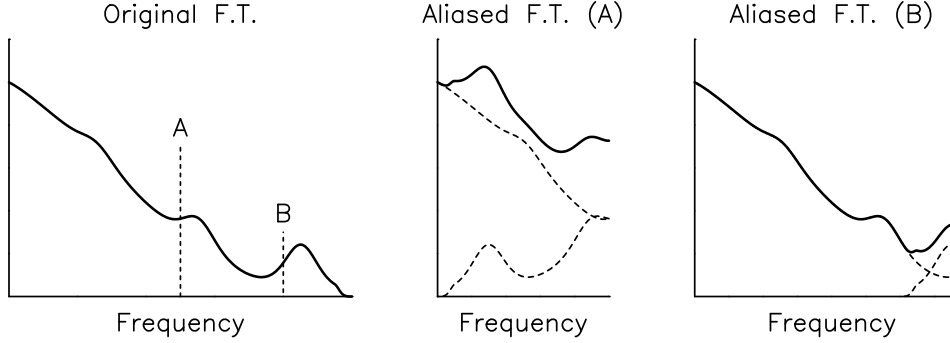


Figure 6.5: The left panel shows the amplitude of a made-up Fourier transform, with two possible locations for the Nyquist frequency. The next two panels show what the transform would be for these two choices, with the original aliases dashed and their sum solid. Choice A gives a badly-aliased result, choice B one that is possibly acceptable, since the only aliasing is near the Nyquist frequency.

It is useful to just consider $|\tilde{x}|$ and ignore the complex conjugates.

Suppose the positive frequency f increases from 0 to f_N . Then the first aliased frequency $f_{1a} = 2f_N - f$ decreases from $2f_N$ to f_N , and the second aliased frequency $f_{2a} = 2f_N - f$ increases from $2f_N$ to $3f_N$. Continuing this indefinitely shows that for $x(t)$ real sampling maps the real line of positive frequencies, from zero to infinity, into the finite interval from zero to f_N ; Figure 6.4 illustrates this. Note that if $x(t)$ is complex, sampling maps the entire real line into $-f_N$ to f_N .

Another way of seeing this is to note that our result (6.8) for the reconstructed $x(t)$ is a sum of sinc functions, and hence will be, like them, bandlimited. Given a sequence of samples, we can construct an infinity of functions on the real line, but only one of these is bandlimited. For real functions and sequences, that bandlimited function has the transform given by mapping $[0, \infty]$ into $[0, f_N]$ according to the rule (6.10), continued to infinite frequency. One way to visualize this rule is as an accordion folding of the frequency axis: a fold at f_N brings $2f_N$ to 0; then another fold at $2f_N$ brings $3f_N$ to f_N , and so on, as shown by the sawtooth function in Figure 6.4. We can write a formula for this: for $f > f_N$, let M be the integer part of f/f_N ; then f maps to

$$f' = \begin{cases} f - Mf_N & \text{for } M \text{ even} \\ (M+1)f_N - f & \text{for } M \text{ odd} \end{cases} \quad (6.10)$$

For example, suppose the sample interval is 0.02 s; this is a sampling frequency of 50 Hz, which makes the Nyquist frequency 25 Hz. Then a frequency of 60 Hz has $f/f_N = 2.4$, so $M = 2$, and the frequency aliases to $60 - 50 = 10$ Hz. A frequency of 90 Hz has $M = 3$, so it also aliases to 10 Hz = $4 \times 25 - 90$.

We can minimize aliasing in two ways:

- Before we sample the data, shape its Fourier transform using an analog filter (physical or electronic) to remove high frequencies: this is the “anti-alias filter” in the block diagram in Figure 6.1.
- Choose Δ so that, in the frequency band of interest, any aliased energy will be much less than the energy in the main transform. Our aim is not to have “significant” contamination, but what level is significant depends on the problem in hand. Figure 6.5 shows an example; while choice B allows some aliasing, the amount is small except near f_N , which may be acceptable. In fact, we cannot avoid problems near f_N : there must be some aliasing unless we apply a strong anti-alias filter—but such a filter will eliminate not just aliasing but the data at those frequencies. A simple rule is to look for successive values with alternating sign (perhaps around a trend); this means that there is substantial energy near f_N , quite likely because of significant aliasing.

A common situation is the effect of 60-Hz noise on data sampled at less than 120 Hz: such noise, which comes from powerlines, is difficult to avoid (Cohen *et al.*, 2010). If Δ is 1 second, N (see above) is 120 ($f_N = \frac{1}{2}$ Hz) and f' is 0. This might be acceptable, except that this “60-Hz” powerline noise is really $60 \text{ Hz} \pm 700\mu \text{Hz}$; the alias maps into 0 to $700 \mu\text{Hz}$ and could interfere, for example, with any signal with a period longer than half an hour. If we sampled at 2048 times per hour, $f_N = 0.2844 \text{ Hz}$, $N = 210$, and $f' = 0.2667 \text{ Hz}$, so that any 60-Hz energy aliases to near the Nyquist, out of the way of lower-frequency signals.

6.5 Decimation

A very common activity in digital signal processing is **decimation**. We say that we have decimated a discrete-time series by n if we take every n -th value to create a new and shorter series with sample interval $n\Delta$. (Another term for this is **down-sampling**.) The new series is related to the one it came from by exactly the same aliasing rules that apply to sampling of a continuous-time series; the only difference is that the folding of the frequency axis extends only to the Nyquist frequency for the original series, instead of to infinity.

For example, if we decimate by two, there is a single folding, so that frequencies between the old Nyquist f_N to the new one ($\frac{1}{2}f_N$) fold into the new interval from 0 to $\frac{1}{2}f_N$. Just as in the continuous case, the degree to which the decimated series is aliased depends on the relative levels of the Fourier transform above and below the new Nyquist frequency; before decimation we may need to digitally filter the data, as described in the next chapter, to avoid aliasing of the output.

The opposite of decimation is putting additional values between each value in a sequence to give a series sampled more often: interpolation, also called **upsam-**

pling. Although it seems counterintuitive, we can do this just by setting the new values to zero and then digitally filtering the series to remove energy above the old Nyquist frequency. One reason for doing such an interpolation would be to create a smooth series for conversion back into analog form: this is standard practice in digital music players.

Decimation and interpolation can be combined to change sample rates; we might, for example, downsample by 5 and then upsample by 3 to get a new rate that is 0.6 of the old. But whatever we do, we need to worry about, and correct for, any possible aliasing.

6.6 Violating the Nyquist Criterion

There are situations in which the data can violate the Nyquist criterion (equation 6.7) without loss of information. A common case is that the signal has a special structure that allows us to sample less often:

- A signal that is actually periodic can be measured adequately while being sampled at random, and even infrequent, times. Astronomy has many cases of this, notably measurements of the brightness curves from regularly variable stars and stars with exoplanets, where the observations may occur at random times over many decades. In such cases the effective Nyquist frequency turns out to be limited by the timing precision (Koen, 2006).
- If the signal can be described by a few parameters, these may be determined even though there is aliasing. For example, the signal produced by the interferometer in an absolute gravimeter is:

$$x(t) = x_0 + \cos[((f_0 + f_1 t)t + \phi)]$$

where the parameter f_1 is related to the local acceleration of gravity. A signal like this, with an increasing frequency, is often called a chirp. Even though the frequency increases to values well above f_N , the special form of the signal means that it can still be processed to find f_0 and f_1 (Parker *et al.*, 1995).

6.7 The Poisson Sum Formula

We can use the sampling and replication properties of the III function to demonstrate another duality between a function and its Fourier transform – though not one related to sampling and aliasing. Consider the sum of replications of a function

$x(t)$ to produce the periodic function y :

$$y(t) = \sum_{k=-\infty}^{\infty} x(t+k) = x(t) * \text{III}(t)$$

which will have the Fourier transform

$$\tilde{y}(f) = \tilde{x}(f)\text{III}(f) = \sum_{n=-\infty}^{\infty} \tilde{x}(f)\delta(f-n)$$

which is to say the sampled-data version of $\tilde{x}(f)$. Now take the inverse Fourier transform of $\tilde{y}(f)$, writing it explicitly

$$\int_{-\infty}^{\infty} \sum_{n=-\infty}^{\infty} \tilde{x}(f)\delta(f-n)e^{2\pi ift} df = \sum_{n=-\infty}^{\infty} \int_{-\infty}^{\infty} \tilde{x}(f)\delta(f-n)e^{2\pi ift} df = \sum_{n=-\infty}^{\infty} \tilde{x}(n)e^{2\pi int}$$

which means that

$$\sum_{k=-\infty}^{\infty} x(t+k) = \sum_{n=-\infty}^{\infty} \tilde{x}(n)e^{2\pi int} \quad (6.11)$$

and if we now set t to zero we find

$$\sum_{k=-\infty}^{\infty} x(k) = \sum_{n=-\infty}^{\infty} \tilde{x}(n) \quad (6.12)$$

which is known as the **Poisson Sum Formula**. One potential use for this is in speeding up the computation of an infinite sum: if the function being summed has a Fourier transform, this may be narrower than the function itself, so that summing over Fourier values would be faster and more accurate. We will see an application in Section 11.5.1.

6.8 Quantization Error

We close by briefly discussing the effects of quantization. Consider the simple (and common) case in which an A-to-D converts a real-valued input voltage to an output integer. A-to-D's are specified by the number of bits in this integer: for example, a 16-bit system outputs values from -32767 to 32768 (plus and minus 2^{15}) over the full range of input voltage. So the more bits, the smaller the voltage corresponding to a unit change in the output (which is known as the **least count** voltage level), and the larger the ratio of the maximum signal to the smallest one that can be detected. This ratio is called the **dynamic range**, for an M -bit A-to-D, it is 2^M , though it is usually expressed in dB, being very nearly $6M$.

The least count in volts may be scaled by the instrument sensitivity to find the least count in the units of whatever is being recorded; we denote this value by ϵ . If the A-to-D rounds or truncates the real value to the nearest integer, the maximum

error is $\epsilon/2$.³ Provided the signal moves by more than ϵ between samples, where it “lands”, relative to the integer boundaries, will be random. Then it is easy to see that this error will be uniformly distributed from $-\epsilon/2$ to $\epsilon/2$, which has a variance of one-twelfth, equivalent to a standard deviation of about 0.3 least counts.

This result suggests that quantization error will usually not be large, and indeed it is usually easy to make quantization error small enough to ignore. But you should always estimate it and compare it to the size of what signal you might wish to record. Once again this is often best done in the frequency domain, though this comparison will require use of the power spectral density (Section 10.2.2).

Sometimes it is actually useful to quantize a time series very coarsely to remove unwanted signals. A good example comes from the very popular procedure of determining seismic wave velocities by cross-correlating noise between seismic stations. When doing this we do not want the correlation to be biased by the occasional large earthquake, which for this application is not signal but noise: something we are not interested in. One way to remove large variations is to quantize the data at the one-bit level (also known as “bang-bang quantization”), so that all amplitude information is lost, and what is left is only the times at which the time series crosses zero. Then large signals (earthquakes) that do not last long have much less weight than small signals (background noise) that are always present; [Bensen et al. \(2007\)](#) compare this and more complicated methods.

³For truncation the error has a bias of $\epsilon/2$, and a random variation between $-\epsilon/2$ and $\epsilon/2$.

CHAPTER 7

DIGITAL FILTERS I: FREQUENCY-SELECTIVE FILTERS

Engineering is the art of doing that thing well with one dollar, which any bungler can do with two after a fashion.

ARTHUR M. WELLINGTON, *The Economic Theory of the Location of Railways* (1887)

7.1 Introduction: Some General Digital Filters

There are many operations we can perform on a discrete-time sequence $\{x_n\}$, the DFT being one example. In this chapter we discuss **filtering** of a series, in which we convolve it with some other series (the **filter**). This means that the filter can be viewed as a system, with the original series as the input and the result as the output.

Specializing to filters that are linear and time-invariant system, with input $\{x_m\}$ and output $\{y_n\}$, the most general form is

$$y_n = \sum_{k=1}^{\infty} a_k y_{n-k} + \sum_{m=-\infty}^{\infty} b_m x_{n-m}$$

that is, each term of the output sequence is a weighted sum of previous values of that sequence, plus another weighted sum over the input sequence. The two sequences $\{a_k\}$ and $\{b_m\}$ are called the **filter weights**.

The infinite sums are of course not computable, so we replace them with finite sums and write the filtering operation as:

$$y_n = \sum_{k=1}^K a_k y_{n-k} + \sum_{m=0}^{M-1} b_m x_{n-m+p} \quad (7.1)$$

so there are K weights a_k and M weights b_m , conventionally numbered from 0 to $M-1$. There are specialized versions of equation (7.1), and these have names (or acronyms) which differ from field to field. One version removes the sum over previous values of the output, so that equation (7.1) becomes

$$y_n = \sum_{m=0}^{M-1} b_m x_{n-m+p} \quad (7.2)$$

and another is to restrict the sum over the x_m 's to a single term:

$$y_n = \sum_{k=1}^K a_k y_{n-k} + b_0 x_{n+p} \quad (7.3)$$

where the variable p allows the filter input to be taken from anywhere in the $\{x_m\}$ sequence; usually this is zero.

Equation	General Name	Signal Processing	Statistics
7.1	Recursive	Infinite Impulse Response (IIR)	Autoregressive Moving Average (ARMA)
7.2	Non-Recursive	Finite Impulse Response (FIR)	Moving Average (MA)
7.3	Recursive	Infinite Impulse Response (IIR)	Autoregressive (AR)

Table 7.1: Different types of filters, and the different names for them.

Table 7.1 gives the names and acronyms for these three versions. The signal processing names refer to what the output looks like for a discrete-time impulse input (equation 5.1). If this is input to equation (7.3), with $b_0 = 1$, it is easy to see that $y_n = (a_0)^n$, which if $|a_0| < 1$ creates a decreasing but always nonzero output: an infinite impulse response. For the same input the output series for equation (7.2) will just be the finite sequence $\{b_n\}$.

For all of these filters, the equation used assumes that the interval between the data values is one; as before, we use ζ for the resulting dimensionless frequency. The Nyquist frequency is $\zeta_N = \frac{1}{2}$. Given a sample interval Δ we can always convert to dimensional frequency using $f = \zeta/\Delta$.

7.1.1 Possible Uses of Filters

For filters described by equation (7.1), **filter design** is the art of deciding on values for the filter parameters (K and M , and the sequences $\{a_k\}$ and $\{b_m\}$) that will give an appropriate level of performance. Obviously, the larger K and M are, the more parameters we have and the better the filter will perform. All filter design is a tradeoff between performance and computational cost: a branch of engineering, in which we seek “good enough” performance, not perfection.

But performance at what? Filters are used for many tasks:

- A. Enhancing or removing energy at certain frequencies, for example removing high frequencies prior to decimation (Section 6.5) to avoid aliasing. This type of filter is the subject of the rest of this chapter.

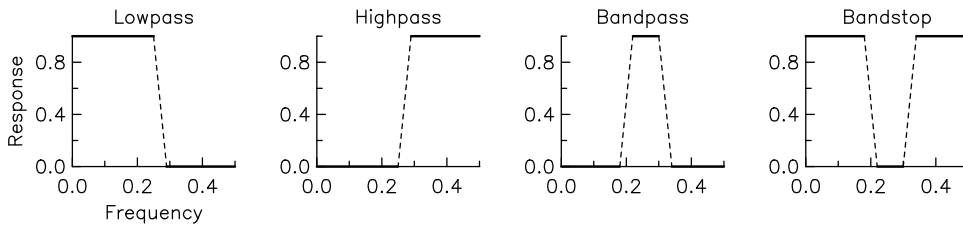


Figure 7.1: Ideal frequency-selective filters: the four commonest types.

The parts of the frequency band for which the response is 1 are called the **passband(s)**; where the response is 0 is the **stopband(s)**. The dashed lines show the region in which (for most design methods) the response goes from 1 to 0, though not necessarily linearly; this is called the **transition band**. Another name for the bandstop filter is **notch filter**.

- B. Differentiating or integrating. These are continuous-time operations, but they be well approximated for properly sampled sequences. We discuss these filters in Section 9.2.
- C. Simulating what a continuous-time linear system would do to a continuous-time series, again assuming that we have a properly sampled sequence. We discuss this type of filter, and concepts relevant to its design, in Chapter 8.
- D. Determining something about one or both of two series when all we have is the convolution of them. This is known as **deconvolution**. Since convolution often smooths a series, deconvolution is often done to recover fine details in, say, a seismic section; downward continuation of magnetic or gravity data measured above its source is another example.
- E. Predicting future values. For this filter design requires that we model the sequence probabilistically, and it often involves simultaneous processing of many input series, to produce at least one output series. We discuss one filter of this type in Section 14.2; other designs, notably the **Kalman filter**, are beyond the scope of this course.
- F. Detecting a signal, often a transient, in a series: for example, a P wave or a sonar return. Such detection can be done using a predictive filter, but it also requires the methods of statistical hypothesis testing, again beyond the scope of the course.

For many of these applications it can advantageous to drop the restriction that the filter be linear and time-invariant. Dropping time invariance allows **adaptive filters**, where the response of the filter changes as the input does. Dropping linearity provides even more flexibility. We will not discuss either generalization.

7.2 FIR Filters for Frequency Selection

For frequency selection, we start by choosing an ideal filter response $\tilde{b}_d(\zeta)$, which is either 1 or 0 over different frequency bands. Figure 7.1 shows and names the commonest filter types.

Until the 1960's analog filters were the only way to approximate these behaviors, and electrical engineers developed methods for designing this type of filter. One way to design a digital filter is to first design an analog filter and then use the methods of Chapter 8 to produce a digital filter, implemented using equation (7.1). Like their analog counterparts, these are IIR filters.

We will only consider FIR filters (equation 7.2). For the same performance these require more computation than an IIR filter, but have two advantages. One is that the output of a FIR filter only depends on a finite timespan of the input; the other, that they can provide minimal distortion.

The action of an FIR filter is just a digital convolution of the weight sequence $\{b_n\}$ with the sequence $\{x_n\}$ to produce a filtered sequence $\{y_n\} = \{b_n\} * \{x_n\}$, so the frequency response of a FIR filter is just the Fourier transform of the weight sequence:

$$\tilde{b}(\zeta) = \sum_{n=0}^{N-1} b_n e^{-2\pi i \zeta n} = \sum_{n=-\infty}^{\infty} b_n e^{-2\pi i \zeta n} \quad \text{for } -\frac{1}{2} \leq \zeta \leq \frac{1}{2} \quad (7.4)$$

N is the number of weights. We can of course consider them to be part of an infinite sequence.

Specializing further, we impose three restrictions:

- The weights are real.
- The number of weights, N , is odd, so we can introduce another integer, M , with $N = 2M + 1$.
- The weights are “symmetric”: $b_{M-k} = b_{M+k} \quad k = 0, \dots, M$

So $b_n = b_{2M-n}$, making the frequency response

$$\begin{aligned} \tilde{b}(\zeta) &= \sum_{n=0}^{2M} b_n e^{-2\pi i \zeta n} = \sum_{n=0}^{M-1} b_n (e^{-2\pi i \zeta n} + e^{-2\pi i \zeta (2M-n)}) + b_M e^{-2\pi i \zeta M} \\ &= e^{-2\pi i \zeta M} \left[b_M + \sum_{n=0}^{M-1} b_n (e^{-2\pi i \zeta (n-M)} + e^{-2\pi i \zeta (M-n)}) \right] \\ &= e^{-2\pi i \zeta M} \left[b_M + 2 \sum_{n=0}^{M-1} b_n \cos 2\pi(M-n)\zeta \right] \end{aligned} \quad (7.5)$$

On the last line the part in square brackets is purely real; if we treat it as complex and use the amplitude and phase form for complex numbers, its phase is zero.

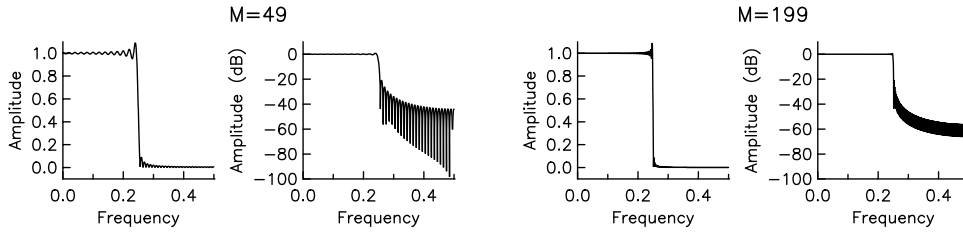


Figure 7.2: Frequency response (shown in both linear and log amplitude) for lowpass filters designed by simple truncation of a sequence of ideal weights. The ideal response $\tilde{b}_d(\zeta)$ has a passband ($\tilde{b}_d = 1$) from 0 to 0.25, and a stopband ($\tilde{b}_d = 0$) from 0.25 to 0.5. The left-hand pair of plots show the response for $M = 49$ (99 weights total), and the right-hand pair for $M = 99$ (199 weights total).

The exponential in front is, by the shift theorem (equation 3.13) equivalent to an M point shift: just a time delay. Since a pure time delay leaves the shape of the series unchanged, a symmetric FIR filter can be said to produce the least distortion of the input. Because the phase shift is linear in frequency, symmetric FIR filters are usually termed **linear phase** filters.

If the filter can be acausal (the output for a step input precedes the step), we can make it symmetrical around $n = 0$, defining $b_n = b_{-n}$ for $n = -M, \dots, M$. The frequency response is then, instead of equation (7.5),

$$\tilde{b}(\zeta) = b_0 + 2 \sum_{n=1}^M b_n \cos 2\pi n f \quad (7.6)$$

which has zero phase shift; this form of FIR filter is called a **zero-phase filter**. In digital systems it is always possible to have an acausal filter, either because it is implemented after the data have been collected, or because we relabel the absolute time of the terms in the output series by changing t_0 in equation (6.1). Acausality is not usually a problem, though seismic data can be an exception: if our interest is in the exact time of arrival of bursts of energy, we do not want the filtering to output any energy before it actually arrives.¹ In Chapter 9 we will see how to make FIR filters that are better suited to this application.

Given an ideal frequency response $\tilde{b}_d(\zeta)$, designing symmetric FIR filters is about choosing the number of weights $M + 1$, and the weights $\{b_n\}$, to make $\tilde{b}(\zeta)$ best approximate $\tilde{b}_d(\zeta)$ —though the meaning of “best” is not unique.

A naive approach to designing FIR filters is to just take the inverse Fourier transform of the ideal filter response: since $\tilde{b}_d(\zeta)$ is real and symmetric, it might

¹Scherbaum and Bouin (1997) shows how this exact problem confounded some interpretations of the initial rupture in earthquakes.

appear that we can use the inverse transform for sequences to get

$$b_n^d = \int_{-\frac{1}{2}}^{\frac{1}{2}} \tilde{b}_d(\zeta) e^{2\pi i \zeta n} d\zeta = 2 \int_0^{\frac{1}{2}} \tilde{b}_d(\zeta) \cos 2\pi \zeta n d\zeta \quad (7.7)$$

But this rarely gives a sequence of finite length, which we must have for any actual FIR filter.

7.2.1 Designs Using Tapers

One method of filter design is to start with the infinitely long sequence $\{b_n^d\}$ given by equation 7.7. We turn this into a finite sequence by multiplying $\{b_n^d\}$ by a **taper** (or **window**) sequence $\{w_n\}$ to create the final weights $b_n = w_n b_n^d$. The taper sequence must be zero: $w_n = 0$ for $n > M$, and the weights $\{w_n\}$ must be symmetric about $n = 0$.

This time-domain multiplication is of course equivalent to a convolution in the frequency domain: and so it is:

$$\begin{aligned} \tilde{b}(\zeta) &= \sum_{n=-\infty}^{\infty} w_n b_n^d e^{2\pi i \zeta n} = \sum_{n=-\infty}^{\infty} w_n e^{2\pi i \zeta n} \int_{-\frac{1}{2}}^{\frac{1}{2}} \tilde{b}_d(u) e^{2\pi i \zeta n u} du \\ &= \int_{-\frac{1}{2}}^{\frac{1}{2}} \tilde{b}_d(u) \sum_{n=-\infty}^{\infty} w_n e^{-2\pi i n(\zeta-u)} du = \int_{-\frac{1}{2}}^{\frac{1}{2}} \tilde{b}_d(u) \tilde{w}(\zeta - u) du \end{aligned}$$

where in the final convolution integral both functions are assumed to be periodic outside the range $[-\frac{1}{2}, \frac{1}{2}]$.

This integral means that the closer $\tilde{w}(\zeta)$, the transform of the taper sequence, is to a delta function, the closer the filter response will be to the ideal $\tilde{b}_d(\zeta)$. What we mean by “close to” will depend on what we think is important: does closeness to a delta-function mean that the peak of $\tilde{w}(\zeta)$ should be narrow or the values away from the peak should be small? Our answer to this will depend on what we want the filter to do.

The simplest taper is the rectangular (boxcar) taper, with $w_n = 1$ for $n \leq M$; this simply truncates the sequence of ideal weights. The corresponding $\tilde{w}(\zeta)$ is:

$$\tilde{w}(\zeta) = \sum_{n=-M}^M e^{-2\pi i \zeta n} = D_{2M+1}(\zeta) = D_N(\zeta)$$

where $D_N(\zeta)$ is the Dirichlet kernel discussed in Section 5.4. Successive maxima of $|D_N(\zeta)|$ do decrease, but only as ζ^{-1} : if what we want is small values away from the peak, this $\tilde{w}(\zeta)$ is not a good approximation to a delta function. Convoluting this $\tilde{w}(\zeta)$ with the ideal response causes much of the passband response to “leak” into the stopband, and vice-versa. Figure 7.2 shows this effect clearly, and also that simply increasing the number of weights M does little to diminish it.

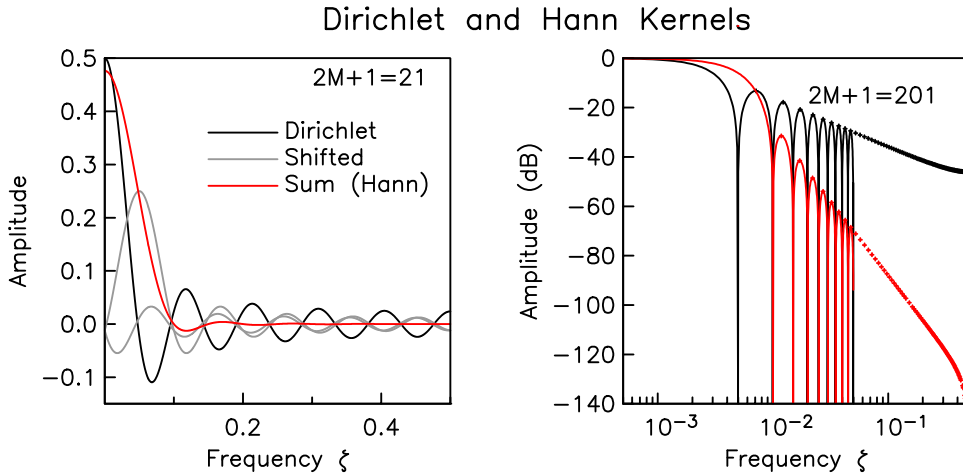


Figure 7.3: The three Dirichlet kernels used in forming the response of the von Hann taper (left, dashed), and that response itself (solid); the normalized kernel D_N^n is shown. The right plot shows $\tilde{w}(\zeta)$ for the Dirichlet (upper) and von Hann (lower) kernels, normalized to be unity at zero frequency, on a log-log scale, for a larger value of M . For frequencies higher than the first 10 peaks, only peak response is shown.

This is a result that might be expected from our discussion of convergence in Section 2.4.1. In taking the rectangular taper we are simply finding partial sums of the Fourier series expression for $\tilde{b}_d(\zeta)$, so the frequency response of these windowed filters converges, but all with problems associated with Gibbs' phenomenon.

A simple taper that has much smaller values away from the central peak is the von Hann taper, also called the Hanning taper, \cos^2 , or $1 + \cos$ taper:²

$$w_n = \frac{1}{2}[1 + \cos(\pi n/M)] = \cos^2(\pi n/2M) \quad \text{for } n = -M, \dots, M$$

which has the transform:

$$\begin{aligned} \tilde{w}(\zeta) &= \sum_{n=-M}^M w_n e^{-2\pi i \zeta n} = \frac{1}{2} \sum_{n=-M}^M e^{-2\pi i \zeta n} + \frac{1}{4} \sum_{n=-M}^M [e^{\pi i n/M} + e^{-\pi i n/M}] e^{-2\pi i \zeta n} \\ &= \frac{1}{2} \sum_{n=-M}^M e^{-2\pi i \zeta n} + \frac{1}{4} \sum_{n=-M}^M e^{-2\pi i (\zeta - 1/2M)n} + \frac{1}{4} \sum_{n=-M}^M e^{-2\pi i (\zeta + 1/2M)n} \\ &= N[\frac{1}{2}D_N(\zeta) + \frac{1}{4}D_N(\zeta - 1/2M) + \frac{1}{4}D_N(\zeta + 1/2M)] \end{aligned}$$

Figure 7.3 shows the three Dirichlet kernels and their sum; as ζ increases, the combination approaches zero much more rapidly than the original Dirichlet kernel does, a point made even more dramatically by a log-log plot.

²The taper was developed (though with slightly different goals) by Julius von Hann, an Austrian meteorologist; calling it a Hanning taper was something of an inside joke by John Tukey, to parallel the name of another taper developed by one of his colleagues at Bell Labs, Richard Hamming.

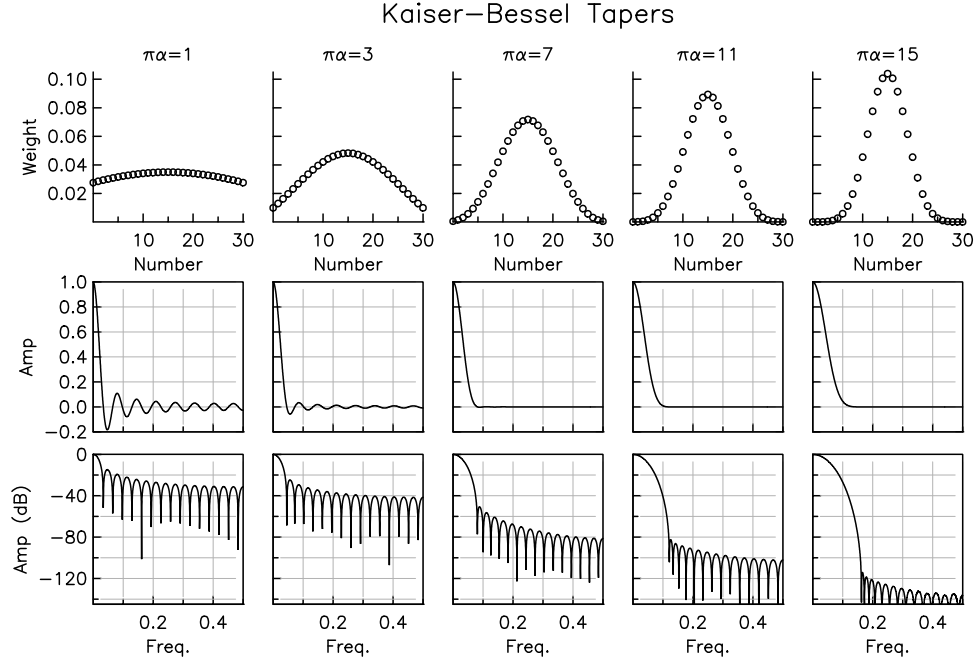


Figure 7.4: Different tapers and their responses. The top row shows five Kaiser-Bessel tapers (length $2M + 1 = 31$, and normalized to sum to one); the middle row shows their Fourier transforms, and the bottom row shows $\tilde{w}(\zeta)$ on a log (dB) scale.

Many other taper sequences have been invented;³ their Fourier transforms vary considerably, but inevitably have a tradeoff between the width of the central peak and smallness of the fluctuations away from it. The usual terminology for this introduces some jargon derived from antenna theory: we say that the tradeoff is between the width of the **main lobe** (the central peak) and the size of the **sidelobes** (all other maxima in the frequency response). Figure 7.4 shows an example of this tradeoff, using a family of tapers known as the **Kaiser-Bessel** tapers, which use a model based on Bessel functions to produce a set of tapers with one parameter (α) that trades off the width of the center lobe (best seen in a linear plot of amplitude) against the size of the sidelobes (best seen in a log plot). The effect of using these different tapers on a filter is shown in Figure 7.5. As expected, the lower the taper sidelobes in Figure 7.4, the better the filter performs in the stopband and the closer the response in the passband is to one.

Kaiser and Reed (1977, 1978) provide some empirical rules for setting the taper parameter and the filter length to meet a given sidelobe level and frequency

³Harris (1976) is a kind of bestiary of every taper then thought of, with plots of the time and frequency responses. Few of these have been useful.

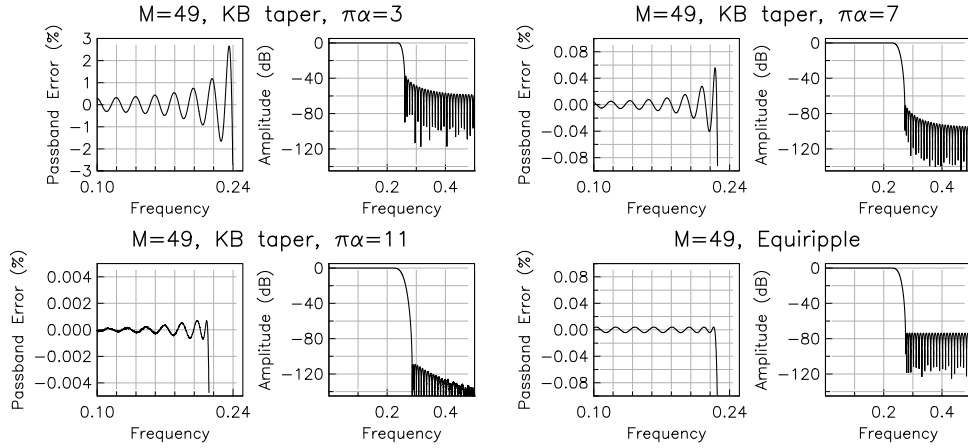


Figure 7.5: Frequency responses of lowpass filters for three of the data tapers shown in 7.4, and also for the minimax design procedure described in Section 7.2.2 For each, the error (departure from unity) is shown over part of the passband (note the different scales), and the complete response is shown in log form.

separation between passband and stopband (the **transition width**). This method offers a convenient and simple method of filter design that is often “good enough”. But filter design using tapers is still somewhat inflexible: because of Gibb’s phenomenon the response is worst right around the transition band, and the amount of ripple in the passband is the same as the size of the sidelobes in the stopband. We can reduce these effects using other techniques, one of which we now describe.

7.2.2 Design by Optimal Fitting of the Frequency Response

A more powerful technique in designing filters is to choose the filter weights to minimize the difference between the ideal response $\tilde{b}_d(\zeta)$ and the actual response $\tilde{b}(\zeta)$. Minimizing the mean-square misfit, by analogy with a least-squares fit, seems like an obvious approach. The quantity to minimize is then an integral over frequency:

$$\epsilon^2 = \int_{-1/2}^{1/2} |\tilde{b}_d(\zeta) - \tilde{b}(\zeta)|^2 df$$

The difference between the ideal and actual responses, in terms of the weights, is

$$\tilde{b}_d(\zeta) - \tilde{b}(\zeta) = \sum_{n=-\infty}^{\infty} (b_n^d - b_n) e^{-2\pi i \zeta n}$$

where the actual weights $\{b_n\}$ are extended to infinity by adding zeroes at both ends. But then we may apply Parseval's theorem for infinite sequences to get:

$$\epsilon^2 = \sum_{n=-\infty}^{\infty} |b_n^d - b_n|^2 = \sum_{n=-\infty}^{-M-1} |b_n^d|^2 + \sum_{n=M+1}^{\infty} |b_n^d|^2 + \sum_{n=-M}^M |b_n^d - b_n|^2$$

and since only the last term is adjustable, we minimize ϵ^2 by setting $b_n = b_n^d$. But this is no different from using a rectangular taper on the ideal sequence – and we have already seen that this produces filters with large sidelobes. Least squares (the L_2 norm) is not always the right choice.

The basic problem with the least-squares approach is that we are fitting to the ideal response using the two-norm (integral over the squared difference) that we introduced in Section 2.2. We get better filter responses if we instead use the infinity norm, and set the weights in equation (7.6) to minimize, over a specified range of frequencies, the maximum value of the misfit $|\tilde{b}_d(\zeta) - \tilde{b}(\zeta)|$. Finding such weights is conceptually and computationally more complicated than anything we have discussed so far, and we will not describe how to do so.

But we can describe the specifications used to design such a filter. We assume K non-overlapping frequency bands, each one bounded by a lower frequency ζ_{Lk} and upper frequency ζ_{Hk} . Then the goal is to find the M weights which minimize

$$c_k \max_{[\zeta_{Lk}, \zeta_{Hk}]} |\tilde{b}_d(\zeta) - \tilde{b}(\zeta)|$$

over all the bands; c_k is a weight applied to each band, which allows the fit to the ideal response to be tighter or looser. The actual amount of misfit mostly depends on the filter length M ; what this misfit actually is can only be determined after the optimal weights are found. Some trial and error is usually needed to decide on the appropriate tradeoff between length and misfit. This procedure gives very good designs, with more flexibility than the tapering method. The resulting filters are termed **equiripple filters**, because the maximum departure of the frequency response from the ideal is the same throughout each frequency band: the sidelobes in the plotted response are all the same size. A filter designed using this method is shown as the fourth example in Figure 7.5: by sacrificing low sidelobes at high frequency, the equiripple design can have a narrower transition band than any of the tapered designs.

The procedure for designing equiripple filters is called the Parks-McClellan algorithm; it is included in MATLAB as routine `firpm`; because this and other implementations are widely available, we do not describe the underlying algorithm, which is known as the Remez exchange method, and involves fitting Chebyshev polynomials (Figure 2.1) to the ideal response $\tilde{b}_d(\zeta)$.

There are many other variants of filter design by optimal fitting; we may, for example, require, as well as a good fit to \tilde{b}_d , that the derivative $d\tilde{b}/df$ have the

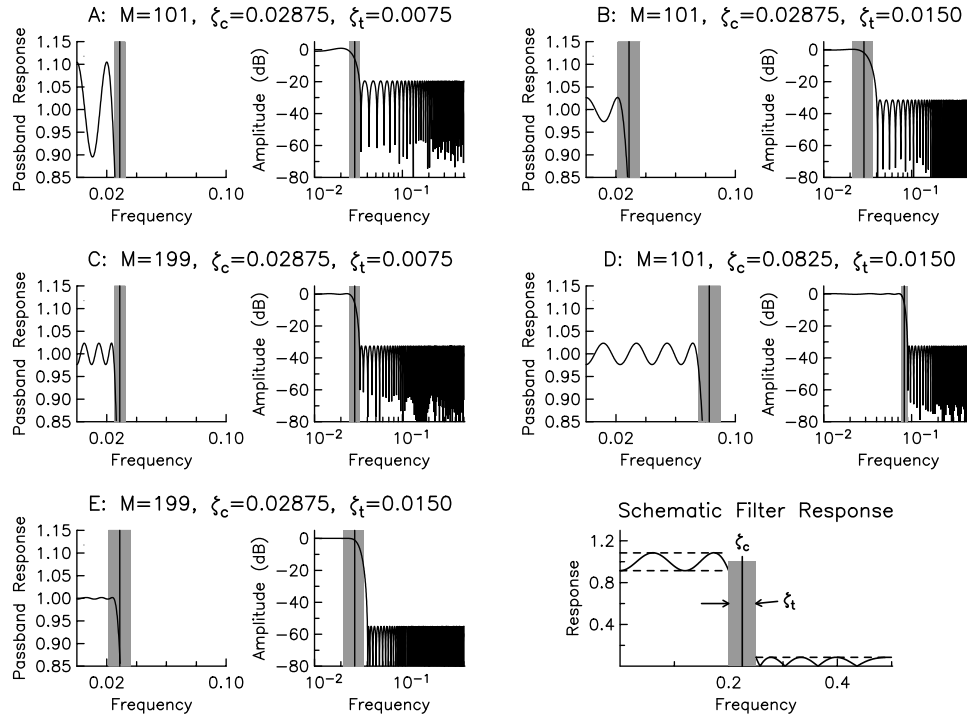


Figure 7.6: Equiripple filter designs. The lower right shows a schematic response, with the frequency parameters indicated. The different designs (A through E), have different frequency settings or lengths M . For each, the passband response is shown on a linear scale, the overall response in decibels.

same sign throughout the passband, to eliminate ripple there.⁴ But most such refinements are rarely important in geophysical data analysis.

7.2.3 A Filtering Example

We close with an example that illustrates how frequency-selective filters can be used, and also illustrates why there are no fixed rules for designing them – what filter you choose depends on the problem you want to solve. The data to be filtered are measurements of strain at Piñon Flat Observatory, made at one-second intervals with a long-base laser strainmeter. For the time period shown, these strain data show the signal from the 1994 Northridge earthquake, 203 km away. This signal, though dominated by the seismic waves from the earthquake, also contains

⁴Steiglitz *et al.* (1992) present a fairly general program for including different kinds of constraints using linear programming: relatively slow, but very flexible. See <http://www.cs.princeton.edu/~ken/meteor.html> for source code and examples.

Northridge Earthquake at PFO: Effects of Different Filters

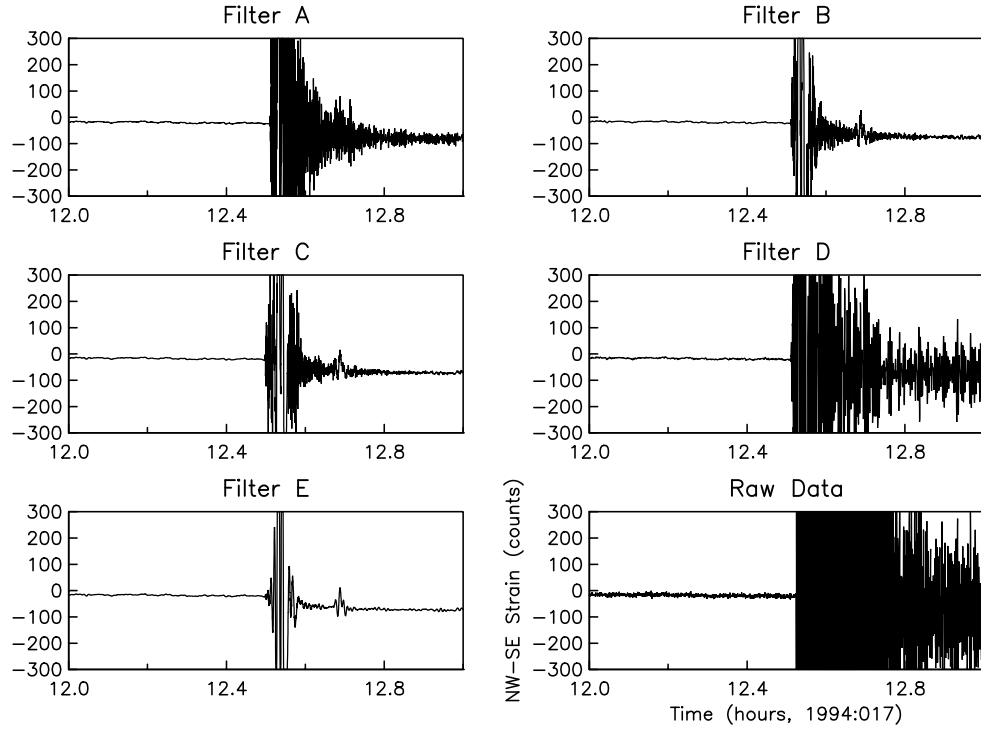


Figure 7.7: Strain variations from the Northridge earthquake recorded on the NW-SE laser strainmeter at Piñon Flat Observatory (PFO). The lower right plot is the original unfiltered data; this actually has a much larger range than is shown. Plots A through E show the results of low-passing the data with the filters whose response is shown in Figure 7.6. Since the data are sampled every second the dimensional values of the frequency, f , are the same as the nondimensional ones ζ .

the static change in strain caused by the elastic deformation of the rock. The aim of the filtering is to remove the “high-frequency” seismic signal so that the static change is shown more clearly.

For maximum flexibility we use the equiripple design; Figure 7.6 shows some possible filter responses. The lower right corner of this figure shows parameters which we can choose: the transition frequency ζ_c and the width of the transition band ζ_t . Once we choose these parameters, we next pick a length for the filter; the program will then find the best design possible, with the smallest amount of ripple in both the passband and stopband. We choose these amounts to be the same so the weights c_k both one, but we could (for example) make the sidelobes smaller while allowing more ripple in the passband.

Our first design (A) has a narrow passband, and a narrow transition band – and the consequence is that the ripple is large, nearly 10%. This means that in the stopband any signal will be only 0.1 of what it was originally – we would say, 20 dB down, which is not a large reduction. To do better, we can try two approaches: (B) make the transition band wider, and (C) use more filter weights (199 instead of 101). Either one gives much less ripple; for these two examples we are trading computation time (filter length) against the width of the passband response. In (D) we try making the passband much larger by increasing ζ_c ; in (E) we combine the larger ζ_t of (B) with the more numerous weights of (C) to get a response even closer to the ideal.

Figure 7.7 shows what these filters do to the data; without filtering the static offset is hidden in the seismic coda. Filter A reduces the code enough that the offset can be seen, but still leaves a lot of energy: looking at this plot, you would (or should) want to say that the “true” signal would be smoother, a sure sign that the data need more filtering. Filters B and C provide this, and since their stopband levels are the same, the results look about the same as well; between the two, B is probably preferable because it is shorter. A much wider passband (D) turns out to be a poor idea, at least for showing the static offset. Filter E is perhaps “best” for this application.

CHAPTER 8

DIGITAL FILTERS II: SIMULATING LINEAR SYSTEMS

Finite arithmetical differences have proved remarkably successful in dealing with differential equations

LEWIS F. RICHARDSON, *Weather Prediction by Numerical Process*
(1922)

8.1 Introduction

We now turn to digital filters used to imitate actual physical systems: specifically the linear time-invariant systems, operating in continuous time, that we introduced in Section 2.5. These are usually called **analog systems**. Consider what is involved in modeling observed seismograms. First we need to compute a synthetic seismogram; this gives, for some source and earth structure, the ground motion that is input to the seismometer. Next, we need a digital simulation of the seismometer, either to produce a synthetic output that can be compared with the observations, or estimate the ground motion from them. The FIR filters of Chapter 7 are not well-suited for this.

Simulation is a relatively narrow topic, but worth a chapter because it leads to ways to describe a particular (but common) class of analog systems. These ways in turn lead to ways to describe the digital filters given by the general equation (7.1). These two descriptions are key to showing how to make a digital filter that will simulate analog systems.

8.2 Lumped-Parameter Systems

We saw in Section 2.5 that we could describe a linear time-invariant system in three ways:

- By its frequency response $\tilde{g}(f)$, which expresses the (complex-valued) ratio between output and input when the input is a pure sinusoid, $e^{2\pi ift}$.

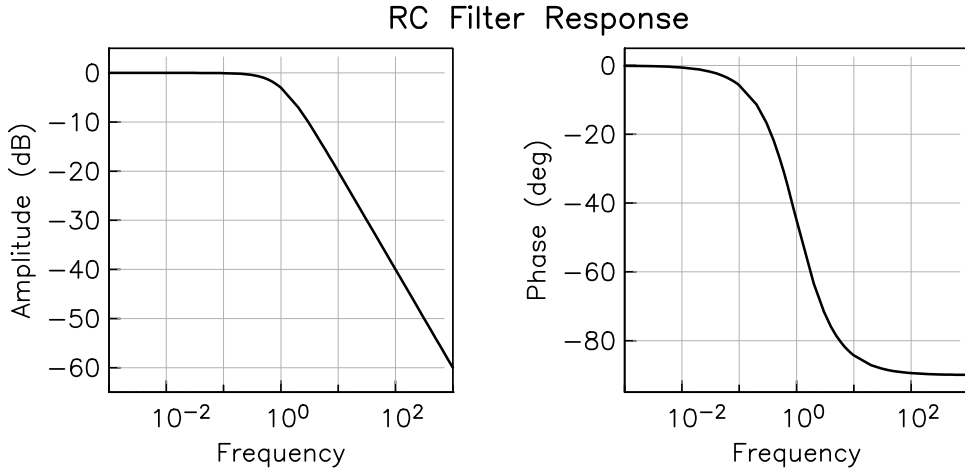


Figure 8.1: Frequency response of an RC filter with $\tau = 1$, shown as log amplitude, and phase, plotted against log frequency.

- By its impulse response $g(t)$: the output when the input is a delta function. The frequency response is $\tilde{g}(f) = \mathcal{F}[g(t)]$.
- By the step response $h(t)$, which is the integral of $g(t)$: something that (unlike $g(t)$) can actually be measured.

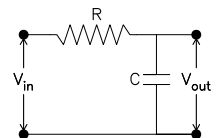
This is completely general; we now focus on a particular class of linear time-invariant systems that is broadly useful in modeling physical processes. This class is systems modeled by constant-coefficient linear differential equations; these are often called **lumped-parameter systems**). In such systems the input x and output y are related through a differential equation

$$\begin{aligned} & a_0 y + a_1 \frac{dy}{dt} + \dots + a_{K-2} \frac{d^{K-2}y}{dt^{K-2}} + a_{K-1} \frac{d^{K-1}y}{dt^{K-1}} \\ &= b_0 x + b_1 \frac{dx}{dt} + \dots + b_{M-2} \frac{d^{M-2}x}{dt^{M-2}} + b_{M-1} \frac{d^{M-1}x}{dt^{M-1}} \end{aligned} \quad (8.1)$$

where the a 's and b 's are the parameters that describe the system.

There are standard procedures for solving these differential equations to get explicit forms for $y(t)$, especially for certain classes of inputs $x(t)$, but we instead look at the frequency response of systems that obey them, starting with a few examples.

- The first example is the simplest analog electronic filter: the RC lowpass filter, which consists of a resistor and capacitor in series, with input and output voltages as shown. The input voltage $V_{in}(t)$ is just the output voltage



$V_{out}(t)$ plus the voltage drop across the resistor, which is given by $RI(t)$, where $I(t)$ is the current flowing through the capacitor. This current is given by $I(t) = CV_{out}(t)$, making the differential equation

$$V_{out}(t) + RC \frac{dV_{out}}{dt}(t) = V_{in}(t) \quad (8.2)$$

To get the frequency response, we assume, as usual, a sinusoidal input $V_{in}(t) = e^{2\pi ift}$; by the definition of \tilde{g} , $V_{out}(t) = \tilde{g}(f)e^{2\pi ift}$. Substituting into equation (8.2) gives

$$\tilde{g}(f) = \frac{1}{1 + 2\pi if\tau} \quad (8.3)$$

where $\tau = RC$ is the time constant of the filter. Figure 8.1 shows, for $\tau = 1$, the amplitude (in dB) and phase of $\tilde{g}(f)$ plotted against the logarithm of the frequency: such depictions are called **Bode plots**. High frequencies are attenuated, so this is a lowpass filter.

- The second example is a seismometer, which we already discussed in Section 2.5.1. As we saw there (equation 2.33), the frequency response to displacement is:

$$\tilde{g}(f) = \frac{-f^2}{-f^2 + i\lambda f_0 f + f_0^2}$$

whose phase and amplitude response we showed in Figure 2.6: these too are Bode plots.

- Our third example is more geophysical: the Earth's polar motion (Lambeck, 1988; Gross, 2015). Time variations in the angular momentum and mass distribution of the fluid parts of the Earth cause the position of the rotation pole of the solid earth to change. This position can be described by two coordinates, p_1 and p_2 , giving the displacement of the North rotation pole toward the Greenwich meridian and at 90° to it. If these changes are small, it can be shown that the relationship between the pole position and the motions of the fluid parts is

$$\frac{1}{\omega_c} \frac{dp_1(t)}{dt} + p_2(t) = \psi_2(t) \quad \frac{1}{\omega_c} \frac{dp_2(t)}{dt} + p_1(t) = \psi_1(t) \quad (8.4)$$

where ψ_1 and ψ_2 are integrals over the mass distribution and velocity of the atmosphere, ocean and fluid core; these are usually called the “excitation”.

For a rigid ellipsoidal body $\omega_c = [(C - A)/A]\Omega$, where C and A are the polar and equatorial moments of inertia, and Ω is the angular frequency of the Earth's spin (2π per day). The values of C and A for the Earth give a value for ω_c that corresponds to a period of 305 days; corrections for the elasticity

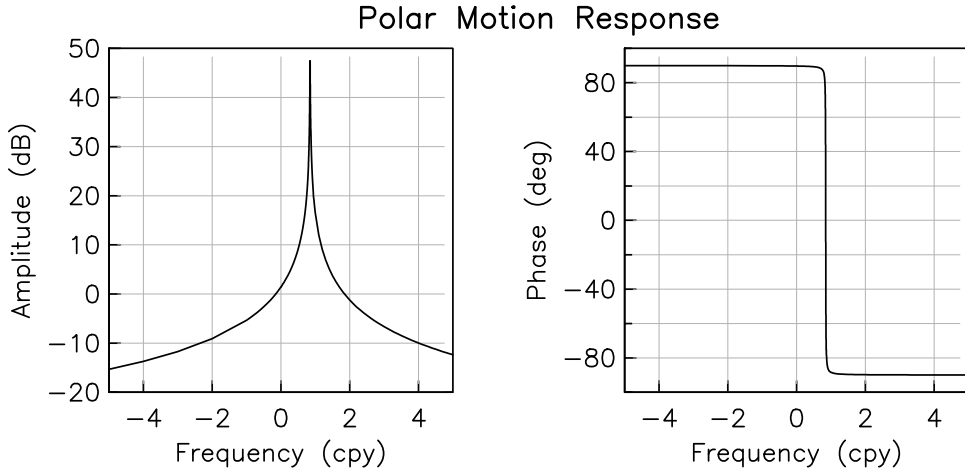


Figure 8.2: Response of the Earth's polar motion to excitation; since we represent the input and output as complex numbers we must show both positive and negative frequency. The response is given for a Q of 100; the Chandler resonance is at 0.849 cycles/year. The rapid change of phase at this frequency makes it difficult to compare the polar motion with excitations.

of the Earth, and for the fluid ocean, make the actual period close to 430 days (Smith and Dahlen, 1981).

As in Appendix B.4, we can write this pair of equations as a single equation by forming the complex variables $\mathbf{p} = p_1 + ip_2$ and $\psi = \psi_1 + i\psi_2$. The two equations (8.4) then become

$$\frac{i}{\omega_c} \dot{\mathbf{p}}(\mathbf{t}) + \mathbf{p}(\mathbf{t}) = \psi(\mathbf{t})$$

If we make the input $e^{2\pi ift}$, and the output $\tilde{g}(f)e^{2\pi ift}$, we find

$$\tilde{g}(f) = \frac{1}{1 - (2\pi f/\omega_c)} \quad (8.5)$$

which has (after we modify ω_c in equation (8.11) below) the form shown in Figure 8.2. Here we do have to show both positive and negative frequency because, as is usual in gyroscopic systems, the response is different for clockwise rotation (negative frequency) and counterclockwise rotation (positive), with a resonance peak (in this case) only for the latter.

8.3 The Laplace Transform: Poles and Zeros

Another way of looking at the response of a lumped-parameter system comes from generalizing the Fourier transform into the **Laplace transform**, which for a function $x(t)$ is defined as

$$\tilde{x}(s) = \int_{-\infty}^{\infty} x(t)e^{-st} dt$$

where s is a complex number. We use $\tilde{\cdot}$ for both Fourier and Laplace transforms and distinguish them by what letter (s , f , or ζ) we use for the argument.

The transform $\tilde{x}(s)$ is defined on the complex plane, and it should be obvious that the Fourier transform $\tilde{x}(f)$ is just $\tilde{x}(s)$ evaluated along the imaginary axis of that plane; that is, $\tilde{x}(f) = \tilde{x}(s)$ for $s = 2\pi if = i\omega$. The Laplace transform can thus be thought of as a generalization of the Fourier transform; but, partly because $\tilde{x}(s)$ is a complex-valued function over the complex plane, the Laplace transform is much more difficult to visualize. We will not be using the inverse Laplace transform, but for completeness, we note that it is

$$x(t) = \frac{1}{2\pi} \int_{c-i\infty}^{c+i\infty} \tilde{x}(s)e^{st} ds$$

The integral is evaluated over a line parallel to the imaginary axis; the value c of the real part of this line depends on the nature of $\tilde{x}(s)$. The Laplace transform pair is thus less symmetric than the Fourier transform pair.

We have introduced the Laplace transform because, for the lumped-parameter systems of equation (8.1), it enables us to understand much about a system without solving the differential equation at all. To see how this works, we first take the Fourier transform of both sides of equation (8.1), which gives us the same result as substituting $e^{2\pi ift}$ as the input; see the examples in Section 8.2. What we mean by “taking the Fourier transform of the system” is to find the equation that describes the connection between the Fourier transforms of the input and output: that is, between $\tilde{x}(f)$ and $\tilde{y}(f)$. We get this equation by applying the theorem for the Fourier transform of the derivative of a function (equation 3.15) to equation (8.1); this converts the differential equation to two polynomials in f :

$$\begin{aligned} \tilde{y}(f)[a_0 + a_1(2\pi if) + \dots + a_{K-2}(2\pi if)^{K-2} + a_{K-1}(2\pi if)^{K-1}] &= \\ \tilde{x}(f)[b_0 + b_1(2\pi if) + \dots + b_{M-2}(2\pi if)^{M-2} + b_{M-1}(2\pi if)^{M-1}] \end{aligned}$$

where \tilde{y} and \tilde{x} are the Fourier transforms of y and x . The frequency response is then

$$\tilde{g}(f) = \frac{\tilde{y}(f)}{\tilde{x}(f)} = \frac{\sum_{m=0}^{M-1} b_j(2\pi if)^j}{\sum_{k=0}^{K-1} a_k(2\pi if)^k} \quad (8.6)$$

We can follow a similar route if we take the Laplace transform of both sides of (8.1). This might at first seem like an unnecessary generalization (who needs the system

response at a complex frequency?), but it leads to a very useful way of describing the system.

To do this we need the derivative theorem for the Laplace transform, which we simply state without proof: if $\tilde{x}(s)$ is the Laplace transform of $x(t)$, the Laplace transform of $\dot{x}(t)$ is $s\tilde{x}(s)$. Applying this rule to the differential equation shows that the ratio of the Laplace transforms of the input and output is

$$\frac{\tilde{y}(s)}{\tilde{x}(s)} = \frac{\sum_{k=0}^{M-1} b_m s^m}{\sum_{k=0}^{K-1} a_k s^k} \quad (8.7)$$

This ratio of two complex polynomials is called the **transfer function**. Comparing equation (8.7) with equation (8.6), we see that the frequency response $\tilde{g}(f)$ is just the transfer function $\tilde{g}(s)$ evaluated for s on the imaginary axis.

8.3.1 Poles and Zeros

The additional insight into the system comes from factoring the polynomials in (8.7) and rewriting them products of monomials, each monomial containing a root of the polynomial:

$$\frac{\tilde{y}(s)}{\tilde{x}(s)} = C \frac{\prod_{m=1}^{M-1} (s - r_m)}{\prod_{k=1}^{K-1} (s - p_k)} \quad (8.8)$$

The polynomial roots in equation (8.8) fall into two categories. The roots r_m of the numerator are called the **zeros**, since if $s = r_m$ the transfer function is zero; the roots p_k of the denominator are called the **poles**, since if $s = p_k$ the transfer function is infinite. The scaling value, C , is needed to make the description complete. If we start with the expression (8.7), the values of r_m and p_k can be found analytically only if K or M is less than five – which is true for our three examples. For higher values of K or M the factors (roots) must be found numerically – which can be quite difficult if these values are large.

Looking at the locations of the poles and zeros, and particularly how close they are to the imaginary axis, provides an immediate sense of the frequency response. We can easily see that frequencies at which the response is large will be those that are near poles that are close to the imaginary axis. Conversely, zeros close to the imaginary axis will produce dips in the amplitude response. For our three examples

- The RC filter has a transfer function

$$\tilde{g}(s) = (1 + \tau s)^{-1} \quad (8.9)$$

which has a single pole on the negative real axis at $s = \tau^{-1}$. This is shown in the lower left frame of Figure 8.3; as is conventional, we use a cross to show the location of a pole.

- The seismometer transfer function is

$$\tilde{g}(s) = \frac{s^2}{s^2 + 2\lambda\omega_0 s + \omega_0^2}$$

which has a pair of zeros at the origin of the s -plane: so \tilde{g} is zero there. The poles lie at $\omega_0[-\lambda \pm \sqrt{\lambda^2 - 1}]$, the top three frames of Figure 8.3 show them for different values of λ . For $\lambda = 0$, the poles are on the imaginary axis, at $\pm i\omega_0$. Since this axis corresponds to the frequency axis for the Fourier transform, these on-axis poles make $\tilde{g}(\pm\omega_0)$ infinite. As λ increases from zero, the two poles leave the imaginary s -axis and follow a circular path about the origin. Because the coefficients of the polynomial are real, its roots (these poles) must be complex conjugates, which makes the frequency response the same for positive and negative frequencies. A value of λ close to 0.8 gives the flattest response in the passband; the electrical engineering description of this would be a two-pole Butterworth filter. At $\lambda = 1$ (critical damping) the poles meet; for larger values they lie on the negative real axis, one approaching and the other receding from the origin.

- The transfer function for polar motion is, from equation (8.5),

$$\tilde{g}(s) = \frac{\mathbf{p}(\mathbf{s})}{\psi(s)} = \frac{1}{1 + is/\omega_c} = \frac{\omega_c}{\omega_c + is} \quad (8.10)$$

which has a single pole, on the imaginary axis, at $s = i\omega_c$. Again, this gives an infinite response for $2\pi f = \omega_c$: in the Earth this resonance gives rise to the Chandler wobble, hence the subscript c on ω_c . In reality dissipation keeps the response from being infinite; we can add this effect to the transfer function by moving the pole slightly away from the imaginary axis. We do so by redefining ω_c as

$$\omega_c = \frac{2\pi}{T_c} \left(1 + \frac{i}{2Q_c} \right) \quad (8.11)$$

where T_c is the period of the resonance, and Q_c a measure of the amount of dissipation.¹ This adjustment illustrates the power of the pole-zero description: we have been able to introduce dissipation without revisiting the differential equation.

For all our examples, including the last one with finite Q_c , the poles are to the left of the imaginary axis. This is good, because a transfer function with poles in the right half-plane describes an unstable system: any nonzero input would lead,

¹It is certain that dissipation occurs in the Chandler wobble, but what causes it remains unclear. Smith and Dahlen (1981) provide an exhaustive discussion of the theoretical values for these two parameters, updated by Benjamin *et al.* (2006).

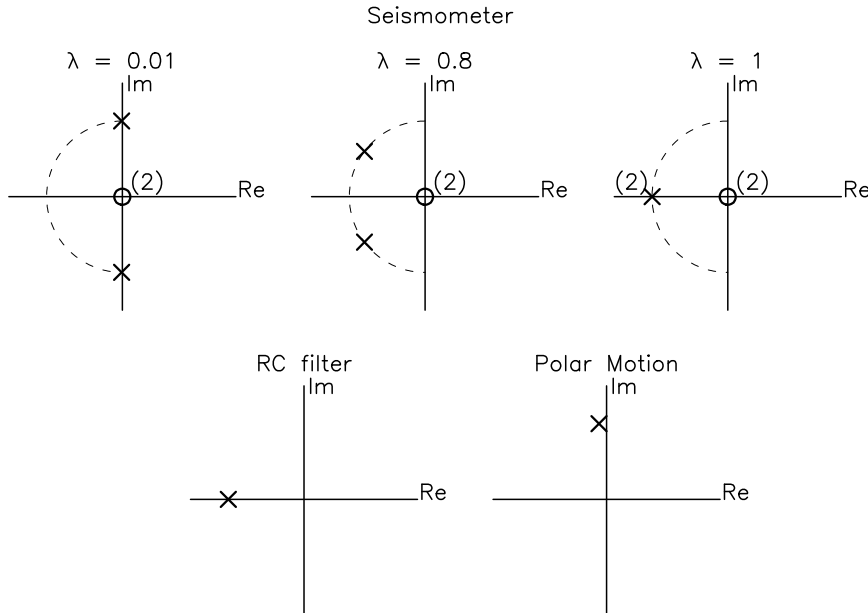


Figure 8.3: Pole-zero plots, showing the locations of these on the complex s -plane for some analog systems. Poles are crosses, zeros circles; multiple roots have numbers next to them.

eventually, to an infinite output. Consider the seismometer equation (2.32), which would have poles in the right half-plane if the damping λ was negative. Looking at its differential equation (2.32), it is easy to see why this would be unstable: the term $2\lambda\omega_0\dot{y}$ would correspond to a force acting in the direction that the mass moves, not against it, which would feed energy into the system for any input motion. While this particular system is unphysical, it is perfectly possible to build actual systems that are unstable. Only for the simplest systems is it obvious from looking at the differential equation whether a system is stable or not; but for any lumped-parameter system, finding the poles of the transfer function shows this immediately.

8.4 The z -transform for Digital Filters

In Chapter 5 we introduced the Fourier transform for sequences. We have seen that the Laplace transform can be regarded as a generalization of the Fourier transform of a continuous function; the equivalent generalization for sequences is called the **z -transform**. An infinite sequence $\{x_n\}$ has a z -transform $\mathcal{Z}[\{x_n\}]$ that

is a function of the complex variable z , and is defined as

$$\mathcal{Z}[\{x_n\}] = \tilde{x}(z) = \sum_{n=-\infty}^{\infty} x_n z^{-n} \quad (8.12)$$

It is important to note that equation (8.12) *not* a definition that is universally followed. In particular, the geophysical exploration industry (which does a lot of signal processing) defines the z -transform as a sum over $x_n z^n$: a positive exponent.² We follow the convention in electrical engineering; so if we call our z variable z_{ee} , and the exploration one z_{oil} , $z_{ee} = z_{oil}^{-1}$. Since z is a complex variable, these usages are equivalent to an inversion of the complex plane on the unit circle: the outside of the circle becomes the inside, and vice-versa, with the origin and infinity mapping into each other. In looking at results, or software, you need to know which convention is used.

We have seen that the Fourier transform can be viewed as the Laplace transform evaluated on the imaginary axis of the s -plane. In the same way, the Fourier transform of a sequence is a special case of the z -transform. Remember that the Fourier transform of a sequence is

$$\tilde{x}(\zeta) = \sum_{n=-\infty}^{\infty} x_n e^{-2\pi i \zeta n} \quad (8.13)$$

This is equivalent to the z -transform for $z = e^{2\pi i \zeta}$; in words, the Fourier transform of a sequence is the z -transform of that sequence on the unit circle in the complex z -plane. By design, this fits in with the “circular frequency” that we introduced in Figure 2.3.

There are other ways of looking at the z -transform; for example, we can regard z^{-1} as a unit delay of the sequence. This may sound peculiar, but is really just a generalization of the Fourier shift theorem for sequences, as described in Section 5.6.1. Suppose y is the same series as x , but delayed by m terms: $y_n = x_{n-m}$. Then the z -transform of y is

$$\tilde{y}(z) = \sum_{n=-\infty}^{\infty} x_{n-m} z^{-n} = \sum_{l=-\infty}^{\infty} x_l z^{-(l+m)} = \tilde{x}(z) z^{-m} = \tilde{x}(z)(z^{-1})^m \quad (8.14)$$

so that the effect of delaying x is to multiply the z -transform by z^{-1} a total of m times: z^{-1} “represents” a delay. (That is, z_{ee}^{-1} does; in the geophysical exploration industry, z_{oil} does.)

Another way to look at the z -transform comes from taking the Laplace transform of the function which is equivalent to the sequence x_n , namely $\sum_{n=-\infty}^{\infty} x(n) \delta(u-n)$ (equation 5.4) which we used in Section 6.2 (modified to equation 6.2) to discuss

²This reflects historical happenstance, namely that Enders Robinson, who introduced digital signal processing into geophysical exploration, used this convention.

Mapping from Sampling the Laplace Transform

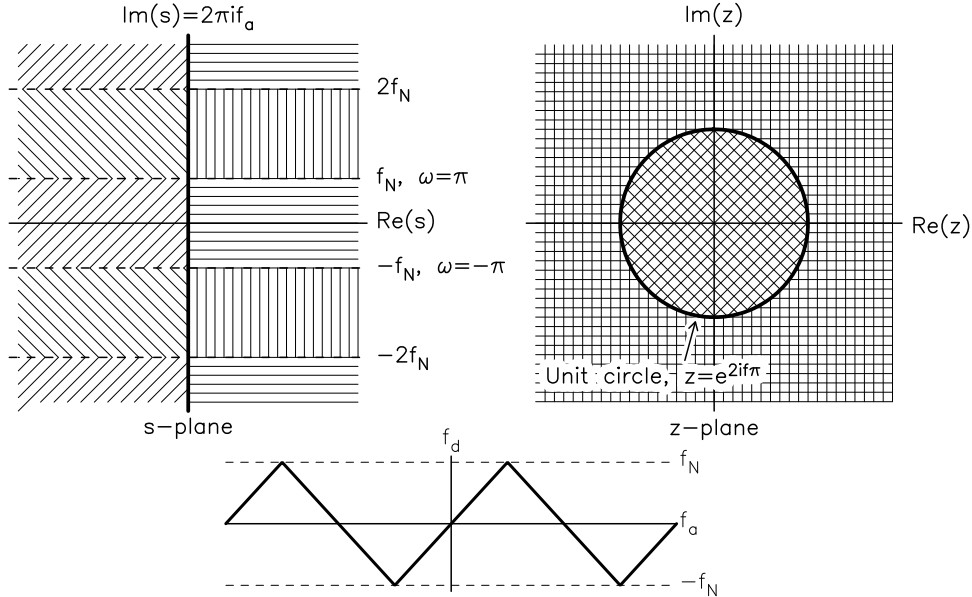


Figure 8.4: Mapping between the *s*-plane and the *z*-plane if the sequence in discrete time is produced by regular sampling in continuous time. The right-hand side of the *s*-plane maps outside the unit circle in the *z*-plane, and the left-hand side to the inside of the unit circle, but in both cases the mapping is not one-to-one. The bottom plot shows how the continuous-time frequency f_a maps into discrete-time frequency f_d .

sampling of a function given in continuous time. The Laplace transform of this infinite sum of delta functions is

$$\int_{-\infty}^{\infty} \sum_{n=-\infty}^{\infty} x_n \delta(t-n) e^{-st} dt = \sum_{n=-\infty}^{\infty} x_n \int_{-\infty}^{\infty} e^{-st} \delta(t-n) dt = \sum_{n=-\infty}^{\infty} x_n e^{-sn}$$

which becomes equivalent to the *z*-transform if we set

$$z = e^s \quad (8.15)$$

a **mapping** from the *s*-plane to the *z*-plane. As we will see, such mappings are important in devising discrete-time (digital) models of continuous-time (analog) systems.

The mapping of equation (8.15), and shown in Figure 8.4, has an important feature, namely that in going from *s* to *z* it is nonunique: different points in the *s*-plane all map to the same point in the *z*-plane: we can find *z* for any *s*. The mapping in the other direction is therefore multivalued, which is not a desirable property.

If we consider the strip for which $|\Im(s)| \leq \pi$ (Figure 8.4) we see that the region of the strip with negative real part maps inside the unit circle, the region with positive real part maps to outside the unit circle, and the segment of the imaginary axis that lies in the strip maps onto the unit circle.³ But exactly the same mapping occurs for each strip defined by $m - \pi \leq \Im(s) \leq m + \pi$, for any integer m . This is yet another example of aliasing: when we form a sequence by sampling a function, one frequency in the sequence could come from many different frequencies in the function (bottom panel in Figure 8.4). The mapping (8.15) can be said to generalize aliasing to complex frequencies.

It is possible to use complex-variable theory to find the inverse of the z -transform, and also to derive extensions to the convolution theorems in order to show, for example, how to convolve two z -transforms to get the z -transform of the product of two sequences. Since these results are not needed to design filters for system simulation, we do not discuss them further; see [Oppenheim and Schafer \(1989\)](#) for the details.

8.5 Recursive Digital Filters

To simulate an analog system we need the more general filter described by equation (7.1), which we rewrite by shifting all the recursive terms to the left side

$$\sum_{k=0}^{K-1} a_k y_{n-k} = \sum_{m=0}^{M-1} b_m x_{n-m} \quad (8.16)$$

where x_n is the input sequence and y_n is the output. Note that the a 's here have the opposite sign of those in equation (7.1), and in that equation a_0 , being just a scaling factor, is set to one. As we noted in Section 7.1, because the sum over k is one-sided, we can compute the “current” value of y , y_n , without needing any values of y except for the “past” ones that we have already computed. Summing over only past values of x is not necessary (except in real-time processing) but is the usual convention for this class of filters.

Just as we used the Laplace transform to find the transfer function of a differential equation, we can use the z -transform to find a transfer function for a discrete-time filter. If we take the z -transforms of both sides of equation (8.16), and use the result (8.14) that the z -transform of a delayed sequence is z^{-m} times the transform of the original sequence, the two sides of (8.16) become polynomials in z . The transfer function is the ratio of these polynomials:

$$\frac{\tilde{y}(z)}{\tilde{x}(z)} = \frac{\sum_{m=0}^{M-1} b_m z^{-m}}{\sum_{k=0}^{K-1} a_k z^{-k}} \quad (8.17)$$

³In geophysical-exploration usage, the mappings to the inside and outside of the circle would be reversed.

An FIR filter will have only the numerator term, and if it is acausal (as zero phase shift FIR filters are) the range of summation will include negative as well as positive values of m .

As in equations (8.7) and (8.8) we can express the polynomials in z as products of their roots:

$$\frac{\tilde{y}(z)}{\tilde{x}(z)} = C \frac{\prod_{m=1}^{M-1} (z - r_m)}{\prod_{k=1}^{K-1} (z - p_k)} \quad (8.18)$$

So we can also describe digital filters in terms of their poles and zeros. In a purely recursive filter, in which only the present value of x is used, $M = 1$ and the numerator is constant, so there are only poles. Similarly, an FIR filter ($K = 1$) has only zeros. As in equation (8.8), at the zeros the transfer function is zero; and at the poles it is infinite. For the frequency response what matters is the proximity of the poles (or zeros) to the unit circle, since the z -transform always maps the frequency axis to this circle. In Section 9.4 we will see how we can design certain kinds of filters by manipulating the locations of these roots.

8.5.1 Recursive Filters for Simulation

The parallel between (8.16) and (8.17) on the one hand, and the differential equation (8.1) and its transfer function (8.7) is quite intentional: this parallelism shows how to simulate an analog system with a digital filter. Given the differential equation (8.1) the simulation problem is one of finding the coefficients of a digital filter (equation 8.16) whose digital transfer function (equations 8.17 or 8.18) will best match the analog transfer function (equation 8.7),

We start with our simplest analog system, the lowpass RC filter, and examine the step response. If $x(t) = x_0$ the solution to the differential equation (8.2) is $y = x_0$. If at time $t = 0$, $x(t)$ changes from x_0 to zero, then for $t > 0$, $y = x_0 e^{-t/\tau}$: an infinitely long response that cannot be reproduced by a FIR filter, or even efficiently approximated. But a very simple recursive filter can give a similar response. This is

$$y_n - ay_{n-1} = x_n(1-a) \quad (8.19)$$

Again, if $x_n = x_0$ then $y_n = x_0$. If x_n is x_0 for $n \leq 0$, and 0 for $n > 0$, it is easy to compute y :

$$y_0 = x_0 \quad y_1 = ax_0 \quad y_2 = a^2x_0 \quad \dots \quad y_m = a^m x_0 = e^{m \ln a} x_0$$

giving the same exponential falloff as in the analog filter. However, the transfer function of this digital filter is

$$\tilde{y}(z)(1 - az^{-1}) = \tilde{x}(z)(1 - a) \quad \text{or} \quad \frac{\tilde{y}(z)}{\tilde{x}(z)} = \frac{1 - a}{1 - az^{-1}}$$

which has the frequency response (using $z = e^{2\pi i \zeta}$)

$$\frac{1-a}{1-ae^{-2\pi i \zeta}} \quad (8.20)$$

where ζ is the dimensionless frequency, with $-\frac{1}{2} \leq \zeta < \frac{1}{2}$ (the range between the Nyquist frequencies). Clearly the analog response (8.3) and the digital response (8.20) are not the same.

Before describing how to design a recursive filter whose response will better match the analog response, we need to describe the stability criterion for digital filters. If we look at the output of the discrete-time filter (equation (8.19), we see that for $a < 1$, the output decays when x goes to zero (from x_0); but if we had $a > 1$ the output would increase exponentially. In this case the value of a determines if the filter is stable or unstable, the boundary being $a = 1$, for which the filter is metastable. In the z -plane, the filter has one pole, at $z = a$, so the condition for stability is that the pole be inside the unit circle. This is a special case of a general result: for a discrete-time filter to be stable, all its poles must be *inside* the unit circle,⁴ just as a stable continuous-time system must have poles only on the negative real half of the s -plane. These stability criteria are important because we want any mapping from the s -plane to the z -plane to preserve stability: the “stable” part of each plane should map only into the stable part of the other.

The mapping given by equation (8.15), corresponding to sampling, fulfills the criterion of mapping the stable part of the s -plane into the stable part of the z -plane, but some others do not. For example, creating discrete-time systems by replacing derivatives by forward differences creates a mapping that fails this requirement: if we perform this substitution on a stable differential equation, the resulting discrete-time filter might not be stable.

8.5.2 The Bilinear Transform

For system simulation a better mapping than equation (8.15) is the **bilinear transformation**. To motivate it, we again construct a discrete-time system from a differential equation, but instead of using numerical differences to approximate derivatives, we use numerical approximations to integrals.

We start with the fundamental theorem of calculus (relating integration and differentiation):

$$y(t) = \int_{t_0}^t \dot{y}(u) du + y(t_0)$$

For equispaced intervals, which we set equal to one, this becomes

$$y(n) = \int_{n-1}^n \dot{y}(u) du + y(n-1)$$

⁴For our convention; for z_{oi} the poles must all be outside the circle.

We now apply the trapezoidal rule for approximating the integral:

$$y(n) = \frac{1}{2}[\dot{y}(n) + \dot{y}(n-1)] + y(n-1)$$

At this point, we need an expression for \dot{y} ; we get this from the differential equation for a linear system, and to keep our derivation as simple as possible we use the one for an RC filter, equation (8.2): $\dot{y}(t) = \tau^{-1}[x(t) - y(t)]$. The expression for $y(n)$ then becomes

$$y(n) = \frac{1}{2\tau}[x(n) + x(n-1) - y(n) - y(n-1)] + y(n-1)$$

which we may, finally, write in the form (8.16) of a recursive filter. Since we are now working with a sequence we use subscripts rather than arguments to get:

$$y_n \left(1 + \frac{1}{2\tau}\right) - y_{n-1} \left(1 - \frac{1}{2\tau}\right) = \frac{1}{2\tau}(x_n + x_{n-1})$$

The transfer function in the z -plane of this discrete-time filter is found in the usual way; we take z -transforms to get

$$\tilde{y}(z) \left[\left(1 + \frac{1}{2\tau}\right) - z^{-1} \left(1 - \frac{1}{2\tau}\right) \right] = \tilde{x}(z) \frac{1+z^{-1}}{2\tau}$$

so that the transfer function is

$$\frac{1}{1 + 2\tau \left(\frac{1-z^{-1}}{1+z^{-1}} \right)}$$

We can equate this with the transfer function for the continuous-time case, equation (8.9), if we make the relationship between s and z

$$s = 2 \left(\frac{1-z^{-1}}{1+z^{-1}} \right) \quad (8.21)$$

which is the bilinear transformation.

In the more general case where the sampling interval is Δ , the same derivation may be used to give the same result, with the leading 2 in equation (8.21) replaced by $2/\Delta$. The inverse mapping from s to z is then

$$z = \frac{1 + \frac{1}{2}s\Delta}{1 - \frac{1}{2}s\Delta} \quad (8.22)$$

While our derivation used a particular differential equation, using multiple integrals for any constant-coefficient linear differential equation will produce the same mapping. This mapping takes the imaginary axis of the s -plane onto the unit circle in the z -plane; since it maps the entire left half of the s -plane into the inside of the unit circle on the z -plane, it maintains stability.

The bilinear transformation thus gives us a design procedure for getting discrete-time filters from continuous-time ones. The steps are:

Mapping for Bilinear Transformation

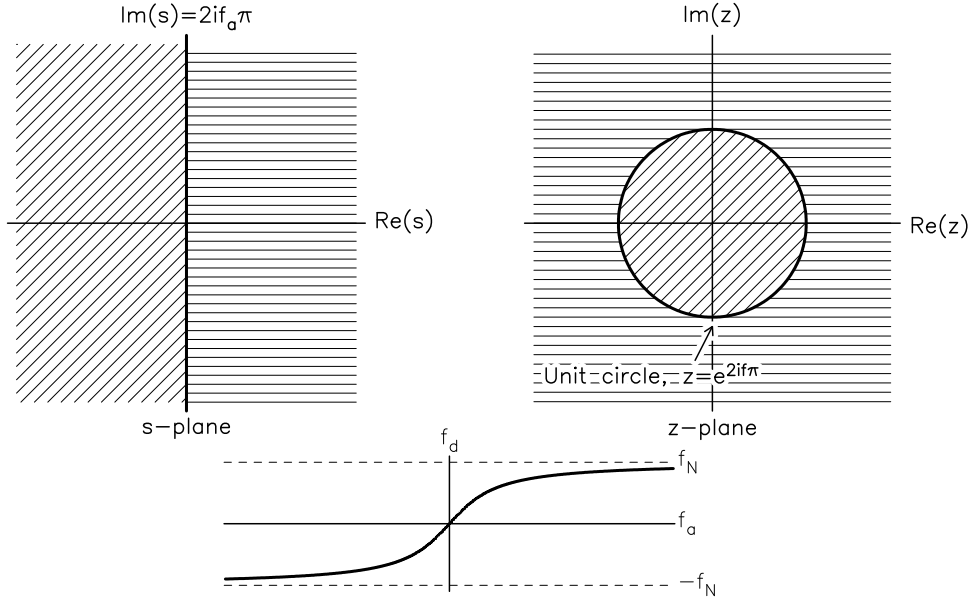


Figure 8.5: Mapping between the s -plane and the z -plane if the bilinear transformation is used. The right-hand side of the s -plane maps outside the unit circle in the z -plane, and the left-hand side to the inside of the unit circle; in both cases the mapping is one-to-one. The bottom plot shows how the continuous-time frequency f_a maps into discrete-time frequency f_d : the mapping is one-to-one, but nonlinear, though approximately linear for $f_a \ll f_N$.

1. Find the transfer function in the s -plane from the differential equation of the system; this will be a ratio of polynomials in s .
2. Perform the bilinear mapping (8.22) to produce a transfer function in the z -plane; reduce this to a ratio of polynomials in z .
3. Get the filter weights from the coefficients of the polynomials, as in the relation between (8.16) and (8.17).

There is often a “step zero”, in which we modify the parameters in the differential equation to minimize the effect of the bilinear mapping on a particular frequency. Let the frequency of the discrete-time system be ζ_d , so that (equation (8.13)) $z = e^{2\pi i \zeta_d}$, and of the analog system be f_a , so that $s = 2\pi i f_a$. Then

$$\frac{1 - z^{-1}}{1 + z^{-1}} = i \tan(\pi \zeta_d)$$

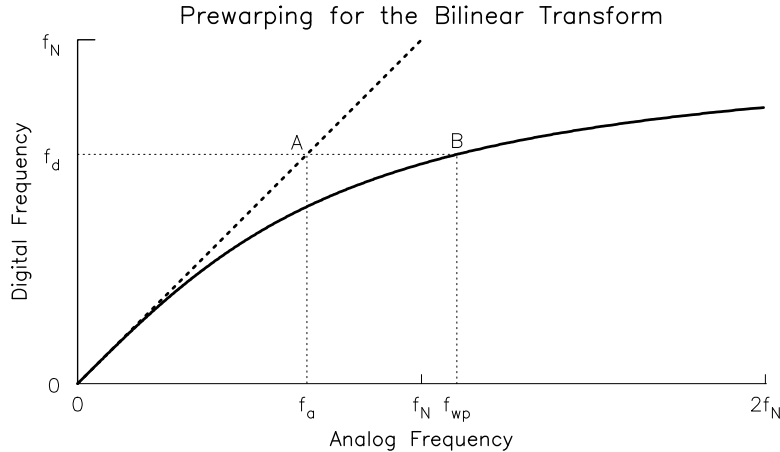


Figure 8.6: Illustration of prewarping for the bilinear transform. The heavy line is the mapping of analog to digital frequency shown in Figure 8.5, for $f \geq 0$. An analog frequency f_a would map to a digital frequency f_d (through the point A) if the mapping were linear (as in Figure 8.4). For the digital simulation to have the appropriate behavior, the frequency f_{wp} (or the equivalent time constant) must be used in the differential equation from which the z -transform and filter weights are derived; this maps through the nonlinear relation (point B) to the appropriate f_d . In the example shown, f_a is two-thirds of the Nyquist frequency f_N , so that f_{wp} has to be substantially larger: indeed, larger than the Nyquist frequency. If we start with an analog frequency greater than f_N , we cannot map it to a digital—but, if the system has a time constant comparable to the sample interval, we cannot model it accurately.

so that the bilinear transformation of the frequencies is

$$\zeta_d = \frac{1}{\pi} \arctan(\pi f_a \Delta)$$

which maps the entire analog frequency axis, from $-\infty$ to ∞ , onto the digital frequencies from $-\frac{1}{2}$ to $\frac{1}{2}$: that is, from the lower to the upper Nyquist frequencies.

This warping of the frequency axis, though it avoids aliasing of the filter response, means that we must adjust the time constants of the differential equation so that after applying the bilinear transformation these have the correct frequency, an adjustment known as **prewarping**, illustrated schematically in Figure 8.6

To give an example that involves all these steps, we design a filter to simulate polar motion, equation (8.4). If we apply the bilinear transformation (8.21) to the transfer function (8.10), and compute the frequency response of the resulting digital filter, we find that it is

$$\frac{\omega'_c}{\omega'_c - (2/\Delta)\tan(\pi f_\Delta)} \quad (8.23)$$

where we have used ω'_c to denote that this parameter is not necessarily the same one as in the actual continuous-time system. For ω_c real, the frequency of the resonance in the continuous-time system is at $f_a = \omega_c/2\pi$; when the series is sampled at an interval Δ , this becomes the (nondimensional) frequency $\omega_c\Delta/2\pi$, providing it is not aliased.

Because of the warping of the frequency axis, the resonance in our discrete-time simulation filter will actually be at an apparent frequency of

$$\zeta_d = \frac{1}{\pi} \arctan\left(\frac{\omega'_c \Delta}{2}\right)$$

Equating these two digital frequencies gives the relationship

$$\omega'_c = \frac{2}{\Delta} \tan\left(\frac{\Delta}{2} \omega_c\right)$$

for the time constant (in this case a frequency) that we need to use in the discrete-time filter if we want to match the resonance frequency actually present in the system. If $\omega_c\Delta \ll 1$, the two are nearly equal; but as this product approaches π more and more correction is needed. In this particular example, a usual sample interval Δ for \mathbf{p} and ψ is 30 days; for $\omega_c = 0.01461\text{rad/day}$, $\omega'_c = 0.01485$, only a 2% change.

Having made this correction, we can compute the actual filter weights by the procedure just described. We find that the polynomial in z is

$$\frac{\omega'_c \Delta + \omega'_c \Delta z^{-1}}{(\omega'_c \Delta + 2i) + (\omega'_c \Delta - 2i)z^{-1}}$$

which gives a recursive filter

$$\mathbf{p}_n(\omega'_c \Delta + 2i) = -\mathbf{p}_{n-1}(\omega'_c \Delta - 2i) + \omega'_c \Delta (\psi_n + \psi_{n-1})$$

for producing simulated polar motion from a possible excitation.

CHAPTER 9

DIGITAL FILTERS III: SPECIALIZED FIR FILTERS

That this analysis was not entirely correct was shown when it was discovered that the compound thiotimoline will dissolve in water — in the proportions of 1 gm/ml — in –1.12 seconds. That is, it will dissolve *before* the water is added.

ISAAC ASIMOV, “The Endochronic Properties of Resublimated Thiotimoline” (1948)

9.1 FIR Filters: Other Applications

In this chapter we look at some other uses for FIR filters than removing bands of frequencies: differentiation, Hilbert transforms, and linear regression. We also describe one type of non-symmetric FIR filter for frequency selection, the minimum-phase filter, which has applications in processing seismic data.

9.2 Differentiators and Digital Hilbert Transformers

We have mentioned before (Section 3.6) that differentiation can be thought of as a linear system; this makes it appropriate for digital filtering. Equation (3.15)

$$\mathcal{F}[\dot{x}(t)] = 2\pi i f \mathcal{F}[x(t)]$$

shows that differentiation is a filter with frequency response $2\pi i f$: that is, a constant phase shift of $\pi/2$ (the i part of the coefficient) and an amplitude response that is proportional to frequency.

To imitate this digitally, we make the number of weights odd, with $N = 2M + 1$, and also make them antisymmetric:

$$b_{-n} = -b_n \quad \text{for } n = 0, \dots, M$$

where we have centered the filter about 0 rather than term M ; this asymmetry means that $b_0 = 0$. Substituting these weights into the general expression (equa-

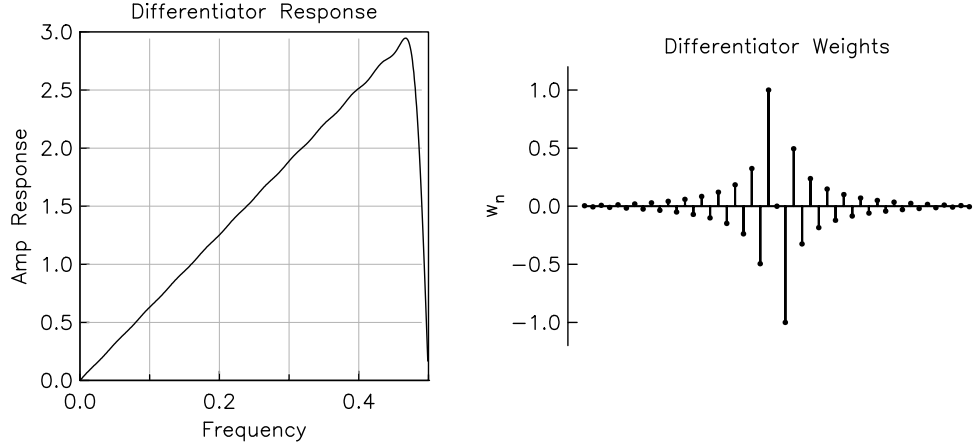


Figure 9.1: The amplitude response, and weights, for a differentiating filter, constructed by tapering the weights for an ideal response with a Kaiser-Bessel taper so that the response at the Nyquist is -40dB .

tion (7.4)) for the frequency response of a FIR filter, we find

$$\tilde{b}(\zeta) = -2i \sum_{n=1}^M b_n \sin 2\pi n \zeta$$

which we may compare with equation (7.6) for a symmetric acausal FIR filter.

Any antisymmetric filter will thus have exactly the same phase response ($\pi/2$) that differentiation does. To get an amplitude response that approximates differentiation, we take the ideal response to be $\tilde{b}(\zeta) = 2\pi i \zeta$ – but, to avoid overamplifying the energy close to the Nyquist, only up to some cutoff frequency α . That is, we want the filter to have an amplitude response that is zero at zero frequency, increases linearly to the cutoff frequency, and then falls to zero.

As with the frequency-selective filters, we can get the filter weights corresponding to this ideal response by taking the inverse Fourier transform of it:

$$\begin{aligned} b_n &= \int_{-\alpha/2}^{\alpha/2} \tilde{b}(\zeta) e^{2\pi i \zeta n} d\zeta = 4\pi i \int_0^{\alpha/2} \zeta i \sin 2\pi \zeta n d\zeta = -4\pi \int_0^{\alpha/2} \zeta \sin 2\pi n \zeta d\zeta \\ &= \frac{1}{\pi n^2} \int_0^{\alpha/2} 2\pi n \zeta \sin 2\pi n \zeta d(2\pi n \zeta) = \frac{1}{\pi n^2} \int_0^{\pi n \alpha} x \sin x dx \\ &= \frac{\alpha \cos(\pi n)}{n} - \frac{\sin \pi n \alpha}{\pi n^2} \end{aligned}$$

where we have made use of the antisymmetry of ζ around zero frequency. As with the ideal lowpass filter, this series of weights goes on forever; and, as in that case, we can approximate the ideal response better if we taper the series of

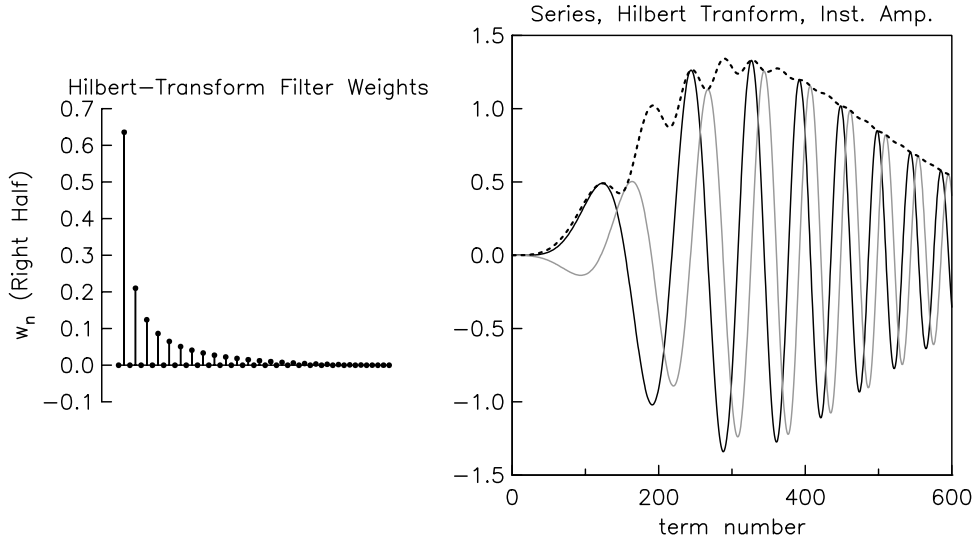


Figure 9.2: On the left, half of the weights for a (windowed) Hilbert transform filter with total length of 97. On the right, a time varying series ($x^3 e^{-x} \sin(1.5x^2)$, where $x = n/10$), shown as the black solid line, its Hilbert transform (gray solid line) and the instantaneous amplitude (dashed line).

weights instead of simply truncating it. Figure 9.1 shows an example. It is also possible to use the equiripple (Parks-McClellan) procedure in designing filters for differentiation.

Antisymmetric filters may have other amplitude responses. An important case is the filter with a constant amplitude response: $|\tilde{b}(\zeta)| = 1$ for $0 \leq \zeta \leq \zeta_N$. This is the digital **Hilbert transform** filter, whose ideal response is

$$\tilde{b}(\zeta) = \begin{cases} i & \zeta < 0 \\ -i & \text{for } \zeta > 0 \end{cases}$$

Note that this has the opposite phase shift from differentiation. The ideal weights are

$$b_n = \frac{2 \sin^2(n\pi/2)}{n\pi}$$

Again, actual filters can be designed by using tapers, (for example, the filter in Figure 9.2) or by using the Parks-McClellan algorithm. Either method will produce a filter with an amplitude response that will approximate the ideal amplitude response; because of the antisymmetry of the filter the phase response will be exact.

If a Hilbert-transform filter is convolved with a series it converts all the cosine components into sines and vice versa. This can be useful for a series that is approximately sinusoidal, since then we can create what is called a complex-valued **analytic series**

$$\{x^a\} = \{x\} + i\{x^h\}$$

where $\{x^h\}$ is the digital Hilbert transform of the original sequence $\{x\}$. From this, we can find the **instantaneous amplitude** (also called the **envelope function**) and **instantaneous phase**; these are the amplitude and phase of each term of $\{x^a\}$; differentiating the phase gives the **instantaneous frequency**. Figure 9.2 shows an example for a gradually-changing sinusoid.

9.3 Least-squares Fits as Filters

Next we show that parameters estimated through least-squares can be regarded as the result of filtering the data – and that thinking of least-squares fitting as a filter can help us understand what the fit is doing. The reason why least-squares is a kind of filter is that any solution to any least-squares problem ends up giving the parameters in terms of a linear combination of the data: that is, a weighted sum. And the weights in a weighted sum can just as well be viewed as filter weights.

Formally, suppose we have a data vector x , to which we aim to fit parameters y by least squares. The expression for y is given by the normal equations:

$$y = (A^T A)^{-1} A^T x$$

where A is the design matrix, which gives the fit if we have the parameters.¹ Now suppose we want to compute some linear combination of the parameters, $z = c^T y$; this includes the case where z is just one of the parameters. The full expression for this is

$$z = c^T (A^T A)^{-1} A^T x \stackrel{\text{def}}{=} b^T x$$

where the weights b are given by $c^T (A^T A)^{-1} A^T$, which can be seen to be an N -term vector, N being the number of data. But this is just a digital convolution (albeit with only one output value) – so we may regard the weights as filter weights, and compute the frequency response by taking their Fourier transform.

A simple and informative example is fitting a straight line to data. Assume we have $2M+1$ values, centered about 0. Then if y_1 is the value of the fit at $n=0$ and y_2 is the slope, the design matrix is

$$A^T = \begin{bmatrix} 1 & 1 & \dots & 1 & 1 & 1 & \dots & 1 & 1 \\ -M & -M+1 & \dots & -1 & 0 & 1 & \dots & M-1 & M \end{bmatrix}$$

¹We have assumed that the errors are identical and independent; if they are not the equations are slightly more complicated but the end result has the same form.

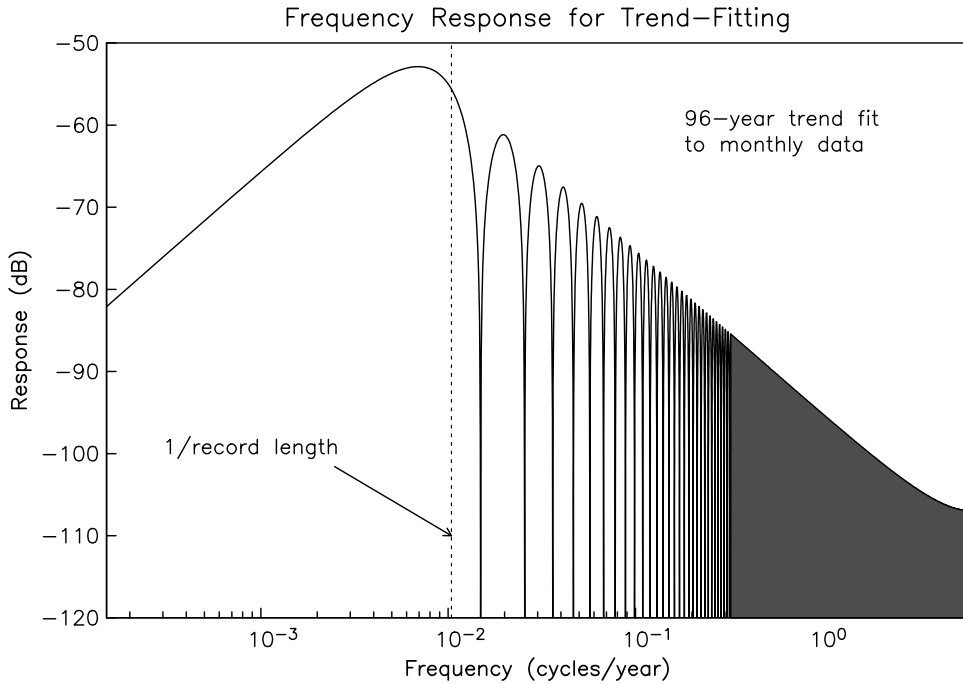


Figure 9.3: An example of the frequency response of a least-squares fit: in this case, for the slope of monthly data, fit over a 96-year span, as was done for Figure 1.1.

These two rows correspond to sequences defined in Section 5.4: the first row to a boxcar sequence Π_n , and the second row to the slope sequence I_n . These are orthogonal, so the matrix for the normal equations is diagonal:

$$A^T A = \begin{bmatrix} 2M+1 & 0 \\ 0 & M(M+1)(2M+1) \end{bmatrix}$$

which in turn makes the weights for finding the slope

$$b_n = \frac{3n}{M(M+1)(2M+1)} = \frac{3}{M(M+1)(2M+1)} I_n$$

These weights are quite different from the weights for finding the derivative, which is a local measure of slope: the weights for the fitted slope are largest far from the center, something that is often stated by saying that such parts of the series have more influence. The frequency response of a filter with such weights is, by equation (5.14):

$$\tilde{b}(\zeta) = \frac{3}{M(M+1)N} \tilde{I}(\zeta) = \tilde{b}(\zeta) = \left(\frac{-3i}{2M(M+1)N} \right) \left(\frac{\sin \pi N \zeta \cos \pi \zeta - N \cos \pi N \zeta \sin \pi \zeta}{\sin^2 \pi \zeta} \right)$$

which depends on $N = 2M + 1$, the length over which the fit is made. Figure 9.3 shows the frequency response for $N = 1153$, the length of the series in Figure 1.1. Note that the response peaks at a period of 140 years, longer than the timespan of the data. This frequency is thus lower than the lowest frequency that is usually resolvable from data, namely one cycle over the record. Why the peak response is where it is becomes more obvious if we think about what kind of sinusoid “looks like” a straight line: namely, one with about a quarter of a cycle over the range of data. Much lower frequencies look more and more like a constant.

The peak location has important practical consequences: if the data consists of a slope plus noise, what determines the error in the estimated slope is the noise power at the peak filter response – which is, always, at a period for which we have no data, so we must extrapolate the noise power from higher frequencies.

9.4 Minimum-Phase Filters

Next, we turn to what are called *minimum-phase* filters. As mentioned in Section 7.2, sometimes we do not want to use zero-phase filters because they lack causality: something that all actual physical systems (outside of science fiction) have. If the data have sudden changes (notably from earthquakes) we may not want leakage of energy into times earlier than the time at which the change occurs. But, also, we usually want the filter to be as compact as possible: that is, we would like the filter to spread any impulses or steps over the minimum possible time span. Making the filter compact, but still causal, turns out to be equivalent to minimizing the phase shift.

The design of such filters depends on the locations of the roots of the z -transform polynomial

$$\tilde{b}(z) = \sum_{k=0}^{N-1} b_k z^{-k}$$

for weights b_0, b_1, \dots, b_{N-1} . This polynomial has $N - 1$ roots, r_1, r_2, \dots, r_{N-1} , so, as we did in going from equation (8.7) to (8.8), we can write the z -transform as a product of degree-one polynomials:

$$\tilde{b}(z) = b_0 \prod_{k=1}^{N-1} (1 - r_k z^{-k})$$

with the b_0 providing appropriate scaling.

For common choices of the weights b_n , there are a number of “symmetry” relationships that apply to the roots r_k . If the weights are real, the roots r_k must either be real, or occur as complex conjugate pairs. If the filter is symmetric, with an odd number $N = 2M + 1$ of weights, then if r_k is a root, so is $r_l = 1/r_k$: the roots occur as reciprocal pairs unless they are on the unit circle. To see this, write the

z -transform as

$$\tilde{b}(z) = \sum_{k=0}^{2M} b_k z^{-k} = z^{-M} \left[b_M + \sum_{k=0}^{M-1} b_k (z^{M-k} + z^{k-M}) \right] = z^{-2M} \tilde{b}(z^{-1})$$

so that if $\tilde{b}(r_k) = 0$, then $\tilde{b}(1/r_k) = 0$ as well.

Combining these results, we have that for real and symmetric weights (the commonest case), the roots of $\tilde{b}(z)$ either form reciprocal pairs or are single roots on the unit circle; all pairs (or single roots) that are not purely real occur as complex conjugate pairs.

If the weights are real and symmetric, the response for a frequency ζ (which corresponds to a z that is on the unit circle) will be

$$\tilde{b}(\zeta) = e^{-2\pi\zeta M} \left[b_M + 2 \sum_{k=0}^{M-1} b_k \cos 2\pi k \zeta \right] = e^{-2\pi\zeta M} \tilde{b}_a(\zeta)$$

where $\tilde{b}_a(\zeta)$ is the amplitude. This is purely real, but may be positive or negative, unlike the usual expression $|\tilde{b}(\zeta)|$. If there are single roots of $\tilde{b}(z)$ on the unit circle, there must be values of ζ for which $\tilde{b}_a(\zeta) \leq 0$. Conversely, if $\tilde{b}_a(\zeta) > 0$ for all ζ , there can be no roots on the unit circle: all roots occur as reciprocal pairs. Quite commonly, $\tilde{b}_a(\zeta)$ is nonnegative, but equal to zero for particular values of ζ ; these values of ζ then correspond to double roots of $\tilde{b}(z)$, for which the root and its reciprocal are equal.

We have discussed the locations of the roots in such detail because of some less obvious results that relate to the goal of obtaining a compact filter. Suppose some sequence b_n , with z -transform $\tilde{b}(z)$, has a root within the unit circle; without loss of generality we can take this to be the “last” root r_{N-1} . Now consider another z -transform polynomial

$$\tilde{b}'(z) = \tilde{b}(z) \frac{z^{-1} - r_{N-1}^*}{1 - r_{N-1} z^{-1}} \stackrel{\text{def}}{=} \tilde{b}(z) \tilde{c}(z) \quad (9.1)$$

The form of the term $\tilde{c}(z)$ means that for the polynomial \tilde{b}' the root at r_{N-1} has been divided out of the polynomial for $\tilde{b}(\zeta)$ and replaced by its reciprocal complex conjugate, which will be outside the unit circle. For $z = e^{-2i\pi\zeta}$,

$$|\tilde{c}(z)|^2 = \left| z^{-1} \frac{1 - r_{N-1}^* z}{1 - r_{N-1} z^{-1}} \right|^2 = 1$$

which means that the amplitude responses $|\tilde{b}(\zeta)|^2$ and $|\tilde{b}'(\zeta)|^2$ are identical. For this reason the filter expressed by the $\tilde{c}(z)$ polynomial is termed an **allpass filter**; note that this is a recursive filter.

We can use the factorization (9.1) to get a relationship between the two sets of weights, b_k and b'_k , that have the responses $\tilde{b}(z)$ and $\tilde{b}'(z)$. Let $\tilde{d}(z)$ be a polynomial

of degree $N - 2$, obtained by factoring out the last root (this is called deflation of the polynomial). Then we can rearrange equation (9.1), to get

$$\tilde{b}(z) = \tilde{d}(z)(1 - r_{N-1}z^{-1}) \quad \text{and} \quad \tilde{b}'(z) = \tilde{d}(z)(z^{-1} - r_{N-1}^*)$$

But these polynomial relationships imply the following expressions for the coefficients of \tilde{b} and \tilde{b}' :

$$\begin{aligned} b_k &= v_n * (1, -r_n) = v_k - r_{N-1}v_{k-1} \\ b'_k &= v_n * (-r_n^*, 1) = -r_{N-1}v_k + v_{k-1} \end{aligned}$$

Next, we compute the difference of the sums of squares of the weights up to the next-to-last term. Most of the terms in the sum cancel, giving

$$\sum_{k=0}^{N-2} |b_k|^2 - |b'_k|^2 = (1 - |r_{N-1}|^2)|v_{N-2}|^2$$

Because $|r_{N-1}| < 1$ (by assumption, we chose a root with this property), this sum has to be positive. This means that the sequence b_k has more energy (measured by the sum of squared amplitudes) concentrated before the last term than the sequence b'_k does.

This result can be extended to show that, among all FIR filters with the same amplitude response $|\tilde{b}(\zeta)|^2$, the one whose z -transform has all its roots on or inside the unit circle will have the most concentration of energy towards the early terms of the sequence; that is,

$$\sum_{k=0}^m |b_k|^2$$

will be maximized for all $m < N - 1$. (For $m = N - 1$ the sum is the same, being the filter response at $\zeta = 0$.) This choice of roots thus makes the filter as compact as possible.

Additional results follow if we express $\tilde{b}(\zeta)$ as amplitude and phase: $\tilde{b}(\zeta) = \tilde{b}_a(\zeta)e^{-\phi(\zeta)}$. The phase of \tilde{b} and \tilde{b}' are related, by equation (9.1), though the phase of the allpass term in equation (9.1). If we write the root in polar form as $r_{N-1} = \rho e^{2\pi i\theta}$, we find that its phase is the phase of

$$e^{-2\pi i\zeta} \left(\frac{1 - \rho e^{2\pi i(\zeta - \theta)}}{1 - \rho e^{-2\pi i(\zeta - \theta)}} \right)$$

which gives a phase

$$\phi(\zeta) = -2\pi\zeta - 2\arctan \left[\frac{\rho \sin 2\pi(\zeta - \theta)}{1 - \rho \cos 2\pi(\zeta - \theta)} \right] \quad (9.2)$$

It is interesting to look at these filters in terms of their group delay $D(\zeta)$, which we introduced in section 3.7.3: it describes the delay of the energy in a signal as a

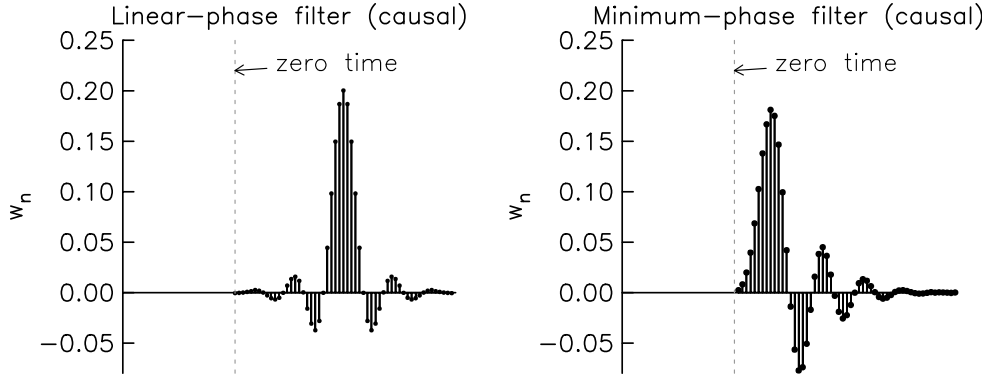


Figure 9.4: Weights for two filters with the same (lowpass) frequency response: on the left, a symmetric filter, on the right, its minimum-phase equivalent. Both are shown as being applied causally.

function of ζ . This delay is given by the derivative of the phase with frequency; if the phase is

$$\phi(\zeta) = \arctan\left(\frac{S(\zeta)}{C(\zeta)}\right)$$

the group delay is

$$D(\zeta) = \frac{1}{2\pi} \frac{d\phi}{d\zeta} = \frac{1}{2\pi} \frac{S'(\zeta)C(\zeta) - C'(\zeta)S(\zeta)}{S^2(\zeta) + C^2(\zeta)}$$

These expressions assume that the separation between the weights is unity; for a sample interval Δ just scale $D(\zeta)$ by Δ , and the argument ζ by Δ^{-1} .

If we apply this definition to equation (9.2) we find that

$$D(\zeta) = \frac{-1 - \rho^2}{1 + \rho^2 - 2\rho \cos 2\pi(\zeta - \theta)}$$

This is negative for $\rho < 0$ (the root inside the unit circle), so that $\tilde{b}'(\zeta)$ has a greater delay, and a larger (more negative) phase than $\tilde{b}(\zeta)$. The sequence with all the roots inside the unit circle is thus not only the most compact; of all the filters with a given amplitude response, it minimizes group delay, and makes the phase lag as small as possible. Such sequences are therefore usually referred to as providing **minimum-phase** FIR filters.

To design such filters requires, besides approximating the desired frequency response, ensuring that the roots of the z -transform all fall inside of or on the unit circle in the complex plane. There are two different ways to accomplish this.

One, suggested by equation (9.1), is to replace all roots outside the unit circle with their reciprocal complex conjugates, leaving roots on the unit circle in place.

This procedure is called the **allpass decomposition**, because of the allpass term in equation (9.1). This equation, generalized to contain as many such factors as there are roots outside the unit circle, becomes the result that any FIR filter can be expressed as the convolution of a minimum-phase FIR filter and an allpass filter. Note that the allpass filter itself is not a FIR filter, but would need to be computed recursively; this is acceptable for correcting for the previous application of a non-causal FIR filter to data (Scherbaum and Bouin, 1997).

A second approach, called **spectral factorization**, depends on the result that, for symmetric filters, if $\tilde{b}_a(\zeta) \geq 0$ on the unit circle, then all the roots can be paired into reciprocals, with double roots on the unit circle. The factorization consists of taking all the roots inside the unit circle and half of the roots on it, and constructing the corresponding sequence.² The resulting filter will have an amplitude response $|\tilde{b}(\zeta)| = \sqrt{\tilde{b}_a(\zeta)}$, which therefore requires that the initial filter have a nonnegative amplitude response, $\tilde{b}(\zeta) \geq 0$. Such a filter can be created using the Parks-McClellan algorithm if we constrain the stopband response to oscillate around the error level ϵ , rather than (as is more usual) zero.

Figure 9.4 shows an example of filter weights for a zero-phase and minimum-phase filter with the same amplitude response.³ It is obvious that the symmetric (linear-phase) filter, if used as a causal filter, is less compact than the minimum-phase filter applied the same way.

²A good description of the procedure, and some pitfalls, is given in Orchard and Willson (2003) – though there have been difficulties with the Newton's method procedure given there.

³This is one of several filters combined to produce 5-minute data from 1-Hz data recorded with the strainmeters installed by the Plate Boundary Observatory. For more details, see Agnew and Hodgkinson (2007),

CHAPTER 10

STOCHASTIC PROCESSES

Sounds may be classed as musical and unmusical; the former for convenience may be called *notes* and the latter *noises*. The extreme cases will raise no dispute; every one recognises the difference between the note of a pianoforte and the creaking of a shoe. But it is not so easy to draw the line of separation.

LORD RAYLEIGH The Theory of Sound, Chapter 1 (1877)

10.1 Ordered Random Data

In Chapter 1 we introduced the idea of data ordered in time or space; Chapters 2 through 9 used, as a mathematical model of these, a function $x(t)$ or an ordered sequence of variables $\{x_n\}$; a model so close to what it is modeling that it is easy to forget that we have made the step from data to model.

We now turn to models in which the values of the x_n 's are random; as before, many of our models will assume infinite sequences, even though we only ever have N data, N a finite number. We will also consider, though to a lesser extent, random functions $X(t)$: the mathematics of random functions can be extremely difficult. We can create a random sequence $\{X_n\}$ by sampling $X(t)$, but will mostly just start with sequences.

What we mean by “random sequence” is that the values $\{X_n\}$ are taken to be random variables. The sequences and functions are called **stochastic processes**: **discrete stochastic process** for a sequence $\{X_n\}$ and **continuous stochastic process** for a random function $X(t)$.

What do we mean when we say “random”? Up to now our sequences and functions used a particular class of mathematical entity, namely one that obeys the rules of algebra. To this point we have just called these entities variables, with no adjective, but we will now be more specific, and call them **algebraic variables**, to distinguish them from new entities termed **random variables**. We indicate random variables by using uppercase letters.¹

¹*Notation alert:* However, some uppercase letters are used for algebraic variables (such as N , the number of data); from here on we will explicitly note this when introducing new variables.

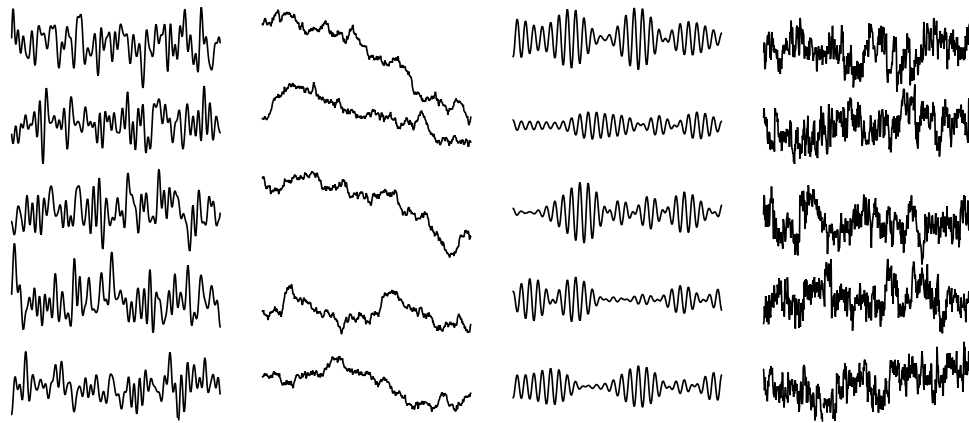


Figure 10.1: Five realizations of each of four different stochastic processes: from left to right, lowpassed white noise, a random walk, a randomly modulated sinusoid, and f^{-1} , or “flicker” noise.

Random variables may seem like algebraic variables, but are described differently and follow different rules:²

- A. An algebraic variable is assumed to have a definite, though perhaps unknown, value. Random variables do *not* have a definite value; instead they are described by a **probability density function**, often abbreviated as **pdf**. The pdf gives the probability density over some range; but note that this range, any parameters of the function for the pdf, and the value of the pdf, are all algebraic variables.
- B. We can add, subtract, multiply, or divide algebraic variables.³ We can define the same operations on random variables, but what happens when we perform them follows a different set of rules. For example, the sum of two random variables is another random variable, but the pdf of this new variable is not the sum of the pdf’s of the two variables that have been added – at its simplest the pdf of the sum is the convolution of the two pdf’s.

Algebraic variables are appropriate for modeling things we want to represent as having some definite, though arbitrary, value: for example, data we have measured. So we could use algebraic variables in our mathematical models for the Fourier transform and signal processing. But for things that are uncertain, the appropriate mathematical model must use random variables.

²Section C.3 provides a longer, though still very condensed, discussion of random variables.

³At least for scalar algebraic variables; for vectors there can be multiple kinds of multiplication and perhaps no division.

You should realize that modeling something by a random variable is a choice: you have to decide what kind of mathematical entity best matches whatever you are studying. There are no absolute rules on when to choose one or another type of variable; depending on what a model is for, we would model the same thing by an algebraic variable in one, and by a random variable in another.

A common way to think about a random variable, or a series of random variables, is as the result of an experiment that can be repeated many times. In this way of thinking, we say that each repetition produces one **realization**, drawn from the **ensemble** of series that would be produced if we repeated the experiment many times. This concept in turn leads to such terminology as the **expected value** of a variable for a particular n or t : this value would be the average, over an infinite number of realizations, of the variable for that n or t . Figure 10.1 shows some realizations of several stochastic processes.

The most general form of a stochastic process is horribly complex, even in discrete time with only N terms. A single random variable needs only a pdf, which is a function of one variable. But to completely specify a collection of such variables we need a joint pdf to express the relationships between each X_n and all the others: to fully describe a stochastic process with N values we need a pdf in N dimensions. Even if we assume all terms of a discrete series have a Gaussian distribution, a full pdf is the joint pdf is the N -dimensional Gaussian function $\phi(\mathbf{x})$ given in equation (C.22). It takes $N(N + 3)/2$ parameters to describe this pdf: always larger, and for typical N much larger, than the number of values N . There is no hope of being able to determine the pdf given only N data values.⁴

We should mention that there are other kinds of stochastic processes than a series of random variables. Another type is the **point process**, for which the randomness applies not to date values but to times: this is used to describe “events” of some type, the time between them being a random variable. Two geophysical phenomena that can be modeled by point processes are magnetic reversals and earthquakes. We discuss point processes a little more in Appendix ??.

10.2 Stationary Processes

To make any progress we limit ourselves to a severely restricted class of stochastic processes: those that are **stationary**, or equivalently are said to possess **stationarity**. In Section 2.5 we encountered *time invariant* systems. For stationary processes, such invariance applies to the pdf: because the values are random variables, they can vary, while the pdf does not depend on time. In **completely stationary** processes, the pdf is completely invariant with time, but there is also partial stationarity, in which only some aspects of the p f (say the mean and vari-

⁴In continuous time even developing the mathematical specification becomes very difficult (Priestley (1981), Chapter 3).

ance) are time invariant but other features are not. Complete stationarity gives the simplest results, and we assume it unless stated otherwise.

Stationarity greatly reduces the number of parameters needed. For example, in a full pdf such as equation (C.22), the mean is a vector of N terms and every term of a stochastic process could have a different expected value. With stationarity the mean of the process must be just one variable, which we denote by $\mathcal{E}[X_n] = \mu$, \mathcal{E} being the expectation operator (equation C.3). To simplify many derivations, we will usually assume that $\mu = 0$. In practice it is rarely problematic to subtract a constant value from a time series. Indeed, for many series, such as the sea level data of Figure 1.1, the original zero level is arbitrary, and we might as well set it to make μ zero. Similarly, the **variance** σ^2 given by equation (C.4) is constant throughout the series.

This sea level data also illustrates an important point, since it shows a typical departure from stationarity, namely a **secular trend**. Stationarity is such a useful property that, whenever possible, the first step in data analysis is convert a nonstationary time series into a series that can plausibly be modeled as stationary. For the sea-level series, this means modeling it as random variables by rewriting equation (1.1) using them:

$$X_j = A_1 + A_2 t_j + \sum_{m=1}^M B_m \sin(2m\pi t_j) + C_m \cos(2m\pi t_j) + R_j \quad (10.1)$$

Here the A 's, B 's, and C 's are random variables that set the size of specified functions of time: as we said in Section 1.2, such functions model what is called **deterministic** behavior. Estimating the best values of the A 's, B 's, and C 's to produce the corresponding algebraic variables in equation (1.1) leaves the residual series $\{r_j\}$, which Figure 1.1 clearly shows is quite plausibly modeled by a stationary stochastic process $\{R_j\}$. Such removal of deterministic components is often needed before modeling actual data by a stochastic process.

10.2.1 Autocovariance

But the most important consequence of stationarity the joint pdf for any two variables. With complete stationarity, this pdf also cannot depend on time, so the only change possible is for the pdf to vary with the time difference, which we will often call the distance between two variables.

Specifically, the second moment of this joint pdf, the **covariance** described in Section C.5, can only depend on but only on how far apart the variables are. So for a sequence we can write this covariance as a sequence⁵ R defined by

$$\mathcal{C}[X_m, X_n] = \mathcal{E}[(X_m - \bar{x})(X_n - \bar{x})] \stackrel{\text{def}}{=} R_{m-n} = R_l \quad (10.2)$$

⁵Notation alert: for consistency with most other treatments, we use uppercase even though R is not a random variable.

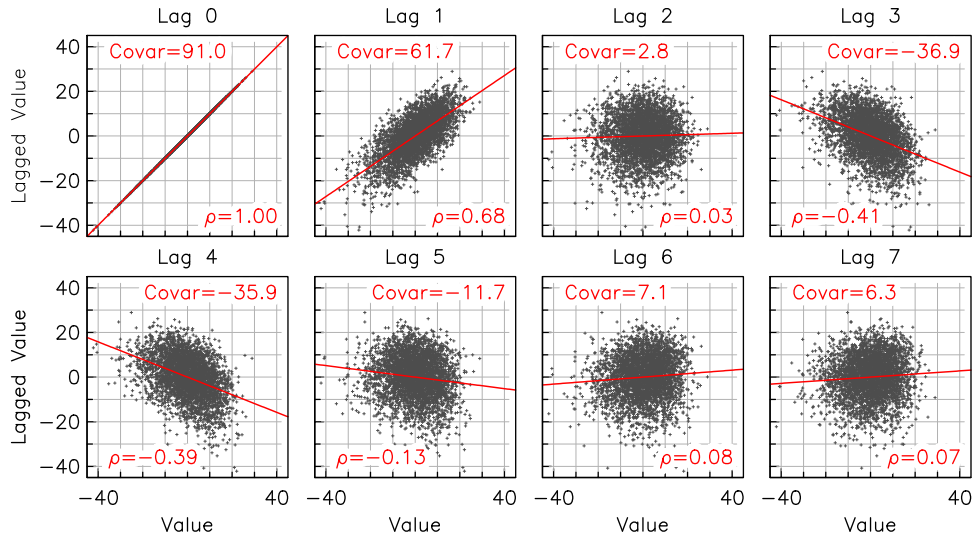


Figure 10.2: Scatterplots of data from the SIO sea-level record shown in Figure 1.4 against the same data shifted by different amounts. The best-fitting regression line, covariance R , and correlation ρ are shown for each plot.

where l is the time difference or distance between the X 's. Likewise for a random function we can write

$$\mathcal{C}[X(t), X(t + \tau)] = R(\tau) \quad (10.3)$$

where τ (like l in the discrete case) is called the **lag**.

This sequence R_l (or function $R(t)$) is called the **autocovariance**.⁶ By the definition of variance and covariance

$$R(0) = R_0 = \sigma^2$$

so the zero-lag autocovariance is just the variance.

Figures 10.2 and 10.3 show the result of applying equation (10.2) to the sea-level data shown in Figure 1.4: data sampled every second and showing the ocean swell. Figure 10.2 shows a series of scatter plots where the x -axis is always the values over some time, and the y -axis is the values over a time span shifted by various amounts of lag. Of course, if the lag is zero, the values line up perfectly. For other values of the lag the shifted data may tend to have the same sign as the reference data ($R > 0$), the opposite sign ($R < 0$), or be equally distributed ($R = 0$).

⁶Notation alert: we will usually use a subscript on R for discrete time and an argument for continuous time.

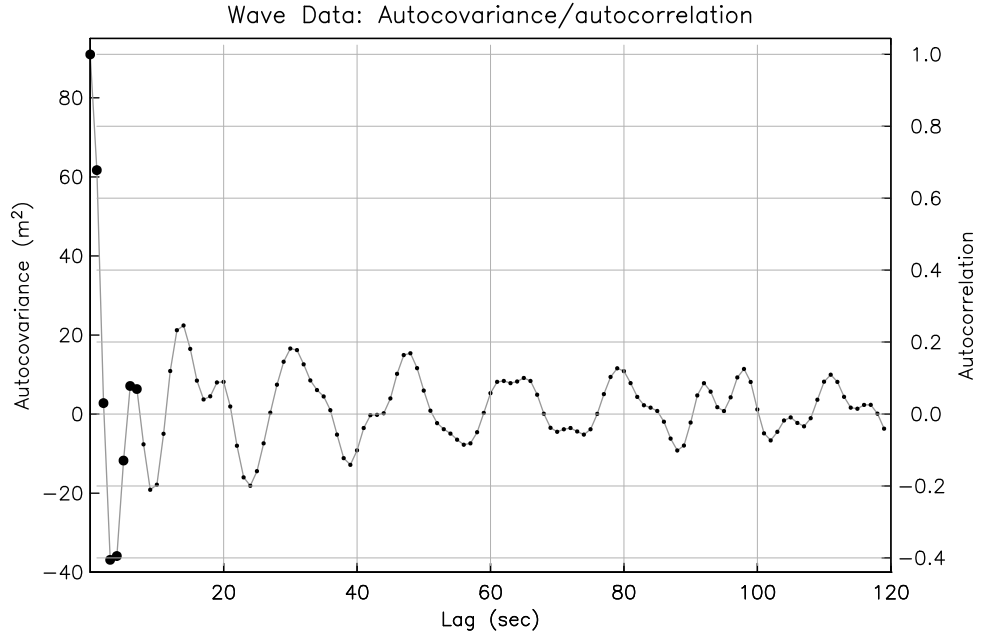


Figure 10.3: The covariances from 10.2 are shown as crosses, and the covariances for larger lags as dots. Since these data are discrete, these quantities only exist for integer values of the lags, but a line has been drawn between them to help show the shape of the sequence $\{R_n\}$. The right-hand y -axis shows the scale if the autocovariance R is divided by the variance σ to produce the autocorrelation ρ .

Stationarity also means that, since R is independent of which time was selected, we can set $s = t - \tau$ in (10.3) and get the same result, so

$$R_{-n} = R_n \quad \text{or} \quad R(-\tau) = R(\tau)$$

That is, the autocovariance function is an even function of the lag: a stationary process does not contain information on which way time is going.

We already saw that for a stochastic process with a Gaussian pdf, as in equation (C.22), stationarity allows us to replace the vector of mean values $\bar{\mathbf{x}}$ with a single parameter. How about the covariance matrix \mathbf{R} ? The j, k th entry of \mathbf{R} becomes

$$R_{jk} = \mathcal{C}[X_j, X_k] \stackrel{\text{def}}{=} R_{l=|j-k|}$$

so that for a stationary process, the covariance matrix is symmetric; indeed each

diagonal of the covariance matrix has the same value, so the matrix looks like:

$$\mathbf{R} = \begin{bmatrix} R_0 & R_1 & R_2 & R_3 & \dots & R_N \\ R_1 & R_0 & R_1 & R_2 & \dots & R_{N-1} \\ R_2 & R_1 & R_0 & R_1 & \dots & R_{N-2} \\ \dots & \dots & \dots & \dots & \dots & \dots \\ R_N & R_{N-1} & R_{N-2} & R_{N-3} & \dots & R_0 \end{bmatrix} \quad (10.4)$$

This type of matrix is called a **Toeplitz** matrix, and is fully specified by $N + 1$ parameters: so a Gaussian stationary process with N values needs only $N + 2$ parameters to describe its pdf, not the $N(N + 3)/2$ of a the general pdf.

The covariance depends on the actual variability of the series, and so will change if (for example) we change the units. To get a function that expresses only the connection between variables, we look at the correlation. The correlation coefficient of two random variables is defined by equation (C.23) as

$$\rho_{12} = \frac{R_{12}}{\sigma_1 \sigma_2}$$

and so we can define the **autocorrelation** by similarly normalizing the autocovariance:

$$\rho(\tau) = \frac{R(\tau)}{\sigma^2} \quad \text{or} \quad \rho_l = \frac{R_l}{\sigma^2}$$

Like the correlation coefficient, ρ must be between -1 and 1 ; the latter value will be the one for zero lag. Figure 10.3 uses a separate scale to show the autocovariance as the autocorrelation.

Our discussion so far has been limited to first and second moments of random variables, and the second moment of the product of two variables; the second moments are taken after setting the first moments to zero. These moments are expressed by the operators \mathcal{E} , \mathcal{V} , and \mathcal{C} . As mentioned in Section C.3 we can define higher order moments of individual variables; and likewise we could find the third-order moments that come from the product of three X 's; for a stationary process this would be a function of two variables (the two lags). But as we have seen, for a stationary process is based on a Gaussian pdf, (equation C.22) the first-order and second-order moments \bar{x} , σ^2 , and R completely specify the pdf and higher moments contain no additional information. Even if the pdf is not Gaussian, much of what is important about a process is contained in its second-order moments, and we will limit our discussion to them.

10.2.2 White Noise

We begin our examples of stationary stochastic processes with the simplest possible: **white noise**. This is any stationary process in which the random variable at

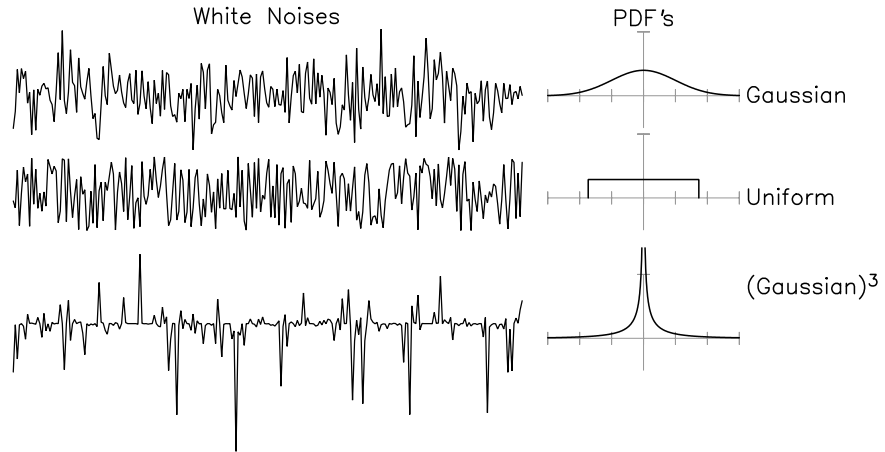


Figure 10.4: Three white noises, all with the same variance, and their pdfs.

any time (or sequence number) is independent of the variable at any other time.⁷ As usual, we assume that the mean value is zero.

In discrete time we thus have

$$R_l = \sigma^2 \delta_{l0}$$

where δ_{jk} is the Kronecker delta symbol. The delta-function correlation means that the joint pdf is just

$$\phi(X_1, X_2, X_3, \dots) = \phi(X_1)\phi(X_2)\phi(X_3)\dots \quad (10.5)$$

where all the pdf's are the same because of stationarity.

While we can define a white noise in continuous time as having

$$R(\tau) = \sigma^2 \delta(\tau) \quad (10.6)$$

this means that the variance (that is, $R(0)$) is infinite – something not physically possible. This is one of a number of places where continuous time, while mathematically convenient in some ways, also leads to difficulties.

A white noise process is genuinely unpredictable: knowing the value at one time tells us nothing about the value at another. All the information about probable values comes from knowing the pdf and its parameters. Given a number of values, we can estimate parameters such as the mean and variance, which (with an

⁷More precisely, the definition is that the correlation between any two times is zero; this can be true for non-Gaussian variables even if the variables are not independent. But such dependence is seen only in the higher moments that we just promised to ignore.

assumed pdf) will tell us something about what value can be expected at any time, but that is all.

Figure 10.4 shows some white noises. One is **Gaussian white noise**, whose pdf (also shown in Figure 10.4) is the one given by equation (C.6), with mean zero. The figure also shows white noise for a uniform distribution, $\phi(X) = b^{-1}[\Pi(X/b) - \frac{1}{2}]$, with $E[X] = 0$ and $V[X] = b^2/12$. As Figure 10.4 shows, this looks different from Gaussian white noise. We have already encountered white noise with this pdf: the quantization noise of Section 6.8. If we have a series that varies by much more than ± 1 between samples, and quantize it to integer values, what we get can be modeled as the true value plus an unpredictable (random) amount. This random part will be distributed uniformly over the interval $(-\frac{1}{2}, \frac{1}{2})$, and usually the consecutive values of the rounding error are uncorrelated. So the recorded series is the true signal with this white noise added, with zero mean and a variance of $\frac{1}{12}$.

While these two examples of white noise are visually different, if we normalize each to the same variance and convert the sequence into sound, the ear cannot tell them apart. If we take Gaussian white noise and cube the values, the smaller values are more concentrated around zero and there are sometimes extremely large values: this white noise will sound and look different. Needless to say, if your data look like this, you should be very careful about applying procedures that assume that the pdf is Gaussian.

10.2.3 Filtered White Noise

Two of the series in Figure 10.1 were produced by filtering white noise. Series generated this way are often used to model data; though we will not use such models, we want to introduce some of them that you might see elsewhere.

To be specific, we can take the different filters described in Section 7.1, and replace the input sequence of algebraic variables $\{x_n\}$ with white noise: a sequence of uncorrelated random variables $\{X_n\}$. Then equations (7.3), (7.2), and (7.1) become

$$Y_n = \sum_{k=1}^K a_k Y_{n-k} + b_0 X_n \quad (10.7)$$

$$Y_n = \sum_{m=0}^{M-1} b_m X_{n-m} \quad (10.8)$$

$$Y_n = \sum_{k=1}^K a_k Y_{n-k} + \sum_{m=0}^{M-1} b_m X_{n-m} \quad (10.9)$$

Since equation (7.3) described an autoregressive filter, we say that $\{Y_n\}$ in equation (10.7) is an **autoregressive process** or **AR process**. Equation (10.8), which applies an FIR filter to white noise, creates a $\{Y_n\}$ that is called a moving-average

or **MA process**. And equation (10.9), which combines these, creates a $\{Y_n\}$ that is called an **autoregressive moving-average** or **ARMA process**.⁸

We saw in Chapter 7 that statisticians and engineers had different names for the same thing, and so it is here. In electrical engineering, equation (10.7), with $K = 1$ and X_n Gaussian, is more likely to be called a **first-order Gauss-Markov process**, the Markov part coming from the $K = 1$ restriction. This restriction does not preclude the more general equation (10.7), because in the engineering literature the random variables X_n and Y_n are usually assumed to be vectors (in the linear-algebra sense) rather than scalars; the (single) a is then a matrix. The Gauss-Markov expression is then

$$\mathbf{Y}_n = \mathbf{a}\mathbf{Y}_{n-1} + \mathbf{b}\mathbf{X}_n \quad (10.10)$$

where we have used boldface to indicate vectors and matrices. This expression is very general, but we may turn it into equation 10.7 by defining the vectors to be of length K :

$$\mathbf{Y}_n = (Y_n, Y_{n-1}, \dots, Y_{n-K+1}) \quad \text{and} \quad \mathbf{X}_n = (X_n, 0, \dots, 0)$$

which means that \mathbf{Y}_{n-1} is the vector with terms from Y_{n-1} through Y_{n-K} . Now take the matrix \mathbf{b} to be zero except for $b_{11} = b$, the first row of the matrix \mathbf{a} to be (a_1, a_2, \dots, a_K) , while the second through the K -th rows of \mathbf{a} each have a single nonzero term, equal to one, in the first through the $K - 1$ th column. Then it should not be difficult to see that the result is just equation (10.7).

What are the autocovariances of these processes? We can start by considering the MA process described by equation (10.8), with the white-noise input $\{X - n\}$ having zero mean. Then we can find the autocovariance of the new sequence using the definition (equation 10.2):

$$\begin{aligned} R_l &= \mathcal{C}[Y_{n+l}, Y_n] = \mathcal{E}[Y_{n+l}Y_n] \\ &= \mathcal{E}\left[\sum_{j=1}^M b_j X_{n+l-j} \sum_{m=1}^M b_m X_{n-m}\right] \\ &= \sum_{j=1}^M \sum_{m=1}^M b_j w_m \mathcal{E}[X_{n+l-j}X_{n-m}] \\ &= \sum_{j=1}^M \sum_{m=1}^M b_j b_m \sigma^2 \delta_{l-j+m, 0} \end{aligned}$$

Since the delta symbol vanishes except when $l - j + m = 0$ or $j = l + m$, the autocovariance becomes

$$R_l = \sigma^2 \sum_{m=1}^M b_m b_{m+l} = \sigma^2 (\{b\} * \{b^r\}) \quad (10.11)$$

⁸The equations in Section 7.1 allowed for a possible time offset in $\{X_n\}$; why is that not needed here?

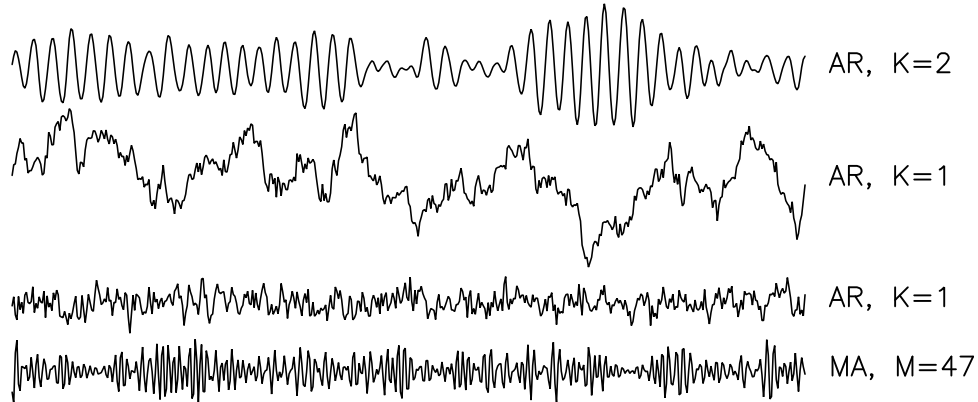


Figure 10.5: Examples of processes generated using equation (10.7) and equation (10.8). The top trace is the AR process produced by using white-noise excitation and the filter described at the end of Section 8.5.2 for simulating the Chandler wobble. The next two are from the simplest possible AR process ($K = 1$) with a_1 set to two different values, 0.95 and 0.45. The bottom trace is an MA process: a bandpass filter applied to white noise.

where $\{b'\}$ is the time-reversed version of the weight sequence $\{b\}$.⁹ So the filtered white noise is correlated, though only over a finite lag, since $R_l = 0$ for $|l| > M$.

You are invited to verify that the same result can be obtained for continuous time: if $Y = b * X$ then $R(t) = \sigma^2 b(t) * b(-t)$.

This result actually provides all we need to find the autocovariances for AR and ARMA processes, since we can express an AR process as an MA process with an infinite number of weights (or an infinitely long function), that are the impulse response of the filter.

There is enough flexibility in equations (10.7) through (10.9) to produce a wide range of stochastic processes. Figure 10.5 shows a few examples. For another, consider the simplest possible AR process:

$$Y_n = Y_{n-1} + X_n$$

which gives a stochastic process known as a **random walk** or a **Brownian process**.¹⁰ This process is actually nonstationary, with a variance that grows with

⁹The autocovariance sum contains the product of $\{b_n\}$ with a shifted version of itself: we need to time-reverse the shifted version for the expression to be a convolution.

¹⁰The “Brownian” name comes from the applicability of this process to explaining the motion of small particles that are moved about by the kinetic motions of (much smaller) molecules, something known as Brownian motion because it was first observed, for pollen in water, by the microscopist Robert Brown.

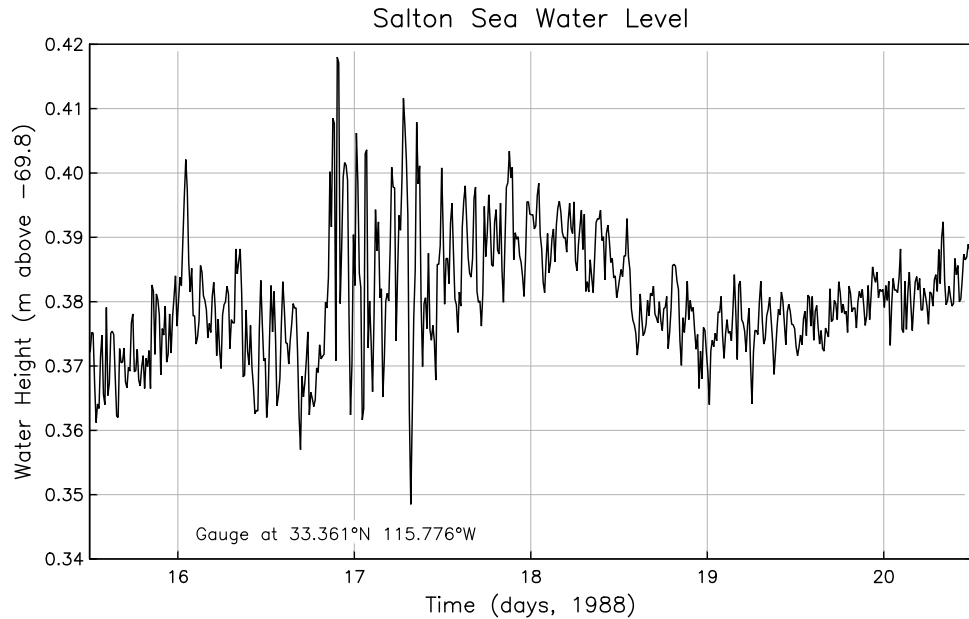


Figure 10.6: Time series of water height on the shore of the Salton Sea, near Bertram siding; data courtesy of Dr. John Beavan. The reference level for the y -axis is 69.8 meters below sea level.

time, though only in proportion to its square root.

Stochastic processes obtained by filtering white noise are called **parametric models**, since only a few things (the filter weights and the pdf of the white noise) are needed to fully describe such a stochastic process. Many statistical treatments of time series focus on such stochastic processes and methods for finding these parameters. In our opinion these models, though sometimes applicable, have limited usefulness for analyzing geophysical data. In particular, applying these models to data is not the best way to reach our goal of describing stochastic processes in the frequency domain. But parametric models form the basis of some popular (though in our view misguided) methods of spectrum estimation – which we relegate to Appendix E.3.

10.3 Some Examples

We now introduce some ordered-data series that we will use in later chapters to illustrate processing methods.

We have already (Chapter 1 introduced the various water levels measured at the end of the SIO pier. We will look in particular at the wave data shown in Figure 1.4; even though we showed, using spectra, that this sequence is not perfectly

stationary, we will assume that it is. This is a common assumption, best thought of as an approximation that makes analysis much easier. Whether or not this assumption is warranted is a matter of judgement: some series are much closer to stationarity than others.

10.3.1 Lake Levels with Seiches

This question of stationarity is well-illustrated by our next time series. Figure 10.6 shows water-height data measured at the edge of the Salton Sea.¹¹ This is a closed basin, and so supports standing waves, which when excited by the wind cause oscillations that are called **seiches**. The data in Figure 10.6 shows variations that suggest periodicity, but they are sufficiently irregular that a stochastic process is an appropriate model. It is less clear that a stationary process is a valid model. But since these oscillations are fairly persistent, and amplitude variations of the type seen here occur repeatedly, we assume that a stationary stochastic process is an adequate mathematical model.

10.3.2 Magnetic Field Profiles

Our next three examples of geophysical data sequences are series of values in space. The first, in Figure 10.7 is the magnetic field measured on an aircraft flying seven km above the south-eastern Pacific Ocean, mostly over young ocean crust. The raw data look smooth, but if we remove a global magnetic-field model (another case of a deterministic component) we get residuals that vary irregularly, without even the suggest of an oscillation seen in Figure 1.4 or Figure 10.6. So a stationary stochastic process is a good model. Notice that the three components appear to be related, varying together in some fashion: there is a lag and perhaps a suggestion of differentiation of the vertical B_3 to obtain the along-track B_1 . Also, the total field is less variable than the individual components. In Chapter 15 we will discuss how to look for relationships between pairs of time series.

Our next dataset is another profile of the magnetic field, but over a much longer distance and measured much higher up: 300-600 km above the Earth's surface. This is the total geomagnetic field strength as measured by the Magsat satellite. The dominant signal is a roughly sinusoidal variation, caused by the satellite going between polar and equatorial fields, in an orbit inclined to the direction of the geomagnetic dipole. We could, as with the data of Figure 10.7, remove a model field; but it is more instructive not to.

¹¹A large (20×50 km), shallow (8.5 m) lake in the southern California desert (Oglesby, 2005).

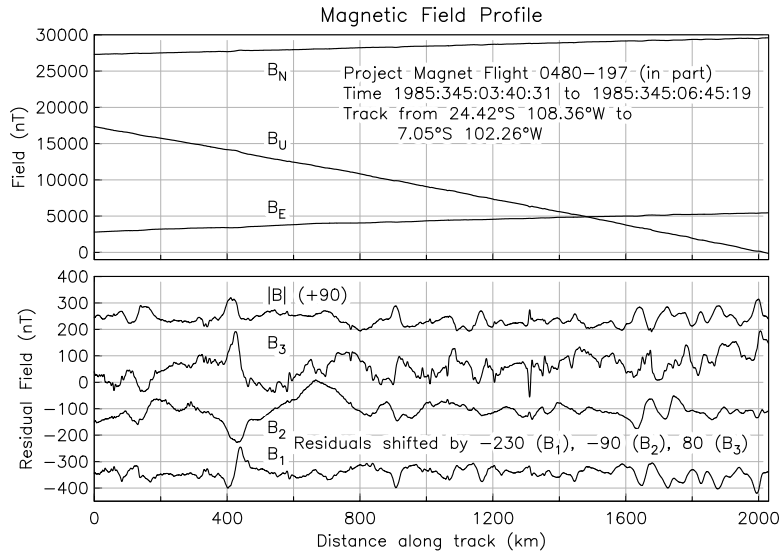


Figure 10.7: Magnetic anomaly profile over the eastern Pacific Ocean, The top frame shows value of three components in the geographical directions (North, East, and Up). The lower frame shows the residual values after the field predicted by a standard geomagnetic model (IGRF11) has been removed; the mean values are nearly zero, but the series have been offset for clarity. In this frame the horizontal components have been rotated so that B_1 is along the track, B_2 perpendicular to it, and the vertical has been relabeled B_3 . The magnitude of the field, $|B|$, has been found from these.

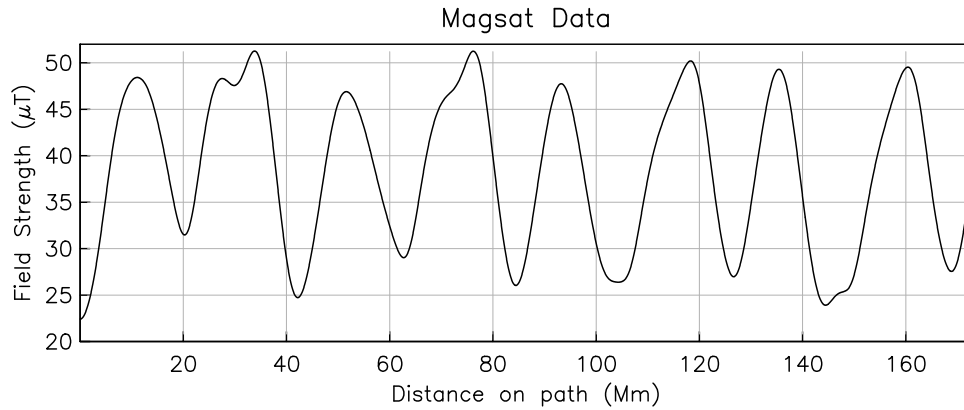


Figure 10.8: Total magnetic field observed over slightly more than four complete orbits of Magsat (Langel *et al.*, 1982): November 5, 1979, minutes 678.0 through 1055.3. The data have been interpolated (from finer sampling) to a spacing of 40 km along the orbit.

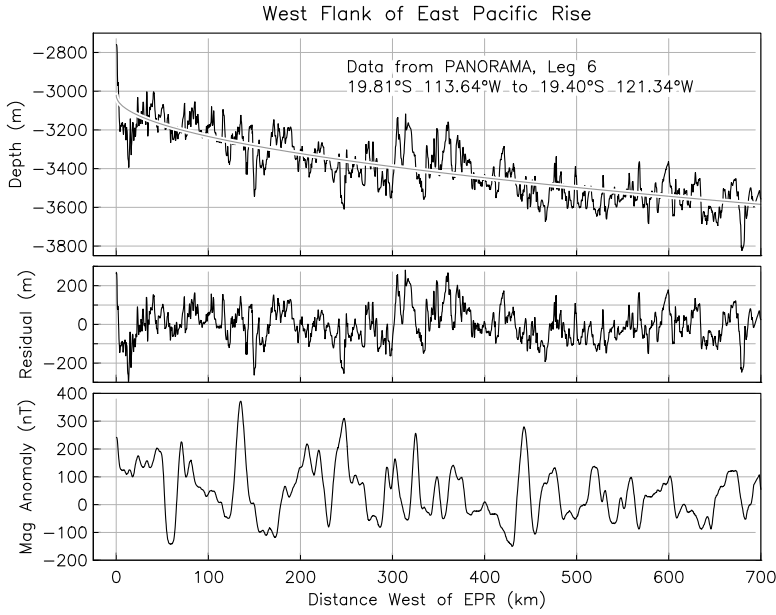


Figure 10.9: The upper panel shows bathymetry collected in April 1998 from R/V *Melville* along an east-west track west of the East Pacific Rise. The smooth curve is the fit to this of a constant plus a part varying as \sqrt{t} ; at this location the spreading rate is steady, so age t is proportional to distance from the axial high. The middle panel shows the residual “depth anomaly” after subtracting this fit. The bottom panel shows the magnetic anomaly measured at sea level.

10.3.3 Bathymetry

Our final example (Figure 10.9) is a profile of bathymetry and (again) magnetic anomalies across one side of the East Pacific Rise: two spatial series, though they could be made into time series if we used the age of seafloor rather than distance. The bathymetry data are very obviously not stationary, because as seafloor ages it sinks, owing to the plate cooling another case of deterministic behavior. Using the famous \sqrt{t} approximation for this depth change we can produce a residual, the depth anomaly, that seems, again, to be plausibly modeled by a stationary process.

10.3.4 Gaussian or Not?

The two assumptions that we place on our stochastic models are that they be stationary, which is fundamental to the analysis, and Gaussian, which ensures that the second moments are complete descriptions. How close the data are to Gaussian is best examined using probability plots (Section C.3.1). While such plots can be used to formally test whether or not the data are strictly consistent with

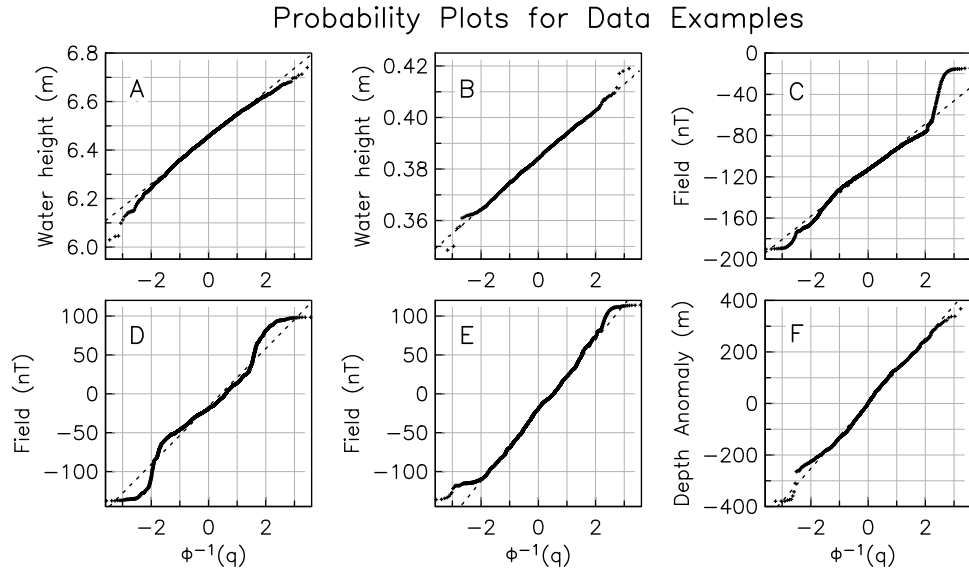


Figure 10.10: Probability plots for some of the data series. A is for an hour of the wave data shown in Figure 1.4. B is for the full water-level data from the Salton Sea; Figure 10.6 shows about half of the total. C, D, and E are for the magnetic-field data shown in Figure 10.7: C is the along-track field, D the cross-track, and E the vertical. F is the bathymetric data from the lower panel of Figure 10.9.

a Gaussian, we shall just take the first step of seeing how closely the data lie on a straight line in the plot. Nongaussian behavior creates a difficulty for filter-based models (equations 10.7, 10.8, and 10.9) since the Central Limit Theorem means that any filtered white noise tends to have a Gaussian distribution, whatever the pdf of the white noise.

Figure 10.10 shows probability plots for many of the data series we have discussed in this chapter and in Chapter 1; see Figure C.4 for plots of two others. The wave data from Figure 1.4 (panel A) are slightly non-Gaussian, being long-tailed for small values and short-tailed for large; by contrast the Salton Sea data (panel B) are almost perfectly Gaussian. The horizontal components of the magnetic field from the Project Magnet data (panels C and D) show some non-Gaussian behavior, being somewhat long-tailed but at the extremes actually truncated relative to a Gaussian. The vertical component (panel E) is asymmetric, with a positive tail and a compressed lower tail. Except for a few points at the extremes, the bathymetry residual data are very nearly Gaussian.

We do not show a probability plot for the Magsat data in Figure 10.8, for the simple reason that it is clearly very near to being sinusoidal – and the pdf of a sinusoid is far from being Gaussian. But once the sinusoidal part is removed,

something we will do in Section 14.3, what is left turns out to be nearly Gaussian.

CHAPTER 11

SPECTRA OF STOCHASTIC PROCESSES

We hold it as scientifically self-evident that knowledge of the power spectrum of some process is often all we want to recover from the measured data.

F. A. DAHLEN AND F. J. SIMONS, Spectral estimation on a sphere in geophysics and cosmology (2008)

11.1 Introduction

You will not be surprised that our preferred description of stochastic processes uses a function of frequency; by analogy with optics, a **spectral analysis**. Many things are simpler when looked at in the frequency domain. As described in Chapters 2 and 8, time-invariant systems, which include differential equations with constant coefficients, are most usefully studied by taking Fourier transforms. For many physical processes, at different frequencies their behavior is dominated by different physical laws, and so is best studied by examining them at various frequencies: in effect, to taking their Fourier transform. As we saw in Chapter 1, this is true for sea level; another example is the time variations of the magnetic field at a point on the Earth's surface. At periods longer than a year ($f = 3 \times 10^{-8}$ Hz), variations arise from the slow-moving liquids of the core dynamo; for periods from a year to 0.1 second ($f = 10$ Hz) from the interactions of the solar wind with the Earth's magnetosphere, and for frequencies from 10 Hz to 10^{10} Hz from electromagnetic radiation by sources natural (lightning) and artificial (radio transmitters).

In this chapter we develop the theory for finding a transform from time to frequency for stationary stochastic processes; in later chapters we discuss how best to actually find this transform, given a finite amount of data.

Up to now our Fourier transforms have been of functions of a real variable: in the terminology of Chapter 10, these functions return algebraic variables. For convenience we repeat the Fourier transform of such a function and its inverse in continuous time:

$$\tilde{x}(f) = \int_{-\infty}^{\infty} x(t) e^{-2\pi i f t} dt \quad x(t) = \int_{-\infty}^{\infty} \tilde{x}(f) e^{2\pi i f t} df \quad (11.1)$$

and for an infinite sequence in discrete time:

$$\tilde{x}(f) = \Delta \sum_{n=-\infty}^{\infty} x_n e^{-2\pi i f n \Delta} \quad x_n = \int_{-1/2\Delta}^{1/2\Delta} \tilde{x}(f) e^{2\pi i f n \Delta} df \quad (11.2)$$

In this expression we have included the sample interval Δ explicitly, rather than using dimensionless frequency $\zeta = f\Delta$.

11.2 Allocating Variance by Frequency

There are two reasons why we cannot apply these definitions to stochastic processes. First, the integral in (11.1), or the sum in (11.2) must actually exist, which means that it must converge as we let the function (or sequence) go from a finite towards an infinite length. For this to happen the function must somehow decrease in amplitude, or energy, as t or n becomes large, and a stationary process does not decrease in this way. Second, if we replace the $x(t)$ in equation (11.1) by a stochastic process $X(t)$ we obtain another random function, whereas we want to characterize $X(t)$ with an algebraic function that describes its properties in frequency, just as the autocovariance function does in time.

There is an intuitive way to see what we need by supposing that we wanted to know how much variability the stationary process exhibits at a frequency f_0 . Imagine a FIR filter with weights $\{w(f_0)\}$ that has a very narrow passband, so that the response is

$$\tilde{w}(f) = \begin{cases} 0 & f < f_0 - \frac{1}{2}f_\delta \\ 1 & f_0 - \frac{1}{2}f_\delta < f < f_0 + \frac{1}{2}f_\delta \\ 0 & f > f_0 + \frac{1}{2}f_\delta \end{cases}$$

where $f_\delta \ll f_0$. Now convolve the random sequence X with that filter: the output will be another stochastic process, though one with a very limited frequency content. Describe the amplitude of this new process by its variance, which we would expect to be proportional to the width f_δ of the bandpass filter (so the average amplitude is proportional to $\sqrt{f_\delta}$), provided that $f_\delta \ll f_0$. Making this assumption, we define

$$S(f_0) = \frac{\mathcal{V}[w(f_0) * X]}{f_\delta} \quad (11.3)$$

as the ratio of the variance of the filtered process to the bandwidth; note that $S(f_0)$ has to be positive. We assume that as f_δ goes to zero, $S(f_0)$ approaches a definite value that will depend on the center frequency f_0 , and is proportional to the variance in X at that frequency. The variance of X in a frequency band is called the **power** in that band and the function $S(f)$ is called the **power spectrum** of X . Equation (11.3) is our informal definition of $S(f)$ for both continuous and discrete processes. Before digital computers, analog spectral analyzers were built using just this method: data were sent into a large number of narrow band-pass filters

whose outputs went to rectifiers whose output showed the variance in each band (Barber, 1961).

11.2.1 PSD Dimensions and Units

Our intuitive description should help to clarify what the dimensions of the power spectrum are: these are often given incorrectly. Our intuitive description shows that the power spectrum is a variance divided by a frequency bandwidth. The dimension of the variance is just that of the original data, squared. So, if our series had the dimension of length (L), as it would if we were measuring sea level, or ground displacement, the dimension of the variance will be L^2 ; the unit would be m^2 . The dimension of the power spectrum would be this divided by frequency, which is to say $L^2F^{-1} = L^2T$, with units m^2/Hz or $m^2\text{s}$. So stated, this result may seem obvious, but it can easily be made obscure by the practice, common in engineering, of taking the square root of $S(f)$, which gives units such as $\text{m}/\sqrt{\text{Hz}}$: valid, but bewildering when first encountered.

The other Fourier representations have different dimensions. The definition of the Fourier transform, equations (11.1 and 11.2), also sets its dimensions, which are just those of x , multiplied by time: so for our example, the dimension of the Fourier transform would be $L/F^{-1} = LT$, and the units would be meter/Hz or meters. We can define the Fourier transform only for functions that are integrable over the real line, which means that they must decrease to zero at large times: they must show transient behavior rather than stationarity. For ground motion, the usual example would be an earthquake, as opposed to the (approximately stationary) fluctuations of background noise, for which a power spectrum is the only correct description.

A third case is that $x(t)$ goes on forever, not because it is stationary, but because it is periodic. Such a function can be represented by a Fourier series:

$$x(t) = \sum_{n=-\infty}^{\infty} C_n e^{2\pi i f_n t}$$

and obviously the dimensions, and units, of the Fourier coefficients are the same as for the original data: so, for our example, the dimension would be L and the unit would be meters. The sea level data discussed in Section 1.1 provide a good examples of all three Fourier representations, since the data include tides (purely periodic), ocean waves (a stochastic process) and, occasionally, a tsunami (a transient).

Using the wrong dimensions, for example showing a spectrum of wave motion in meters, or a power spectrum of tides or tsunami, is a marker of ignorance: in terms of spectra, these different phenomena are not apples and oranges, but apples and beef. This means that you *cannot* show these different kinds of spectra on the same plot – though, with some care, it is possible to intercompare them.

11.3 Two Definitions of the Power Spectrum

We now provide a more formal development of the power spectrum, for which a more precise name is the **Power Spectral Density** or **PSD**. We assume we have a stationary process $X(t)$, defined on the real line; we assume zero mean. As noted above, there are two problems with applying the Fourier transform directly:

1. The Fourier transform of X would not be defined because the integral cannot be found on the infinite interval.
2. The result would be a random function, not an algebraic one.

To fix the first problem we define $X_T(t)$ as the process $X(t)$ on the finite interval $(-T/2, T/2)$:

$$X_T(t) = \begin{cases} X(t) & -T/2 \leq t \leq T/2 \\ 0 & \text{otherwise.} \end{cases}$$

This is not stationary, but that is all right for now. Any particular realization of this process has a bounded 2-norm and thus has an ordinary Fourier transform:

$$\tilde{X}_T(f) = \mathcal{F}[X_T(t)] = \int_{-\infty}^{\infty} X_T(t) e^{-2\pi i f t} dt = \int_{-T/2}^{T/2} X(t) e^{-2\pi i f t} dt$$

But \tilde{X}_T is still a random function of f ; to remove this, we find its squared magnitude and take the expected value: $\mathcal{E}[|\tilde{X}_T(f)|^2]$.

We then let T tend to infinity; but we can easily see that if we do this, the integral, and hence the expected value, would grow to infinity – so we divide it by the interval length T to tame the growth. We thus get a function of frequency

$$\begin{aligned} S(f) &= \lim_{T \rightarrow \infty} \frac{1}{T} \mathcal{E}[|\tilde{X}_T(f)|^2] \\ &= \lim_{T \rightarrow \infty} \mathcal{E} \left[\frac{1}{T} \left| \int_{-T/2}^{T/2} X(t) e^{-2\pi i f t} dt \right|^2 \right] \end{aligned} \tag{11.4}$$

which defines the power spectral density. It can be shown that $S(f)$ exists for all stationary processes X with zero mean and a bounded variance. It is, obviously, real and non-negative.

You should be aware that equation (11.4) defines a normalization for the PSD that is not always used – indeed it is probably the less common choice. Equation (11.4) defines what is called the **two-sided PSD**, because in it f runs from $-\infty$ to ∞ . As with the Fourier transform of a real function, when X is real the power spectrum $S(f)$ is even, so we only need the values for $f \geq 0$. For real-valued series the normalization most often seen is the **one-sided PSD**, which is given by $2S(f)$ for $f \geq 0$; we explain the factor of two below. In using other people's spectra, you should be aware that the spectrum, unspecified, might be either the two-sided

spectrum shown for positive f only, or the one-sided spectrum – and you should, even if it seems pedantic, specify which one you use.

Looking at equation (11.4) we see that $S(f)$ is obtained from products of X with itself; it thus is related only to the second order moment of X – no third or higher order moments are involved. We already introduced a function involving second-order moments of X , namely the autocovariance $R(\tau)$, defined in equations (10.2) and (10.3). Does $S(f)$ provide independent information about X , or is there a connection between $R(\tau)$ and $S(f)$? Somewhat surprisingly the answer is that the functions $R(\tau)$ and $S(f)$ contain *exactly* the same information, because $S(f)$ is just the Fourier transform of $R(\tau)$

$$S(f) = \mathcal{F}[R(t)] = \int_{-\infty}^{\infty} R(t)e^{-2\pi i f t} dt \quad (11.5)$$

Equation (11.5) is often used as an alternative definition of the PSD, not least because it is (as we will see) more convenient than equation (11.4) for proving theorems about the PSD.

$R(\tau)$ is always even. For real data, it is also real and we can write

$$S(f) = \frac{1}{2} \int_0^{\infty} R(t) \cos(2\pi f t) dt \quad (11.6)$$

where $S(f)$ is still the two-sided spectrum; the $\frac{1}{2}$ absorbs a factor of two produced when we change the limits of the integral. If we used the one-sided spectrum (as makes sense for a real series) we would omit the $\frac{1}{2}$; for generality we will use the definition given by equation (11.5).

Before we establish the truth of (11.5) we note a few consequences of it. Since $R(t)$ is a real even function of t , (11.5) implies that $S(f)$ is also a real and even function of f . But clearly not every even function will have a positive Fourier transform, so the requirement that $S(f)$ must be non-negative puts severe restrictions on what functions $R(t)$ might be autocovariances;

The inverse transform of (11.5) is

$$R(t) = \int_{-\infty}^{\infty} S(f) e^{2\pi i f t} df \quad (11.7)$$

and recall from the definition of $R(t)$ that

$$R(0) = \mathcal{E}[X(t)X(t)] = \mathcal{V}[X] = \sigma^2$$

remembering that X is a zero-mean process. Setting $t = 0$ in (11.5) gives an important result:

$$\sigma^2 = \int_{-\infty}^{\infty} S(f) df \quad (11.8)$$

That is, *the area under the power spectrum is the variance of the process*. It is to preserve this property that we double $S(f)$ if we use the one-sided PSD; then, even

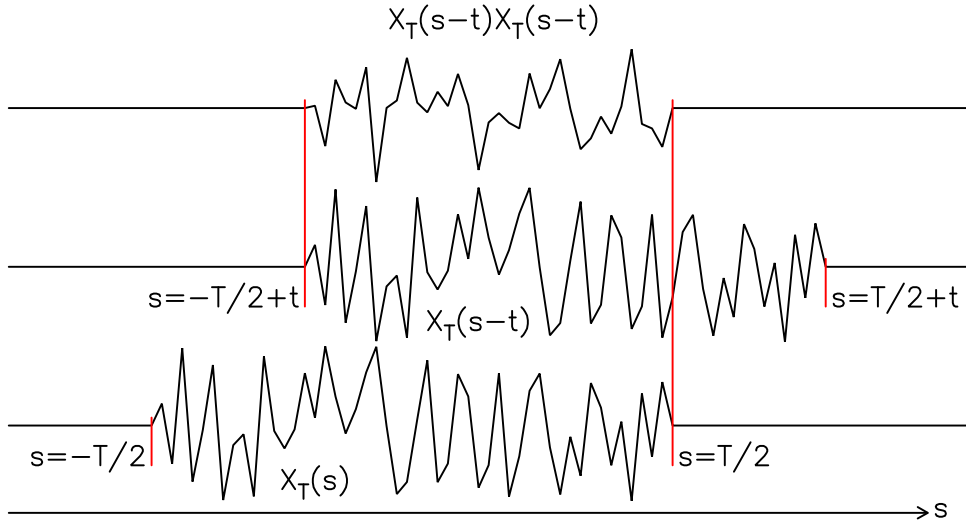


Figure 11.1: The integrand of equation (11.12)

though we integrate $S(f)$ only over positive frequencies, the integrated area is still the variance.

Now we verify (11.5); the argument follows the lines of the one given in Section 3.7.4, except that here we are considering random functions, and there we were considering algebraic functions. We start with the squared magnitude of the Fourier transform of the windowed function X_T :

$$|\tilde{X}_T|^2 = \tilde{X}_T \tilde{X}_T^* \quad (11.9)$$

Recall that the Fourier transform of a convolution is the product of the Fourier transforms; and, since X_T is real

$$\tilde{X}_T^*(f) = \int_{-\infty}^{\infty} X_T(t) e^{2\pi i f t} dt = \int_{-\infty}^{\infty} X_T(-t) e^{-2\pi i f t} dt = \mathcal{F}[X_T(-t)] \quad (11.10)$$

Note that the integrals are over the whole real line even though X_T is only nonzero over part of it.

Combining the convolution theorem with (11.10) and (11.9), we have

$$|\tilde{X}_T|^2 = \mathcal{F}[X_T(t) * X_T(-t)] = \mathcal{F} \left[\int_{-\infty}^{\infty} X_T(s) X_T(s-t) ds \right] \quad (11.11)$$

In (11.4) we have normalized by the interval T , so we put that into the definition of another function:

$$C_T(t) = \frac{1}{T} X_T(t) * X_T(-t) = \frac{1}{T} \int_{-\infty}^{\infty} X_T(s) X_T(s-t) ds \quad (11.12)$$

which is stochastic.

Then by (11.11), the Fourier transform of C_T is

$$\mathcal{F}[C_T] \stackrel{\text{def}}{=} \int_{-\infty}^{\infty} e^{-2\pi ift} C_T(t) dt = \frac{1}{T} \mathcal{F}[X_T(t) * X_T(-t)] = \frac{|\tilde{X}_T|^2}{T} \quad (11.13)$$

Our definition of the PSD is (11.4); let us plug (11.13) into that so that we get

$$S(f) = \lim_{T \rightarrow \infty} \mathcal{E}\left[\frac{|\tilde{X}_T|^2}{T}\right] = \lim_{T \rightarrow \infty} \int_{-\infty}^{\infty} e^{-2\pi ift} \mathcal{E}[C_T(t)] dt \quad (11.14)$$

From (11.12) we see that $C_T(t)$ is even in t , so we can always write $C_T(t) = C_T(|t|)$; in the following we will assume $t \geq 0$ and then replace t by $|t|$ at the end. We know $X_T(s)$ vanishes outside the interval $(-T/2, T/2)$ and therefore the integrand of (11.12) must vanish when $s > T/2$ or when $|s-t| > T/2$; see Figure 11.1. Therefore we can reduce the interval of integration in (11.12) to be over $(-T/2+t, T/2)$ instead of the whole real line. Also observe that, once $t > T/2$, the nonzero sections cease to overlap, and the integrand is identically zero.

These considerations lead to the result

$$C_T(t) = \begin{cases} \frac{1}{T} \int_{-T/2+t}^{T/2} X_T(s) X_T(s-t) ds & 0 \leq t < T/2 \\ 0 & t \geq T/2 \end{cases} \quad (11.15)$$

Further simplifications ensue when we take the expected value, as dictated by (11.14); for the segment $0 \leq t < T/2$

$$\mathcal{E}[C_T(t)] = \frac{1}{T} \int_{-T/2+t}^{T/2} \mathcal{E}[X_T(s) X_T(s-t)] ds = \frac{1}{T} \int_{-T/2+t}^{T/2} R(-t) ds$$

where we have, finally, introduced the actual autocovariance of the process, $R(t)$. Since $R(-t) = R(t)$, which is independent of s , we can evaluate the s integral explicitly:

$$\mathcal{E}[R_T(t)] = \frac{R(t)}{T} \int_{-T/2+t}^{T/2} 1 \cdot ds = R(t) \left[1 - \frac{t}{T} \right] \quad \text{for } 0 \leq t \leq T \quad (11.16)$$

From (11.15) $\mathcal{E}[R_T(t)] = 0$ when $t \geq T$. Recalling that R_T is even, we can write the negative t behavior from $R_T(t) = R_T(-t)$, and obtain the following complete description for the expected value of R_T :

$$\mathcal{E}[R_T(t)] = R(t) \Lambda_T(t) \quad (11.17)$$

where

$$\Lambda_T(t) = \begin{cases} 1 - |t|/T & |t| \leq T \\ 0 & |t| > T \end{cases}$$

which is a triangle function of unit height and width $2T$.

Substituting (11.17) into (11.14) gives us the following very plausible expression for the PSD:

$$S(f) = \lim_{T \rightarrow \infty} \mathcal{F}[R(t)\Lambda_T(t)] = \lim_{T \rightarrow \infty} \int_{-\infty}^{\infty} e^{-2\pi ift} R(t)\Lambda_T(t) dt \quad (11.18)$$

If we can put the limit in equation (11.18) inside the integral, and since $\Lambda_T(s) \rightarrow 1$ as $T \rightarrow \infty$, we then have the result we claimed: equation (11.5). This last step is where some care is needed. [Priestley \(1981\)](#) (pp. 211-215) uses the Lebesgue Dominated Convergence Theorem, and the further condition that

$$\int_{-\infty}^{\infty} |R(t)| dt < \infty \quad (11.19)$$

to prove that it is permitted to reverse the order of the limit and the integral. Section 11.7 contains a proof (by Parker) that makes a different set of assumptions about $R(t)$.

11.4 Some Properties of the PSD

We now examine the PSD further for processes in continuous time, relying for our proofs on the definition given by equation (11.5).

The simplest possible PSD is for white noise. By equation (10.6) in Chapter 10, a white noise in continuous time has a δ -function autocovariance; this makes the PSD

$$S(f) = \int_{-\infty}^{\infty} R(t)e^{-2\pi ift} dt = \int_{-\infty}^{\infty} \sigma^2 \delta(t)e^{-2\pi ift} dt = \sigma^2$$

which is a constant, independent of frequency. White noise therefore has the same power at every frequency, which is where the name comes from: white light is, ideally, light with the same power at each frequency. However, recall from (11.8) that the area under the PSD is the variance of the process. For ideal white noise this would be infinite, so continuous-time white noise is not a physically realizable phenomenon.

We next consider what happens to the PSD of a white-noise process if it is filtered by a time-invariant linear system. We already know that we can represent this filtering as a convolution, $Y = g * X$, where g is a filter function, possibly infinite in extent. How is S_Y related to S_X ? The simplest way to get the result is to compute the autocovariance of Y . Assume X has zero mean; then Y will also,

and

$$\begin{aligned}
 R_Y(t) &= \mathcal{E}[Y(s)Y(s+t)] \\
 &= \mathcal{E} \left[\int_{-\infty}^{\infty} du g(u)X(s-u) \int_{-\infty}^{\infty} dv g(v)X(s+t-v) \right] \\
 &= \int_{-\infty}^{\infty} \int_{-\infty}^{\infty} \mathcal{E}[X(s-u)X(s+t-v)]g(u)g(v)du\,dv \\
 &= \int_{-\infty}^{\infty} \int_{-\infty}^{\infty} R_X(t+u-v)g(u)g(v)du\,dv
 \end{aligned} \tag{11.20}$$

Now replace the autocovariance on the right with its representation in terms of S_X by applying equation (11.7):

$$\begin{aligned}
 R_Y(t) &= \int_{-\infty}^{\infty} \int_{-\infty}^{\infty} \int_{-\infty}^{\infty} S_X(f) e^{2\pi if(t+u-v)} g(u)g(v)du\,dv\,df \\
 &= \int_{-\infty}^{\infty} e^{2\pi ift} S_X(f) df \int_{-\infty}^{\infty} e^{2\pi ifu} g(u)du \int_{-\infty}^{\infty} e^{-2\pi ifv} g(v)dv \\
 &= \int_{-\infty}^{\infty} e^{2\pi ift} [S_X(f)\tilde{g}(f)^*\tilde{g}(f)] df \\
 &= \mathcal{F}^{-1}[S_X(f)\tilde{g}(f)^*\tilde{g}(f)]
 \end{aligned} \tag{11.21}$$

Next we take the Fourier transform of (11.21); since the Fourier transform of R_Y is the PSD of the output, S_Y , we find that

$$\begin{aligned}
 S_Y(f) &= \tilde{g}(f)^*\tilde{g}(f)S_X(f) \\
 &= |\tilde{g}(f)|^2 S_X(f)
 \end{aligned} \tag{11.22}$$

This is a very important result: it is the parallel, for stochastic processes, of the convolution theorem for algebraic functions. For such functions, the Fourier transform of a function produced by convolution is the Fourier transform of the original, multiplied by the Fourier transform of the convolving function. For a stochastic process the new power spectrum is found by multiplying the original spectrum by the squared magnitude of the Fourier transform of the convolving function. This result provides a rigorous foundation for the idea described in Section 11.2, that we could obtain a power spectrum by applying a series of ideal, narrow band-pass filters the stochastic process.

Another useful result is the relationship between the PSD of a continuous process and the PSD of the time derivative of the process. We also get this result by starting with the autocovariance $R(t) = \mathcal{E}[X(s)X(s+t)]$, differentiating with respect to t gives

$$\frac{dR}{dt} = \mathcal{E}[X(s)X'(s+t)]$$

where we use prime as a shorthand for the time derivative. Under the expectation operator, change variables so that $u = s + t$:

$$\frac{dR}{dt} = \mathcal{E}[X(u-t)X'(u)]$$

and differentiate again:

$$\frac{d^2R}{dt^2} = -\mathcal{E}[X'(u-t)X'(u)] = -R_{Xp}(-t)$$

where we use the Xp subscript to denote that this is R for X' . Now rearrange and take the Fourier transform, recalling that for any function g , $\mathcal{F}[g'] = 2\pi i f \mathcal{F}[g]$; this means that

$$\mathcal{F}[R_{X'}(-t)] = -\mathcal{F}\left[\frac{d^2R}{dt^2}\right] = 4\pi^2 f^2 \mathcal{F}[R_X]$$

and since we know the Fourier transform of $R(t)$ is just the PSD we see that the PSD of the derivative is

$$S_{X'}(f) = 4\pi^2 f^2 S(f) \quad (11.23)$$

which is to say that taking the derivative multiplies the PSD by $(2\pi f)^2$ – so it raises the level for high frequencies compared to low. In the next section we will see that the parallel operation in discrete time has very similar effects; taking derivatives (or more rarely integrals) before trying to find the spectrum is often worthwhile, for reasons we address in later chapters.

11.5 Power Spectral Density for Discrete Processes

Every result for a continuous-time stationary stochastic process has a similar result for discrete-time sequences; we state these without derivation. First, the definition of the PSD as a limit of discrete Fourier transforms is

$$S(f) = \lim_{N \rightarrow \infty} \frac{1}{N\Delta} \mathcal{E} \left[\left| \Delta \sum_{n=-N/2}^{N/2} X_n e^{-2\pi i n f \Delta} \right|^2 \right] \quad \text{for } -\frac{1}{2} \leq f \Delta \leq \frac{1}{2} \quad (11.24)$$

while the alternative definition through the autocovariance is

$$S(f) = \Delta \sum_{n=-\infty}^{\infty} R_n e^{-2\pi i n f \Delta} \quad \text{for } -\frac{1}{2} \leq f \Delta \leq \frac{1}{2} \quad (11.25)$$

which immediately means that we can obtain the autocovariance from the PSD: it is just the coefficients of the Fourier series expansion in (11.25):

$$R_n = \int_{-1/2\Delta}^{1/2\Delta} S(f) e^{2\pi i n f \Delta} df \quad (11.26)$$

Note that the PSD, even though it is derived from a discrete-time process, is a function of the real-valued frequency f .

If we set $n = 0$ in equation (11.26) we find

$$\sigma^2 = \int_{-1/2\Delta}^{1/2\Delta} S(f) df$$

so that the variance is again the integral of the PSD over frequency. And again, we need to be careful of normalization; for the two-sided spectrum $S_2(f)$ the expression is

$$\sigma^2 = \int_0^{1/2\Delta} S(f) df$$

which provides an easy way to check which normalization is being used by a computer program.

If we restrict ourselves to convolution filters, then filtering a discrete sequence gives the power spectrum

$$S_{g*X}(f) = |\tilde{g}(f)|^2 S_X(f) \quad (11.27)$$

where

$$\tilde{g}(f) = \sum_{n=-\infty}^{\infty} g_n e^{-2\pi i n f \Delta} \quad (11.28)$$

We can use this result directly to get the effect of taking a derivative; remember that in Section 9.2 we showed how to make a filter that was a close approximation to the derivative, with amplitude response approximating $|2\pi f|$; then equations (11.27) and (11.28) give the same result as equation (11.23) for continuous time.

11.5.1 Aliasing in the PSD

In Chapter 6 we looked at sampling of functions and the resulting aliasing of their Fourier transforms. We now examine how sampling of a stochastic process modifies its PSD: an important practical issue because for a continuous time series whose spectrum we want, we usually have only sampled data.

We again start with a continuous-time process $X(t)$, and from it get the discrete process produced by sampling:

$$X_j = X(j\Delta) \quad j = 0, \pm 1, \pm 2, \dots$$

As usual, it is easiest to derive the spectrum from the autocovariance. The autocovariance of the sampled series is

$$\begin{aligned} R_n &= \mathcal{E}[X_j X_{j+n}] \\ &= \mathcal{E}[X(j\Delta) X((j+n)\Delta)] = R(n\Delta) \end{aligned} \quad (11.29)$$

which is to say that the autocovariance of X_n is simply the sampled autocovariance of $X(t)$.

The PSD of the discrete process is given by (11.25), which we modify by including Δ in the exponent to scale the frequencies, replacing the Nyquist frequency of $\frac{1}{2}$ in (11.25) by $\frac{1}{2\Delta}$, and also scaling the expression by the same quantity:

$$S(f) = \Delta \sum_{n=-\infty}^{\infty} R_n e^{-2\pi i n f \Delta} \quad \text{for } -\frac{1}{2\Delta} \leq f \leq \frac{1}{2\Delta}$$

Now substitute (11.29)

$$S(f) = \Delta \sum_{n=-\infty}^{\infty} R(n\Delta) e^{-2\pi i n f \Delta}$$

To sum this series we appeal to the Poisson Sum Formula given in equation 6.12 and find

$$S(f) = \Delta \sum_{m=-\infty}^{\infty} \int_{-\infty}^{\infty} R(n\Delta) e^{-2\pi i n f \Delta} e^{-2\pi i n m} dn$$

We change variables in the integral, set $t = n\Delta$, and then recognize the definition of PSD for the continuous process:

$$\begin{aligned} S(f) &= \sum_{m=-\infty}^{\infty} \int_{-\infty}^{\infty} R(t) e^{-2\pi i t (f + m/\Delta)} dt \\ &= \sum_{m=-\infty}^{\infty} S_c(f + m/\Delta) \end{aligned}$$

where S_c is the spectrum of the original continuous process. The discrete process PSD is thus the sum of these spectra, shifted by multiples of twice the Nyquist frequency $f_N = 1/2\Delta$. This is exactly parallel to the summing and shifting of the Fourier transform that takes place when we sample a nonrandom function, so we can again view it as a series of foldings of the frequency axis – $-\infty, \infty$ which maps it all into the interval $[-f_N, f_N]$ – or for real-valued processes, maps the range $[0, \infty$ to the interval $[0, f_N]$. If the power in the continuous process falls to low levels at and above the Nyquist frequency, the PSD of $S(f)$ will be a good approximation to $S_c(f)$ – but not otherwise. So, to get a good PSD we must set the sampling rate high enough to avoid aliasing at a level that would significantly distort the spectrum: where “significantly” and “high enough” depend on our judgement, and on what we think the spectrum of the continuous process is.

11.5.2 Sampling and Normalization

Sampling brings up another issue that, though trivial, is easy to miss. Most PSD computations are done using routines that do not explicitly include the value of the sample interval, but we want the spectrum to have physical units, including an actual frequency: Hz, cycles per year, or km^{-1} . (For time series, we strongly recommend that you use Hz for the frequency unit in the power spectrum unless there is some physical reason not to; for example, in earth-rotation studies cycles/d is more meaningful.)

To give a computed spectrum the appropriate units, we thus need to find what the program assumes the sample interval to be, though it is most useful to work in terms of an assumed Nyquist frequency f_{NP} . Remember that for real data we assumed the spectrum was one-sided, so that the integral of the spectral values,

taken from zero to the actual Nyquist frequency f_N , will equal the variance. To find f_{NP} , make the input a white noise with variance σ^2 . If the computed spectrum has an average value of S_w , the integral will be σ^2 if $f_{NP} = \sigma^2/S_w$, meaning an assumed sample interval $\Delta_P = S_w/2\sigma^2$. For example, if $\sigma^2 = 1$ (a convenient value) and $S_w = 1$, $f_{NP} = 1$, and the implicit sample interval is $1/2$.

Then to convert the PSD to actual frequency units, scale the spectrum by f_{NP}/f_N , where $f_N = \frac{1}{2\Delta}$ is the Nyquist frequency in whatever units we use. So the overall scaling, given Δ , σ^2 , and S_w , is the dimensionless quantity $2\Delta\sigma^2/S_w$. We give an example in Section 11.6.1.

11.6 Some PSD Examples

We now look at some PSD's estimated from actual data; how to make such an estimate we leave to Chapters 12 and 13. But we include here some discussion of how best to plot a spectrum, something often done badly.

11.6.1 Data with Resonances

We begin with the Salton Sea data. Figure 11.2 is an estimate of the PSD of the 260 hours (1300 data points) that are available (more than were shown in Figure 10.6). We saw in Chapter 10 that the data time series suggests a number of resonances excited by the wind. The PSD indeed contains a number of peaks, well separated in frequency, with the lowest-frequency one being at 0.169MHz, or a period of 94.5 minutes.¹

The peaks are far from being delta functions because frictional losses damp the lake resonances and broaden the peaks. The four peaks picked out are certainly significant; there are other smaller ones that may or may not actually be present.

As in nearly all our plots of spectra, we use a logarithmic scale for the $S(f)$ -axis by expressing the power spectral density in dB relative to a reference level. Notice that for power, which is the square of the amplitude, the conversion to dB is $10\log_{10}(S(f))$, equivalent to taking $20\log_{10}$ of the amplitude. We need this logarithmic scaling because, as is almost universally true for geophysical data, the spectrum has a large dynamic range: the ratio between the largest and smallest value, which we first introduced in Section 6.8. If we used a linear scale for the PSD level, only the leftmost part of the plot would be visibly different from zero.

As we stated in section 11.2.1 the PSD, being a measure of variance per unit frequency, has the dimensions of X^2T , where X is the dimension of the original data. So here the PSD level is dB relative to $1 \text{ m}^2/\text{Hz}$. To get this result required two scalings. First, scaling the data from digital units (counts) to meters. Second,

¹This is actually not the lowest-frequency mode of oscillation of the lake; as it happens, this particular measurement was made at a nodal point for this mode.

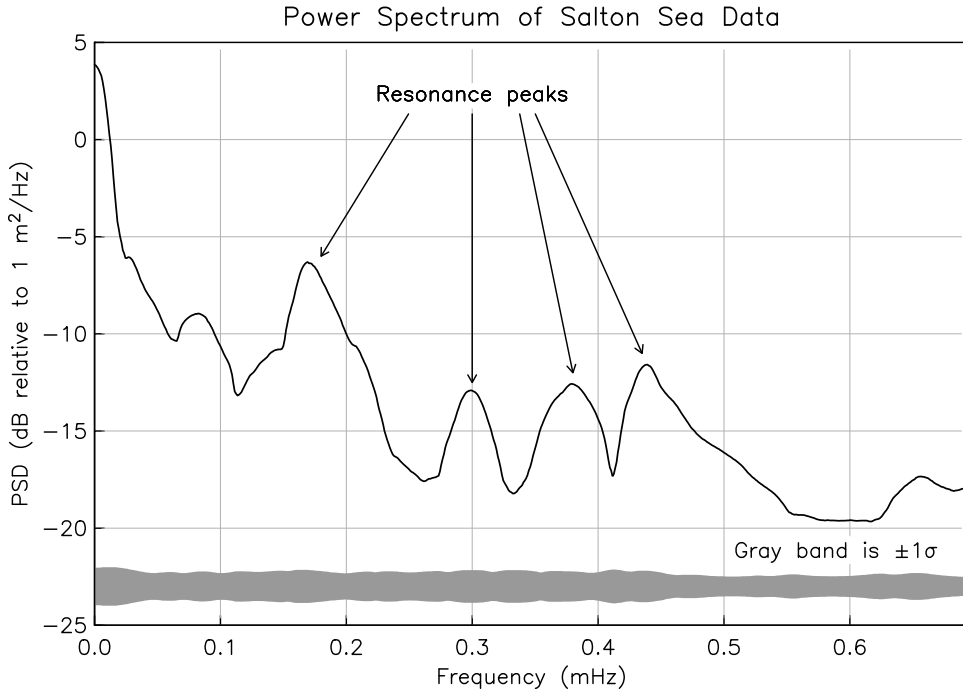


Figure 11.2: Power spectral density of Salton Sea data. The gray band shows the one-standard-deviation error estimates; this is smaller for frequencies where the spectrum is varying gradually with frequency and larger if it changes more abruptly.

we found that for unit-variance noise put in, our power-spectrum program output a value $S_w = 2$; so the scaling to go to from the output of our program to m^2/Hz was $2\Delta\sigma^2/S_w = \Delta$, which was 720 s. So we had to multiply the levels by 720, or equivalently add 28.6 dB ($10\log_{10}(720)$) to the output of the program.

With a properly normalized spectrum, we can find the variance associated with the different peaks. For example, the lowest peak at 0.3 mHz (period just under an hour) has a value of about -12 dB, or $0.063\text{m}^2/\text{Hz}$, and a width of about 0.1 mHz, so the variance is $6.3 \times 10^{-6}\text{m}^2$; the square root of this, σ , is 2.5 mm: not very large. For time series σ is often called the **root-mean-square** or **rms**; since Gaussian data would stay between $\pm 2\sigma$ 95% of the time, the rms σ is a good approximation to what we would, just looking at the time series, say was the amplitude.

Observe the rise in power at the lowest frequencies: this behavior, common in geophysical data, is called having a **red spectrum**, the color being that of light which has power concentrated towards long wavelengths and low frequencies. Red spectra are common partly because natural behaviors (for example, seismic losses, or upward continuation in potential fields) act as low-pass filters.

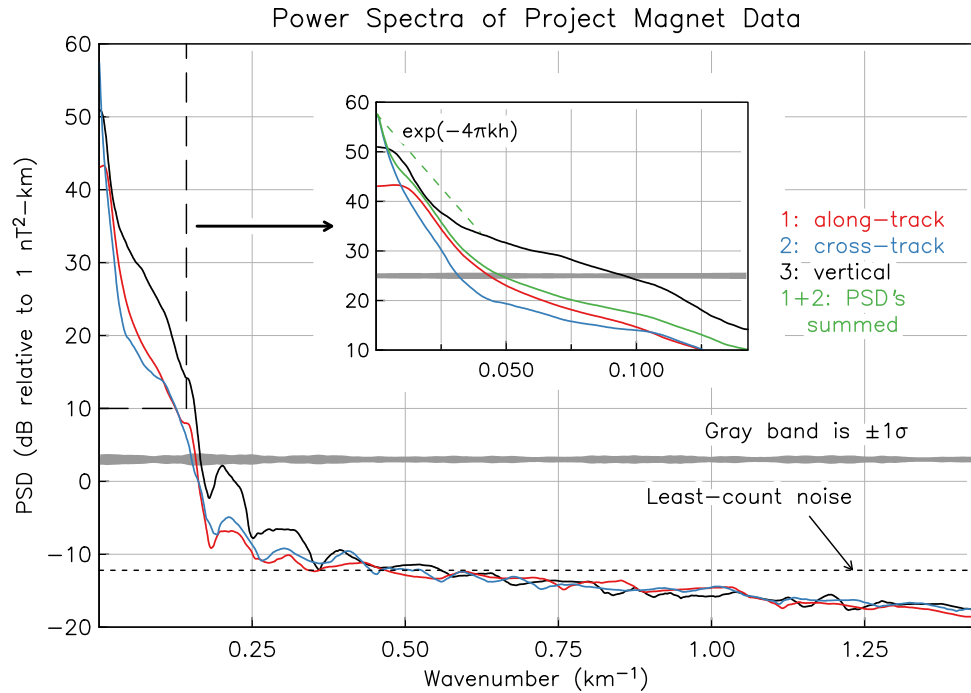


Figure 11.3: Estimated PSD of the three components of magnetic data shown in Figure 10.7. The gray band gives the error of the spectral estimate. The inset shows the low-frequency part (dashed box in main plot) in more detail. The field values are sampled every 350 m, so the Nyquist frequency f_N is $\frac{1}{2 \times 0.35} = 1.43 \text{ km}^{-1}$.

11.6.2 Mostly Redundant Data

We next look at the spectrum of the magnetic field data from Figure 10.7. Figure 11.3 shows the whole spectrum up to the Nyquist frequency (or, to be pedantic, the Nyquist wavenumber). Notice the very large dynamic range of the PSD. The claimed accuracy of the magnetometer is $\pm 1 \text{ nT}$. From Section 6.8 on quantization noise, we would expect this to mean that there is uncorrelated noise with a variance of $1/12 = 0.083 \text{nT}^2$. The dashed horizontal line in Figure 11.3 corresponds to the spectrum of white noise with this variance: a level of $10 \log_{10}(0.083/1.43) = -12.3 \text{ dB}$. For two-thirds of the wavenumber axis all the spectra are close to this level: any actual geophysical signal is totally obscured by quantization noise. So while the data are in no way aliased, higher precision would have been useful. This is an example of a general rule: if the PSD levels off at high frequency, instrument noise has probably overwhelmed the signal of interest, so any high-frequency be-

havior in the time series is probably not geophysical.²

In the inset to Figure 11.3 we have expanded the wavenumber scale to show the small-wavenumber part of the spectrum more clearly. We see that at this scale the PSD approximates two intersecting straight lines. The theory of upward continuation of static magnetic fields shows that at a height h above the source of the field, it is attenuated by a filter with frequency response $\tilde{g}(k) = e^{-2\pi kh}$, where k is the wavenumber. Recall that the effect of the filter on the PSD is to square this response. The plot includes a line corresponding to $|\tilde{g}|^2$ for $h = 11\text{ km}$, the aircraft height (7 km) plus the average ocean depth (4 km). It is plausible to assume that the PSD near the crustal sources of the field is relatively flat (a white PSD); after upward continuation the observed spectrum fits that prediction quite well. What then is the source of the straight-line dependence of the PSD on wavenumber for wavenumbers from about 0.03 km^{-1} to 0.13 km^{-1} ? Parker and O'Brien (1997) showed that the power in this wavenumber band comes from imperfections in the system that keeps the magnetometer oriented in a constant direction. So only for wavenumbers below $k = 0.03\text{ km}^{-1}$, the lowest 3% of the spectrum, do the observations contain actual information about the crustal field. The inset also shows that the horizontal components have less power than the vertical, and also that at the very lowest frequencies the cross-track PSD is larger than the along-track.

So the PSD can reveal properties of the original signal that could not be deduced from visual inspection of the original sequence or from the autocorrelation function. In this case we could learn even more by comparing the B_1 , B_2 and B_3 components using what is called a cross-spectrum. We will describe this in Chapter 15 and in Chapter 16 will apply it to these data.

11.6.3 Fractal Bathymetry

Finally, we look at the PSD (Figure 11.4) estimated from the detrended marine bathymetry data (Figure 10.9). Here we have used a log scale for the wavenumber axis, as well as the PSD level, to show that the power spectrum is approximated well by a straight line, which means that the PSD is proportional to a power of the frequency: this is called a **power-law spectrum**, with $S(k) = \beta k^{-q}$; in this case q is about 2.6.

A time series with a power-law spectrum has no intrinsic time or length scale: the process will look the same at any magnification – which is the hallmark of a **fractal**. This ideal behavior is never true for all scales: here it breaks down at wavelengths longer than about three km. The geological process responsible for this spectrum is repeated fracturing and faulting; there are some theories (Fox and Hayes, 1985) that predict fractal behavior, although it does not seem to be possible to predict the exponent q very well.

²Unfortunately, over-interpretation of high-frequency wiggles remains common.

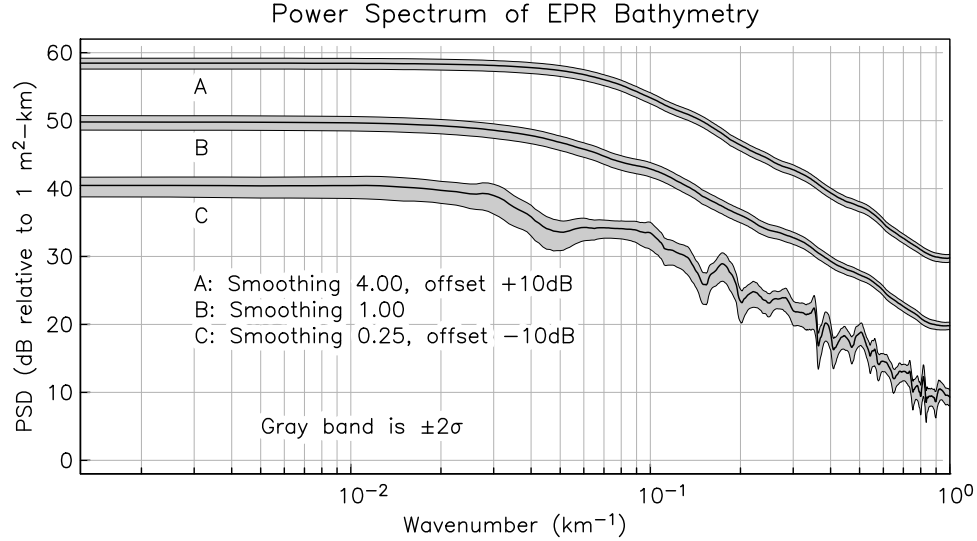


Figure 11.4: PSD of ocean rise bathymetry. The Reidel-Sidorenko method used here allows adjustment of the amount of smoothness imposed; here we show the spectra for three different values, offset for clarity. As the smoothness is decreased the error band becomes wider.

11.7 Appendix: Proof of Equation (11.18)

In Section 11.3 we left the proof of the validity of the interchange of the integral and limit to a reference to Priestley. There is a reason why Priestley's proof is not entirely satisfactory, namely, the additional restriction (11.19) is too severe, since it excludes autocovariance functions behaving like the sinc function, which are associated with a discontinuity in $S(f)$. Here is an alternative proof.

We examine the difference between the desired result and the function within the limit, and show that the difference vanishes under some mild restrictions, as T becomes large. We measure the discrepancy with the 2-norm:

$$\|f(t)\|^2 = \int_{-\infty}^{\infty} |f(t)|^2 dt$$

Define the number

$$A_T = \|\mathcal{F}[\Lambda_T R - R]\| = \|\Lambda_T R - R\| \quad (11.30)$$

The second equality follows from the Power Theorem, the invariance of the 2-norm

under the Fourier transform. Then, since Λ_T and R are both real and even,

$$\begin{aligned} A_T^2 &= \int_0^\infty (\Lambda_T(t) - 1)^2 R(t)^2 dt \\ &= \int_0^T (\Lambda_T(t) - 1)^2 R(t)^2 dt + \int_T^\infty R(t)^2 dt \\ &= \int_0^T \frac{t^2}{T^2} R(t)^2 dt + \int_T^\infty R(t)^2 dt \end{aligned}$$

To proceed we need to assume something more about the behavior of $R(t)$. We know $R(t)$ is never greater than σ^2 , so it is bounded; we will assume that it dies away for large t , but more rapidly than some power v :

$$|R(t)| < \frac{c}{(1+t)^v} \quad (11.31)$$

for some fixed values of c and v . With this constraint we can see that

$$A_T^2 < \frac{1}{T^2} \int_0^T \frac{c^2 t^2}{(1+t)^{2v}} dt + \int_T^\infty \frac{c^2}{(1+t)^{2v}} dt = \frac{A_T}{T^2} + B_T \quad (11.32)$$

Our interest lies in the behavior of A_T as T tends to infinity. Applying L'Hopital's rule of elementary calculus to the first term:

$$\begin{aligned} \lim_{T \rightarrow \infty} \frac{A(T)}{T^2} &= \lim_{T \rightarrow \infty} \frac{A'(T)}{T} \\ &= \lim_{T \rightarrow \infty} \frac{T c^2}{(1+T)^{2v}} = 0 \quad \text{when } v > \frac{1}{2} \end{aligned}$$

In the second term we find

$$B(T) < \int_T^\infty \frac{2c^2}{t^{2v}} dt = \frac{2c^2}{2v-1} \frac{1}{(T)^{2v-1}}$$

and, provided that $v > \frac{1}{2}$, $B(T)$ tends to zero with large T . Thus if $v > \frac{1}{2}$, both terms in (11.32) tend to zero for large T and this means that A_T vanishes: hence, the discrepancy between the Fourier transform of R and the $\mathcal{F}[\Lambda_T R]$ also vanishes in the limit. In the context of bounded functions like $R(t)$ our class of functions in (11.31) is much bigger than the one in Priestley's proof and includes, for example, the sinc function.

CHAPTER 12

ESTIMATING POWER SPECTRA: THEORY AND CHALLENGES

There was the periodogram in front of us; and if there were any new facts it seemed that they would reveal themselves to us in its eccentricities. I think we have had an indication this afternoon that when we have got this periodogram the work is only beginning.

H. H. TURNER, Discussion of a paper presented by Prof. A. Schuster,
The Observatory, **29**, 47 (1906).

12.1 Introduction

Once we assume that we can model a data set by a stationary stochastic process, we have automatically assumed that it has a PSD. We would like to make “good” estimates of this PSD, or (much more rarely) of the autocovariance function. In estimating either function we face a challenge not present for many statistical estimates: from a finite number, N , of data values we are trying to estimate not just a few parameters, but a function with infinitely many values. We always have to settle for a simplified version of the function, usually one that is somehow required to be “smooth” as f varies.

We model our data by a discrete stochastic process $\{X_n\}$, with a sampling interval $\Delta = 1$. Being stationary, this process extends over infinite time; but we must form our estimate from only N values. We first assume that there is no perfectly periodic behavior, as this would correspond to a delta function in the PSD, and make estimation much more difficult. So an important preprocessing step is to remove any periodic components by fitting and subtracting sinusoids with the appropriate periods.

Finally, for our theoretical development, we must assume the process is **ergodic**. What does this term mean? When developing the theory of the PSD in Chapter 11, we used the expectation operator freely; but this only makes sense if we assume that it is possible to generate as many realizations of the process as required, so that when the expectation \mathcal{E} is needed, we can take the average over the realizations. We might think of this as having many series, all produced at once from many simultaneous experiments.

But in geophysics we cannot always say that there are, many realizations, since there is just the one Earth. Sometimes we can get many realizations by sampling different regions, but usually all we have is a single data series such as the time history of the Earth's magnetic field. We then must model this as *one* realization of the stochastic process. We will see that to get a good spectrum estimate, it is absolutely essential to average something; if we cannot average over realizations, we must average over time. For this to work, the process must be one for which averaging over infinite time gives the same answer as averaging over infinitely many realizations. Such equality of averages does not occur for all stationary processes, but only for ergodic ones. We can guess that a process would be ergodic if the autocorrelation dies away fast enough that two well-separated sections of the data series will also be independent. It can be shown that a discrete process X_n is ergodic if

$$\sum_{n=-\infty}^{\infty} R^2(n) = \int_{-1/2}^{1/2} S^2(f) df \quad (12.1)$$

with both integrals finite. This is a pretty mild condition, indeed one that is satisfied by any process with a bounded spectrum.

Spectral estimation has a huge literature describing an enormous variety of methods. We will describe statistical considerations that distinguish better methods from worse ones; unfortunately ignorance or inertia lead many people to still use some of the worse ones. We describe the more popular of these inferior methods in Appendix E,¹ when you see them used you will know that the estimates could have been better.

12.2 Statistical Estimation

In discussing the performance of power spectrum estimation methods, usually termed **estimators**, we are entering the branch of statistics called **estimation theory**. Here we provide only some terminology and symbols, with a fuller development in Section C.4.

Our finite data set is $\{x_n\}$, which we model by N random variables $\{X_n\}$. We have some kind of procedure (the estimator) that produces, from these data, a value for some parameter, or parameters, that describe some aspect of the probability properties of X : for example the expected value $\mathcal{E}[X]$, the variance, or the power spectral density at some frequency. We use θ for this parameter, and θ_t for its true value: both of these are algebraic variables. Applying our estimation procedure to the data $\{x_n\}$ then gives us an estimate of θ_t . Our symbol for this estimate is $\hat{\theta}$, with the hat ($\hat{\cdot}$) symbol denoting an estimate.

Now, if we apply the same procedure to the random variables $\{X_n\}$, we get another random variable, $\hat{\Theta}$, whose properties tell us something about how good,

¹The introductory section of Thomson (1982) gives a more complete catalog of such methods.

or bad, the estimator is at finding θ_t —which, remember, is a parameter used to create $\{X_n\}$, so not unknown at all.² Three measures of the quality of an estimator are:

1. What is the expected value of the difference between $\hat{\Theta}$ and θ_t , that is, $\mathcal{E}[\hat{\Theta} - \theta_t]$? That is, on average will $\hat{\Theta}$ give the true value? If $\mathcal{E}[\hat{\Theta} - \theta_t] = 0$ we call $\hat{\Theta}$ an **unbiased estimate**, otherwise it is a **biased estimate**. The value of $\mathcal{E}[\hat{\Theta} - \theta_t]$ can depend on N ; if as $N \rightarrow \infty$, $\mathcal{E}[\hat{\Theta} - \theta_t] \rightarrow 0$ we call $\hat{\Theta}$ **asymptotically unbiased**: more data give a better answer.
2. How does the variance of $\hat{\Theta}$, $\mathcal{V}[\hat{\Theta} - \mathcal{E}[\hat{\Theta}]]$, change as $N \rightarrow \infty$? We would certainly like this variance to shrink. If $\mathcal{V}[\hat{\Theta} - \mathcal{E}[\hat{\Theta}]] \rightarrow 0$ as $N \rightarrow \infty$, we call the estimator (or the estimate it produces) **consistent**;³ if not, the estimate or estimator is **inconsistent**. Inconsistency, like asymptotic bias, means that more data will not improve anything: not what we would want.
3. As described in Section C.4, we can combine bias and variance to create an overall performance number for an estimator, the **mean square error**, equation (C.15). This is useful when there is a tradeoff between bias and variance.

12.3 The Periodogram

To start, we apply the same approach as we just used for the mean: use the formula that defines the PSD as the formula for estimating it, but replace the expectation by an average. We use equation (11.4), which is the limit over longer and longer sections of a discrete Fourier transform of the data. Applying this to data gives what is called the **periodogram estimator**.

While a modified version of this procedure will be the basis of our preferred estimator, the unmodified periodogram itself is a poor estimator. Far too many spectra are estimated by simply applying equation (11.24) directly to the data:

$$\hat{S}(\zeta) = \frac{1}{N} \left| \sum_{n=0}^{N-1} x_n e^{-2\pi i n \zeta} \right|^2 \quad \text{or} \quad \hat{S}_k = \frac{|\tilde{X}_k|^2}{N} = \frac{1}{N} \left| \sum_{n=0}^{N-1} x_n e^{-2\pi i n k / N} \right|^2 \quad (12.2)$$

In the left-hand equation we have assumed a dimensionless sample interval of one, and so have reverted to the nondimensional frequency ζ for the expression in

²In most discussions the $\{X_n\}$ are called a sample, and $\hat{\Theta}$ a sample estimate: both terms reflect the idea that our data are a subset of a much larger collection. We prefer to just say that we are using some random-variable model for our data.

³This is a simplification: the full definition of consistency is that the pdf of the estimate approaches a delta function as $N \rightarrow \infty$, which of course leads to the variance going to zero.

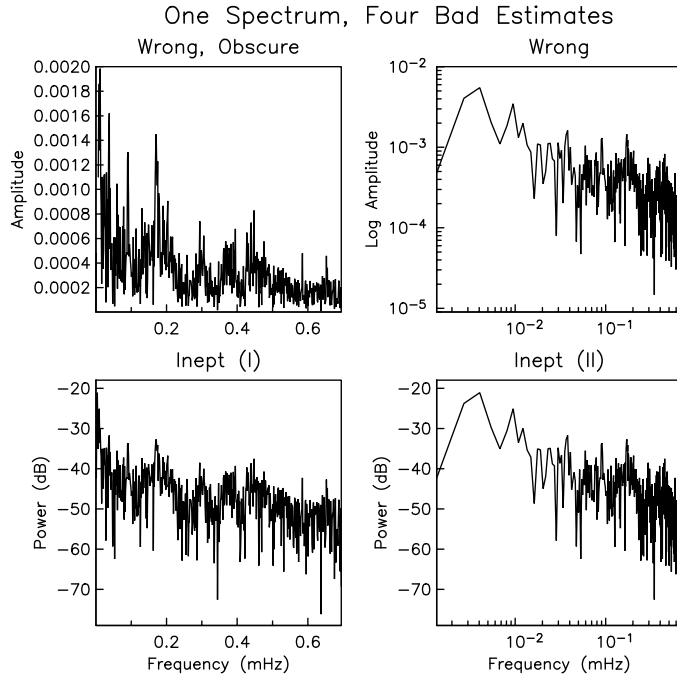


Figure 12.1: Several flavors of “spectra” that aren’t, or are badly estimated: all are for the seiche data shown in Figure 10.6. On the upper left, the Fourier amplitude (meaningless for a stochastic process) plotted on a linear scale (which fails to show the dynamic range adequately); the plot on the upper right fixes this mistaken plotting choice, but is still meaningless. The two lower plots show the power spectral density, on the left without units (another solecism), and on the right estimated using the periodogram.

real-valued frequency, with $-\frac{1}{2} \leq \zeta \leq \frac{1}{2}$. This should be looked at as the definition of the periodogram, even though most periodograms are computed for the discrete frequencies of the DFT as in the right-hand equation, with index k falling in the range $-\frac{1}{2}N < k \leq \frac{1}{2}N$.

Equation (12.2) is superficially appealing: it seems natural to just take the FFT and square the magnitudes of the coefficients to estimate of the PSD, this is sometimes called a **direct spectral estimate**. Even though this estimator is a poor one, we will discuss it in some detail, both to show why it is poor and because we will end up recommending modifications of it. Understanding why the periodogram is a bad estimator shows what needs to be done to fix its problems.

The spectra shown in Figure 12.1 are, alas, typical of many in the literature; the top two are not even power spectra, because they are normalized to give the Fourier amplitude, a meaningless quantity for a stochastic process. The lower

plots show a periodogram estimate, and one of its typical features, namely lots of dense wiggles at high frequency:⁴ if you see a spectrum with this feature, you know the author needs to learn more about spectral estimation! In Figure 11.2 we already showed a properly-estimated spectrum of these data plotted with meaningful units. Comparing Figures 11.2 and 12.1 will show you how much more clearly the salient features of the data appear when the spectrum is estimated intelligently.

12.3.1 The Periodogram for White Noise

We first examine the periodogram by using it to estimate the spectrum of the simplest possible stochastic process, namely the white noise of Section 10.2.2), in particular Gaussian white noise. a sequence of independent Gaussian random variables with zero mean and variance σ^2 . The autocovariance is $R(n) = \sigma^2 \delta_{n0}$. So the true PSD $S(\zeta)$, the Fourier transform of this, is constant and equal to σ^2 for $-1/2 \leq \zeta \leq 1/2$.

The right-hand expression in equation (12.2) is the estimate of the PSD at the $N + 1$ equally-spaced frequencies that come from using the DFT, evenly sampling the frequency range $-1/2 \leq \zeta \leq 1/2$. As we saw in Section 5.5, this choice of frequencies makes the Fourier transform easy to calculate; there turn out to be other reasons to choose them for the periodogram.

For convenience we take N to be even. Define the real and imaginary parts of the DFT in equation (12.2) as $\tilde{X}_k^R = \mathcal{R}[\tilde{X}_k]$ and $\tilde{X}_k^I = \mathcal{I}[\tilde{X}_k]$. We can then write the periodogram estimate as

$$\hat{S}_k = \frac{(\tilde{X}_k^R)^2 + (\tilde{X}_k^I)^2}{N} \quad -\frac{1}{2}N < k < \frac{1}{2}N \quad (12.3)$$

To get the statistical properties of the periodogram for white noise, we start by finding the pdf's of \tilde{X}_k^R and \tilde{X}_k^I . The definition of \tilde{X}_k means that these are just sums of samples from a Gaussian process, weighted by the exponential values: this means that all the \tilde{X}_m^R 's and \tilde{X}_m^I 's also have a Gaussian distribution. This in turn means that the pdf's are completely specified by the mean value and variances of each variable, and the covariances between them, as in equation (C.22 from Appendix C).

It is simple to find the mean values:

$$\mathcal{E}[\tilde{X}_k^R] = \mathcal{R} \left[\sum_{n=0}^{N-1} \mathcal{E}[X_n] e^{-2\pi i n k / N} \right] = 0 = \mathcal{E}[\tilde{X}_k^I] = 0$$

To calculate the variances and covariances we start by looking at the DFT variables \tilde{X}_k . The covariance between these at two frequencies can be written in two

⁴The usual jargon for this is to say that the spectrum is extremely **noisy**.

ways: first, in terms of \tilde{X}^R and \tilde{X}^I , and second, as a product of the DFT's:

$$\begin{aligned}\mathcal{E}[\tilde{X}_j \tilde{X}_k^*] &= \mathcal{E}[\tilde{X}_j^R \tilde{X}_k^R + \tilde{X}_j^I \tilde{X}_k^I] - i\mathcal{E}[\tilde{X}_j^R \tilde{X}_k^I - \tilde{X}_k^R \tilde{X}_j^I] \\ &= \sum_{m=0}^{N-1} \sum_{n=0}^{N-1} \mathcal{E}[X_m X_n] e^{-2\pi i m j / N} e^{2\pi i n k / N} \\ &= \sum_{m=0}^{N-1} \sum_{n=0}^{N-1} \sigma^2 \delta_{mn} e^{-2\pi i (mj - nk) / N} \\ &= \sigma^2 \sum_{m=0}^{N-1} e^{-2\pi i m(j-k) / N}\end{aligned}$$

where we have made use of the white-noise nature of X . The sum at the end is an expression we have seen before in Section 5.5: from equation (5.19), we know that this sum vanishes unless $j = k$, in which case it is N . Therefore

$$\mathcal{E}[\tilde{X}_j^R \tilde{X}_k^R + \tilde{X}_j^I \tilde{X}_k^I] - i\mathcal{E}[\tilde{X}_j^R \tilde{X}_k^I - \tilde{X}_k^R \tilde{X}_j^I] = N\sigma^2 \delta_{jk} \quad (12.4)$$

In an exactly similar way we can calculate

$$\mathcal{E}[\tilde{X}_j \tilde{X}_k] = N\sigma^2 \delta_{j,-k}$$

and so find that

$$\mathcal{E}[\tilde{X}_j^R \tilde{X}_k^R - \tilde{X}_j^I \tilde{X}_k^I] + i\mathcal{E}[\tilde{X}_j^R \tilde{X}_k^I + \tilde{X}_k^R \tilde{X}_j^I] = N\sigma^2 \delta_{j,-k} \quad (12.5)$$

For each frequency pair (j, k) equations (12.4) and (12.5) give two complex equations in $\mathcal{E}[\tilde{X}_j^R \tilde{X}_k^R]$, $\mathcal{E}[\tilde{X}_j^I \tilde{X}_k^I]$, and $\mathcal{E}[\tilde{X}_j^R \tilde{X}_k^I]$. We solve for these quantities and, after some simple manipulations, find that $\mathcal{C}[\tilde{X}_j^R, \tilde{X}_k^I] = 0$ for all j and k , including $j = k$, and also that

$$\begin{aligned}\mathcal{C}[\tilde{X}_j^R, \tilde{X}_k^R] &= \mathcal{C}[\tilde{X}_j^I, \tilde{X}_k^I] = 0 && \text{for } j \neq k \\ \mathcal{V}[\tilde{X}_j^R] &= \mathcal{V}[\tilde{X}_j^I] = \frac{1}{2}N\sigma^2 && \text{for } j \neq 0, \pm \frac{1}{2}N\end{aligned}$$

while for $j = 0, \pm \frac{1}{2}N$, $\mathcal{V}[\tilde{X}_j^R] = N\sigma^2$ and $\mathcal{V}[\tilde{X}_j^I] = 0$. Because the covariances are all zero, the \tilde{X}_j^R and \tilde{X}_j^I are completely uncorrelated; the individual variables all have a variance of $\frac{1}{2}N\sigma^2$ except at $j = 0$ and $j = \pm \frac{1}{2}N$ (which we will call the Nyquist frequency). So the DFT of white noise is just a collection of independent Gaussian random variables with zero mean and variance (almost always) $\frac{1}{2}N\sigma^2$: almost exactly “Gaussian white noise in, Gaussian white noise out.”

Having gotten the pdf of the DFT of white noise, we can now find what we really want, namely the pdf of the estimated PSD \hat{S}_k in equation (12.3), and of its log, $\hat{P}_k = 10 \log_{10}(\hat{S}_k)$. For simplicity, we ignore zero and the Nyquist frequency.

We start by defining two normalized random variables, \tilde{U}^R and \tilde{U}^I , such that

$$\sigma\sqrt{\frac{1}{2}N}\tilde{U}^R = \tilde{X}^R \quad \text{and} \quad \sigma\sqrt{\frac{1}{2}N}\tilde{U}^I = \tilde{X}^I$$

which are Gaussian-distributed with zero mean and unit variance. Then equation (12.3) becomes

$$\hat{S}_k = \frac{1}{2}\sigma^2 \left[(\tilde{U}_k^R)^2 + (\tilde{U}_k^I)^2 \right]$$

The part of this expression between the square brackets is the sum of two independent and identical unit Gaussians; we denote it by U . Its pdf is⁵

$$\phi(u) = \frac{1}{2}e^{-u/2}$$

and so, by equation (C.9), the pdf for $\hat{S}_k = \frac{1}{2}\sigma^2 U$ is

$$\frac{e^{-s/\sigma^2}}{\sigma^2} \quad (12.6)$$

which has the first and second moments

$$\int_0^\infty \frac{se^{-s/\sigma^2}}{\sigma^2} ds = \sigma^2 \quad \text{and} \quad \int_0^\infty \frac{(s - \sigma^2)^2 e^{-s/\sigma^2}}{\sigma^2} ds = \sigma^4 \quad (12.7)$$

The good news is that the expected value of the estimate \hat{S} is just the true value of the PSD, so the periodogram estimator is unbiased – at least in the case where the input is white noise. It turns out that this is also true at zero frequency and the Nyquist frequencies.

But the second moment shows that the standard deviation of \hat{S} is also equal to σ^2 ; at zero frequency and the Nyquist frequencies it becomes $\sqrt{2}\sigma^2$. Thus, the standard deviation of the estimate is *equal to the estimate itself*. An uncertainty as large as the value is bad enough, but what is worse is that this uncertainty is independent of the number of data N . As N grows, the variance does not decrease at all: an example of what we called, in the previous section, an **inconsistent** estimate. This behavior can be easily understood just by counting information in and out. The periodogram gives $\frac{1}{2}N$ independent estimates from N data; so in some sense the number of data that go into an estimate at one frequency is always two, independent of N .⁶ So we are not averaging over more data per estimate as we increase N , and it is no surprise that the variance does not get any smaller.

Now consider the pdf of what we usually plot,

$$\hat{P}_k = 10 \log_{10}(\hat{S}_k) = b \ln(aU)$$

⁵This is the chi-squared distribution with two degrees of freedom.

⁶At zero frequency and the Nyquist we have, effectively, only one data value because the periodogram amounts to a sine or cosine transform.

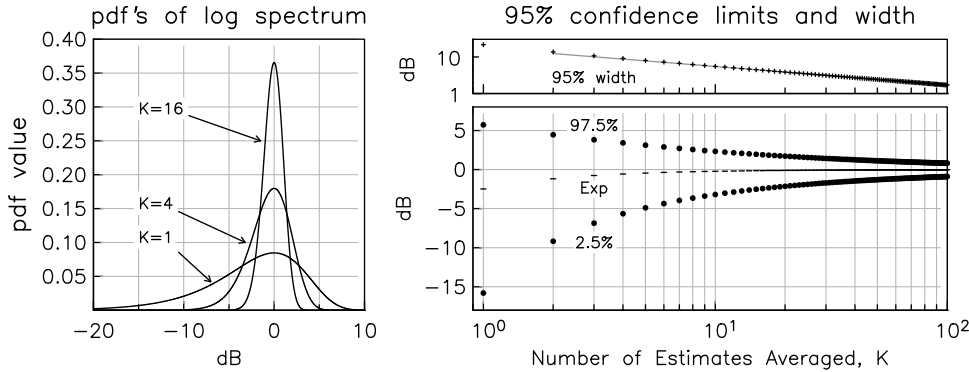


Figure 12.2: Probability density functions for the log spectrum for different amounts of averaging. The left panel shows the pdf's for the periodogram ($K = 1$, no averaging) and for averaging 4 and 16 estimates. The low right panel shows the expected value and 95% confidence limits for averaging 1 to 100 estimates. The upper right panel shows the width of the 95% confidence limits; this is adequately approximated by $5.5/\sqrt{K}/10$ (gray line) for $K \geq 2$.

where for dB, $b = 10/\ln 10 = 4.343$, and $a = \frac{1}{2}\sigma^2$. By equation (C.10), and some algebra to turn exponentials into powers of 10,

$$\phi_P(p) = \frac{10}{\sigma^2 \ln 10} \exp\left(-\frac{10^{p/10}}{\sigma^2}\right) 10^{p/10} \quad (12.8)$$

If we define a normalized log power level $p' = p - 10 \log_{10}(\sigma^2)$, the pdf becomes

$$\phi_P(p') = \frac{10}{\ln 10} \exp\left(-10^{p'/10}\right) 10^{p'/10}$$

so the form of the pdf does not depend on the level of σ^2 . A major reason for plotting power spectra in dB is this invariance of the pdf in such a plot; in a linear plot, the pdf becomes narrower as S becomes smaller, but not because the relative accuracy is any better. Figure 12.2 shows this pdf ($K = 1$), which is clearly asymmetrical, with the longer tail for negative values leading to two consequences. First, the expected value of the log of the spectrum, unlike the spectrum itself, is biased, about 3 dB downwards. Second, there will be many more estimates below than above the visual average value, causing the many “downwards spikes” (Figure 1.7) in a plot of the log periodogram.

12.3.2 Averaging The Periodogram for Lower Variance

We will see below that whatever the spectrum, the variance of periodogram estimates is always the square of the estimated value no matter what N is. The estimate remains inconsistent, unavoidably, because as the ratio of estimates to data

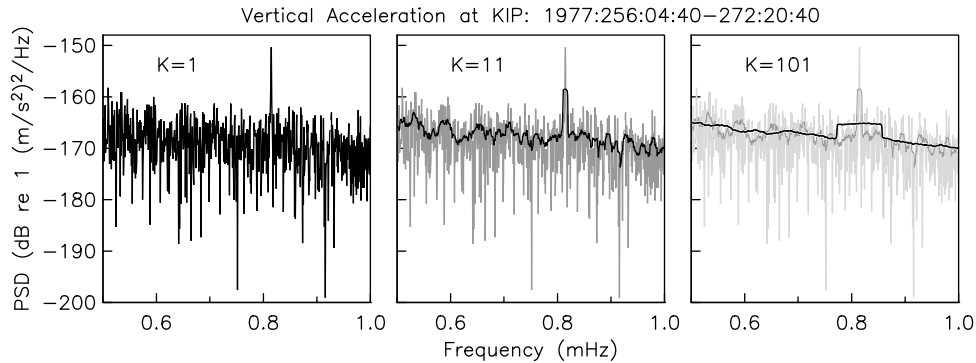


Figure 12.3: Periodogram estimates of the PSD for seismic motion recorded at station KIP (see Figure 1.7). At each frequency of the original periodogram, $(K - 1)/2$ estimates on each side, and the estimate at that frequency, are averaged to produce a new estimate: so $K = 1$ is the original periodogram. In the plots for $K > 1$ the unaveraged periodograms are shown in gray.

does not change with N . So we can reduce the variance only by applying some kind of averaging that reduces the number of independent spectrum estimates: so a reduced variance unavoidably creates lower resolution in frequency.

As noted above, the pdf of a periodogram estimate is that of the sum of two squared normally-distributed random variables. Suppose we apply the most obvious kind of averaging, which is to make each new estimate the average of K periodogram estimates. In the white-noise case, when the original estimates are uncorrelated, this new estimate will have the pdf of the sum of $2K$ squared normally-distributed random variables, divided by K .⁷ Averaging K consecutive estimates together scales the variance down by a factor close to K^{-1} ; from (12.9)

$$\mathcal{V}[\langle \hat{S}(\zeta) \rangle_K] \approx \frac{S(\zeta)^2}{K}$$

As Figure 12.2 shows, this averaging not only decreases the variance of the spectrum estimate, but also moves its pdf closer to a Gaussian. Even very modest amounts of averaging (small K) nearly eliminates the bias of the spectrum when plotted in dB.

Figure 12.3 shows an example of frequency-domain averaging to illustrate its merits and demerits. Increasing the number of estimates averaged, K , appears to give a much improved plot of the spectrum over most of the frequencies shown, where it would seem the spectrum is in fact smooth; but such averaging can badly distort the actual peak in the spectrum from the ${}_0\text{S}_0$ free oscillation. Such

⁷This is the chi-squared distribution with $2K$ degrees of freedom.

loss of **spectral resolution** is inescapable; we must balance our desire to see detail in the PSD against better statistical reliability. In this example, it is clear that different parts of the spectrum need different amounts of smoothing, depending on the spectral shape; we will see one approach to such adaptive smoothing in Section 13.5.

12.3.3 The Periodogram for Nonwhite Spectra

How do these results generalize to the spectra of processes other than white noise? For such “colored” power spectra, we will show that the periodogram estimator is asymptotically unbiased: as $N \rightarrow \infty$ the expected value of the estimate approaches the actual value of the PSD. But as $N \rightarrow \infty$, the variance behaves just as it does for white noise:

$$\mathcal{V}[\hat{S}(\zeta)] \rightarrow (S(\zeta))^2. \quad (12.9)$$

which is to say that, again, the variance remains finite and the standard deviation of the estimate approaches the estimated value.

We start by calculating the bias for a finite number of samples N . We skip some algebra, which is the same as the proof (Sections 11.3 and 11.7) showing the equivalence of the two definitions of PSD for continuous time, and find that the discrete periodogram estimator (12.2) can also be written, without approximation, as

$$\hat{S}(\zeta) = \sum_{n=-N+1}^{N-1} \left(1 - \frac{|n|}{N}\right) \hat{R}_n e^{-2\pi i n \zeta} \quad (12.10)$$

where \hat{R}_n is this estimator of the autocovariance function:

$$\hat{R}_n = \frac{1}{N - |n|} \sum_{k=0}^{N-|n|} X_k X_{k+n}$$

This estimator is unbiased, as we discuss in Section E.2. To find the bias of the PSD estimator in (12.10) we take the expectation:

$$\begin{aligned} \mathcal{E}[\hat{S}(\zeta)] &= \sum_{n=-N+1}^{N-1} \left(1 - \frac{|n|}{N}\right) \mathcal{E}[\hat{R}_n] e^{-2\pi i n \zeta} \\ &= \sum_{n=-N+1}^{N-1} \left(1 - \frac{|n|}{N}\right) R_n e^{-2\pi i n \zeta} \end{aligned}$$

Now recall that R_n is the inverse Fourier transform of the true PSD, (equation

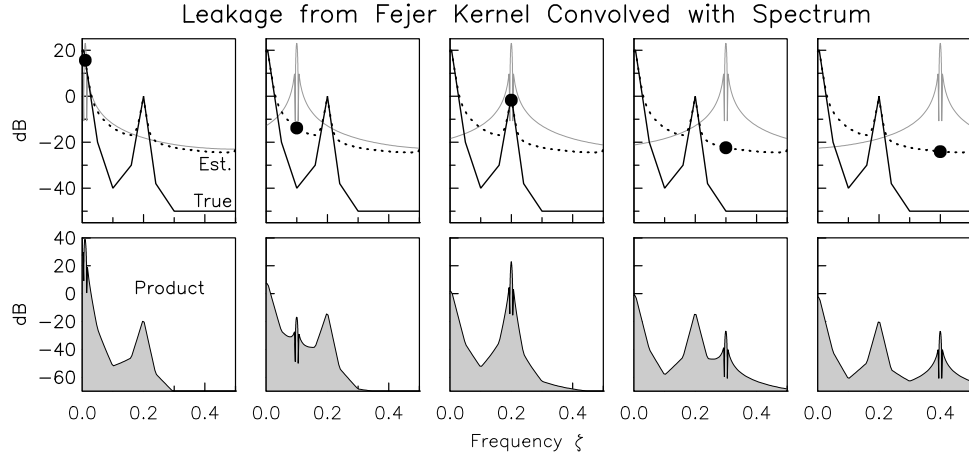


Figure 12.4: Schematic (though computationally accurate) plot to show the effect of leakage on a PSD estimated using the periodogram. In the top panels, the solid black line is the true spectrum, the Fejer kernel (shown for a different frequency in each panel) is in gray. The bottom panel shows the product of these, which are integrated (the gray region) to give the spectral estimate (black dot) in the upper pane. Done for all frequencies this gives the estimated spectrum (dashed line).

(11.5) of Chapter 11) and substitute this inverse transform in, to get:

$$\begin{aligned}
 \mathcal{E}[\hat{S}(\zeta)] &= \sum_{n=-N+1}^{N-1} \left(1 - \frac{|n|}{N}\right) \int_{-\frac{1}{2}}^{\frac{1}{2}} S(\zeta') e^{2\pi i \zeta' n} e^{-2\pi i \zeta n} d\zeta' \\
 &= \int_{-\frac{1}{2}}^{\frac{1}{2}} S(\zeta') \left[\sum_{n=-N+1}^{N-1} \left(1 - \frac{|n|}{N}\right) e^{-2\pi i (\zeta - \zeta') n} \right] d\zeta' \\
 &= \int_{-\frac{1}{2}}^{\frac{1}{2}} S(\zeta') F_N(\zeta' - \zeta) d\zeta'
 \end{aligned} \tag{12.11}$$

where F_N in the last line of equation (12.11) is the Fejér kernel that we introduced in Section 5.4.

Equation (12.11) demonstrates that the periodogram estimator *convolves the true spectrum with the Fejér kernel*, which has considerable amplitude away from the central peak. So the estimate at one frequency is affected by values at others. When the spectrum is flat the convolution works out to have no effect and the spectrum is unbiased. But when there are peaks or other variations in the spectrum, and particularly when the PSD has a large dynamic range, this convolution can seriously distort the spectrum by biasing the estimates. This bias is called **spectral leakage** because it causes parts of the spectrum with a lot of power to leak out and affect parts where the power is low. Figure 12.4 shows how this works: the

gray regions in the bottom panels are what contribute to the estimated spectrum. Even for $\zeta = 0.4$, the two largest contributions come, not from the frequencies close to that, but from more distant frequencies where the spectrum is larger.

Note that all this is consistent with the statements made earlier about asymptotic behavior: As $N \rightarrow \infty$ the Fejér kernel gets closer and closer to a delta function, and a delta function in the convolution integral of equation (12.11) would make the estimated spectrum equal to the true one. But the convergence to the delta function is very slow: in practice more data won't solve the problem.

So the periodogram has two problems:

1. It is inconsistent.
2. If the spectrum is not flat, the periodogram can be biased in regions where the spectrum is much smaller than it is in other regions.

The rest of this chapter will be devoted to ways to ameliorate (for we cannot eliminate) these two problems.

But first, to see what damage leakage can do, we look at the spectrum of the data in Figure 10.8: the series looks very smooth, which suggests that the high-frequency part of the spectrum is much less than the low-frequency part, making the overall spectral range very high. Figure 12.5 shows two periodogram-based estimates of the spectrum for low wavenumbers: the Nyquist wavenumber is 0.0132km^{-1} .

But for wavenumbers above $k = 0.0003\text{km}^{-1}$ the periodogram becomes smooth, which for an unaveraged spectrum, is a sure sign of spectral leakage. The variability in the periodogram estimate is an unavoidable consequence of how it is defined; if the result is *not* highly variable from frequency to frequency, something is wrong. Bias is the usual cause of too smooth a spectrum, often from large amounts of energy at low frequencies. A very smooth spectrum can also indicate that there is a large outlier somewhere, this, like a delta function, distributes energy over all frequencies.

12.3.4 Bias Reduction with Tapers

So we have a case where over most of the frequency range the spectral estimate is clearly biased. What can we do to reduce this?

For the periodogram the bias-producing kernel in (12.11) the square of the Dirichlet kernel, which itself is the Fourier transform of a boxcar sequence. By the technique used in Section 12.3.3 we can show a more general result. Suppose that we multiply the data series by a weight series w_n , with $\sum_0^{N-1} w_n^2 = 1$, and perform a periodogram estimate on this new series:

$$\hat{S}(\zeta) = \frac{1}{N} \left| \sum_{n=0}^{N-1} w_n x_n e^{-2\pi i n \zeta} \right|^2$$

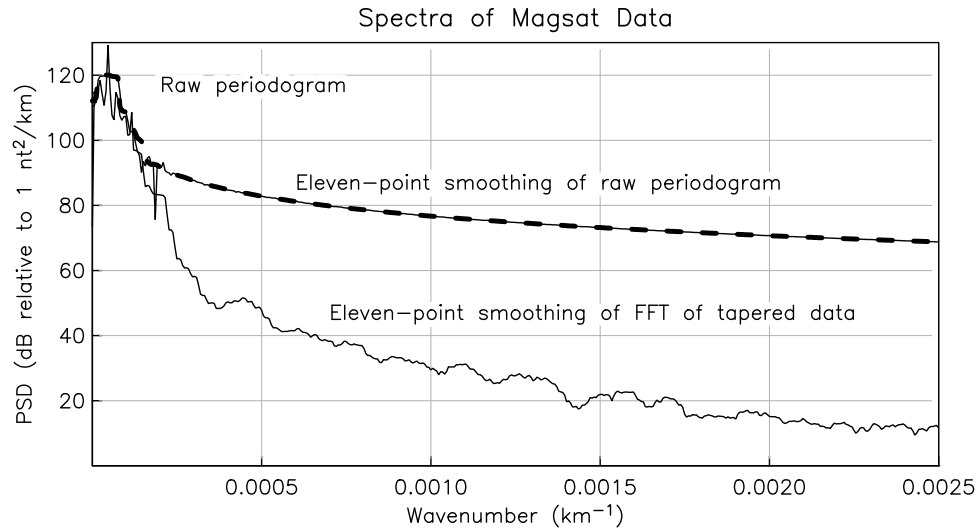


Figure 12.5: Periodogram of the data in Figure 10.8 The thin black curve is the raw periodogram; at the lowest wavenumbers this varies considerably one frequency to the next, giving a “noisy” spectrum. The thick dashed black line shows the result of averaging 11 consecutive periodogram estimates: the variance becomes much smaller – averaging does smooth the spectrum.

The expected value of the estimator is then

$$\mathcal{E}[\hat{S}(\zeta)] = \int_{-\frac{1}{2}}^{\frac{1}{2}} S(\zeta') \tilde{w}^k(\zeta' - \zeta) d\zeta' \quad (12.12)$$

where the convolving function \tilde{w}^k is approximated by

$$\tilde{w}^k(\zeta) = \frac{1}{N} |\tilde{w}(\zeta)|^2 = \frac{1}{N} |\mathcal{F}[w]|^2 \quad (12.13)$$

That is, the **convolving function** for the PSD estimate is the squared magnitude of the Fourier transform of the weight series: if all the weights are one, we get the the Fejér kernel.

In developing the theory further we will work in continuous time, since we get rid of one variable, the length N . Thus for the raw periodogram we would take the weights to be a boxcar function $w(t)$:

$$w(t) = \Pi\left(\frac{t}{N} - \frac{1}{2}\right)$$

which means that equation (12.13) becomes

$$\tilde{w}(\zeta) = N e^{\pi i N \zeta} \text{sinc}(N \zeta) \quad (12.14)$$

What equation (12.12) means is that we can reduce the bias from spectral leakage by choosing $w(n)$ to be a function whose Fourier transform falls away with frequency more steeply than sinc^2 does: for large frequencies this means faster than ζ^{-2} . We can get this if $w(t)$ has smooth behavior in the transitions at $n = 0$ and $n = N - 1$, the ends of the interval, because the leakage is a consequence of poor convergence of the Fourier transform of a function with a discontinuity: yet another example of Gibb's phenomenon.

For convenience we change to a continuous-time approximation, replacing n by t and $N - 1$ by T , so that the observations are on the time interval $(0, T)$. We introduce a function $w(t)$ which we call a **taper**, just as we did for the similar functions used in designing FIR filters.⁸ As we discussed in section 7.2.1 there are many choices for $w(t)$, some of which we showed there. In Chapter 13 we will develop taper design methods that have made such *ad hoc* designs obsolete; but first, we illustrate the effect of tapering on spectral bias using the von Hann taper, which we discussed in some detail in Section 7.2.1 and showed in Figure 7.3. Normalized to give unit area under $|\tilde{w}|^2$, this taper is

$$w(t) = \begin{cases} (8/3T)^{1/2} \sin^2(\pi t/T) & 0 \leq t \leq T \\ 0 & \text{otherwise} \end{cases}$$

and its Fourier transform is

$$\tilde{w}(f) = \left(\frac{2T}{3}\right)^{1/2} [\text{sinc}(fT) + \frac{1}{2}\text{sinc}(fT - 1) + \frac{1}{2}\text{sinc}(fT + 1)]$$

In getting a good spectrum estimate, the suppression of leakage from large peaks into low-amplitude parts of the spectrum is nearly always *much* more important than the loss of frequency resolution introduced by the wider peak. As we saw in Section 7.2.1, the Fourier transform of a von Hann taper has much lower sidelobes than the transform of a boxcar. Figures 12.4 and 12.6 show how the von Hann taper eliminates the bias present with no tapering.

What about the Magsat data? Figure 12.5 includes a spectral estimate of this series with the von Hann taper. For the frequencies where the periodogram estimate is smooth, the von Hann taper lowers the estimated spectral level by almost 60 dB: six orders of magnitude. The von Hann taper seems to pretty well eliminate the effects of leakage; in Section 13.3 we will see a way of checking this.

12.3.5 Weighted Overlap Section Averaging

We have combined tapering with averaging in frequency, but a more common form of averaging is what is called **Weighted Overlap Section Averaging**, or **Welch's**

⁸In the older literature such a function was often called as a “data window,” and in some fields it is called the “apodizing function.”

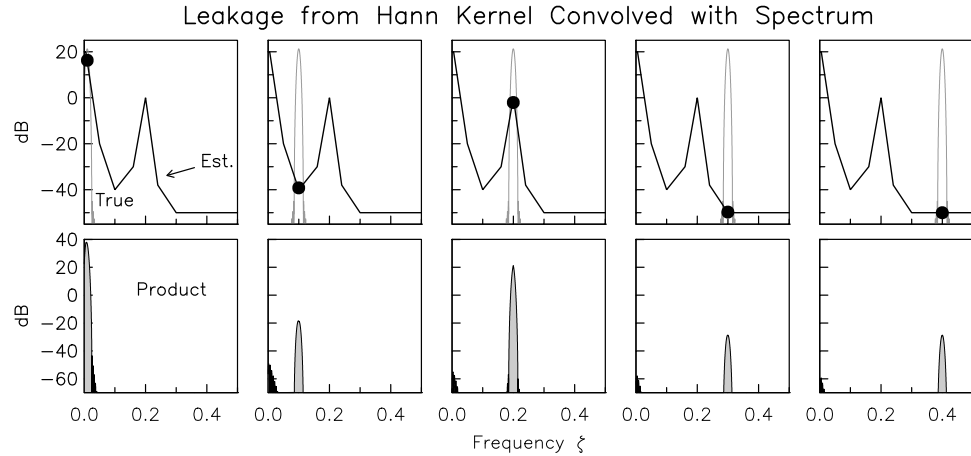


Figure 12.6: Plot showing the effect of using a von Hann taper for the schematic spectrum shown in Figure 12.4. Because its sidelobes are so much smaller, the lower panels all show that the spectral estimate is controlled by the size of the spectrum at the frequency of interest, not anywhere else: so the estimated and true spectra coincide.

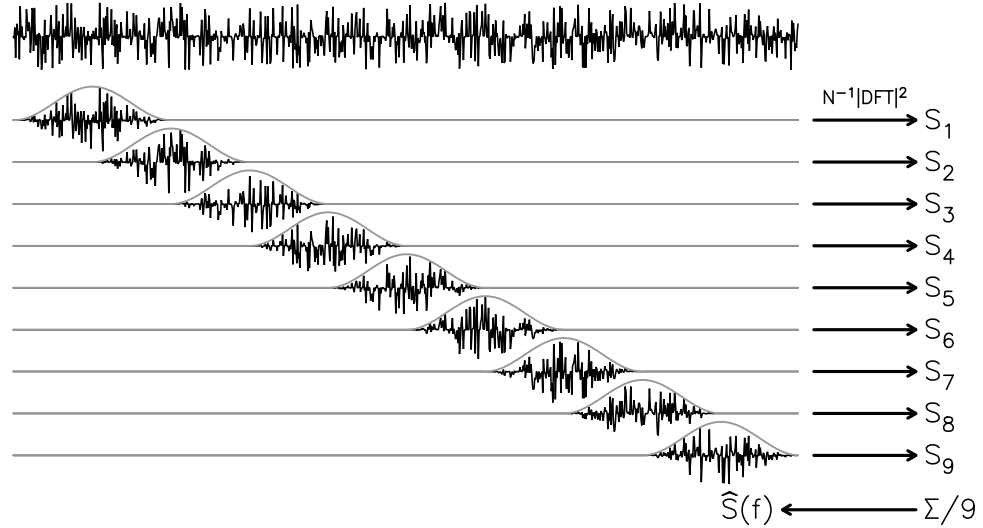


Figure 12.7: Cartoon illustrating the method of Weighted Overlapping Section Averages (Welch's method), using a von Hann taper and 50% overlap. For the section length shown, this gives nine estimates which are averaged to produce the final estimate \hat{S} . Notice that this can be viewed as a multaper method.

method (Welch, 1967). In this method, we split the original record into K segments of equal length, taper each one, compute its periodogram, and finally average the K periodogram amplitudes we have at each frequency. If the sections do not overlap, the data series are approximately independent, and thus each one provides a statistically independent estimate of the PSD at each frequency; averaging the section estimates reduces the variance by as much as averaging over frequency does. Just as with frequency averaging, we lose spectral resolution, because now the interval between consecutive frequencies in the estimated PSD becomes K/N instead of the $1/N$ it would be if we used the whole record. Since we are tapering each section, it is usual to overlap the sections somewhat so that data that is downweighted by the taper in one section will be highly weighted in the next: a standard approach is to use 50% overlap with a von Hann taper.

This method is appealingly simple, and also well-suited to series with gaps: it is easy to just skip these in forming the sections. But we must choose a section length, and in doing so must, as usual, trade spectral resolution (best if we use long sections) against the variance of the estimate (best if we use short sections). Usually this choice is done by trial-and-error, with a fair amount of subjectivity involved. For this reason we regard section averaging as an obsolescent method: there are better choices.

But a slightly different view of section averaging is a good bridge to the methods we will recommend. We can view the K estimated spectra as being the result of applying K different tapers to the data, each taper being zero except in the relevant section. Section averaging is thus an example of **multitaper spectral estimation**.

The obvious question is, are there better choices for the K tapers than the rather *ad-hoc* shapes created by splitting the series into sections? The answer is yes, there are; we will find out about them in the next chapter.

CHAPTER 13

ESTIMATING POWER SPECTRA: MULTITAPERS

13.1 Introduction

In the previous chapter we have seen how a spectrum spectrum estimate can be biased. While there are many ways to reduce the variance of the final estimate, none can reduce bias: if we start with biased estimates, there is no way we can unbias them. So it is crucial for any estimation procedure to minimize bias, which can be done only by applying tapers to the data before computing Fourier transforms.

We say “tapers” and “transforms” rather than “a taper” and “a transform” because the best estimation procedures all apply different tapers to the data, compute the DFT’s of the each tapered series, and combine these DFT’s into a **multitaper** estimate of the PSD. These methods reduce variance by averaging, not over frequency or time, but by averaging the individual estimates created by these DFT’s. This simple description may seem at odds with the reputation that multitaper methods have of being arcane and complicated. But this reputation comes more from the mathematics of some of the tapers used than from the method itself. As noted in Section 12.3.5, the long-established Welch’s method is a multitaper estimate.

In this chapter we describe methods that use families of tapers which

1. minimize bias of some kind
2. are orthogonal functions or sequences

Orthogonality is important because it means that the PSD estimate at any frequency produced by each taper-and-transform operation will be uncorrelated with the estimate produced using another taper. Combining uncorrelated estimates will reduce the variance of the spectrum estimate by the largest amount. We say “combine” because there is more than one way to get a single estimate from multiple ones. In Welch’s method, and in some other multitaper methods, we simply take the average, but there are other approaches.

In Sections 7.2.1 and 12.3.5 we limited ourselves to tapers that were everywhere non-negative; but these can be orthogonal only if they do not overlap. [Thomson](#)

(1982) had the crucial insight that we can use tapers that are both positive and negative, in which case orthogonality is compatible with much better choices of taper.

In this chapter we examine two families of tapers; each family is designed to minimize a bias, though not the same one. What we look for is easy to describe:

1. Find a function whose Fourier transform maximizes (or minimizes) some property, to give the first taper.
2. Find another function, orthogonal to the first taper, whose transform maximizes (or minimizes) the same property,
3. And so on: find more functions that satisfy the extreme property, subject to being orthogonal to the previous tapers.

For the properties we will minimize, we will obtain a series of tapers for which the orthogonality arises automatically.

So multitaper methods are not *completely* automatic; we must still decide how to trade off better frequency resolution against increased variance, as shown in Figure 10.9. This amounts to asking, how many tapers should we use? Broadly speaking, this depends on the spectrum and on our aims in doing the analysis. More specifically, we must answer two questions:

1. How much resolution in frequency do we think is needed? The less resolution the better the estimates will be.
2. How much possible bias can we tolerate?

The answer may not be the same for all frequencies. By allowing the number of tapered estimates to change with frequency we can make the frequency resolution, and hence the amount of variance reduction, frequency-dependent: such an **adaptive spectrum estimate** is often appropriate.

13.2 The Minimum-Leakage Tapers

As just stated, we must, above all else, avoid bias. Since bias commonly comes from spectral leakage, our first collection of tapers is designed to minimize this. Guided by the examples in Figures 12.4 and 12.6, in which better results come from the taper with the lower sidelobes, we can ask, what taper has the lowest sidelobes of all? More precisely, what function $w(t)$, nonzero only over the interval $(-T/2, T/2)$, has a Fourier transform whose energy is most concentrated in frequency? As is often true the question is easier to ask than to answer.

When we developed equation (12.13) to compute the approximation $|\tilde{w}|^2$ for the convolving kernel $\tilde{w}^k(f)$ in equation (12.12) we worked in continuous time, and we

will continue to do so; to simplify the algebra we put the time origin at the center of the data span.¹

We first define **spectral concentration**, $\mathcal{N}[|\tilde{w}|^2]$; we use square brackets around $|\tilde{w}|^2$ because $|\tilde{w}|^2$ is a function, not a variable, so $\mathcal{N}[|\tilde{w}|^2]$, which finds a scalar given a function, is a **functional**. (The choice of letter is to suggest narrowness). Our definition of $\mathcal{N}[|\tilde{w}|^2]$ and a related quantity $L[|\tilde{w}|^2]$ is:

$$\mathcal{N}[\tilde{w}] = \frac{\int_{-f_b}^{f_b} |\tilde{w}(f)|^2 df}{\int_{-\infty}^{\infty} |\tilde{w}(f)|^2 df} \quad \text{and} \quad L[|\tilde{w}|^2] = 1 - \mathcal{N}[|\tilde{w}|^2] \quad (13.1)$$

The definition of the functional \mathcal{N} , as illustrated in Figure 13.1, provides a measure of frequency concentration for any taper w , with $\mathcal{N}[|\tilde{w}|^2] \leq 1$ and $L[|\tilde{w}|^2] \geq 0$ by definition. For spectral analysis we actually care more about L , the **leakage factor**, because this gives the amount of energy outside the frequency band of concentration. Ideally L would be zero; L close to one would mean that there is no concentration at all, and would produce a spectral estimate in which the results at any frequency would be contaminated by the results at all the others.

Note that $\mathcal{N}[|\tilde{w}|^2]$ depends on the bandwidth parameter f_b ; in equation (13.1). In terms of the unavoidable tradeoff of resolution against variance, our choice is made by choosing a value for f_b . In developing the taper formulae, we regard as f_b as a parameter, and so we are asking what taper maximizes $\mathcal{N}[|\tilde{w}|^2]$ (or equivalently minimizes $L[|\tilde{w}|^2]$) for any particular f_b . In other words, we choose f_b to be the width of the frequency interval over which we are willing to accept leakage (a form of averaging); then, for that interval, we seek the taper that maximizes $\mathcal{N}[|\tilde{w}|^2]$.

How might we choose f_b ? It should not be smaller than T^{-1} , since that is the lowest frequency accessible from a record of length T . If we make $f_b = T^{-1}$ and consider some simple tapers, we can ask what values we get for L , the amount of energy outside the peak, something we will call “sideband energy”. Integrating the transforms of tapers gives $\mathcal{N} = 0.902$ ($L = 0.098$) for no taper, $L = 0.03$ for a sine taper (a taper that looks like half the cycle of a sine wave), and $L = 0.082$ for the von Hann taper. If the bandwidth f_b is this narrow, the sine taper has the most concentrated Fourier transform and hence the least sideband energy. The von Hann taper is worse because more of the central peak of its transform falls outside the limits and is counted as sideband energy.

But if instead we choose $f_b = 4T^{-1}$ the numbers for L are instead 2.5×10^{-2} for no tapering, 2.7×10^{-4} for a sine taper, and 1.4×10^{-5} for a von Hann taper; if we are willing to average over this wider bandwidth, the von Hann taper produces the least leakage.

¹The following draws on, though it does not follow exactly, Percival and Walden (1993), pages 75–81 and 101–116.

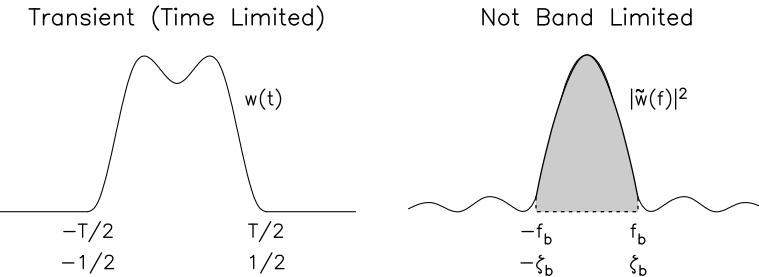


Figure 13.1: A (cartoon) transform pair: on the left, a time-limited function, or transient, and on the right, the square of its Fourier transform, which is nonzero for the whole real line. The concentration factor $\mathcal{N}[|w|^2]$ is the shaded area normalized against the whole area of $|w|^2$ and depends on the bandwidth parameter f_b .

Appendix G describes how to find the functions that maximize \mathcal{N} (minimize L). Here we simply state the result, which is that these tapers are the solution to an eigenvalue problem:

$$\int_{-1}^1 \frac{\sin \pi p(x-y)}{\pi(x-y)} \psi_n(y) dy = \mu_n \psi_n(x) \quad \text{for } |x| \leq 1 \quad (13.2)$$

where the eigenvalues μ_n are the concentration factors for the n -th taper, and the eigenfunctions ψ_n are just the tapers u_n fitted into the interval $[-1, 1]$: $u_n(t) = \psi_n(2t/T)$. Rescaling the interval in this way means that there is only one parameter that determines the solutions, namely the dimensionless quantity $p = Tf_b$, which is called the **time-bandwidth product**. We already considered two values of this; when looking at concentration factors (or sideband energy) for $f_b = T^{-1}$ and $f_b = 4T^{-1}$ we were considering $p = 1$ and $p = 4$. As we mentioned above, a band narrower than $1/T$ is not a good idea: we always choose $p > 1$,

For any value of p , equation 13.2 has infinitely many distinct, real, and positive eigenvalues with

$$1 > \mu_0 > \mu_1 > \mu_2 > \dots \quad (13.3)$$

and as $n \rightarrow \infty$, $\mu_n \rightarrow 0$. Since the concentration function $\mathcal{N}[\psi_n] = \mu_n$, the first eigenfunction, ψ_0 , has the most concentration (lowest L) for the chosen value of p . Another important result is that the eigenfunctions (which give the tapers) are mutually orthogonal on $(-1, 1)$:

$$\int_{-1}^1 \psi_m(x) \psi_n(x) dx = 0 \quad \text{for } m \neq n \quad (13.4)$$

Appendix G describes where the usual name for these functions, **prolate spheroidal wavefunctions**, comes from; we instead will use the name **Slepian functions**,

after David Slepian (of Bell Labs) who discovered that they are the functions with the most-concentrated Fourier transforms. This name has become used for similar maximally-concentrated functions in more than one dimension, including on all or part of the surface of a sphere. Appendix G also summarizes the discrete-time version of these functions, which are known as **discrete prolate spheroidal sequences**; we prefer the simpler name **Slepian sequences**. For these we need to specify both the time-bandwidth product p and the number of points N ; we use them when we want the absolute best result, or have very few data so that N is small. For large N these sequences become close to sampled versions of the Slepian functions; we will just use the term **Slepian tapers** when we want to refer to either the sequence or the function.

How little leakage do the Fourier transforms of these tapers have? The leakage L will be smallest for the largest eigenvalue in (13.3). Consider $p = 4$, corresponding to $f_b = 4/T$, for which the von Hann taper has $L[w] = 1.4 \times 10^{-5}$. For this value of p the largest eigenvalue μ_0 is so close to unity that $L[\psi_0] = 5.8 \times 10^{-10}$. Outside the central peak $\tilde{\psi}_0$ is nearly four orders of magnitude smaller than the squared transform for the von Hann taper – but the latter has a much narrower center lobe.

So, we can minimize spectral leakage by using $\psi_0(t)$, the taper with the smallest L . The first step in *any* spectral analysis should be to taper the data with ψ_0 for several values of $p \geq 4$, and compute the periodogram of the tapered data. If the range of the spectrum is the same for (say) $p = 4$ and $p = 6$, then you will have established what the dynamic range of the spectrum is, and can arrange further calculations to avoid contaminating any part of the spectrum with leakage from another part.

13.3 Multitaper Spectral Estimation with Slepian Functions

The previous section shows the advantages of the taper with minimum leakage. But can we also use the other functions that satisfy equation (13.2)? Yes: as we mentioned in section 12.1, at each frequency these can be applied to the data to give additional, statistically independent, estimates of the spectrum – additional estimates that we can combine to reduce the variance. But in order to do this without introducing bias from leakage, the leakage values L_n need to be small: that is, the eigenvalues μ_n associated with these additional tapers need to be close to one.

Figure 13.3 shows how L depends on p for $0 \leq n \leq 15$; $n = 0$ gives the smallest values of L , which is around -120 dB for $p = 4$: about the best we can do in double-precision computations. For each value of n (each curve in Figure 13.3) there is some value of p below which L_n is close to 0 dB; above that value L falls

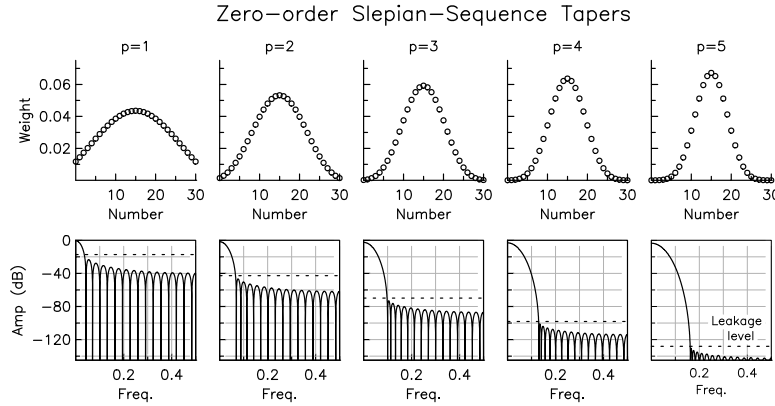


Figure 13.2: For several values of the time-bandwidth product p , the most concentrated taper ψ_0 , for the discrete-time case with $N = 31$, and its Fourier transform (plotted in dB). The dashed line shows the “leakage” level L . The Kaiser-Bessel tapers (Figure 7.4) are very similar, but have slightly larger sidebands.

as p increases. Similarly, for any value of p (the x -axis in Figure 13.3) successive tapers with larger n have larger values of L , asymptotically reaching $L = 1$ (0 dB), when the leakage is so large that the taper is useless. It is often said that for each value of p there is some value of n below which μ_n is close to one (L small), and above which μ_n “abruptly” goes towards zero; plotting, as here, the logarithm of $L_n = 1 - \mu_n$ shows that the change from small L to $L = 1$ is not abrupt.

Once leakage occurs it cannot be undone, so we should, to be conservative, use tapers with less leakage than the dynamic range of the spectrum. For example, suppose this range was 60 dB. Then Figure 13.3 shows that for a time-bandwidth product $p = 4$ we can use only three tapers ($n = 0, 1, 2$). But with $p = 8$ we could use ten tapers. The number of tapers to use ($K = n + 1$) is sometimes taken to be proportional to p . In Figure 13.3 the symbols connected by dashed lines connect values of L for successive tapers with n equal to a fixed constant times p ; the larger this constant, the larger the value of p needed to keep L below a particular level. These lines show that, for a given level of acceptable leakage (a constant value of L), when p increases the ratio of the number of usable tapers to p also increases.

Figure 13.4 shows the first five tapers for the time bandwidth product $p = 4$; from Figure 13.3 the maximum value of L is then -20 dB. Figure 13.4 brings out another advantage of using multiple tapers: the higher-order ones will give more weight to the ends of the series than the zero-order one does. One objection to tapering is that the usual single tapers downweight much of the data; multitaper estimates ameliorate this.

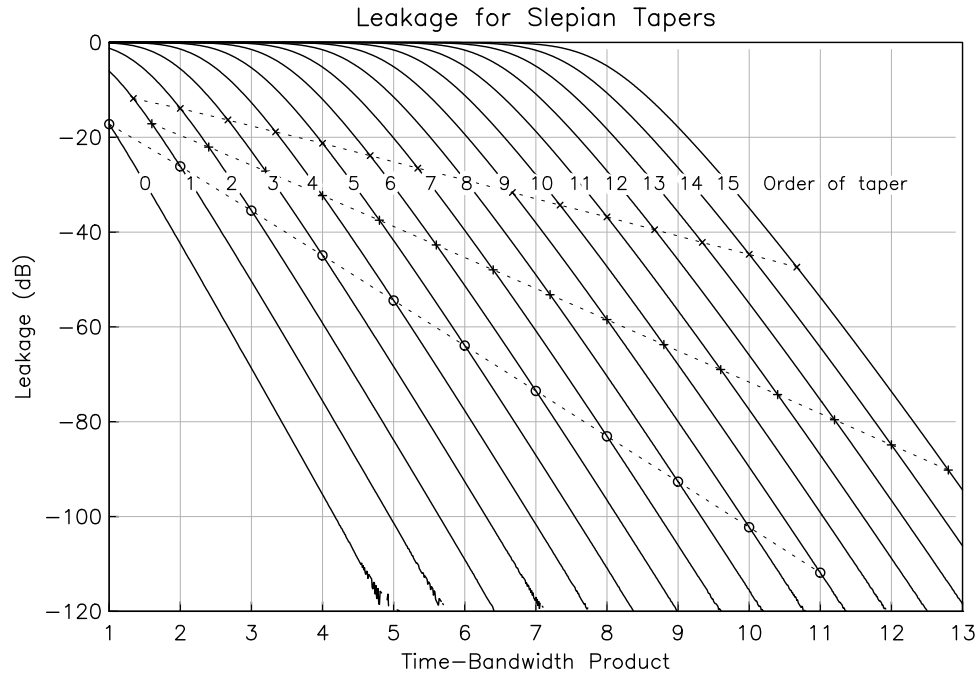


Figure 13.3: Leakage L_n as a function of time-bandwidth product p , for n from zero to fifteen. As the values of L approach 10^{-6} (-120 dB) some numerical noise is evident. The dashed lines connect the points on the $p - L$ curves for which $p = K$ (circles), $p = 1.25K$ (plus) and $p = 1.5K$ (crosses), where $K = n + 1$ is the number of tapers. Any fixed proportion between p and K will produce decreasing leakage as p increases.

13.3.1 A Multitaper Example

Figures 13.5 through 13.7 show how we might estimate the PSD of the Magsat data with multiple tapers. Figure 13.5 shows the spectra estimated by taking the periodogram of the data after applying each of two zero-order tapers, one with time-bandwidth product $p = 4$ and the other with $p = 5$. The resulting periodograms look very similar, and plotting the difference between these shows that they do indeed give similar results: the mean difference is only 0.05 dB. So we can conclude that both estimates show the full dynamic range of the spectrum: 115 dB overall, and about 70 dB from the peak to a point where the spectrum falls off more gradually with frequency.

So we choose a time-bandwidth product of 5 – and it is important to emphasize that this choice is *arbitrary*, or, more precisely, governed by our sense of how smooth the spectrum is.

Figure 13.3 shows that for $p = 5$ we get less than 50 dB of leakage if the number of tapers is $K = 6$. This might seem like too much given the range of the spectrum,

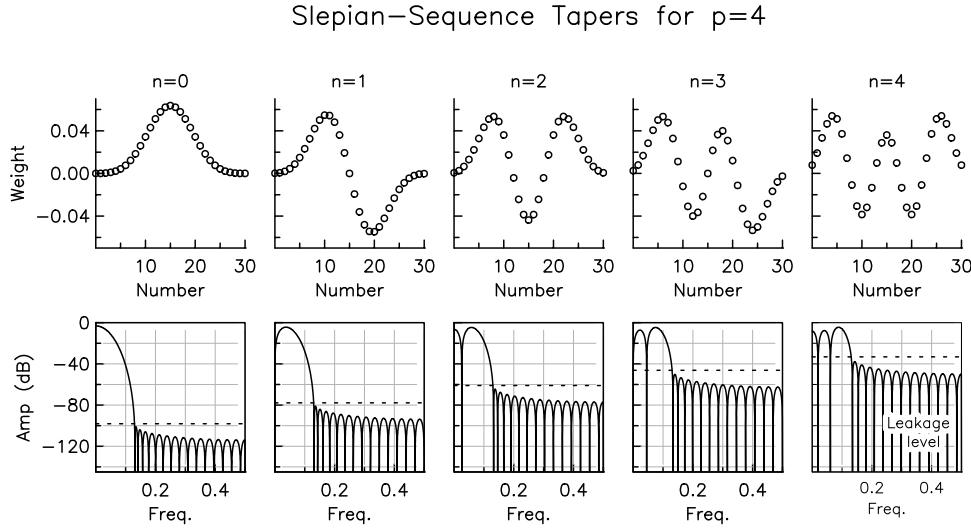


Figure 13.4: The first five tapers for $p = 4$, shown as in Figure 13.2.

and so it turns out to be. Figure 13.6 shows the spectra estimated by taking the periodogram of the data after applying each of the first six tapers. It is evident that each of the first three estimates, while showing the large variations expected for a periodogram, all appear to overlay each other at all frequencies. This is not true for the next three estimate: there is a slight evidence of biase for the fourth taper, while for the fifth and sixth it is very obvious indeed, with the spectrum systematically higher than for the first three estimates.

So for this choice of p we can only do a modest amount of averaging. Figure 13.7 shows the results, ranging from using one taper, to average spectral esitmates using the first three spectra in Figure 13.6; note that we need to average the actual spectral values, not the logarithmic (dB) values shown in the plots. Figure 13.7 shows, unsurprisingly, that such averaging produces a spectrum estimates with less variance than what the individual spectra have. Looking at Figure 13.4 shows that the multitaper estimate makes better use of the data than a single taper, since it downweights the ends of the data much less.

13.3.2 Problems with the Slepian Multitaper

The Thomson/Slepian multitaper method is certainly the best way to estimate a spectrum with large dynamic range, such as one with a sharp falloff or a strong peak – though actual sinusoids, which would put delta functions into the spectrum, should always be removed before making any spectrum estimate. Used as we have described, where we fix p , and choose a single value for K to avoid bias, the averaging bandwidth will be the same for all frequencies. But a fixed bandwidth

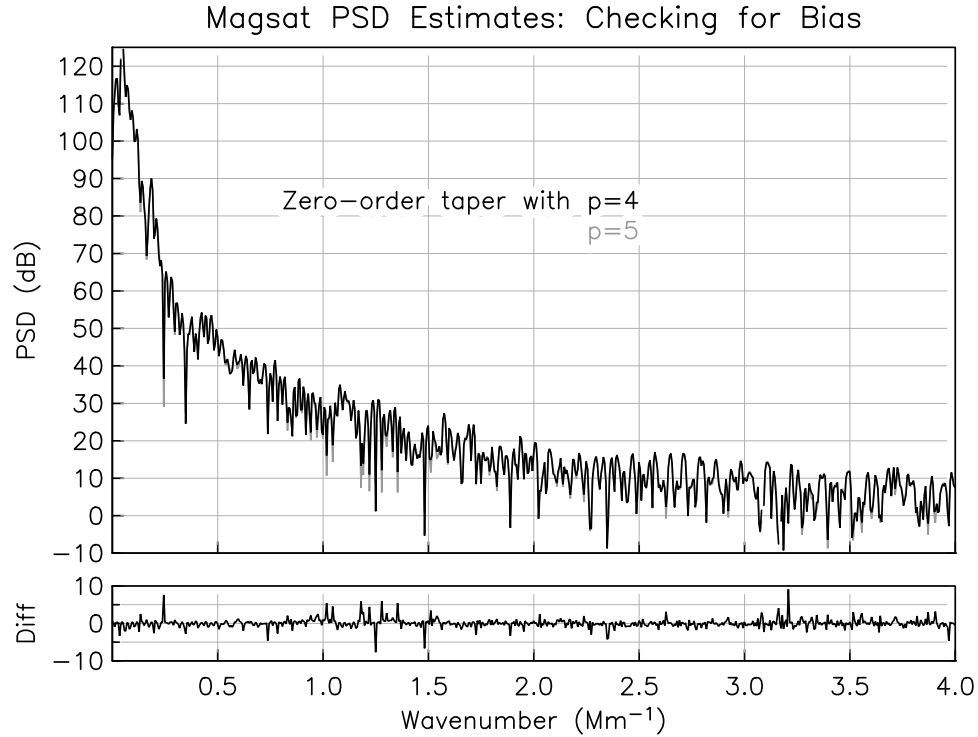


Figure 13.5: PSD estimates for the Magsat data shown in Figure 10.8. In the upper panel, black is the spectrum estimated using a $p = 4$ and gray that estimated using $p = 5$; since these are nearly indistinguishable, the lower panel shows the difference between these two estimates, on the same scale as in the upper panel.

may be less than ideal over different parts of the spectrum: if the spectrum varies rapidly with frequency it might be better to have it smaller, while if the spectrum is relatively smooth it would be better to make it larger.

In principle we could use a different bandwidth for different parts of the spectrum, with smooth regions getting a larger bandwidth; for a given level of bias, this would allow us to use more tapers and decrease the variance in such regions. With the prolate tapers it is not easy to vary the bandwidth in this way, because we would have to produce a new set of tapers and a new set of spectral estimates for each bandwidth, and at each frequency decide which bandwidth and how many tapers to use. While this is possible it is also complicated. So we next look at a different set of tapers, developed by [Riedel and Sidorenko \(1995, 1996\)](#), which make it easy to vary the bandwidth with frequency. These tapers have different, and for many spectra more useful, bias properties than the prolates do, and it is these properties that we discuss next.

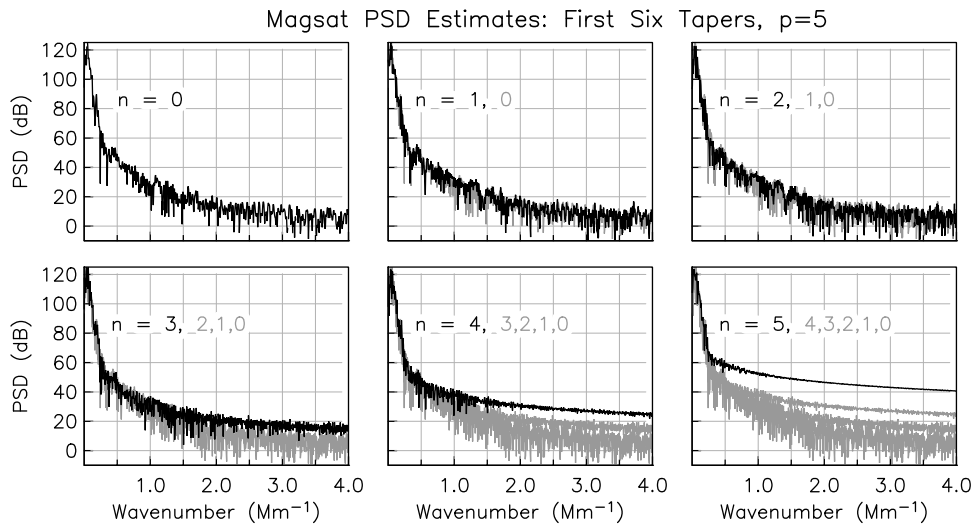


Figure 13.6: Magsat PSD estimates for the first six tapers with $p = 5$. In the i -th panel, black is the periodogram of data tapered using the i -th taper, and gray shows the periodograms using the first $i - 1$ tapers.

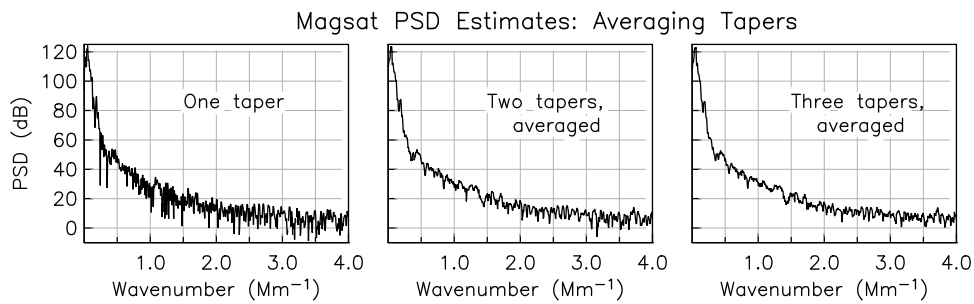


Figure 13.7: PSD estimates for the Magsat data. The three panels show the spectrum found by averaging over one, two, and three tapers with $p = 5$.

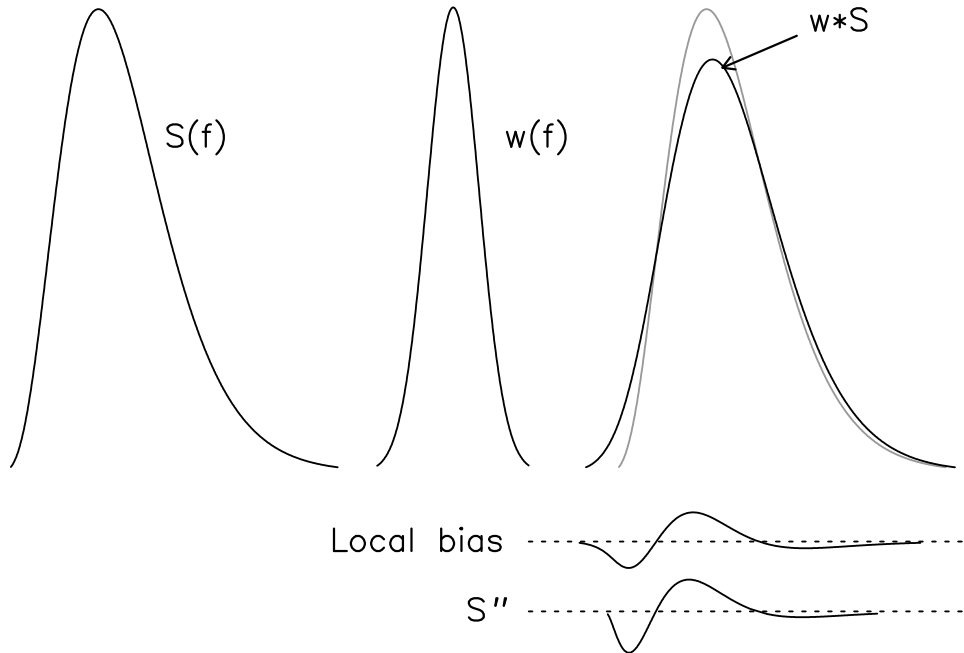


Figure 13.8: Cartoon showing how smoothing of the true PSD introduces bias: the convolution flattens peaks and widens their flanks. The difference between the true spectrum and the smoothed spectrum is similar to the second derivative of the spectrum.

13.4 Local Bias Minimization

Again, we start with the fact (Section 12.3.4) that the periodogram of a tapered time series is the convolution of the true spectrum with the convolving kernel $\tilde{w}^k(f)$ in equation (12.12). If the spectrum has peaks or troughs, this convolution, while smoothing the spectrum, also introduces a **local bias**, shown schematically in Figure 13.8. Even if the spectrum has a moderate dynamic range, so that spectral leakage does not matter, this local bias can be a problem, so we ask what tapers will minimize this bias. Following Riedel and Sidorenko (1995) the quantity we minimize is the difference between the expected value and the true value of the PSD:

$$\beta = \mathcal{E}[\hat{S}(f_0)] - S(f_0) = \int_{-1/2}^{1/2} S(f) \tilde{w}^k(f - f_0) df - S(f_0) \quad (13.5)$$

where \tilde{w}^k is the convolving function; see equations (12.12) and (12.13). The area under $\tilde{w}^k(f)$ is always chosen to be unity, and hence equation (13.5) can be written

$$\beta = \int_{-1/2}^{1/2} [S(f) - S(f_0)] \tilde{w}^k(f - f_0) df \quad (13.6)$$

For practical tapers, \tilde{w}^k also dies away to zero fairly fast; [Riedel and Sidorenko \(1995\)](#) approximate the factor in brackets by a local Taylor series:

$$S(f) - S(f_0) = (f - f_0)S'(f_0) + \frac{1}{2}(f - f_0)^2 S''(f_0) + O(f - f_0)^3 \quad (13.7)$$

Next we substitute equation (13.7) into equation (13.6) and integrate. The odd derivative terms vanish because $\tilde{w}^k(f)$ is always an even function of f , and the local bias β is approximated by:

$$\beta = \int_{-\frac{1}{2}}^{\frac{1}{2}} \frac{1}{2}S''(f_0)(f - f_0)^2 \tilde{w}^k(f - f_0) df \quad (13.8)$$

This expression is only valid if $S''(f_0) \neq 0$; if this is true, the error in the expression depends on the fourth derivative $S^{iv}(f_0)$. You can see in Figure 13.8 how the discrepancy between the true S and $\tilde{w}^k * S$ is greatest where the second derivative of the PSD is largest in magnitude, just as predicted by equation (13.8). For this bias there is no bandwidth parameter to choose.

So we seek the taper $w(t)$ that minimizes $\beta[w]$, just as the Slepian tapers minimize $L[w]$. We omit the details, and simply note that we again end up with an eigenvalue problem, whose eigenfunctions are another family of orthogonal functions. And an amazing thing happens: to a remarkably good approximation, *those orthogonal functions are the sines*. In continuous time they are:

$$\phi_n(t) = \sqrt{\frac{2}{T}} \sin \frac{\pi n t}{T} \quad 0 \leq t \leq T \quad (13.9)$$

13.5 An Adaptive Multitaper Estimate

Since the sines are orthogonal, we can again apply them to form statistically independent estimates of the spectrum – estimates that we can average to reduce the variance. In Figure 13.9 we plot the convolving kernels (squared transforms) for the different tapers. Recall that

$$\tilde{w}_n^k(f) = |\hat{\phi}_n(f)|^2$$

We find the following simple result:

$$\tilde{w}_n^k(f) = \frac{2n^2 T}{(n + 2fT)^2} \text{sinc}(fT - \frac{1}{2}n)^2$$

Thus when $fT \gg n$ the kernel decays like $n^2/2\pi^2 T^3 f^4$ times a squared sine function. The peak of $\tilde{w}_n^k(f)$ is roughly at $f = n/2T$ for $n > 1$ and is at $f = 0$ when $n = 1$. Unlike the Slepian tapers, which attempt to concentrate energy inside the bandwidth F , these functions spread it out over a wider and wider frequency band

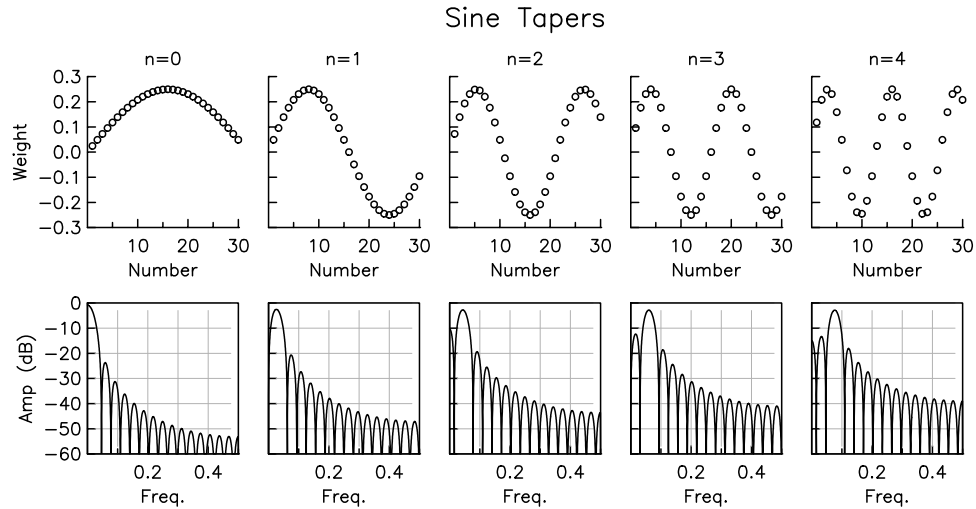


Figure 13.9: The first five sine tapers and their convolving kernels.

as n increases, because there is no fixed scale parameter corresponding to F . We obviously have much more spectral leakage; in Chapter 14 we will show how we can, for many spectra, get away with using tapers with higher leakage.

Once again we have to decide how many ϕ_n to use; as before we use K for this number of tapers. Riedel and Sidorenko integrate equation (13.8) with the \tilde{w}_n^k inserted to demonstrate that, if we average the K spectral estimates from using the first K tapers from equation (13.9) β is approximately

$$|\beta| = \frac{|S''(f_0)|K^2}{24T^2}$$

The local bias increases as K^2 while, because we are averaging independent estimates, the variance decreases as K^{-1} : We find

$$\mathcal{V}[\hat{S}(f_0)] = \frac{S(f_0)^2}{K}$$

Many statistical estimates involve a tradeoff between bias and variance; one common choice is then to minimize the **mean square error**: the linear combination

$$M^2 = \beta^2 + \mathcal{V}[\hat{S}(f_0)]$$

It is a simple calculus problem to find what value of K minimizes M^2 . We write

$$M^2 = \frac{S''(f_0)^2 K^4}{576T^4} + \frac{S(f_0)^2}{K}$$

with derivative

$$\frac{dM^2}{dK} = \frac{S''(f_0)^2 K^3}{144T^4} - \frac{S(f_0)^2}{K^2}$$

Setting this to zero gives what we may reasonably call an optimal number of tapers:

$$K_{opt} = \left(\frac{12T^2 S(f_0)}{|S''(f_0)|} \right)^{\frac{2}{5}} \quad (13.10)$$

We can use equation (13.10) to find this optimal number *at each frequency*. Where the spectrum is smooth the local bias is small, and according to equation (13.10) we should use many tapers to reduce the variance; but where there are narrow peaks or troughs in the spectrum, we should use fewer tapers, giving higher variance but less local bias, which means better frequency resolution. Equation (13.10) thus provides us with an optimal bandwidth, so we do not need to guess a suitable value for it as we did with the Slepian tapers.

But there are two problems. First, we do not actually know S or S'' , since that is what we are trying to estimate: a chicken-and-egg problem. For our first estimate, we simply pick a constant value for the number of tapers to be used. We then use this estimate in equation (13.10); because these estimates are noisy, we will need to smooth to get a reasonably reliable approximation for S'' ; but we know from our initial choice of K a local bandwidth over which the spectrum should be relatively smooth, which guides the range of smoothing needed. Now we can apply equation (13.10) to find $K_{opt}(f)$; we use this to apply a varying number of tapers with frequency, and so find another estimate of $S(f)$, which we again use in equation (13.10). In practice two or three iterations of this process converge to a stable result, though there is no known proof guaranteeing this.

A second problem is that the theory all depends on $S''(f_0)$ not being zero: if the second derivative vanishes, the bias calculation is invalid, and using it gives $K_{opt} = \infty$. Because the spectral estimates have a finite variance, random variations in S with frequency can cause $S''(f)$ to pass through zero quite often. A somewhat *ad hoc* approach (used in Parker's code `psd`) looks for runaway growth in K_{opt} and limits the increase as a function of f .

Using sine multitapers seems to provide a very convenient way of performing spectral estimation, because it does not require the user to guess various parameters, such as p (as when using Slepian tapers) or the section length (as in Welch's method). And it is also very fast for an interesting reason: because all the tapers are sinusoids, we only need to Fourier transform the original data sequence *once!* Every other method requires many Fourier transforms; here the different estimates can be made simply by combining the Fourier coefficients from the DFT in different ways – so there is no computational penalty for very large K_{opt} , which it will be if the spectrum is in fact smooth – and this is not uncommon. In contrast, if

we use Slepian tapers and vary the time-bandwidth products or number of tapers with frequency, the computation time will increase substantially.

We should note that [Prieto *et al.* \(2007\)](#) have developed a method, **quadratic multitaper estimation**, that combines some of these local-bias considerations with the Slepian tapers to produce a better estimate. And the Slepian tapers remain the preferred choice if the series is very short or has very large dynamic range over a narrow frequency band, since then it is crucial to minimize leakage.

The sine tapers do not have the low leakage of Slepian tapers; given how much we have stressed the importance of not allowing bias, you might think this higher leakage was a fatal flaw. But we can often keep it from being a problem by pre-processing the data series to reduce the dynamic range, before we estimate the spectrum. And to find out how to do this, you will need to read the next chapter.

CHAPTER 14

ESTIMATING POWER SPECTRA: PREWHITENING

Every valley shall be filled, and every mountain and hill shall be brought low; and the crooked shall be made straight, and the rough ways shall be made smooth.

LUKE 3:5 (KJV)

14.1 Introduction

Most geophysical spectra with large dynamic range have the most power at the lowest frequencies (a “red spectrum”), often with $S(f)$ varying as $f^{-\alpha}$ or $e^{-\alpha f}$. The Slepian tapers are effective in suppressing leakage from low to higher frequencies; but their relatively broad central lobe can cause local leakage around the low-frequency peak, distorting this part of the spectrum. Because they have less local leakage, the sine multitapers produce less of this local distortion – but their relatively large sidelobes mean that leakage from the low frequencies can corrupt the higher-frequency estimates.

We can reduce, or even eliminate, this problem if, before we form the spectral estimates, we preprocess the data to create derived values whose spectrum has a lower dynamic range, and then estimate the spectrum of these values. This procedure, called **prewhitening**, works especially well with red spectra, but should be considered when estimating any spectrum.

To prewhiten data, we design a filter that, when applied to the original series $\{X_n\}$ in the time domain, produces an output series $\{Y_n\}$ whose spectrum has a lower dynamic range: ideally, the flat spectrum of white noise. For example, if $S_X(f)$ was a red spectrum, $S_Y(f)$ would be less concentrated at low frequencies. We call $\{Y_n\}$ the **prewhitened** series. We then estimate the spectrum of the filtered series ($\hat{S}_Y(f)$); because the lower dynamic range of $S_Y(f)$ makes bias from leakage much smaller, we can use the sine tapers, with their lower local bias and easy use in adaptive estimation.

In Section 11.4 we showed that if the frequency response of a filter applied to a series is $\tilde{g}(f)$, then $S_Y(f) = |\tilde{g}(f)|^2 S_X(f)$. So if we multiply the estimated spectrum

for the prewhitened data, $\hat{S}_Y(f)$, by the inverse of the squared filter response, we get an estimate of $S_X(f)$:

$$\hat{S}_X(f) = \frac{\hat{S}_Y(f)}{|\tilde{g}(f)|^2}$$

Since the filter is something we design, we know the response $\tilde{g}(f)$ exactly: this correction introduces neither error or uncertainty.

14.2 Prewhitenning with Prediction-Error Filters

How do we design a prewhitening filter? Our goal is to make $\{Y_n\}$ as close as possible to white noise, but even a very poor approximation to this can still make the dynamic range of $S_Y(f)$ much less than that of $S_X(f)$.

A filter that works particularly well for processes with a red spectrum is an IIR (recursive) one, which uses a linear combination of the values before a data point to predict its value. We can then use the errors in the prediction as the prewhitened series $\{Y_n\}$. For the simplest possible prediction – that each term has the same value as the previous one – the prediction errors are just the first differences. At frequencies much less than the Nyquist frequency, the response $|\tilde{g}(f)|^2$ of this “filter” is approximately f^{-2} : so even this simple approach can flatten a very red spectrum.

But we can do better. We write the equation for a recursive prediction-error filter as

$$Y_n = X_n - \sum_{m=1}^M a_m X_{n-m} \quad (14.1)$$

which is to say that the prediction error Y_n is the difference between the actual value X_n and a linear combination of the previous M values; M is called the **order** of the filter. Our design method is then, for a particular value of M , to determine the a 's that minimize the variance of the error series Y . To find each a , we take the derivative of equation (14.1) squared with respect to a_i and set it to zero:

$$-2\mathcal{E} \left[\left(X_n - \sum_{m=1}^M a_m X_{n-m} \right) X_i \right] = 0 \quad (14.2)$$

Equation (10.2) tells us that when we apply the expected-value operator to the products of the X 's we get the autocovariances, so equation (14.2) becomes

$$R_{n-i} = \sum_{m=1}^M a_m R_{n-m-i} \quad (14.3)$$

where the R 's are the autocovariances, with the argument expressed as a subscript. A change of variables turns equation (14.3) into

$$R_j = \sum_{m=1}^M a_m R_{j-m} \quad \text{for } j = 1, \dots, M \quad (14.4)$$

which are called the **Yule-Walker equations**. Solving these for the a 's gives the best recursive prediction filter based on the autocovariances, which has more uses than just prewhitening.

This derivation also gives us another way of looking at prediction error. Equation (14.2) amounts to $\mathcal{E}[Y_n X_n] = 0$, which is to say that the error series $\{Y_n\}$ is uncorrelated with the original series $\{X_n\}$. We can then rearrange equation (14.1) to be

$$X_n = \sum_{m=1}^M a_m X_{n-m} + Y_n \quad (14.5)$$

This says that to produce the original stochastic process $\{X_n\}$, we apply a recursive filter (specified by the weights a_m) to an input $\{Y_n\}$, which will be uncorrelated with $\{X_n\}$. Using the terminology for recursive filters from Section 8.5, we say that $\{X_n\}$ is produced by an autoregressive (AR) filter. The input $\{Y_n\}$ is called the **innovations process**. If we want to model $\{X_n\}$ as the result of a recursive filter applied to some other series, and also assume that this other series (the innovations) is white noise, we will again get equation (14.4).

We can also use the Yule-Walker equations to derive an explicit expression for the variance of the prediction error, $\mathcal{E}[Y_n^2]$, which we denote by P^M ; note that here and for the rest of this chapter, a superscript M denotes not a power of the variable, but the order M of the filter. The expression for P^M is:

$$\begin{aligned} P^M &= \mathcal{E} \left[\left(X_m - \sum_{m=1}^M a_m X_{n-m} \right)^2 \right] \\ &= R_0 - 2 \sum_{m=1}^M a_m R_m + \sum_{m=1}^M a_m \sum_{l=1}^M a_l R_{l-m} \\ &= R_0 - \sum_{m=1}^M a_m R_m \end{aligned} \quad (14.6)$$

The Yule-Walker equations (14.4) are a linear system of equations for the unknown weights, which we can write in matrix form:

$$\mathbf{R}^M = \mathbf{C}^M \mathbf{a}^M \quad (14.7)$$

where there are two vectors:

$$\mathbf{R}^M = (R_1, R_2, \dots, R_M)^T \quad \text{and} \quad \mathbf{a}^M = (a_1^M, a_2^M, \dots, a_m^M)^T$$

and \mathbf{C}^M is the matrix of autocovariances defined by equation (10.4), with N in that definition being set to $M - 1$. We could of course solve this by inverting \mathbf{C}^M to find \mathbf{a}^M ; but the special form of \mathbf{C}^M , namely that it is a Toeplitz matrix, makes it possible to use a faster algorithm than the usual matrix inversion methods. This procedure, called the **Durbin-Levinson** algorithm, has the additional advantage

that it computes \mathbf{a}^M , and the mean-square prediction error P^M , for successively increasing values of M . We describe this algorithm in Appendix H.

As M increases, P^M will decrease, which suggests that we might choose M to be the smallest value for which increasing it by one does not decrease P^M very much. If we were trying to model the original series $\{X_n\}$ using an autoregressive model such as equation (14.5), we would want to make M as “correct” as possible: a difficult task. But since we are only trying to produce an approximately white series for spectrum analysis, we do not need to worry too much about what value of M to choose.

The final challenge in prewhitening is that, since we do not know the spectrum, we also do not know the R_m ’s! So we need to start by estimating the PSD, $\hat{S}_X(f)$, using a bias-resistant procedure, and then take its DFT to get preliminary values for the R_m ’s. Next, we solve the Yule-Walker equations (14.4), typically for $M < 10$, and use the resulting filter to compute the error series $\{Y_n\}$ according to equation (14.1); we inevitably lose M terms off the front of $\{X_n\}$ when we do. We then estimate $\hat{S}_Y(f)$, and finally apply the inverse of the square of the filter response:

$$\hat{S}_X(f) = \frac{\hat{S}_Y(f)}{\left|1 - \sum_{m=1}^M a_m e^{-2\pi i m f}\right|^2} \quad (14.8)$$

We could iterate by finding new R_m ’s from $\hat{S}_X(f)$, use these to find new filter weights a_m , prewhiten again, and so on – but this is rarely necessary if we are careful to minimize bias in our initial estimate of $S_X(f)$.

14.3 A Prewhitenning Example

To demonstrate prewhitening, we again consider the Magsat data in Figure 10.8. We have already computed its power spectrum using both the Hann taper and Slepian multitapers. Given the large dynamic range shown by these estimates (Figure 13.7), we might expect a sine multitaper estimate to suffer from spectral leakage over a broad range of frequencies. It does; but we can use prewhitening to eliminate this problem and also to show that one feature of these earlier estimates, the rather flat PSD near $k = 0$, was caused by local bias.

Our initial spectrum estimate is the smoothed Hann-taper estimate (Figure 12.5); we take the DFT of this to get the autocovariances. Since we only need a few autocovariances it is most efficient to use a “slow” Fourier transform (Appendix Section F.4). We then solve the Yule-Walker equations using the Durbin-Levinson algorithm (Appendix H); because this proceeds iteratively, we can use each iteration to see how we should choose the filter order M .

Figure 14.1 and Table 14.3 show the results. The weights for $M \leq 3$ are very close to first, second, and third differences. But more importantly, the figure and table also show that for $M > 2$ the rms prediction error, σ^2 , actually increases.

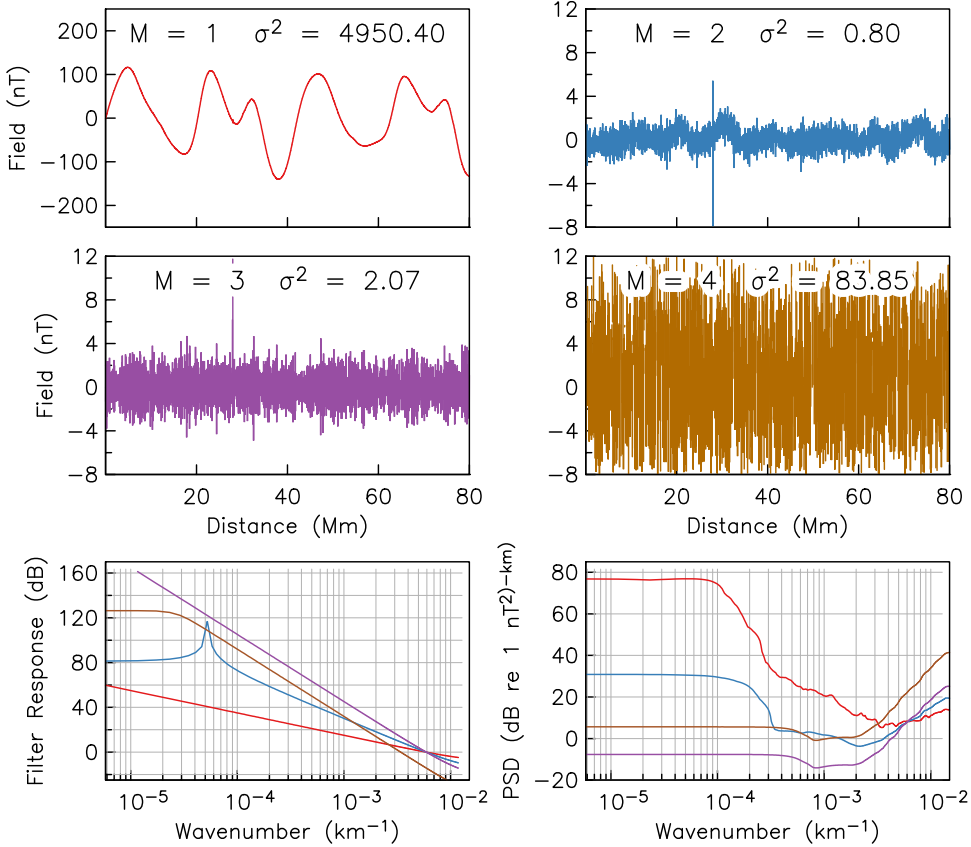


Figure 14.1: The top four plots show the prediction error for part of the Magsat data for filters of order M , for $1 \leq M \leq 4$. Note the improvement from $M = 1$ to $M = 2$; followed by poorer performance as the order increases. The bottom left plot shows the response of the inverse of the prediction filter for the different values of M and the bottom right plot shows the PSD's of the prediction error series.

M	σ^2	a_0	a_1	a_2	a_3	a_4
1	4950.40	-1.0	0.999957			
2	0.80	-1.0	1.999957	-1.000043		
3	2.07	-1.0	3.000000	-3.000000	1.000000	
4	83.85	-1.0	8.580145	-19.740436	17.740436	-5.580145

According to the mathematical development shown in Appendix H this is impossible; it happens because of the finite precision of the actual calculations. In finding prediction-error filters of higher and higher order this growth of error is not unusual; it arises, not from numerical instability of the Durbin-Levinson algorithm (Cybenko, 1980) but because for a well-correlated series, such as the Magsat data, the matrix \mathbf{C}^M becomes increasingly ill-conditioned as M increases. So any inversion with finite-precision arithmetic will be unstable.

The prediction-error series in Figure 14.1 shows another important reason to prewhiten the data: problems such as outliers and nonstationarity become more visible. The prewhitened data for $M = 2$ very clearly show a spike in the series, suggesting a possible error; this spike is not visible even in the series for $M = 1$ (not to mention the original series) because the overall variation is much larger.¹

The bottom left panel of Figure ref 14.1 shows the inverse response of the prediction-error filter for $1 \leq M \leq 4$, while the bottom right panel shows the PSD's, estimated using sine multitapers, for the corresponding prewhitened series. In these plots we use a logarithmic scale for frequency to show the low-frequency behavior more clearly. Note that for $M = 2$ the inverse response, but not the prewhitened spectrum, shows a low-frequency peak; what the prediction-error filter is mostly predicting is the sinusoidal variation of the series. The prediction-error filter for $M = 2$ includes a pair of poles close to $0.999935 \pm 0.009283i$ in the z -plane; these correspond to a resonance with a wavelength of 20,000 km, which is halfway around the Earth.

None of the prediction-error spectra are white; but for all of them the range is much less than the 110 dB of the estimated spectrum in Figure 13.7. For $M = 2$, when we divide the spectrum of the prediction error by the response of the filter (equation 14.8), we get the estimate plotted in black in Figure 14.2.

This shows, first, that if we use prewhitening, the sine multitaper estimate is no more affected by bias from spectral leakage than the prolate multitaper estimate was – and the sine multitaper estimate is much smoother. And, as expected from the discussion above, the estimate using prewhitening and sine multitapers shows a peak at the lowest wavenumbers, where the other two estimators gave a flat spectrum. This peak is quite real: it comes from the quasi-sinusoidal variation caused by the satellite orbiting through the dipole part of the field. Without the prewhitening and adaptive estimation the energy in this gets spread into a broader band at low frequencies, as can be seen in the spectrum in Figure 13.7.

¹This outlier is not in the original data, but was added to show the value of prediction-error filtering. It was an offset of one value by 5 nT, obviously small relative to the 30,000 nT variations in the original signal shown in Figure 10.8.

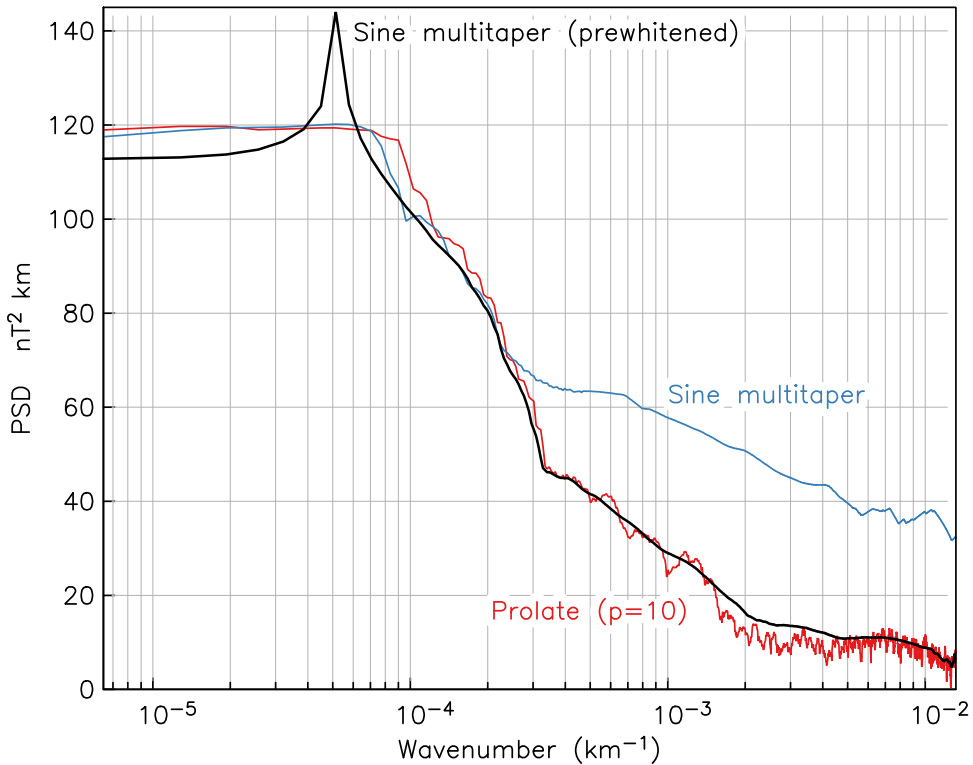


Figure 14.2: Three PSD estimates for the MAGSAT data. The red is the estimate using prolate multitapers, shown above in Figure 13.7. Blue is the sine multitaper estimate for the original series, and black the sine multitaper estimate for the prewhitened data, corrected using the response of the prewhitening filter for $M = 2$.

14.4 Spectrum Estimation: Summary and Suggestions

So what procedure do we suggest for estimating the power spectral density? The most important things to know are that there is no single method that is best for all data, and that there is no escape from using your judgement to decide, for example, how best to remove bias, or how much the spectrum should be smoothed. With these warnings, we suggest the following approach:

1. Remove any purely periodic variations – though you may need to look at the power spectrum first to find them. Almost always you should remove the mean and a trend, especially if you have reason to think either of these has a different source than the other variations. For example in the Project Magnet data (Figure 10.7) the mean and trend come from the core, and the other variations from the crust. The data shown in Figure 1.1 are a more difficult

case: while the mean is arbitrary, the trend might or might not be driven by the same processes as the other fluctuations. You should always remember that the trend might simply represent actual variations at a period longer than the record length, and that by removing the trend you might be biasing the spectrum at the very lowest frequencies.

2. If the data have short gaps, fill these in by some form of interpolation. For very large datasets with occasional large gaps, you may wish to apply Welch's method; if you do, make sure the tapering is adequate to eliminate bias from spectral leakage. Any large outliers ("spikes") will add energy at all frequencies, and should be usually be removed: even if they are real (rather than caused by instrument malfunction) they still represent nonstationary behavior.
3. Taper your data with a prolate taper, such as the 4π prolate, that has very low sidelobes, and compute the periodogram of the result. The result should show you if the spectrum has a very large dynamic range. While sometimes (as with the Magsat data) this can be obvious from the time series, there are data for which this is not so: for example, a spectrum with a very low level (a "notch") over some range of frequencies.
4. If the dynamic range of the spectrum is small, you should use a sine multitaper estimate.
5. If the dynamic range of the spectrum is high in a way that cannot easily be reduced by prewhitening, or if the number of data points is small, you should make a multitaper estimate using the prolate tapers. It is up to you to decide what level of frequency averaging is appropriate.
6. If you can prewhiten the data, you should; the resulting time series should again be checked for possible problems such as outliers. Then make a sine multitaper estimate, and correct it by the inverse of the prewhitening filter. Be sure to check that the spectrum estimated using the prewhitened data is indeed free from bias by comparing it to the single-taper estimate you did as a first step.
7. Plot your estimate using a log scale for the PSD, preferably in dB relative to some level, which should have the proper dimensions (using SI units if possible). Unless you have complex-valued data use the single-sided spectrum normalization. Sometimes a linear frequency scale will be appropriate; other times a log scale may be more informative. Avoid the temptation to plot the PSD against period rather than frequency.

CHAPTER 15

MULTIVARIATE SPECTRA

Like most scientific discoverers, ... [Vacquier] sought for some way to confirm the correlation with statistical rigor. ... Accordingly he consulted with a statistician, only to be told that the statistical approach was a waste of time. The wiggly lines [magnetic anomalies] matched perfectly enough.

H. W. MENARD (1986), page 76

15.1 Introduction

In geophysics we often encounter time series that are (or might be) related to one another. Some examples would be:

- The input signal and the instrument output for a seismometer calibration, as in Figure 2.4.
- Two components of a vector field measured along a path in space, as in Figure 10.7.
- Ground elevation and the strength of gravity along a profile or in a region.
- Time variation of the north electric field and the east magnetic field at the same location.

We now turn to methods that show if two series are related and, if they are, describe the relationship. If the relationship between two series is through some process that can be modeled as a linear time-invariant system, Section 2.5 shows that this relationship can be described by a complex-valued function of frequency: the frequency response. So we want to be able to estimate this.

The methods for these tasks are called **multivariate** spectral estimators, by analogy with the generalizing of single random variables (univariate probability and statistics) to multiple random variables, which may be connected by their joint pdf's. Appendix C.5 gives a very brief treatment of the relevant theory, in which we introduce several concepts:

- The covariance between two variables, which shows how they are related in terms each having a linear relationship to the other.
- The correlation, the normalized (or standardized) form of the covariance, which gives a measure of how strong this linear relationship is.
- Linear regression, which is how we estimate what the relationship is.

We have already encountered the first two in Section 10.2.1, where we used them to describe how each point in a time series is related to others closer or farther from it, in the form of the autocovariance. But now we want to consider two different series, in order to develop, as we did with the power spectrum, frequency-domain descriptions. As we have done in Chapters 10 through 14, we first develop the theory for pairs of stochastic processes, and then describe procedures for estimating the frequency-domain connection from a finite set of data.

15.2 Pairs of Random Sinusoids

We start by developing an approximate way of looking at the relation between two stationary time series. In Section 11.2 we developed an intuitive way of thinking about the power spectrum, which was to view it as the result of (1) convolving the time series with a narrow-band filter to isolate a given frequency component, (2) taking the variance, and (3) normalizing by the bandwidth of the filter to get the power spectral density.

We can take a corresponding approach to pairs of time series. Imagine that we filter both series using a bandpass filter with a very narrow passband. Each output series will look like a sinusoid, which as usual we view as the real part of the complex quantity $\tilde{x}e^{2i\pi f t}$ with \tilde{x} complex; we use \tilde{x}_1 for one series and \tilde{x}_2 for the other. If we had many realizations of the time series, filtering each realization would give a different value of \tilde{x}_1 and \tilde{x}_2 .

Now consider a *complex* scatterplot of \tilde{x}_1 against \tilde{x}_2 ; any relationship will appear, as in a conventional scatterplot, as an elongated cloud of points. But since the \tilde{x} 's are complex, we have four real quantities to compare with each other, not just two, and we need to make four scatterplots to show all the possibilities for interrelationships.

Figure 15.1 shows an example, using the two of the series of magnetic data in Figure 10.7. To get multiple realizations we divided the data into sections; to filter to a narrow frequency, we took DFT's of each pair of sections, and selected the DFT coefficients corresponding to a wavelength of 60-100 km. Figure 15.1 shows scatterplots of all four possible combinations of real and imaginary parts of the two series for the series x_1 and x_3 ; the DFT coefficients, being in the frequency domain, are \tilde{x}_1 and \tilde{x}_3 . There is no correlation between the real parts or the imaginary

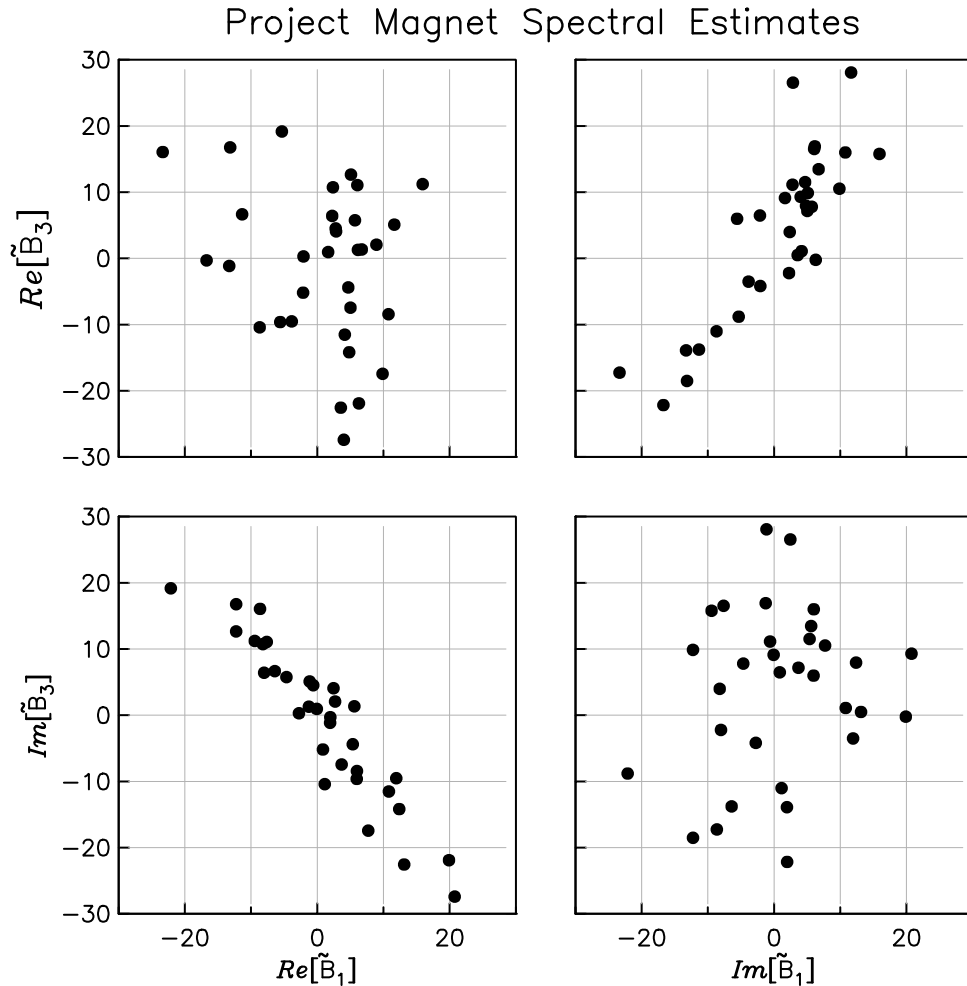


Figure 15.1: Scatter plots of the real and imaginary parts of DFTs from the data in Figure 10.7, for wavelengths of 60-100 km, and fields B_1 and B_3 (called x_1 and x_3 in the text). The DFT's were taken over 750 values (262.5 km), overlapping by 250 terms.

parts, but there clearly is between the real part of one and the imaginary part of the other.

A probability model of this collection of complex sinusoids would be two, possibly correlated, random variables. This model gives the same results that we will find for the spectral analysis of pairs of series; but since it involves only two random variables, it is easier to see the parallels to Section C.5's treatment of pairs of random variables.

Formally, the two sinusoids are

$$X_1(t) = \tilde{X}_1 e^{2\pi i f t} \quad X_2(t) = \tilde{X}_2 e^{2\pi i f t}$$

where \tilde{X}_1 and \tilde{X}_2 are complex-valued random variables and we take the real part of the complex sinusoids to produce real-valued time series.

We assume that both the real and imaginary parts of \tilde{X}_1 and \tilde{X}_2 are zero-mean. The variance of \tilde{X}_1 , which we denote by σ_1^2 , requires us to use the complex conjugate to make the result real-valued:

$$\begin{aligned} \mathcal{V}[\tilde{X}_1] &= \mathcal{E}[\tilde{X}_1 \tilde{X}_1^*] = \mathcal{E}[(\tilde{X}_1^R)^2 + (\tilde{X}_1^I)^2] \\ &= \mathcal{E}[(\tilde{X}_1^R)^2] + \mathcal{E}[(\tilde{X}_1^I)^2] = \mathcal{V}[\tilde{X}_1^R] + \mathcal{V}[\tilde{X}_1^I] \end{aligned} \quad (15.1)$$

where we have re-used the labels from equation (12.3) for the real and imaginary parts of the Fourier coefficient, though there the subscript referred to frequency, while here it refers to which series has been filtered.

Similarly, we can write the covariance $\mathcal{C}[X_1, X_2]$ as:

$$\begin{aligned} \mathcal{C}[\tilde{X}_1 \tilde{X}_2^*] &= \mathcal{E}[(\tilde{X}_1^R + i\tilde{X}_1^I)(\tilde{X}_2^R - i\tilde{X}_2^I)] \\ &= \mathcal{E}[(\tilde{X}_1^R \tilde{X}_2^R - \tilde{X}_1^I \tilde{X}_2^I) + i(\tilde{X}_1^I \tilde{X}_2^R + \tilde{X}_1^R \tilde{X}_2^I)] \\ &= R_{rr} - R_{ii} + i(R_{ir} + R_{ri}) \end{aligned} \quad (15.2)$$

where the R 's are shorthand for the covariances of the different combinations of real and imaginary parts. In general $\mathcal{C}[\tilde{X}_1, \tilde{X}_2]$ is complex-valued, as it needs to be to cover, for example, what we see in Figure 15.1, in which a decrease in the real part of \tilde{X}_2 when the imaginary part of \tilde{X}_1 increases, meaning that $C_{ir} = \mathcal{E}[\tilde{X}_1^I \tilde{X}_2^R]$ is negative.

What, in this case, is the analog to the correlation defined by equation (C.23) in Appendix C? Again, we need to take complex conjugates, this time of the covariance itself, and then normalize by the variances of the two variables:

$$\gamma^2 = \frac{\mathcal{C}[\tilde{X}_1, \tilde{X}_2] \mathcal{C}^*[\tilde{X}_1, \tilde{X}_2]}{\sigma_1^2 \sigma_2^2} \quad (15.3)$$

Now suppose $\tilde{X}_2 = g\tilde{X}_1 + \tilde{X}_3$, where g is complex and \tilde{X}_1 and \tilde{X}_3 are uncorrelated. Then

$$\mathcal{C}[\tilde{X}_1 \tilde{X}_2^*] = g \sigma_1^2 \quad \text{and} \quad \sigma_2^2 = \mathcal{E}[\tilde{X}_2 \tilde{X}_2^*] = gg^* \sigma_1^2 + \sigma_3^2$$

which means that

$$\begin{aligned} \gamma^2 &= \frac{\mathcal{C}[\tilde{X}_1, \tilde{X}_2] \mathcal{C}^*[\tilde{X}_1, \tilde{X}_2]}{\mathcal{E}[\tilde{X}_1 \tilde{X}_1^*] \mathcal{E}[\tilde{X}_2 \tilde{X}_2^*]} = \frac{|g|^2 \sigma_1^4}{\sigma_1^2 (|g|^2 \sigma_1^2 + \sigma_3^2)} \\ &= \frac{|g|^2}{(|g|^2 + \sigma_3^2) / \sigma_1^2} \end{aligned}$$

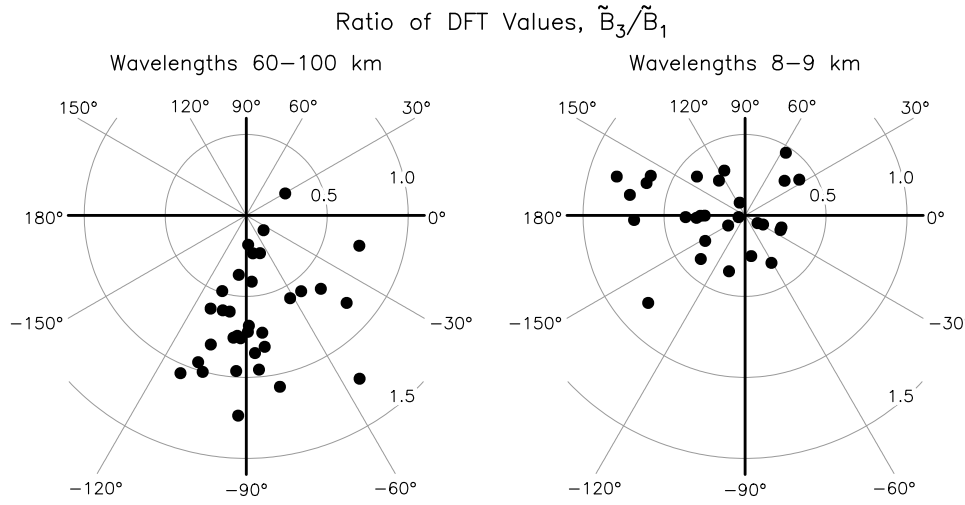


Figure 15.2: Ratio of DFT coefficients for two different frequency bands, plotted on the complex plan (labelled as a phasor diagram). The left panel shows the result for the same frequency range as shown in Figure 15.1, the right for higher frequencies.

We thus see that γ^2 will be one for perfect correlation (X_3 absent, so $\sigma_3^2 = 0$), independent of g , and zero for no correlation (a zero). We call γ^2 the **squared coherence**, the “squared” part indicating that (unlike the correlation) it cannot be negative.

The correlation between \tilde{X}_1^R and \tilde{X}_2^I , and between \tilde{X}_1^I and \tilde{X}_2^R , and 15.1 shows that there is some relationship between the series, and also suggests what it is. Multiplying a complex number by an imaginary one converts its real part to a complex part, and vice versa, which suggests that the constant g in $\tilde{X}_2 = g\tilde{X}_1$ must be imaginary, or in other words have a phase shift of 90° .

Finding the constant g is the equivalent of finding the regression of one random variable on another (Section C.5.1), something that only makes sense if the variables are correlated, but which gives additional information about their exact relationship. If the variables are connected by a relationship $X_2 = aX_1$, a naive approach is to look at the ratio X_2/X_1 . Figure 15.2 shows the ratio \tilde{X}_2/\tilde{X}_1 for two sets of DFT coefficients, with the complex plane labelled in amplitude and phase. The ones on the left are for the DFT coefficients shown in Figure 15.1, and these do indeed cluster around a phase of -90° and an amplitude ratio of about 0.75. The plot on the right is for much higher wavenumbers (shorter wavelengths), and suggests a phase of about 180° , though with a smaller amplitude and more scatter.

15.3 Pairs of Stationary Signals

We are now ready to consider actual random time series; we will see that, as with the power spectrum, we can develop the theory most easily by taking Fourier transforms of time-domain correlations.

Consider two stationary stochastic processes $X_1(t)$ and $X_2(t)$, both with zero mean; we define the **cross-covariance** between them as

$$R_{21}(\tau) = \mathcal{E}[X_1(t)X_2^*(t + \tau)] = \mathcal{E}[X_1(t)X_2^*(t + \tau)]$$

We use subscripts to indicate the different series because it is then more obvious that we can generalize this for M series, to define a **cross-covariance matrix** in which each matrix element is a function:

$$R_{kj}(\tau) = \mathcal{E}[X_j(t)X_k^*(t + \tau)] \quad \text{for } j, k = 1, 2, \dots, M \quad (15.4)$$

Notice the (somewhat illogical looking) reversal of the order of the indices in the function and under the expectation. Because the processes are stationary, R_{jk} depends only on τ even though t appears in the equation. Some trivial algebra gives $R_{12}(\tau) = R_{21}^*(-\tau)$, so the cross-covariance matrix is Hermitian.

We defined the power spectral density (PSD) as the Fourier transform of the autocovariance function; in equation (15.4) we would have M such power spectra, each one obtained by taking the transform of one of the functions R_{jj} that are on the diagonal of the matrix.¹

We will use the term **cross-spectrum** for the transform of the covariance between (for example) $X_1(t)$ and $X_2(t)$:

$$S_{12}(f) = \mathcal{F}[R_{12}(t)] = \int_{-\infty}^{\infty} R_{12}(t)e^{-2\pi ift} dt \quad (15.5)$$

As with the power spectrum, this relationship is useful for theory, but it is as poor a way to estimate the cross spectrum from data as the Blackman-Tukey method is for the power spectrum.

We have seen (Section 11.3) that because the autocovariance is symmetric and real-valued, the PSD is always real and non-negative. But the cross-covariance is usually not symmetric, and so the cross-spectrum, unsurprisingly given our early results for sinusoids, will be complex-valued. If the series are real, the cross-spectrum is still complex, but Hermitian, so that, as with the PSD, negative frequencies provide only redundant information.²

¹Sometimes these are called **autospectra**, but we will keep calling them power spectra.

²Two more names that others use, but we will not, are **cospectrum**, for the real part of $S_{12}(f)$, and **quadrature spectrum**, for the imaginary part.

The most important two combinations of the real and imaginary parts of $S_{12}(f)$ are the **amplitude spectrum**, defined as $\sqrt{\mathcal{I}[S_{12}]^2 + (\mathcal{R}[S_{12}])^2}$ and the **phase spectrum**, defined as

$$\arctan\left(\frac{-\mathcal{I}[S_{12}]}{\mathcal{R}[S_{12}]}\right) \quad (15.6)$$

where the arctan function is understood to return values from $-\pi$ to π . These two spectral quantities are the most intuitive way to express the cross-spectrum, though because they are nonlinear functions of $S_{12}(f)$ the probability distribution of their estimators turns out to be quite complicated.

We can normalize the cross-spectrum by the two power spectra to get what is called the **coherency**:

$$\frac{S_{12}}{\sqrt{S_{11}S_{22}}}$$

but this complex-valued quantity is not very useful; a better measure of correlation is the **coherence** spectrum, which is the squared magnitude of the coherency:

$$\gamma_{12}^2(f) = \frac{|S_{12}|^2}{S_{11}S_{22}} = \frac{\mathcal{R}[S_{12}]^2 + \mathcal{I}[S_{12}]^2}{S_{11}S_{22}} \quad (15.7)$$

where the square again indicates that the value must be nonnegative. Just like equation (15.8), equation (15.7) gives a correlation coefficient between the two signals as a function of frequency.

One important result that does not require us to use the correlation functions comes from considering two stochastic processes Y_1 and Y_2 , both produced by convolutions of a third process X :

$$Y_1 = g_1 * X \quad Y_2 = g_2 * X$$

We can then ask how the cross spectrum S_{12} is related to the PSD of X , S_X . The answer, which takes a few lines of simple algebra, is:

$$S_{12} = \tilde{g}_1 \tilde{g}_2^* S_X \quad (15.8)$$

This result is valid for processes of a single variable or for any higher dimensions. When $g_1 = g_2$, so that $Y_1 = Y_2$, we get the usual result, equation (11.21), that the PSD of Y is $S_Y = |\tilde{g}|^2 S_X$

15.4 Estimating Cross Spectra

For estimating cross-spectra, the same approaches we developed for power spectra remain the best methods – though with some complications. For estimation, we ignore the definitions in terms of the autocovariance and cross-covariance, and work with DFT's of the series. To reduce (some) bias we taper both series (in the same

way) before computing the DFT; as usual, to reduce the variance of the estimates, we have to average over something. We are thus led, again, to multitaper estimation: we average over DFT values found for the series multiplied by an orthogonal set of tapers, a set we choose in order to minimize bias from spectral leakage. As in the power-spectrum case, it is also a good idea to prefilter the series to make the dynamic range smaller.

15.4.1 Bias in the Cross-Spectrum

Unfortunately the cross-spectrum has additional biases, which create the need for another kind of prefiltering before estimating cross-spectra. Suppose we have two uncorrelated white-noise time series, and compute the components of the spectral matrix without any averaging: that is, we apply the periodogram estimator to the cross spectrum. We know that for white noise this estimator is unbiased for the power spectrum, albeit with very large variance. What about the cross-spectrum?

This cross-spectrum is just

$$\hat{S}_{12}(m) = \left(\sum_{j=0}^{N-1} X_{1j} e^{-2\pi jm/N} \right) \left(\sum_{k=0}^{N-1} X_{2k} e^{-2\pi km/N} \right)^*$$

where we use two subscripts on X , the first to indicate the series number, and the second for the term number. If we ask for the expected value of \hat{S}_{12} , we see that it is the sum of a collection of expected values of products, $\mathcal{E}[X_{1j}X_{2k}]$ – but since the series are uncorrelated, all these expected values are zero, and so is $\mathcal{E}[\hat{S}_{12}]$: since the true value is zero, this estimate of the cross-spectrum is, in this case, unbiased.

Unfortunately this cannot be said of some of the spectral estimates found from \hat{S}_{12} . In particular, consider the squared coherence:

$$\begin{aligned} \hat{\gamma}^2(m) &= \frac{\hat{S}_{12}(m)\hat{S}_{12}^*(m)}{\hat{S}_{11}(m)\hat{S}_{22}(m)} \\ &= \frac{(\sum X_{1j} e^{-2\pi jm/N})^* (\sum X_{2k} e^{-2\pi km/N}) (\sum X_{1j} e^{-2\pi jm/N}) (\sum X_{2k} e^{-2\pi km/N})^*}{(\sum X_{1j} e^{-2\pi jm/N}) (\sum X_{1j} e^{-2\pi jm/N})^* (\sum X_{2k} e^{-2\pi km/N}) (\sum X_{2k} e^{-2\pi km/N})^*} \end{aligned} \quad (15.9)$$

which can be seen to be exactly equal to one, irrespective of the values of X_1 and X_2 . Since the maximum value for γ^2 is one, and the true value in this case is zero, this estimate of the coherence is as badly biased as it can be. As with the high variance of the power-spectrum estimate, this result comes from insufficient averaging. The parallel with the results in Appendix C.5 is that one pair of data values cannot tell us if the data are correlated or not. Since much of the interest in the cross-spectrum lies in looking for coherence (or not) between series, bias in the

estimated coherence is a much more serious defect than the high variance of the power-spectrum estimate – and averaging is, correspondingly, more important.

But it turns out that there is another source of bias, somewhat connected with spectral leakage, in that it comes from variations in the cross-spectrum with frequency. Remember that in Section 13.4 we showed that local bias in the power-spectrum estimate depends on the second derivative of the power spectral density. The same is true for the cross-spectrum; what is different is that it is very easy to make this second derivative large even if it might seem that the cross-spectrum would vary only slightly with frequency. To see how this can be, we write the cross-spectrum in polar form:

$$S_{12}(f) = A(f)e^{i\theta(f)}$$

Then the first derivative is

$$S'(f) = \frac{dS_{12}(f)}{df} = A'e^{i\theta} + A i\theta' e^{i\theta}$$

and the second derivative is (using primes for differentiation with respect to frequency):

$$S''(f) = \frac{d^2S_{12}(f)}{df^2} = A''e^{i\theta} - A(\theta')^2 e^{i\theta} + i \left[2A'\theta' e^{i\theta} + A\theta'' e^{i\theta} \right] \quad (15.10)$$

If we multiply S''_{12} by $e^{-i\theta(f)}$, it becomes clear that the real part of equation (15.10) is the amplitude of S''_{12} , and the imaginary part is the part in quadrature, which accounts for the phase of S''_{12} relative to S_{12} . The amplitude part of S''_{12} is thus $A'' - A(\theta')^2$; the first term is of course what we would get if S were purely real, as it is for the power spectrum.

But even if $|A(f)|$ is constant, making A'' equal to zero, the amplitude of S''_{12} can be nonzero because of the $-A(\theta')^2$ term. And, by the shift theorem (equation 3.13) we can make $\theta'(f)$ arbitrarily large just by shifting (delaying or advancing) one series with respect to the other. A delay, or any other phase shift with frequency, will thus bias the amplitude of the cross-spectrum downwards: because the coherence depends on this amplitude, it too will be biased down.

It is not difficult to see intuitively how a delay would lower the coherence: if we had two perfectly correlated series, one of which was delayed, and we took a sample length less than the delay, the samples we would have would in fact be uncorrelated. So it is standard practice to make sure that series are “aligned” to minimize any delay before estimating the cross-spectrum. As with prewhitening, shifting one series introduces a known change in the transfer function, one that is easy to remove after the estimates have been found.

15.4.2 Other Estimation Issues

To find the cross-spectrum, we can form tapered series and apply a DFT; to preserve the independence of estimates with different tapers, we must use the same taper set for X_1 and X_2 . This is true even if the two processes are very different, which would mean that the optimal tapers for suppressing leakage would be different too. When K tapers are used the variance is, as usual, multiplied by K^{-1} .

Estimates of coherence and phase are usually based on the definitions

$$\hat{\gamma}_{12}^2 = \frac{|\hat{S}_{12}|^2}{\hat{S}_1 \hat{S}_2} \quad \text{and} \quad \hat{\theta}_{12} = \arctan \left(\frac{-\mathcal{I}[\hat{S}_{12}]}{\mathcal{R}[\hat{S}_{12}]} \right)$$

As we noted above, the coherence estimator is *not* unbiased, even when the various spectra and cross spectra are. If we were foolish enough to use different sets of tapers on the two series, the coherence can even exceed one.

Uncertainty estimates can be formed based on Gaussian statistics, but the modern way is the jackknife estimator, which makes no such assumptions. One exception is the case when we want to know if the coherence differs significantly from zero. Priestley shows that if we average K independent estimates to find $\hat{\gamma}_{12}$, and assume X_1 and X_2 are Gaussian, then the statistic Γ defined by

$$\Gamma = \frac{2K\hat{\gamma}_{12}}{1 - \hat{\gamma}_{12}}$$

has an $F_{2,4K}$ distribution. This allows a simple test for the hypothesis that γ_{12} exceeds zero (or any other value):

$$\mathcal{P}(|\hat{\gamma}_{12}| \geq z) = (1 - z^2)^{K-1}$$

Often whether or not two series are coherent at some frequency is the most important thing to know.

15.5 An Example: Seismometer Calibration

For an example, we consider the pair of time series shown in Figure 2.4, which were recorded as part of the calibration of a seismometer. The input is (effectively) shaking it with a random signal: though in this case the shaking is done by adding a voltage to the system, and the signal is not really random, since it is generated by circuits in the datalogger. We model this as

$$x_2(t) = g * x_1(t) + x_3(t) \tag{15.11}$$

where $x_2(t)$ is the output voltage, g is the impulse response of the seismometer (the output for a delta-function input), $x_1(t)$ is the input signal, and $x_3(t)$ is noise,

in this case coming from ground motion, which the system cannot be isolated from (Berger *et al.*, 1979). If the transition times were entirely random x_1 would have a white spectrum; because the transitions are allowed only on multiples of five data samples, the actual spectrum is not exactly flat.

If we possessed an infinite noise-free record we could just divide the Fourier transforms of input and output and obtain

$$\hat{\tilde{g}}(f) = \frac{\hat{\tilde{x}}_2}{\hat{\tilde{x}}_1} \quad (15.12)$$

where $\tilde{g}(f)$ is the frequency response of the seismometer. But we want to estimate $\hat{\tilde{g}}$ when x_2 and x_1 are stochastic processes and there is unknown noise x_3 present in the output. Taking the DFT of both time series and using equation (15.12) is no more a good estimate of \tilde{g} than the periodogram is of the power spectra $S_1(f)$ and $S_2(f)$.

Notice that in (15.11) we have the same situation as we did with equation (C.27): the noise is present in only one of the signals. For stationary stochastic processes the estimate is the analog of equation (C.29):

$$\hat{\tilde{g}}(f) = \frac{S_{12}(f)}{S_1(f)} \quad (15.13)$$

that is, the best estimate is the cross spectrum of x_2 with x_1 , divided by the PSD of x_1 . The magnitude $|\hat{\tilde{g}}|$ is then the gain of the system; equation (15.6) gives the estimated phase.

To prove equation (15.13) we must assume that $x_3(t)$ in equation (15.11) is uncorrelated with the input $x_1(t)$. The cross-covariance is then:

$$\begin{aligned} R_{12}(\tau) &= R_{21}(-\tau) = \mathcal{E}[X_2(t)X_1(t-\tau)] = \mathcal{E}[(g * X_1 + X_3)(t)X_1(t-\tau)] \\ &= \mathcal{E}[(g * X_1)(t)X_1(t-\tau)] \\ &= \mathcal{E}\left[\int g(p)X_1(t-p)X_1(t-\tau)\right] dp \\ &= \int g(p)R_1(p-\tau)dp = \int g(p)R_1(\tau-p)dp \end{aligned} \quad (15.14)$$

where in (15.14) we used the definition of R_1 to evaluate $\mathcal{E}[X_1(t-p)X_1(t-s)]$, having moved the expectation under the integral. Now take the Fourier transform of (15.14), which by definition is the cross spectrum between X_2 and X_1 :

$$\begin{aligned} S_{12}(f) &= \int_{-\infty}^{\infty} \int_{-\infty}^{\infty} e^{-2\pi i \tau f} g(p)R_1(\tau-p)dp d\tau \\ &= \int_{-\infty}^{\infty} \left[\int_{-\infty}^{\infty} e^{-2\pi i (\tau-p)f} R_1(\tau-p) \right] e^{-2\pi i p f} g(p) dp d\tau \\ &= S_1(f) \hat{\tilde{g}}(f) \end{aligned} \quad (15.15)$$

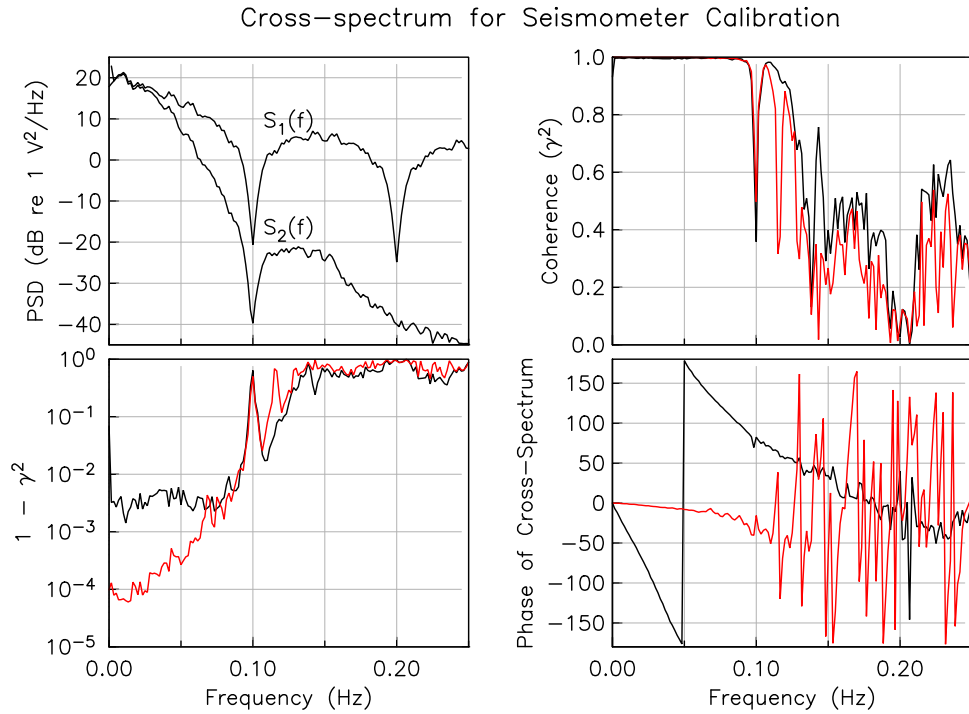


Figure 15.3: Spectral estimates from the seismometer calibration data of Figure 2.4. The upper left panel shows the power spectra of the input and output; the upper right and lower left panels show the coherence in two ways; and the bottom left panel shows the estimated phase. In the three plots derived from the cross-spectrum, black shows the results using the original series, and red the results when the input has been prefiltered.

and this is just (15.13).

This is not of course a proper derivation of an estimator. What it shows is that if all the noise is in one of the stationary processes, the transfer function would be given exactly by the ratio of the cross spectrum to the PSD of the input. It can be shown (see Priestley) that \hat{g} is an unbiased estimator when estimates of S_{12} and S_1 are used rather than the exact functions.

Figure 15.3 shows results from a cross-spectral analysis of the seismometer calibration data of Figure 2.4. The power spectra (upper left) show that the random telegraph spectrum has two “holes” at 0.1 and 0.2 Hz, because of the five-sample restriction. The output spectrum is much lower at high frequencies, so this signal is not aliased. Neither, despite its spectrum, is the input signal: because the signal has only two levels, and because the transitions are synchronized with the sampling, the input can be interpolated as finely as desired without any error.

The other three plots show results derived from the cross-spectrum, in this case the coherence and phase; the black lines show the results of finding the cross-spectrum between the series as recorded. At low frequencies the coherence is very close to one; it falls where the input power is low, and also at higher frequencies as the seismometer response becomes small. The phase plot shows a rapid change of phase with frequency, which suggests, based on the results of Section 15.4.1, that there may be bias in the estimate of the cross-spectrum.

To eliminate this bias, we need to make the two series resemble each other more closely. There are versions of the prediction-error filter that can be used, but a simpler approach also works: we convolve the input with a guess at the impulse response³ and compute the cross-spectrum for between this “imitation” output and the actual output. The red lines show what differences this makes: first of all, we have removed almost all of the phase change with frequency. This means that at lowest frequencies the coherence becomes even closer to one (as shown by the plot of $1 - \gamma^2$ on the lower left), making the phase and gain estimates much more reliable.

Cross-spectral analysis is commonly applied in geomagnetic and magnetotelluric sounding, where such analysis, from time series of different components of the electric and magnetic fields are used to estimate the impedance of the Earth as a function of frequency; from this in turn electrical conductivity structure can be inferred. A complication in that case is that both signals are subject to noise, so that the approach described for calibration, while often used, is not strictly valid; alternatives to avoid this problem sometimes involve a special experimental setup called a remote reference station (Gamble *et al.*, 1979; Egbert and Booker, 1986).

Another important use of cross-spectral analysis is for comparing topography and gravity data to understand the response of the Earth (or a planet) to loading. In this application the transfer function from topography to gravity, called the **isostatic response**, is a function of wavenumber; its shape yields insight into crustal and lithospheric strength. In this case it is plausible to assert that the gravity data are far more prone to error than the topography, and we may estimate the transfer function as we did for the seismometer calibration. Chapter 5 of Watts (2001) gives many details. However, for this analysis we often need to examine data over an area, rather than profiles – and that brings us to our next subject, spectra in more than one dimension.

³In fact, we simply use the instrument response at the start of the record, since before this the input voltage was zero.

CHAPTER 16

MULTIDIMENSIONAL SPECTRA

16.1 Introduction

We now look at spectra of stochastic processes that depend on more than one variable: that is, **multidimensional** processes and spectra. For time series, a single argument is enough; to look at quantities in space, or space and time, we need more dimensions. But a complication is that, very often, the data we actually have are a sample with a lower dimension. For example, the magnetic field exists in three dimensions, but the magnetic profile of Figure 10.7 is a sample of it in one dimension. Similarly, the bathymetry data of Figure 10.9 is a one-dimensional sample of a two-dimensional function. As we saw in Chapter 4, we can apply one-dimensional Fourier theory to multidimensional data sampled along a line; but our results will depend on the full multidimensional spectrum.

In saying that the magnetic and bathymetry data are sampled along a line, we are implicitly treating the Earth as flat, which is an acceptable approximation given the limited extent of the data. But we cannot do this for such cases as the Magsat data in Figure 10.8; so in Section 16.4 of this chapter we discuss, very briefly, analogs to the power spectrum for data defined on a sphere.

16.2 Stationary Processes in the Plane

Suppose we have a stationary process defined by a random function $Y(x_1, x_2)$ in the plane. We can follow the single-variable recipe to define the autocovariance:

$$R(\mathbf{s}) = \mathcal{E}[Y(\mathbf{x})Y(\mathbf{x} + \mathbf{s})] \quad (16.1)$$

where \mathbf{s} and \mathbf{x} are two-dimensional real-valued vectors; \mathbf{s} is the lag, in two dimensions. The two-dimensional power spectral density of Y is then, as you might expect, the two-dimensional Fourier transform (equation 4.1) of $R(\mathbf{s})$:

$$S(\mathbf{k}) = \mathcal{F}[R(\mathbf{s})](\mathbf{k}) = \int_{\mathbb{R}^2} R(\mathbf{s}) e^{-2\pi i \mathbf{k} \cdot \mathbf{s}} d^2 \mathbf{s} \quad (16.2)$$

where the Fourier variable is the wavenumber vector \mathbf{k} ; \mathbb{R}^2 denotes the entire plane.

Now suppose we have measurements along a line, which is a slice through a two-dimensional random field; how do we collapse the two-dimensional spectrum to get the spectrum on the profile? This is done using the **Slice theorem** for spectra and cross spectra. In Section 4.2.2 we saw this theorem for ordinary functions: for a function y with two-dimensional Fourier transform \tilde{y} , the one-dimensional Fourier transform of y along the line $x_2 = 0$ is:

$$\mathcal{F}[y(x_1, 0)](k) = \int_{-\infty}^{\infty} \tilde{y}(k_1, k_2) dk_2$$

that is, to get the one-dimensional Fourier transform in a direction $\check{\mathbf{k}}$,¹ we integrate the two-dimensional Fourier transform of the function in the direction perpendicular to $\check{\mathbf{k}}$.

Exactly the same result holds for power spectra and cross spectra; we prove it for the power spectrum. Assume that we sample Y along the x_1 axis to produce a one-dimensional stationary process Z . If the autocovariance of Y is R_Y , the autocovariance of Z is a slice of this:

$$R_Z(x) = R_Y(\check{\mathbf{x}}_1 x) = R_Y(x_1, 0) \quad (16.3)$$

where $\check{\mathbf{x}}_1$ is the unit vector in the 1 direction. By equation (16.2), S_Y , the PSD of Y , is the two-dimensional Fourier transform of R_Y . Conversely,

$$R_Y(\mathbf{x}) = \mathcal{F}^{-1}[S_Y(\mathbf{k})] = \int_{\mathbb{R}^2} e^{2\pi i \mathbf{x} \cdot \mathbf{k}} S_Y(\mathbf{k}) d^2 \mathbf{k} \quad (16.4)$$

Substituting (16.4) into (16.3) gives

$$\begin{aligned} R_Z(x) &= \int_{\mathbb{R}^2} e^{2\pi i x \check{\mathbf{x}}_1 \cdot \mathbf{k}} S_Y(\mathbf{k}) d^2 \mathbf{k} \\ &= \int_{-\infty}^{\infty} e^{2\pi i k_1 x_1} \int_{-\infty}^{\infty} S_Y(k_1, k_2) dk_2 dk_1 \\ &= \mathcal{F}_1^{-1} \left[\int_{-\infty}^{\infty} S_Y(k_1, k_2) dk_2 \right] \end{aligned}$$

where \mathcal{F}_1 is a reminder that we will be taking a one-dimensional Fourier transform. But since the PSD of Z is the one-dimensional Fourier transform of R_Z , this means that

$$\begin{aligned} S_Z(k) &= \mathcal{F}_1 \left(\mathcal{F}_1^{-1} \left[\int_{-\infty}^{\infty} S_Y(k_1, k_2) dk_2 \right] \right) \\ &= \int_{-\infty}^{\infty} S_Y(k_1, k_2) dk_2 \end{aligned} \quad (16.5)$$

¹We use $\check{\mathbf{k}}$ for the unit vector in the direction of \mathbf{k} ; that is, $\check{\mathbf{k}} = \mathbf{k}/|\mathbf{k}|$, which would usually be denoted $\hat{\mathbf{k}}$; our notation here avoids confusion with our use of $\hat{\cdot}$ for estimated values.

which is the slice theorem for power spectra. The result is the same for cross spectra: simply integrate the two-dimensional cross-spectrum in the wavenumber domain along the perpendicular direction. Looking at the one-dimensional spectra and cross spectra of measurements made through a random field of higher dimension is a very common practice in physical oceanography, where it is taken as obvious that you get a version that simply integrates over the unexplored directions in wavenumber space, but this is often forgotten in most of geophysics.

16.2.1 Isotropic Processes

In more than one dimension, we can impose an additional property on stochastic processes, namely that they be **isotropic**. This property means that the autocovariance depends only on the distance between two points, $|\mathbf{s}|$, independent of the direction from one to the other. We can then write $R(\mathbf{s}) = R(|\mathbf{s}|) \stackrel{\text{def}}{=} R(r)$. So for an isotropic process in two dimensions the autocovariance is circularly symmetric. The PSD is still the Fourier transform of R , $S(\mathbf{k}) = \mathcal{F}[R(\mathbf{x})]$, but, as we saw in Section 4.3, if a function is circularly symmetric its Fourier transform will be also. We can thus write the spectrum as $S(\kappa)$, where $\kappa = |\mathbf{k}|$. R and S can then be defined on the positive part of the real line, and they are related by the Hankel transform, equation (4.6):

$$S(\kappa) = \mathcal{H}[R(r)] = 2\pi \int_0^\infty R(r) J_0(2\pi\kappa r) r dr \quad (16.6)$$

where $J_0(r)$ is the zero-order Bessel function.

What this means is that if a process on a plane is isotropic, it is only necessary to have data on a straight profile to find the full PSD. The stationarity of the random process means that there is no special location in space that the function is radially symmetric around; rather, the autocovariance is always symmetric about zero lag, and along a straight line in any direction the autocovariance is always $R(r)$.

This result allows us to bring in the slice theorem again. Suppose we have observations of an isotropic process along a straight line, which we can, because the process is isotropic, designate the 1-axis. From the data along the line we can find the PSD profile in two ways. One way is to find the one-dimensional Fourier transform of the autocovariance:

$$S(k_1) = \mathcal{F}[R(x_1)] \quad (16.7)$$

which, from the slice theorem, is

$$S(k_1) = \int_{-\infty}^{\infty} S(k_1, k_2) dk_2 = \int_{-\infty}^{\infty} S\left(\sqrt{k_1^2 + k_2^2}\right) dk_2 \quad (16.8)$$

In practice, one may have observations on a profile and hence knowledge of $S(k)$, which one would like to convert into the two-dimensional PSD function $S(\mathbf{k})$ –

or more properly, given the isotropy, $S(|\mathbf{k}|)$. The way to do this is clear: we invert (16.7), then apply (16.6) to find $S(k)$. This combination of a one-dimensional Fourier transform followed by a Hankel transform can be expressed as another transform:

$$S(|\mathbf{k}|) = \mathcal{H}[\mathcal{F}^{-1}[S(k_1)]] = -\frac{1}{\pi} \int_k^\infty \frac{dS(k_1)}{dk_1} \frac{1}{\sqrt{k_1^2 - k^2}} dk_1 \quad (16.9)$$

which is the inverse Abel transform that we encountered in Section 4.3.1. For an isotropic process the inverse Abel transform takes us directly from a profile power spectrum to the two-dimensional power spectrum; equation (16.8) goes the opposite way.

16.3 An Example: Magnetics over the Ocean

We can use two-dimensional transforms to develop some theory for the aeromagnetic signals of Figure 10.7. The three magnetic field components (B_1 , B_2 , and B_3) are the gradients of V , the scalar magnetic potential. Above the sources of this potential, V obeys Laplace's equation, $\nabla^2 V = 0$; this means that if we know it on the plane $x_3 = 0$ (also above the sources) it can be upward continued to any other value of x_3 . This upward continuation is

$$\tilde{V}(\mathbf{k}, x_3) = \tilde{V}(\mathbf{k}, 0) e^{-2\pi i |\mathbf{k}| x_3} \quad (16.10)$$

where \tilde{V} is the Fourier transform of V in a plane of constant x_3 : and the wavenumbers \mathbf{k} are in that plane:

$$\tilde{V}(\mathbf{k}, x_3) = \int_{\mathbb{R}^2} V(\mathbf{x}, x_3) e^{-2\pi i \mathbf{k} \cdot \mathbf{x}} d^2 \mathbf{x}$$

If we take the inverse two-dimensional Fourier transform of (16.10), and use the convolution theorem (backwards), we find

$$V(\mathbf{x}, x_3) = V_0 * g = g * V_0$$

where $V_0 = V(\mathbf{x}, 0)$ and

$$g(\mathbf{x}) = \mathcal{F}^{-1}\left[e^{-2\pi i |\mathbf{k}| x_3}\right] = \frac{x_3}{2\pi(x_3^2 + |\mathbf{x}|^2)^{3/2}} \quad (16.11)$$

But what we observe is the vector $\mathbf{B} = -\nabla V$. From the definition of convolution it follows that

$$B_3 = -\frac{\partial V(\mathbf{x}, x_3)}{\partial x_3} = -\frac{\partial g}{\partial x_3} * V_0 \stackrel{\text{def}}{=} g_3 * V_0 \quad (16.12)$$

where we use g_3 for the derivative of g with respect to x_3 ; there are similar expressions for the other components.

So far we have been considering V and B_3 to be ordinary functions. Now suppose instead that V_0 is a random field, which we model as a stationary stochastic process in the plane $x_3 = 0$. Then equation (16.12) means that the vertical magnetic field is also such a process. Denote the (two-dimensional) PSD of V_0 by $S_V(\mathbf{k})$. Then, by equation (11.22) the two-dimensional PSD of B_3 is

$$S_3 = |\tilde{g}_3|^2 S_V$$

where \tilde{g}_3 is the two-dimensional Fourier transform of g_3 . But by equation (16.11), g is the inverse Fourier transform of the exponential in (16.10), so it follows that

$$\tilde{g}(\mathbf{k}) = e^{-2\pi|\mathbf{k}|x_3}$$

hence

$$\tilde{g}_3 = -\frac{\partial \tilde{g}}{\partial x_3} = 2\pi|\mathbf{k}|e^{-2\pi|\mathbf{k}|x_3} \quad (16.13)$$

We can calculate the spectrum of $B_1 = -\partial V / \partial x_1$ in the same way:

$$B_1 = -\frac{\partial V(\mathbf{x}, x_3)}{\partial x_1} = -\frac{\partial g}{\partial x_1} * V_0 = g_1 * V_0$$

where

$$\tilde{g}_1 = 2\pi i k_1 e^{-2\pi|\mathbf{k}|x_3} \quad (16.14)$$

so that

$$S_1(k) = |\tilde{g}_1|^2 S_V \quad (16.15)$$

and the spectrum of B_2 follows in the same way from

$$\tilde{g}_2 = 2\pi i k_2 e^{-2\pi|\mathbf{k}|x_3} \quad (16.16)$$

These results, combined with equation (15.8), also give us the various cross-spectra; for example, the cross spectrum, between B_1 and B_3 is

$$S_{13}(k) = \tilde{g}_1(\tilde{g}_3)^* S_V \quad (16.17)$$

So what we have is a two-dimensional system in which the three stochastic processes B_1, B_2, B_3 are each given by convolutions of different functions with a single stochastic process V . This means that these three components are closely related. For example, because $|\mathbf{k}|^2 = k_1^2 + k_2^2$, the power spectra are related by

$$S_3(\mathbf{k}) = S_1(\mathbf{k}) + S_2(\mathbf{k}) \quad (16.18)$$

That is, the vertical component of a field \mathbf{B} generated from random sources is always larger on average than either of the other two; but the sum of the spectra of the two horizontal components should equal that of the vertical one.

We now have all the pieces to be able to say something interesting about the magnetic profile in Figure 10.7. To look at the power and cross spectrum of the profile data we simply apply the slice theorem to equations (16.13) through (16.17).

$$S_1(k_1) = \int_{-\infty}^{\infty} |\tilde{g}_1(\mathbf{k})|^2 S_V(\mathbf{k}) dk_2 \quad (16.19)$$

$$S_2(k_1) = \int_{-\infty}^{\infty} |\tilde{g}_2(\mathbf{k})|^2 S_V(\mathbf{k}) dk_2 \quad (16.20)$$

$$S_3(k_1) = \int_{-\infty}^{\infty} |\tilde{g}_3(\mathbf{k})|^2 S_V(\mathbf{k}) dk_2 \quad (16.21)$$

$$S_{13}(k_1) = \int_{-\infty}^{\infty} \tilde{g}_1(\mathbf{k}) \tilde{g}_3(\mathbf{k})^* S_V(\mathbf{k}) dk_2 \quad (16.22)$$

Observe that we have the same relationship between the profile PSD's of the components as we did in the two-dimensional system (equation 16.18):

$$S_3(k_1) = S_1(k_1) + S_2(k_1) \quad (16.23)$$

This relationship can be called the **Power Sum Rule**. Another thing to notice (equations 16.13 through 16.16) is that while \tilde{g}_3 is real, \tilde{g}_1 and \tilde{g}_2 are purely imaginary. Thus whatever the spectrum is for S_V , equation (16.22) shows that the phase spectrum between either B_1 and B_3 , or B_2 and B_3 , must be constant for all k_1 , and equal to $\pi/2$: a very strong prediction.

We can compare this prediction with the estimated power spectra and cross spectra for the data of Figure 10.7, as was done by Parker and O'Brien (1997). Figure 11.3 shows the PSD's of all three components, with the inset showing the spectra for the lowest 10% of the wavenumbers, since at higher wavenumbers (shorter wavelengths) the spectrum is just instrument noise. (Section 11.6.2). To a first approximation, all the spectra fall off exponentially at the lowest wavenumbers, and all change slope dramatically at about $k_1 = 0.025 \text{ km}^{-1}$. If the spectrum of the sources, S_V , is fairly flat, equations (16.19) through (16.21) suggest that the spectrum should decay approximately as an exponential, proportional to $e^{-4\pi k_1 x_3}$. The slope of the power spectra in Figure 11.3, at the lowest wavenumbers at least, is about right: with a water depth of four km and aircraft altitude of seven km, x_3 is eleven km. It would be plausible for the spectrum of the field to fall off even more steeply than this because S_V itself can be expected to have the red spectrum typical of many geophysical power spectra. But clearly something happens when $k_1 > 0.025 \text{ km}^{-1}$.

Next look at the black line, which is the value of $S_1 + S_2$. According to the power sum rule (equation 16.23) this should coincide with the green S_3 line. Again things go as we might expect for $k_1 < 0.025 \text{ km}^{-1}$, but not for larger wavenumbers.

Figure 16.1: Coherence and phase spectra between the components B_1 and B_3 of the magnetic field for the magnetic anomaly data shown in Figure 10.7,

For further clues to solving this mystery we look at one of the cross spectra: S_{13} , the one between B_1 and B_3 . Figure 16.1 shows the phase and coherence spectra derived from S_{13} : for the longer wavelengths the phase is about 90° although it wanders off very close to $k_1 = 0$. The theory we presented predicts the 90° phase for potential fields with sources below the plane. Like the PSD's this shows that the magnetic signals are coming from sources in the crust only for $k < 0.025 \text{ km}^{-1}$: wavelengths greater than 40 km.

As Parker and O'Brien (1997) explain, the spectrum at higher wavenumbers is from error in the orientation of the magnetometers. Figure 10.7 shows that while the anomalies are about 100 nT; the main geomagnetic field is over 30,000 nT, roughly horizontal, and points North. Even small errors in the vertical orientation of the gyro-stabilized platform will cause some of the horizontal field to appear on the B_3 sensor; the other components are also corrupted, though less so. This is the source of the excess level of S_3 above S_1 and S_2 in Figure 11.3. Because the main field points upward in the southern hemisphere, the rocking platform causes a signal that is 180° out of phase between B_3 and B_1 , which is just what we see in Figure 16.1; this mechanism also predicts the observed high coherence.

What these spectra show is that 90% of the bandwidth of the record from this Project Magnet data is noise! Only signals with wavelengths longer than 40 km can be interpreted as geology. To avoid overinterpreting these data we ought to first lowpass them – though we might actually want to use a bandpass filter, since the very longest-wavelength signals are also not from the crust: over the two hours spent collecting these data time variations in the magnetic field can cause apparent long-wavelength spatial signals, which may not have been properly corrected. Figure 11.3 shows that the B_2 component has more power than the B_3 near $k_1 = 0$, which the Power Sum rule again says can never happen; the improper phase spectrum there also suggests a problem. These time changes come from sources above the measurements, so the theory we have developed does not apply to them.

16.4 Stationary Processes on a Sphere

We can also generalize the power spectrum to processes defined on the sphere. It is only an approximation to say that the surface of the Earth is a plane; we can ask what happens if the region is so large that we must account for curvature, or even larger still, so that the domain of the random process is the whole surface of the Earth.

Spherical power spectra are used to describe the geomagnetic and gravitational potential fields; in seismology and geodynamics to characterize velocity and temperature structure at a particular radius within the Earth; and, most recently, to characterize the cosmic microwave background, since the spectrum of this depends on the very early history of the universe. One of the most successful uses of the stochastic model on the sphere has been in studying the geomagnetic field over geological time: if we exclude the dipole and a few other harmonics, the remaining field appears to be spatially stationary and to have a “white” spectrum (Constable and Parker, 1988).

The following is one way of approaching the problem. Stationarity means that the statistics of a stationary random process on the sphere cannot depend on the position $\check{\mathbf{r}}$.² We will assume that the process $X(\check{\mathbf{r}})$ has zero mean; then $\mathcal{E}[X] = 0$ is obviously position independent. The second-order statistics are once again captured by the autocovariance:

$$R(c) = \mathcal{C}[X(\check{\mathbf{r}}), X(\check{\mathbf{s}})] = \mathcal{E}[X(\check{\mathbf{r}})X(\check{\mathbf{s}})] \quad (16.24)$$

where the argument is

$$c = \cos(\Delta_c) = \check{\mathbf{r}} \cdot \check{\mathbf{s}}$$

with Δ_c is the angle at the center of the sphere between the two unit vectors $\check{\mathbf{r}}$ and $\check{\mathbf{s}}$. On the sphere, being independent of location means that every unit vector is the same as every other, so that any reorientation of the sphere must leave $R(c)$ unaltered.

If this is the autocovariance, what is the corresponding PSD? How do we decompose a function on a sphere into different wavelength components? You will not be surprised to hear that the answer uses spherical harmonics – and, as usual with spherical harmonics, everyone feels free to define different normalizations, so factors of π , l , $l + 1$ and $2l + 1$ appear in various places in the papers of various authors.

The analog of the result that the autocovariance is the Fourier transform of the PSD is this expansion of $R(c)$:

$$R(c) = \sum_{l=0}^{\infty} S_l P_l(c) \quad (16.25)$$

Here S_l is the variance of X in the part of the function with spherical harmonic degree l ; P_l is the Legendre polynomail of degree l . Since $P_l(1) = 1$ we see that

$$R(1) = \mathcal{V}[X] = \sum_{l=0}^{\infty} S_l$$

²Again, we use the notation $\check{\mathbf{r}}$ for a unit vector along the direction of a vector \mathbf{r} .

which is the equivalent the variance of a random process on a line or in the plane being the area under the PSD. The sequence S_l is our candidate for the **Spherical Power Spectrum**.

Since Legendre polynomials P_l are orthogonal the inverse of (16.25) is

$$\begin{aligned} S_l &= (l + \frac{1}{2}) \int_0^\pi R(\cos\theta) P_l(\cos\theta) \sin\theta d\theta \\ &= \sqrt{(2l+1)\pi} \int_{S^2(1)} R(c) Y_l^0(\check{\mathbf{s}})^* d^2\check{\mathbf{s}} \end{aligned} \quad (16.26)$$

where $S^2(1)$ denotes the surface of the unit sphere, and the spherical harmonics are normalized so that

$$\int_{S^2(1)} |Y_l^m|^2 d^2\check{\mathbf{s}} \stackrel{\text{def}}{=} \|Y_l^m\|^2 = 1$$

Equation (16.26) is the analog to the fact that the PSD is the Fourier transform of the autocovariance.

An alternative definition proceeds as follows: imagine that the stationary process is written out as a spherical harmonic expansion on the unit sphere:

$$X(\check{\mathbf{r}}) = \sum_{l=0}^{\infty} \sum_{m=-l}^l C_{lm} Y_l^m(\check{\mathbf{r}}) \quad (16.27)$$

where C_{lm} are random complex coefficients. Plugging this into (16.24), it turns out that the only way to get $R(c)$ to be independent of the vectors $\check{\mathbf{r}}$ and $\check{\mathbf{s}}$ in (16.24) is to have

$$\mathcal{E}[C_{lm}, C_{nk}^*] = 0 \quad \text{unless} \quad l = n \quad \text{and} \quad m = k \quad (16.28)$$

That is, the coefficients in the expansion must be uncorrelated random variables. Furthermore, we find that we can define a variance

$$\mathcal{E}[|C_{lm}|^2] = \sigma_l^2 \quad (16.29)$$

independent of the order m . Then, using the fact that X is real valued, and equations (16.24), (16.27) and (16.28), we find

$$\begin{aligned} R(\check{\mathbf{r}} \cdot \check{\mathbf{s}}) &= \mathcal{E}[X(\check{\mathbf{r}}) X(\check{\mathbf{s}})] = \mathcal{E}[X(\check{\mathbf{r}}) X(\check{\mathbf{s}})^*] \\ &= \mathcal{E}\left[\sum_l \sum_m C_{lm} Y_l^m(\check{\mathbf{r}}) \sum_n \sum_k C_{nk}^* Y_n^k(\check{\mathbf{s}})^*\right] \\ &= \sum_{l=0}^{\infty} \sum_{m=-l}^l \mathcal{E}[|C_{lm}|^2] Y_l^m(\check{\mathbf{r}}) Y_l^m(\check{\mathbf{s}})^* \end{aligned}$$

Now we use the spherical harmonic addition formula together with (16.29) to get

$$R(\check{\mathbf{r}} \cdot \check{\mathbf{s}}) = \sum_{l=0}^{\infty} \frac{(2l+1)\sigma_l^2}{4\pi} P_l(\check{\mathbf{r}} \cdot \check{\mathbf{s}})$$

Compare this to (16.25) and we see that

$$\sigma_l^2 = \frac{4\pi S_l}{2l+1}$$

The seemingly unnecessary factor of 4π here could be eliminated if we were willing to use spherical harmonics normalized as $\|Y_l^m\|^2 = 4\pi$.

The surprising fact is that on a sphere there are only isotropic stationary processes, analogous to those described in Section 16.2.1; there cannot be processes with the more general behavior described by equation (16.1). This is because on a sphere parallel lines (defined as pairs of lines perpendicular to a third line) eventually meet, so anisotropy has to produce nonstationarity. For example, suppose we decide to have a process which, at the North Pole, has a spectrum that is small along the meridian with 0° longitude, and large along the meridian with 90° longitude. Then, go along the 0° longitude meridian until we reach the Equator: because the large spectrum is perpendicular to the small one, this would mean a large spectrum along the Equator. But, bad luck, this means that on the Equator at 90° longitude we will have a large spectrum in two perpendicular directions – which violates stationarity. We can do the same over any other pairs of lines, with the result that on the sphere a stationary process must be isotropic.

APPENDIX A

NOTATION AND SYMBOLS

We know that intellectual food is sometimes more easily digested, if not taken in the most condensed form. It will be asked, To what extent can specialized notations be adopted with profit? To this question we reply, *only experience can tell.*

FLORIAN CAJORI *A History of Mathematical Notations*, vol 2, p. 77
(1928).

It is difficult to devise a set of symbols for any subject that spans several disciplines; different communities of researchers inevitably develop different conventions, and it is impossible to match all of them.

We have tried to be consistent in which types of symbols we use for what, and we have also tried to keep the notation uncluttered. To reduce clutter we do not specify particular parameters unless they are needed, in accordance with the principle that the utility of a mathematical notation is proportional to the amount of information it *hides*. Some treatments of multitaper methods (Thomson, 1982; Percival and Walden, 1993) try to be as precise as possible by placing many subscripts and superscripts on variables and functions; but these treatments are generally agreed to be hard to read. We believe that one reason for this is that the novice reader has to remember what all these labels mean. Excessive labeling may also come from trying to match the style of computer languages, in which variable labels must be unambiguous – but of course the computer has a flawless memory.

Although people have less perfect memories, they can infer meaning from context; so when we write (for example) $\hat{S}(f)$ for the estimated power spectral density, we are assuming that you will realize that when we are discussing the periodogram \hat{S} refers to that estimate, but in a section on prolate multitaper estimation \hat{S} refers instead to this other estimate. We also sometimes use the argument of a function to distinguish functions with the same symbol (see below), and also to show what dimension the argument of the function is in.

Taking the letter b to represent a variable or function, we would write:

b	algebraic variable
b^*	complex conjugate of b
$b(t)$	algebraic-variable function
\dot{b}	derivative of b , usually against time
b'	derivative of b
$\tilde{b}(f)$	Fourier transform of function
$\tilde{b}(s)$	Laplace transform of function
$\{b_n\}$	sequence of algebraic variables
$\tilde{b}(\zeta)$	Fourier transform of sequence
$\tilde{b}(z)$	z-transform of sequence
B	random variable or function
$\mathcal{B}[\cdot]$	an operator on a function
\hat{b}	estimate of a variable, function, or sequence

We almost always restrict uppercase to random variables and random functions; but we use R and S for the autocovariance and power spectrum respectively, and N (or M or similar letters) for total numbers of terms in a finite sequence. R and S also violate our rule for denoting Fourier transforms, according to which we should write the power spectrum as \tilde{R} – but we think it deserves its own symbol.

Symbol	Meaning	Page
\mathbf{a}^M	Prediction weights for order- K filter	203
\mathcal{A}	Abel transform	58
AR	Autoregressive	96
ARMA	Autoregressive moving average	96
\mathcal{C}	Covariance	139
\mathbf{C}^M	Toeplitz matrix of covariances in Yule-Walker equations	203
D_N	Dirichelet kernel	65
DFT	Discrete (-time) Fourier Transform	61
\mathcal{E}	Expectation operator	242
E	Estimation procedure	248
f_δ	frequency width of bandpass	153
\mathcal{F}	Fourier transform	32
f_a	analog frequency in binlinear mapping	122
f	frequency	27
f_N	Nyquist frequency	87
f_0	center frequency of bandpass	153
F_N	Fejer kernel	67
f_b	bandwidth for multitaper estimate	188
FIR	Finite Impulse Response	96
FFT	Fast Fourier Transform	78
g^p	projection of function g	57
\mathcal{H}	Hankel transform	58
IIR	Infinite Impulse Response	96
J	jump function	35
\mathbf{k}	unit vector, wavenumber	223

k	wavenumber	53
\mathbf{k}	vector wavenumber	222
MA	Moving average	96
\mathcal{N}	Concentration of function	188
N	number of observations	170
\mathcal{P}	Probability	218
P^M	Mean-square prediction error for order- M filter	203
p	time-bandwidth product	189
pdf	probability density function	241
PSD	Power Spectral Density	155
\Re	Real line	54
\mathbf{R}^M	Vector covariances in Yule-Walker equations	203
\mathcal{S}	Section operator	??
$S(f)$	power spectral density	155
$S_{ij}(f)$	Auto- or cross-spectral density	214
s	Laplace-transform variable	112
\mathbf{v}	reference relative position	28
\mathcal{V}	Variance operator	243
\tilde{w}^k	convolution kernel for power spectrum	182
\tilde{w}_n^k	n -th convolution kernel for power spectrum	197
\mathbf{X}	vector of random variables	253
\mathbf{x}	vector position	222
$\check{\mathbf{x}}$	unit vector, position	223
\mathcal{Z}	Z transform	116
β	generic estimator bias	γ^2 squared coherence 213
Δ	sample interval	83
ζ	dimensionless frequency	26
ζ_d	digital frequency in bilinear mapping	122
θ_L	location parameter for a pdf	242
θ_S	shape parameter for a pdf	242
θ_W	width parameter for a pdf	242
θ	parameter to be estimated	248
θ_t	true value of a parameter	248
$\hat{\Theta}$	statistic for an estimated parameter $\hat{\theta}$	249
Π	boxcar function	33
ρ	correlation coefficient	254
σ^2	variance (second moment)	243
$\hat{\sigma}_\theta$	square root of variance of a statistic	249
$\stackrel{\text{def}}{=}$	is defined to be	13
.	vector scalar product	13
III	shah (sampling) function	85
\mathcal{I}	slope function	35
sinc	sinc function	33

APPENDIX B

COMPLEX VARIABLES AND COMPLEX SINUSOIDS

We have shown the symbol $\sqrt{-a}$ to be void of meaning, or rather self-contradictory and absurd.

AUGUSTUS DE MORGAN, *On the Study and Difficulties of Mathematics*
(1831).

B.1 Complex Variables

One potential stumbling block to learning Fourier theory comes in understanding why, given that data are real-valued, we use complex variables, and particularly complex exponentials. The answer is that doing this usually makes our derivations and results simpler and briefer.

Usually, the first encounter with complex numbers and complex variables is when finding solutions to algebraic equations, but that aspect of complex variables is not important for Fourier procedures. Instead, we proceed by defining a complex variable as the sum of one real variable and another real variable multiplied by a constant which we denote by i . This constant obeys the usual rules of algebra and has the property that $i^2 = -1$. So we write a complex variable c as $a + bi$, where a is called the **real part**, and b the **imaginary part**. It is very helpful to represent such a variable by a point in the **complex plane**, in which the two orthogonal coordinates are the real and imaginary parts; this graphical representation is called the **Argand diagram**.

Such a geometrical representation suggests another set of parameters for a complex variable. If we draw a line from the origin $0 + 0i$ to $c = a + bi$, we can describe the variable by the length of the line and the angle of the line to the real axis. The length is called the **magnitude** of the complex variable; this is symbolized by $|c| = |a + bi| = \sqrt{a^2 + b^2}$, and is always positive. The angle is called the **argument** of the complex variable; this is symbolized by $\text{Arg}(c) = \text{Arg}(a + bi)$ and, like any angle, falls into the range $[0, 2\pi]$ or if we prefer $[-\pi, \pi]$. Trigonometry shows that if $\theta = \text{Arg}(c)$ $a + bi = |c|[\cos(\theta) + i \sin(\theta)]$. There are variety of ways to show that the expression in brackets is in fact equal to a complex power of e ,

namely $e^{i\theta}$; given this equality we can write $c = |c|e^{i\theta}$, giving us the relationship needed to get from magnitude and argument to the complex variable.

If a complex variable is $c = a + bi$ and another is $d = a - bi$, then c and d are called **complex conjugates**; the complex conjugate of a complex variable c is usually symbolized by c^* . Then $cc^* = a^2 + b^2 = |c|^2$.

B.2 Sinusoids

Now consider, in keeping with our focus on Fourier analysis, a sinusoidal function $x(t)$, with frequency f . There are seven different ways to write this function, each using a different set of parameters:

$$\begin{aligned} x(t) &= a_1 \cos(2\pi ft - \phi_1) \\ x(t) &= a_2 \cos(2\pi ft + \phi_2) \\ x(t) &= a_3 \sin(2\pi ft - \phi_3) \\ x(t) &= a_4 \sin(2\pi ft + \phi_4) \\ x(t) &= a_5 \cos(2\pi ft) - a_6 \sin(2\pi ft) \\ x(t) &= a_7 \cos(2\pi ft) + a_8 \sin(2\pi ft) \\ x(t) &= \Re[a_9 e^{i2\pi ft}] \end{aligned} \tag{B.1}$$

where a_1, \dots, a_8 , and ϕ_1, \dots, ϕ_4 are all real; a_9 is complex, and so we take the real part (\Re) of the expression to get our function $x(t)$. Except for a_9 , the a 's are all **amplitudes**, and the ϕ 's are different variables representing the **phase**.

The amplitude and phase are physically appealing: one tells us how big the function is, and the other when it will be zero, or at a maximum or minimum. The list shows two potential sources of confusion: some writers add the phase, others subtract it, and not everyone uses cos rather than sin; if you want to use amplitude and phase, be sure to specify your choices. But using amplitude and phase makes algebra with sinusoids very difficult; if we have $x(t) = a_x \sin(2\pi ft + \phi_x)$ and $y(t) = a_y \sin(2\pi ft + \phi_y)$, the amplitude and phase of the sum $x(t) + y(t)$ will not have any simple relationship with the original parameters a_x, ϕ_y, a_y , and ϕ_y . Using the sine and cosine parameterization avoids this; if we write $x(t)$ as $a_{x1} \cos(2\pi ft) + a_{x2} \sin(2\pi ft)$, with a_{y1} and a_{y2} for the same form of $y(t)$, we can simply add the a_1 's and a_2 's to get the parameters for $x(t) + y(t)$.

The complex form is easier to use if we want to describe how a sinusoid is modified by a linear system; because such a system can change both the amplitude and the phase, we need a complex frequency response, $\tilde{g}(f)$, to describe what it does. Multiplying \tilde{g} by a_9 and taking the real part gives the correct changes in the amplitude and phase of the sinusoid. We could of course take the real and imaginary parts of \tilde{g} and combine them with a_5 and a_6 , but this is cumbersome. In this case it is in fact easy to work with amplitude and phase: the new amplitude is $|\tilde{g}|a_1$ and the new phase is $\phi_1 + \text{Arg}[\tilde{g}]$. But only the complex form is easy both for this and for summing sinusoids.

Note that we cannot use the complex form if we multiply two sinusoids. If we have two complex quantities a_x and a_y , $\Re[a_x a_y] \neq \Re[a_x] \Re[a_y]$, and so if we have $x(t) = \Re[a_x e^{2\pi f t}]$ and $y(t) = \Re[a_y e^{2\pi f t}]$, with both a_x and the product $x(t)y(t)$ will not be $\Re[a_x a_y e^{4\pi f t}]$. (An easy example is to set the a 's to be one; $\Re[e^{4\pi f t}] \neq \cos^2(2\pi f t)$.)

Of course we can convert between the different forms given in equation (B.1). If

$$\begin{aligned} x(t) &= \Re[a_9 e^{2\pi i f t}] = \frac{1}{2}[a_9 e^{2\pi i f t} + a_9^* e^{-2\pi i f t}] \\ &= \Re[a_9] \cos 2\pi f t - \Im[a_9] \sin 2\pi f t = a_1 \cos(2\pi f t - \phi_1) \end{aligned}$$

so that we can write the complex amplitude a_9 as $a_1(\cos \phi_1 - i \sin \phi_1) = a_1 e^{i\phi_1}$, a complex variable which itself can be written in terms of its magnitude $|a_9| = a_1$, and argument $\text{Arg}[a_9] = \phi_1$ – that is, just the amplitude and phase.

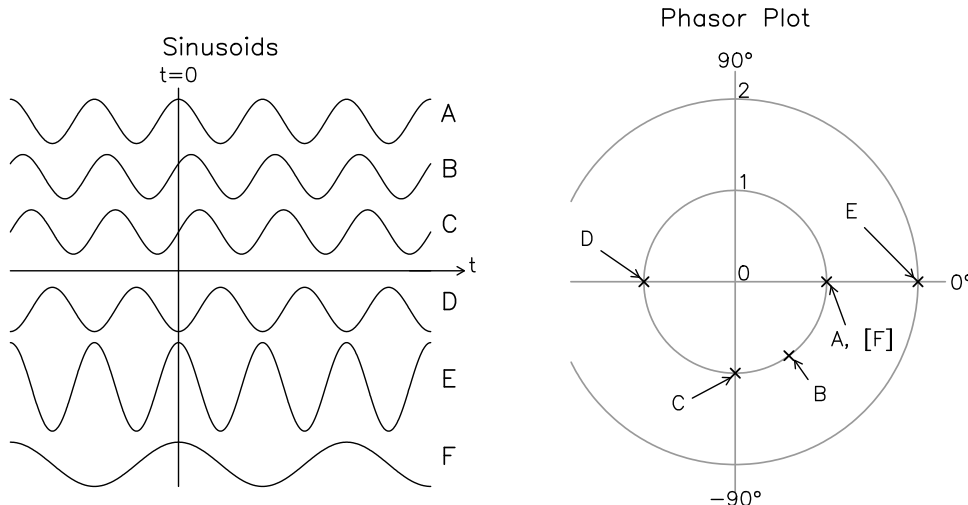


Figure B.1: Some sinusoids and how they are shown on phasor plots. **A** is a unit sinusoid with 0° phase shift. **B** is a unit sinusoid with -30° phase shift (a delay); **C** is a unit sinusoid with -90° phase shift (we say that it is **in quadrature** with **A**); **D** is a unit sinusoid with $\pm 180^\circ$ phase shift; and **E** is a sinusoid with amplitude 2 and a 0° phase shift. **F** is another unit sinusoid with 0° phase shift, but a different frequency; in the phasor diagram, it plots in the same location as **A** though usually a single phasor diagram is taken to refer to sinusoids of the same frequency.

As with a complex variable, we can represent a sinusoid as a point on the complex plane. When representing sinusoids the resulting picture is usually called a **phasor diagram** or vibration diagram. We show some examples of sinusoids, and their phasor-diagram representations, in Figure B.1.

B.3 Conventions

Some of the expressions in equation (B.1) may look like very minor variations on a theme. And so they are – but they will not seem minor when, having chosen one, you have to worry about whether the numbers you are using came from somebody who chose a different one.

Of course the periodicity of sin and cos mean that cases (2) and (4) are just (1) and (3) with a time shift; to decide which is being used, you have to decide if $t = 0$ is the time of a maximum, or a zero-crossing. General usage tends to favor the former, so the appropriate function is a cosine. More problematic is the sign of the phase, which distinguishes ϕ_2 from ϕ_1 and a_6 from a_8 . This comes down to which sign of ϕ represents a lag (or lead). Consider our sample sinusoid, $a_2 \cos(2\pi f t + \phi_2)$. If $\phi_2 = 0$, a maximum will occur at $t = 0$. If ϕ_2 is slightly greater than 0, this maximum will be at $t < 0$, and the waveform will be advanced (we reach the maximum sooner in time) relative to $\phi_2 = 0$; similarly for $\phi_2 < 0$, we reach the maximum later (a delay). Then $\phi_2 < 0$ is a **phase lag**, and $\phi_2 > 0$ a **phase lead**; this convention corresponds to our definition of the Fourier transform (equation 3.4).

This sign convention is not universal; while it is conventional in electrical engineering (and hence in signal processing), much of the older geophysical literature (for example, in tidal studies) takes phase lags to be positive, which amounts to using ϕ_1 .

B.4 Complex Representation of Two-Dimensional Vectors

So far we have treated complex values as a convenience. But if we have a varying two-dimensional vector quantity, for example horizontal displacement or velocity, complex numbers become the appropriate representation. We can map, for example, North displacement x_N and East displacement x_E , into a complex quantity $x = x_E + i x_N$; unfortunately there isn't something like this for vectors in three dimensions. There is then no conceptual challenge in using complex exponentials: a sinusoidal variation is just written as

$$x(t) = a e^{i 2\pi f t} \quad (\text{B.2})$$

without taking the real part:

With $x(t)$ complex, the transform has no symmetries (Table 3.1), and frequencies can be positive or negative. This is meaningful: the sign of the frequency f tells us whether the vector-valued data rotates clockwise (deasil) or anticlockwise (widdershins) about the origin. For systems in which gyroscopic forces are impor-

tant, the sense of rotation can be physically important, as we illustrate in Section 8.2.

APPENDIX C

PROBABILITY AND STATISTICS

Chance itself pours in at every avenue of sense; it is of all things the most obtrusive.

CHARLES SANDERS PIERCE, 1893

C.1 Introduction

This Appendix presents some background information on aspects of probability and statistics that are used in the main text, as a reference and reminder. If these fields are new to you, you should first read an introductory textbook; Appendix I lists some of the many available.¹

C.2 Probability

We start with probability, and how applicable it is to geophysical problems. Probability can be thought of in (at least) three ways:

1. The relative frequency of occurrence of something in a repeated series of experiments. This idea is a good fit for the kind of gambling problems in which probability was first introduced. If we throw a fair die many times, we expect that each number will appear equally often. This view of probability also makes sense for repeated measurements of something unchanging, for example, repeated GPS measurements of the distance between two points on a stable plate. In such applications the changing part is often called the “error” and the unchanging part the “true value”.
2. The relative frequency of something in a large population. This arose from the problems for which much of statistics was developed, namely the distributions of different quantities in some group of people. A geophysical example of such a population would be the magnitudes of all earthquakes recorded in a given region and timespan.

¹Some of the terminology of probability and (especially) statistics makes them more difficult to learn. When we use alternate terminology, we provide the usual terms in a footnote like this one.

3. Our judgement of how likely it is that something is true: say, that a quantity falls into a certain range of values. While we cannot give a precise number for our belief that something is true, we can certainly say that we are more certain of the truth of A than the truth of B; and also, our certainty runs over a finite range, from complete disbelief to “not a shadow of doubt”.

The first two interpretations are called the “frequentist” interpretation of probability; the third is called the “subjective” or (for historical reasons) the Bayesian interpretation.

In geophysics all of these interpretations can seem unsatisfactory. Consider the distribution of density in the Earth. There is only one Earth, so the idea of a “population” makes no sense; and it was created once, so the idea of repeated experiments doesn’t seem right either. The subjective interpretation avoids these problems, but does suffer from our inability to assign numerical values to levels of certainty; though Bayesian methods of statistics address that problem.

We believe that it is pointless to ask what probability “means”; rather, we should regard it as we do other parts of mathematics: a logical development from a set of axioms. We can use this mathematics to model various phenomena that we study, including games of chance, occurrences in a population, fluctuations in repeated measurements, and degrees of belief. But the value of using probability as a model does not imply that the system modeled is somehow the foundation of that theory. We can certainly apply the mathematics of probability to model properties of unique things; whether or not we are right to do so is an empirical question, one partly answered by how much the use of probability clarifies or confuses our understanding of what we study.²

C.3 Single Random Variables

Probability models of phenomena often use **random variables**. The usual variables of algebra have a definite, if unknown, value, which could be an integer, a real number, a complex number, or a vector. A random variable has no definite value; instead, it is described through the probability that it will take on some value or range of values. This probability is given by its **probability density function** or **pdf**; the arguments of this function, and the function itself, are algebraic variables. The pdf $\phi(x)$ is related to probability through

$$\mathcal{P}[a \leq X \leq b] = \int_a^b \phi(u) du \quad (\text{C.1})$$

²See Kass (2011) for a similar view. Attempts to answer the question “What is probability?” continue; see, for example, the (very good) book by Clayton (2021). But nobody asks this question about complex numbers.

which is to say that the probability of the random variable X being between a and b is the integral of the pdf ϕ between these limits. Note that we use an uppercase letter for the random variable X , and lowercase letters for the other variables, which are all algebraic. A shorthand for equation (C.1) is $X \sim \phi(x)$, which stands for “ X is distributed as $\phi(x)$ ”.

For example, consider the random variable that is the value produced by throwing a single cubical die: the numbers one through six are equally likely. The pdf for this is six delta functions at these integer values, each scaled to one-sixth, so that integrating from zero to seven gives a total probability of one, since it is certain that the values will be one of the six integers.³ All pdf's integrate to one over the possible range of the variables, and have to be zero or positive within that range.

We can write pdf's, in general, in the form

$$\theta_W \phi\left(\theta_S, \frac{x - \theta_L}{\theta_W}\right) \stackrel{\text{def}}{=} \phi(\theta_S, u) \quad (\text{C.2})$$

where the θ 's are parameters of the pdf: knowing these, plus the actual functional form of ϕ , tells us everything there is to know about X . The parameters θ_L and θ_W change the location⁴ and width of the pdf; θ_S , only used in some pdf's, is a shape parameter that can be varied to create a whole family of pdf's. Figure C.1 shows some pdf's, one of which is shown for two shape parameters. The θ_W appears in front of the $\phi(x)$ expression to maintain the integral at one. Equation (C.2) also introduces the variable $u = (x - \theta_L)/\theta_W$: a nondimensional quantity that makes the expression for pdf's less complicated.

One way to obtain θ_L and θ_W is to take the **moments** of the pdf.⁵ The first moment of the pdf $\phi(x)$ is

$$\int_{-\infty}^{\infty} u \phi(u) du \stackrel{\text{def}}{=} \mathcal{E}[X] \stackrel{\text{def}}{=} \mu \quad (\text{C.3})$$

where we have defined the **expectation operator** \mathcal{E} , which acts on the random variable X to return the algebraic variable μ , which is called the **mean value** of X . For many, though not all, pdf's, μ is a good descriptor of where most of the probability is found, and so is an appropriate value for θ_L .

For the width of the pdf, we can take the second moment of $\phi(x - \mu)$:

$$\int_{-\infty}^{\infty} x^2 \phi(x - \mu) dx = \int_{-\infty}^{\infty} (y + \mu)^2 \phi(y) dy \stackrel{\text{def}}{=} \mathcal{V}[X] \stackrel{\text{def}}{=} \sigma^2 \quad (\text{C.4})$$

where we have shifted the pdf so that its mean is zero; if we do not, the second moment is the width about zero, which is largely determined by the mean. Then

³A random variable whose pdf is a single delta function is equivalent to an algebraic variable.

⁴Some pdf's, for example the exponential, do not have a location parameter.

⁵Moment, like density, is a term used by analogy with mechanics.

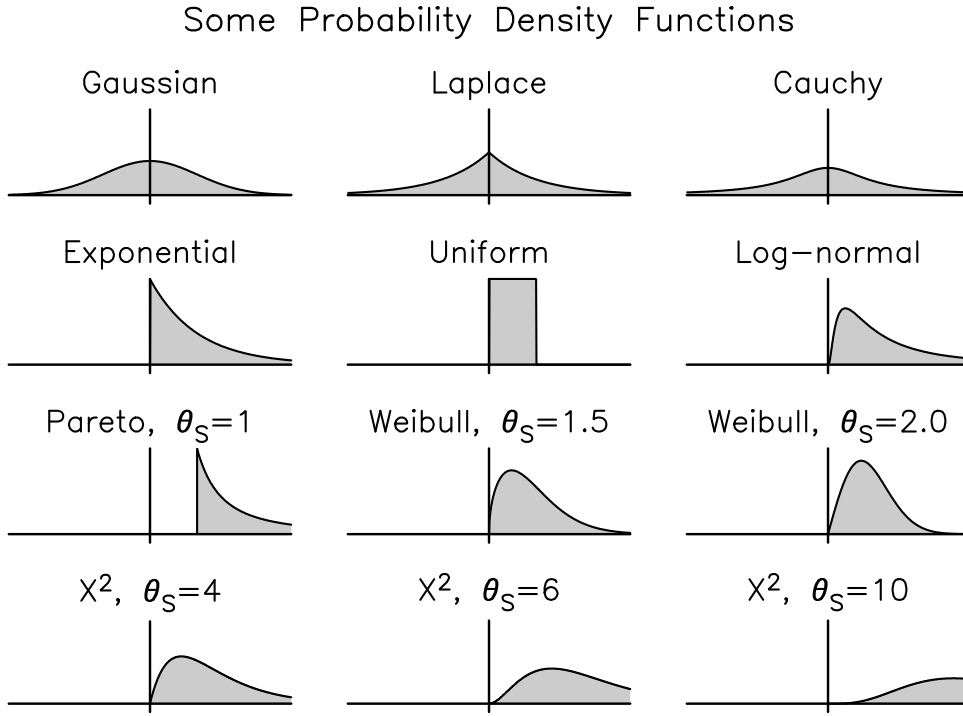


Figure C.1: Some commonly-used probability density functions. The top row shows pdf's that extend over the whole real line; the next three rows show pdf's for random variables that must be nonnegative. The Uniform pdf is what random number generators usually produce. The Weibull pdf is a relatively flexible form; depending on the shape factor θ_S it can be peaked at the origin or away from it. In the top three rows the x limits are ± 3 and the y limits from 0 to 1; for the bottom row, showing the χ^2 pdf's, the x limits are ± 9 and the y limits from 0 to 0.33.

σ^2 is the **variance**, which approximates the square of the width for many pdf's; σ , is called the **standard deviation**. \mathcal{V} is the **variance operator**. The particular nondimensional variable given by

$$u = (x - \mu)/\sigma \quad (\text{C.5})$$

is called a **standardized variable**.

We can continue by defining higher-order moments of pdf's; the n -th moment is

$$\int_{-\infty}^{\infty} x^n \phi(x - \mu) dx = \int_{-\infty}^{\infty} (y - \mu)^n \phi(y) dy$$

but often these are much less important than μ and σ ; for example, these two parameters completely determine the Gaussian, or normal, distribution, which

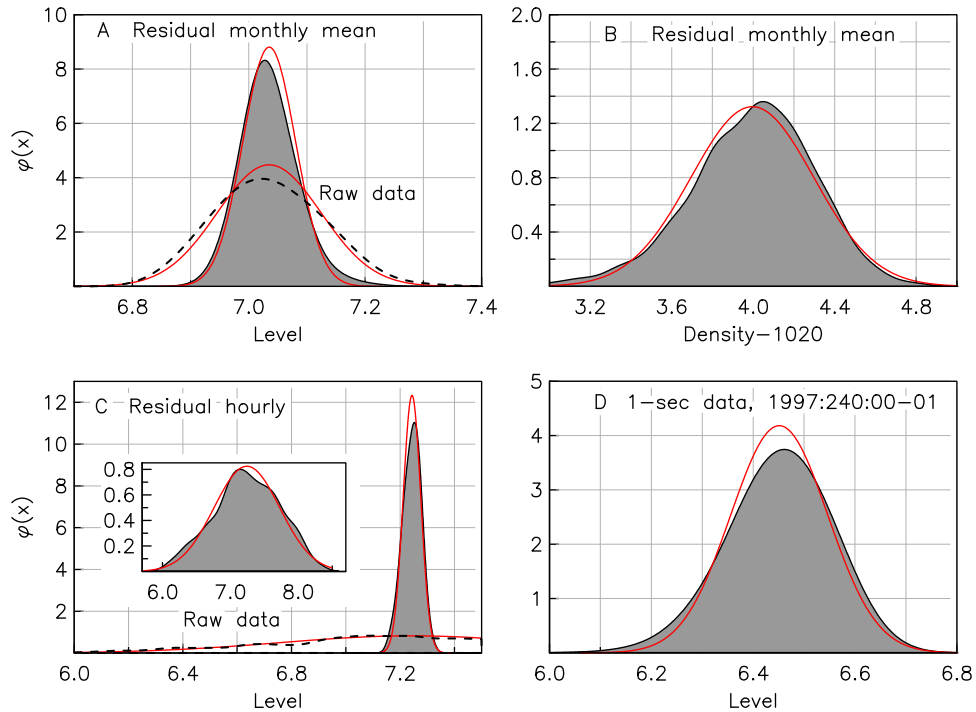


Figure C.2: Probability density functions for the residual data shown in Figures 1.1 (A), 1.2 (B), 1.3 (C), and the original data from 1.4 (D). Panels A and C also show the pdf's for the raw data from Figure 1.1, and Figure 1.3. Panel D is actually for a full hour of data. Gaussian pdf's with the same mean and variance have been overplotted in red.

has the pdf

$$\phi(x) = \frac{\sigma}{\sqrt{2\pi}} e^{-(x-\mu)^2/\sigma^2} \quad \text{or} \quad \phi(u) = \frac{1}{\sqrt{2\pi}} e^{-u^2} \quad (\text{C.6})$$

where u is the standardized variable from equation (C.5).

The pdf is fundamental to all operations with random variables. Just as we can add algebraic variables, so also can we define a random variable formed by summing two random variables. But the rules are very different, since it is meaningless to sum two pdf's, at its simplest, the pdf of the sum of two random variables is the convolution of their two pdf's.⁶

⁶And for this reason a good many proofs of theorems for random variables are done in the Fourier domain, using the Fourier transforms of pdfs – though in probability theory these are called characteristic functions.

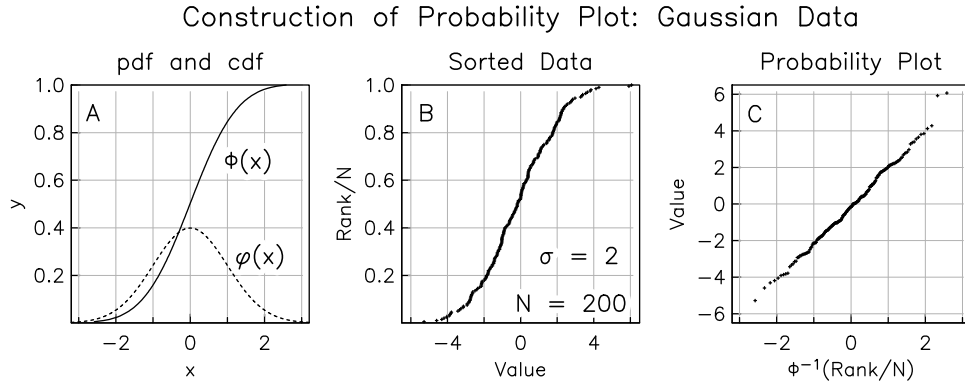


Figure C.3: Cartoon to show how a probability plot is constructed. Panel A shows the pdf ϕ (dotted) and cumulative distribution function (cdf) Φ for a Gaussian with unit variance and zero mean. Panel B plots 200 data values from a Gaussian pdf with variance of four; for each data value the x -axis is the value and the y -axis the rank of that value, divided by the number of data. Panel C is the probability plot, in which, for each point, the inverse cdf Φ^{-1} is applied to the normalized rank, which is shown on the x -axis, with the data value on the y -axis.

C.3.1 Probability Plots

, Figure C.2 suggests that for the sea-level datasets discussed in Chapter 1, the Gaussian approximates the actual pdf pretty well. These plots show a Gaussian pdf with the same mean and variance as the data, along with an **empirical pdf**, meaning one estimated from the data, in this case using a kernel estimator (Silverman, 1986), a useful alternative to the familiar histogram. But both histograms and kernel estimators have the same undesirable feature, namely a need to decide how much averaging to do: too small and there are a lot of fluctuations, but too large and important features can be smoothed over.

A better way of comparing the data distribution with a Gaussian (or any other) pdf is what is called a **probability plot**. Figure C.3 shows the idea behind such a plot. For any pdf there is a **cumulative distribution function** (cdf):

$$\Phi(x) = \int_{-\infty}^x \phi(u) du$$

that gives the probability of a random variable X being less than x . Panel A of the figure shows the pdf and cdf for a Gaussian distribution. If we sort N data from smallest to largest, the location of a data value in the resulting list is called its **rank**, running from 1 to N . Panel B of the figure plots the data in rank order, against their actual values. Since the rank is a kind of cumulative value, the result looks very much like the cdf Φ . So if we apply the inverse of the cdf, Φ^{-1} , to the

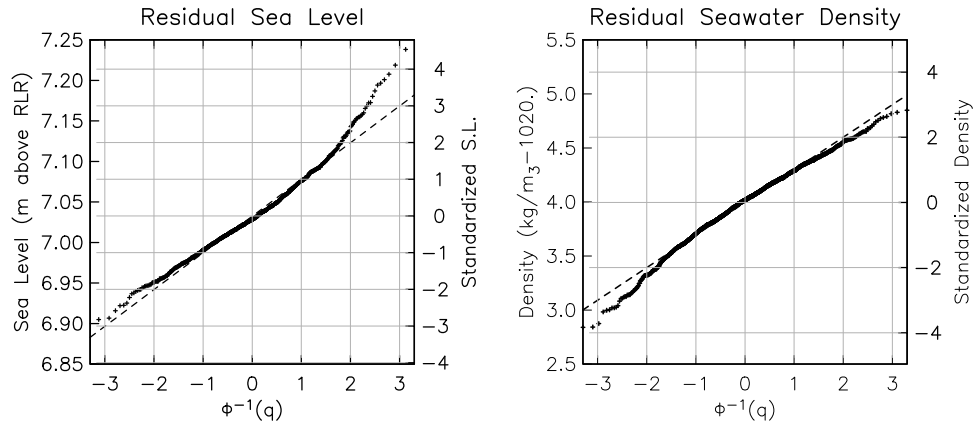


Figure C.4: Probability plots for the residual sea level and density data shown in Figures 1.1 and 1.2.

normalized rank values, this should, if the data actually follow the assumed cdf, transform the axis to give numbers that are uniformly distributed.

Panel C, the probability plot, does this, while also (as is conventional) plotting the data values on the vertical axis rather than the horizontal one used in Panel B. We see that the data, so plotted, fall very close to a straight line with a slope of two, corresponding to the standard deviation of the data. The largest values depart from this line, but if we had more the rank values for these particular data points will decrease, and usually will fall closer to the line.

A probability plot thus allows us to see if data, particularly the larger or smaller values, are consistent with an assumed pdf (in this case the Gaussian), without the averaging inherent in making a histogram. Figure C.4 shows probability plots for the residual sea level and density data shown in Figures 1.1 and 1.2 – that is, the data with seasonal cycles and long-term trends removed. In each plot, a dashed line shows where the data should be if they had a Gaussian distribution with the same mean and variance. Values of the data, standardized by the mean and variance, are shown on the right axis: in these units the dashed line always has a slope of one.

Looking first at the sea level data, the largest values are much larger than would be expected for a Gaussian (the dashed line); the upper tail of the data distribution is longer than for the Gaussian and we would say that the data are **heavy-tailed** on this side of the distribution. The same upward curvature for the lowest data values means just the opposite: the data are closer to the mean than would be expected. These behaviors are just visible in the pdf in Figure C.2. The density plot shows that the data are long-tailed for low values, and short-tailed for large ones. The two long tails are caused by recent ocean warming, which has moved the temperature, density, and sea level outside their previous range.

C.3.2 Transformations of Random Variables

The cumulative distribution function is also useful for seeing how the pdf of a random variable X changes if we transform it to another variable, $Y = g(X)$, where g is some function. For spectrum estimation the case of most interest is converting a spectral value S to dB, the transformation being $10\log_{10}(S)$.

We first show how to get the cdf of the transformed variable. We have to assume that $g(X)$ is monotonic, so that there will be an inverse function $X = g^{-1}(Y)$. We successively replace variables in the definition of the cdf $\Phi_Y(y)$ and get

$$\Phi_Y(y) = \Pr[Y \leq y] = \Pr[g(X) \leq y] = \Pr[X \leq g^{-1}(y)] = \Phi_X(g^{-1}(y)) \quad (\text{C.7})$$

Next we differentiate this using the chain rule and get

$$\phi_Y(y) = \frac{d}{dy} \Phi_Y = \frac{d}{dy} \Phi_X(g^{-1}(y)) = \phi_X(g^{-1}(y)) \left| \frac{d}{dy} (g^{-1}(y)) \right| \quad (\text{C.8})$$

where the absolute value is present to deal with the case in which Y decreases as X increases.

The simplest case is when we scale a random variable, defining Y as aX , so $g^{-1}(y) = y/a$. Then equation (C.8) becomes

$$\phi_Y(y) = \frac{\phi_X(y/a)}{|a|} \quad (\text{C.9})$$

As noted above, the case $Y = b \ln(aX)$ is of particular interest; for dB, $b = 10/\ln 10 = 4.343$. If $y = g(x) = b \ln(ax)$, $x = g^{-1}(y) = e^{(y-b \ln a)/b} = e^{y/b}/a$ and equation (C.8) becomes

$$\phi_Y(y) = \frac{\phi_X(e^{(y-b \ln a)/b}) e^{(y-b \ln a)/b}}{|b|} = \frac{\phi_X(e^{y/b}/a) e^{y/b}}{|ab|} \quad (\text{C.10})$$

If we were to shift y by writing $z = y - b \ln a$ this expression would become

$$\frac{\phi_X(e^{z/b}) e^{z/b}}{|b|}$$

which is just a scaled version of X : so scaling X shifts but does not otherwise alter the pdf of the log.

C.4 Estimation

We now turn from probability to statistics, which might be considered a subfield of probability, but for historical reasons is usually somewhat separate. This is perhaps reasonable, given how different the aim of statistics is, namely to learn about something from data, using the mathematics of probability to relate the

something (whatever it is) to the data. While the data are numbers (usually), not random variables, statistical reasoning uses such variables as models for data.

Our particular interest is the subfield of statistics known as **estimation theory**: the development and evaluation of procedures to estimate, from the data, parameters of a pdf that is supposed to model them. The most familiar example is finding the two parameters of a one-dimensional Gaussian pdf (equation C.6) that is the model assumed for the data; that is, finding the mean μ and variance σ^2 .

Given a dataset with N values x_1, x_2, \dots, x_N the usual methods for finding these parameters emulate the moment integrals: equations (C.3) and (C.4). These integrals suggest estimating the mean by taking the average:

$$\hat{\mu} = \frac{1}{N} \sum_{i=1}^N x_i \quad (\text{C.11})$$

and estimating the variance by computing

$$\hat{\sigma}^2 = \frac{1}{N} \sum_{i=1}^N (x_i - \hat{\mu})^2 \quad (\text{C.12})$$

where the $\hat{\cdot}$ indicates that we are finding an estimate of the parameter.⁷

We can put this estimation step into a more general form. First, we have a finite data set $\{x_n\}$. Second, we have some kind of procedure, the **estimator**, that produces, from $\{x_n\}$, a value for some parameter, or parameters, that describe the probability properties of X , the random variable whose pdf we have chosen to model the data. For the example above, these parameters would be μ and σ^2 , and equations (C.11) and (C.12) describe the estimators. But for our general treatment, we use θ to denote some parameter to be found, with θ_t being its true value. Both of these are algebraic variables. In this general framework, applying our estimation procedure to the data $\{x_n\}$ gives us an estimate of θ_t , which we denote by $\hat{\theta}$; that is,

$$\hat{\theta} = E[\{x_n\}] \quad (\text{C.13})$$

where we use E to represent the statistical estimation procedure. This might be an algebraic expression such as is used in equations (C.11) and (C.12), or a complicated algorithm.

To evaluate an estimation procedure E we replace the data $\{x_n\}$ by N random variables $\{X_n\}$ with a specified pdf, and write

$$\hat{\Theta} = E[\{X_n\}] \quad (\text{C.14})$$

⁷The usual statistical names for these expressions are the **sample mean** and the **sample variance** because the N data are viewed as being a subset created by sampling from a much larger collection: a view only sometimes applicable to geophysical data.

where we are using a Greek capital letter (Θ) because $\hat{\Theta}$, just like $\{X_n\}$, is a random variable. But since $\{X_n\}$ is a random variable we have chosen, we know the true value θ_t for any parameter of the pdf.

It is important to remember that the pdf of $\hat{\Theta}$, for any estimator, will depend on the pdf we choose for the X 's, which means that our results for $\hat{\Theta}$ will be more or less applicable to our data depending on whether the pdf we assume for X models the data well or badly. In addition, the pdf of $\hat{\Theta}$ may depend on the number of data, N – as we will see, it had better.

For the specific case of the estimator given by equation (C.11), we would have

$$\hat{\Theta}_L = \frac{1}{N} \sum_{i=1}^N X_i$$

If we assume that the X 's used to model the data are by independent⁸ random variables X_i with a Gaussian pdf (equation C.6) with first moment μ and second moment σ^2 , then it can be shown that $\hat{\Theta}_L$

1. has a Gaussian distribution;
2. with a first moment, or expected value equal to μ : $\mathcal{E}[\hat{\Theta}_L] - \mu = 0$;
3. a second moment, or variance, equal to σ^2/N ; we use $\hat{\sigma}_\theta$ to denote the square root of this second moment.

What item (2) means is that the average is an **unbiased** estimate of the true mean value μ : if we imagine having many data sets, no average will be exactly equal to it, but the many averages would themselves have a pdf centered on the true value. Item (3) tells us that the pdf of $\hat{\Theta}_L$ becomes narrower and narrower as N increases: having more data improves the estimate because $\hat{\sigma}_\theta$ varies as $1/\sqrt{N}$. This narrowing of the pdf, plus the lack of bias, means that the average is a **consistent** estimate of the mean value: as N goes to infinity, the pdf of $\hat{\Theta}_L$ approaches a delta function.⁹

For an example of how important the assumed pdf of the X 's can be, suppose that it is instead the Cauchy pdf shown in Figure C.2, which is

$$\phi(u) = \frac{1}{\pi(1+u^2)}$$

which for large u obviously decreases much more gradually than does a Gaussian pdf. Then it can be shown that the pdf of $\hat{\Theta}_L$ is a Cauchy pdf, and also is independent of N . This independence makes $\hat{\Theta}_L$ found by averaging an **inconsistent** estimator: not only does the pdf not approach a delta function as N increases, it

⁸We explain “independence” in Section C.5 below.

⁹A random variable with a delta-function pdf is equivalent to an algebraic variable.

does not change at all! Worse yet, the first moment of the Cauchy distribution is infinite: the estimate from averaging does not even have an expected value. So trying to find the location parameter by averaging just does not work. That is not to say that there is no way to do this: if instead we find $\hat{\Theta}_L$ by taking the median of N data, it has a pdf with an expected value equal to the actual location parameter, so it is unbiased; the variance of this pdf, for large N , varies as $1/N$, so the median is a consistent estimator for this pdf.

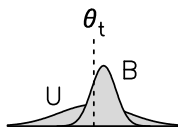
Now go back to the case of Gaussian variables, and consider finding an estimate for the variance. We again create a random variable by using X instead of x in equation (C.12):

$$\hat{\Theta}_W^2 = \frac{1}{N} \sum_{i=1}^N (X_i - \hat{\Theta}_L)^2$$

where $\hat{\Theta}_W$ is the random variable for our estimate of σ . Note that we are using the estimate $\hat{\Theta}_L$ in this expression, not the true value μ . It can be shown that

$$\mathcal{E}[\hat{\Theta}_W^2] = \sigma^2 \left(1 + \frac{1}{N}\right)$$

which means that the bias $\beta = \mathcal{E}[\hat{\Theta}_W^2] - \sigma^2 \neq 0$, making $\hat{\Theta}_W$ a **biased estimate**. That is, we know that using equation (C.12) on many data sets will, on average, produce estimates that are too large. However, as N goes to infinity, $\mathcal{E}[\hat{\Theta}_W^2]$ approaches σ^2 ; to describe this behavior we say that the estimate is **asymptotically unbiased**. In this case the bias is not large even for small N . An asymptotically unbiased estimation procedure is usually acceptable, since we know that with more data we can reduce the bias to a negligible amount. But if an estimator is **asymptotically biased**, it should be used only if no alternative is available.



Now consider two estimators, either different procedures, or the same procedure used with different values of some adjustable parameter. If a biased estimator, B , has a much smaller variance than an unbiased estimator, U , we might prefer A to B even though B is biased. For some estimation procedures the bias $\beta = \hat{\Theta} - \theta_t$ and the variance $\mathcal{V}[\hat{\Theta}]$ trade off: if we decrease one the other increases. It is then useful to consider the **mean square error**, which combines bias and variance:

$$m_{sq}^2 = \beta^2 + \mathcal{V}[\hat{\Theta}] = (\mathcal{E}[\hat{\Theta} - \theta_t])^2 + \mathcal{V}[\hat{\Theta} - \mathcal{E}[\hat{\Theta}]] \quad (\text{C.15})$$

If there is a tradeoff, we can try to choose whatever makes m^2 smallest.

We have seen that for the Cauchy distribution one procedure (the median) is consistent while another (the average) is not, and indeed does not exist. A general measure of the relative goodness of two procedures A and B is the ratio of the variances of the random variable produced by them; the quantity

$$\frac{\mathcal{V}[\hat{\Theta}_A]}{\mathcal{V}[\hat{\Theta}_B]}$$

is called the **relative efficiency** of B compared to A (if B has a larger variance, its efficiency is lower); this can be a function of N , or, as with the bias, we can consider what it is for $N \rightarrow \infty$, which is (what else) the asymptotic relative efficiency. We have seen that for Cauchy random variables, the average has a relative efficiency of zero compared to the median; but for Gaussian random variables, the median has a relative efficiency of 0.64.

C.4.1 Confidence Limits

Up to this point we have discussed how to get a “good” estimate of some parameter θ , something known as **point estimation**. Certainly we want this, but it is just as important to have some idea about how good our estimate is. One way to describe this is through **confidence intervals**. Given a pdf ϕ_θ for $\hat{\Theta}$, we can choose values θ_b and θ_t such that

$$\int_{\theta_b}^{\theta_t} \phi_\theta \parallel d\theta = \alpha \quad (\text{C.16})$$

for any α between zero and one (since the integral just gives a probability). This equation does not determine θ_b and θ_t uniquely; almost always they are chosen to minimize $\theta_t - \theta_b$, the length of the interval.

It is conventional to take $\alpha = 0.95$ and call the range $[\theta_b, \theta_t]$, a **95% confidence interval**: if we had repeated estimates of a parameter, this interval would be different each time, but 95% of the intervals would include the true value. This is preferable to giving the standard deviation σ because the meaning of the latter depends on the shape of the pdf of $\hat{\Theta}$.

C.5 Multiple Random Variables: Covariance and Correlation

We now return to probability theory, which becomes more interesting, useful, and complicated when we consider, not just a single random variable X with a pdf $\phi(x)$, but N random variables X_1, X_2, \dots, X_N , which we can denote by the vector \mathbf{X} . These also are described by a pdf, but it becomes a function of N dimensions, $\phi(\mathbf{x})$, where \mathbf{x} is an N -dimensional vector of algebraic variables. Such a pdf is often called a **joint pdf**, and can model the very common systematic but variable relationships between quantities.

Considering only two variables, a function tells us that a particular value of an algebraic variable x_1 is associated with a particular value of $x_2 = f(x)$. A joint pdf tells us the probability that, if a random variable X_1 falls in a certain range, another random variable X_2 will fall in some other range. The notation and formula

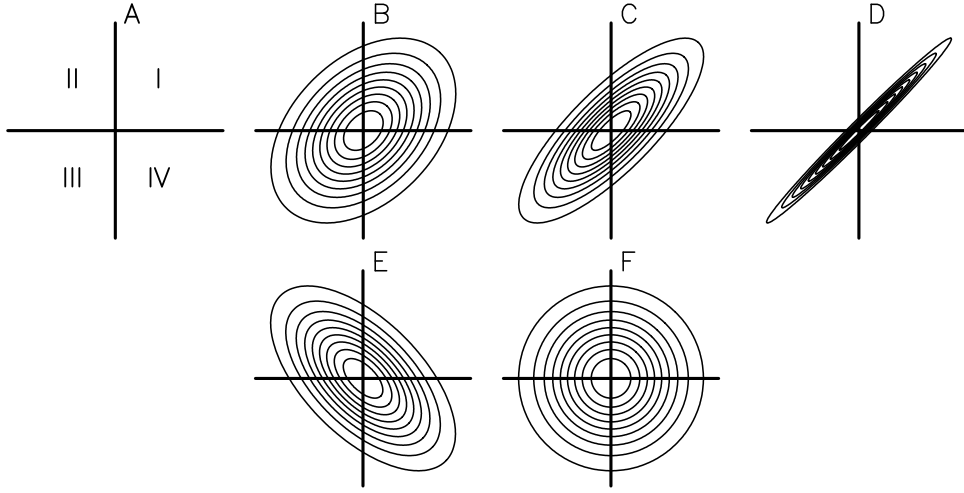


Figure C.5: Cartoon of different probability density functions in two dimensions (shown as contour plots). Panel A shows the division into quadrants discussed in the text; panels B through D show pdf's for which the second moment R_{12} becomes larger relative to the variances; panel E shows a pdf with negative R_{12} , and panel F one for which $R_{12} = 0$.

for this is

$$\mathcal{P}[a_2 \leq X_2 \leq b_2 | a_1 \leq X_1 \leq b_1] = \int_{a_1}^{b_1} \int_{a_2}^{b_2} \phi(u_1, u_2) du_1 du_2 \quad (\text{C.17})$$

where the notation $\mathcal{P}[A|B]$ means “probability of A given that B is true”, which is called **conditional probability**.

Sticking with two dimensions, we can again determine the moments of the pdf: two means (first moments)

$$\bar{x}_i = \int_{-\infty}^{\infty} \int_{-\infty}^{\infty} u_i \phi(u_1, u_2) du_1 du_2 \quad \text{for } i = 1, 2$$

and two variances (second moments)

$$\sigma_i^2 = \int_{-\infty}^{\infty} \int_{-\infty}^{\infty} (u_i - \bar{x}_i)^2 \phi(u_1, u_2) du_1 du_2 \quad \text{for } i = 1, 2$$

But there is an additional second moment

$$\begin{aligned} & \int_{-\infty}^{\infty} \int_{-\infty}^{\infty} (u_1 - \bar{x}_1)(u_2 - \bar{x}_2) \phi(u_1, u_2) du_1 du_2 \\ &= \mathcal{E}[(X - \mathcal{E}[X])(Y - \mathcal{E}[Y])] \\ &\stackrel{\text{def}}{=} \mathcal{C}[X_1, X_2] \end{aligned} \quad (\text{C.18})$$

where the second line shows how to write the integrals in terms of the expectation operator.

To simplify the discussion, suppose the means \bar{x}_1 and \bar{x}_2 are both zero; then this second moment is

$$\int_{-\infty}^{\infty} \int_{-\infty}^{\infty} u_1 u_2 \phi(u_1, u_2) du_1 du_2 \quad (\text{C.19})$$

Looking at the integrand, the product $u_1 u_2$ will be positive in the quadrant with $u_1 > 0$ and $u_2 > 0$, and the opposite quadrant in which both are negative (I and III in Figure C.5 – and negative in the other two quadrants (II and IV). So if most of the pdf is in quadrants I and III, the integral in equation (C.19), which is $\mathcal{C}[X_1, X_2]$, will be positive. But a pdf of this form means that when $X_1 > 0$, X_2 probably is too (or the converse, going from X_2 to X_1); likewise, when $X_2 < 0$, X_1 probably is also (and the converse). Hence if the two random variables X_1 and X_2 vary together, or **co-vary**, the **covariance** $\mathcal{C}[X_1, X_2]$ will be positive. If $X_1 > 0$ was associated with $X_2 < 0$, the most of the pdf would be in quadrants II and III, and $\mathcal{C}[X_1, X_2]$ would be negative. Finally, if the sign of X_1 conveys no information about the sign of X_2 , the pdf will be so distributed that $\mathcal{C}[X_1, X_2]$ will be close to zero.

Thus, this particular second moment tells us something about probabilistic associations between two random variables, something that can be generalized to more than two dimensions: given N random variables, the covariances are

$$\mathcal{C}[X_i, X_j] = \int_{-\infty}^{\infty} \int_{-\infty}^{\infty} \dots \int_{-\infty}^{\infty} \int_{-\infty}^{\infty} u_i u_j \phi(\mathbf{u}) d\mathbf{u} \stackrel{\text{def}}{=} R_{ij} \quad (\text{C.20})$$

creating a matrix \mathbf{R} , which is called the **covariance matrix**. Because of the symmetry in equation (C.20), this matrix is symmetric. The terms on the diagonal are

$$R_{ii} = \int_{-\infty}^{\infty} \int_{-\infty}^{\infty} u_i u_j \phi(u_i) \phi(u_j) du_i du_j \int_{-\infty}^{\infty} u_i \phi(u_i) du_i \int_{-\infty}^{\infty} u_j \phi(u_j) du_j = \sigma_i^2 \quad (\text{C.21})$$

which is to say that they are the variances.

An example of an N -dimensional, or **multivariate** pdf is the Gaussian probability density function $\phi(\mathbf{x})$ its argument being an N -vector $\mathbf{x} = (x_1, x_2, \dots, x_N)^T$. The pdf is

$$\phi(\mathbf{x}) = \frac{1}{(2\pi)^{N/2}} \det(\mathbf{R}) \exp[-\frac{1}{2}(\mathbf{x} - \bar{\mathbf{x}})^T \mathbf{R}^{-1}(\mathbf{x} - \bar{\mathbf{x}})] \quad (\text{C.22})$$

This expression contains N parameters $\bar{\mathbf{x}}$, the vector of mean values, and N^2 more in the covariance matrix \mathbf{R} . Because it is symmetric, only $N(N + 1)/2$ values R_{ij} are needed to specify it completely. The total number of free parameters is thus N means, N variances, and $N(N - 1)/2$ covariances.

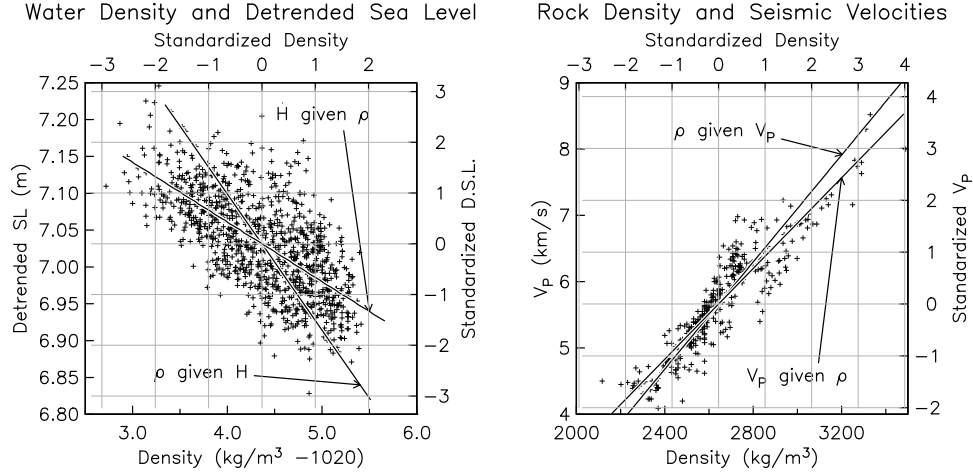


Figure C.6: Scatterplots of two datasets. The left panel shows the water height and density data shown in the top panels of Figure 1.1 (but with the trend removed) and Figure 1.2, so the data include the annual cycles. The right panel shows observed densities and seismic velocities for rocks from laboratory measurements or data from deeper boreholes (Brocher, 2005). In both panels the scales on the bottom and left are for the actual values while the scales on the top and right are for the standardized values. The diagonal lines in both plots are the linear regressions of each variable on the other (Section C.5.1).

Such a pdf is difficult to visualize except in two dimensions, so Figure C.5 shows a variety of two dimensional Gaussian pdf's to illustrate different amounts of association between variables: clearly panel D illustrates a much more definite association than panel B does.

To measure how strongly two random variables X_i and X_j are associated, we divide the covariance by the product of the individual variances:

$$\frac{\mathcal{C}[X_i, X_j]}{\sqrt{\mathcal{V}[X_i]\mathcal{V}[X_j]}} = \frac{R_{ij}}{\sigma_i\sigma_j} \stackrel{\text{def}}{=} \rho_{ij} \quad (\text{C.23})$$

where ρ_{ij} is called the **correlation coefficient** for the random variables X_i and X_j .

Since $R_{ii} = \sigma_i^2$, $\rho_{ii} = 1$: the correlation of a variable X_i with itself is one. It should be obvious that if $X_j = -X_i$, $\rho_{ij} = -1$; and also that this remains true for any scaling $X_j = -aX_i$. The correlation must fall into the range $[-1, 1]$, with the two extremes occurring when there is a definite linear relation between two random variables. Because of their similar sound (and common usage) it can be difficult to remember the distinction between covariance and correlation: the distinction is that the former includes information about how much the two variables

actually vary, and has the dimension that is the product of the dimensions of the two variables: so if, for example, we compare rock density to seismic velocity, the covariance has the dimension of density times velocity. The correlation has the variance information removed, and is a nondimensional measure of how closely associated the two variables are. Equivalently the correlation is the covariance between two standardized variables created by applying equation (C.5) to the original variables.

As an example of standardization (in this statistical sense), Figure C.6 shows **scatterplots** for two different data sets. One is the sea level and water density from Figures 1.1 and 1.2; the other density and seismic velocity for many different kinds of geological materials.

The left panel shows that sea level is negatively correlated with density increase. This is expected on physical grounds, since the denser the surface layer of water, the less volume it occupies and the lower the sea level is. The correlation coefficient is only -0.66 , implying that density changes are not the only cause of sea level fluctuations. The right panel shows a much stronger correlation, $\rho = 0.92$, between the two rock properties.

The correlation coefficients for these datasets were found by replacing the integrals in equation C.23) by sums to find the estimated correlation $\hat{\rho}$:

$$\hat{\rho} = \frac{\sum_j (x_j - \hat{x})(y_j - \hat{y})}{\left(\sum_j (x_j - \hat{x})^2 \sum_k (y_k - \hat{y})^2 \right)^{1/2}} \quad (\text{C.24})$$

where \hat{x} and \hat{y} are the estimates of the means from taking the average. This equation suggests another way to look at ρ : if we consider the data to form two N -dimensional vectors, equation (C.24) is then the inner (dot) product of the two vectors, divided by their Euclidean norms. Schwarz's inequality for vectors, $(\mathbf{x}, \mathbf{y}) \leq \|\mathbf{x}\| \|\mathbf{y}\|$, shows that $|\rho_{XY}| \leq 1$; that is, $-1 \leq \rho \leq 1$. The inequality also shows that $\rho = \pm 1$ only if these “data-vectors” have the same direction: then a scatterplot would show all the points lying along a straight line, and we would say that the two variables are perfectly correlated. Conversely, $\rho = 0$ corresponds to no correlation between the two; the two data-vectors would be perpendicular.

For actual data we would not expect $\hat{\rho}$ to be zero even if the data pairs were in fact uncorrelated. For a particular value of $|\hat{\rho}|$, deciding if it indicates actual correlation, or just the variations that would be expected even for uncorrelated data, is a matter of **hypothesis testing**.

For power spectra, for which the amount of variation matters, we use the covariance; when we examine the connection between two series, we instead focus on an analog to the correlation.

In describing correlation we used the phrase “definite linear relation”; here “linear” is more important than might be expected. The second moment can only capture a linear dependence of one variable on another; but there can be other

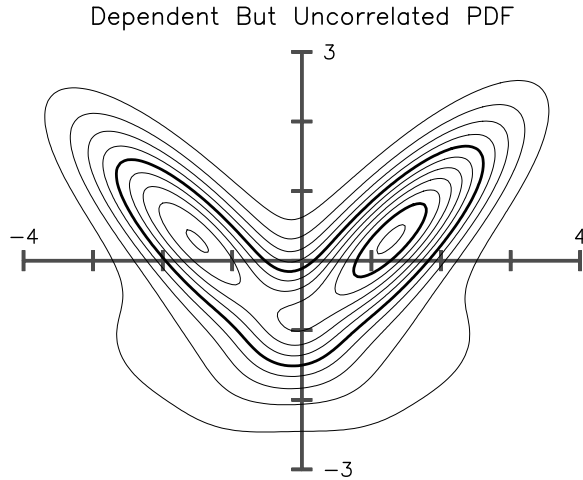


Figure C.7: Pdf of a pair of random variables, shown as a contour plot (contour interval 0.01, heavy lines at 0.05 and 0.10). The means are zero, the standard deviations are 1.82 and 1.20, and the covariance is 0.11; so the correlation is 0.05. The two variables are dependent, but there is not a linear relationship so they are nearly uncorrelated.

kinds of dependence. Figure C.7 is an example – admittedly a somewhat artificial one,¹⁰ in which the pdf is designed so that the probability of X_2 depends (roughly) on X_1^2 . Since X_2 and X_1 are connected (probabilistically) they are not **independent** random variables: the pdf of one depends on the assumed (or conditional) value of the other. But because the dependence is not linear these two variables are (nearly) **uncorrelated**. It is common to confuse independence with lack of correlation, but while it is true that if random variables are independent they will be uncorrelated, the converse may not be true.

One of the reasons why Gaussian pdf's are appealing is that for them, as equation (C.22) suggests, knowing the first two moments (means and covariances) completely determines the pdf: higher moments exist but contain no additional information.

C.5.1 Linear Regression

Given correlation between random variables, we usually want to say something about what value of one variable to expect if we know the value of the other: e.g., for the rock properties we might have a P-wave velocity and want to know the most likely value of the density. That is, we want to know

$$b_2(x_1) = \mathcal{E}[X_2 | X_1 = x_1] \quad (\text{C.25})$$

¹⁰We owe the germ of this example to R. A. Haubrich.

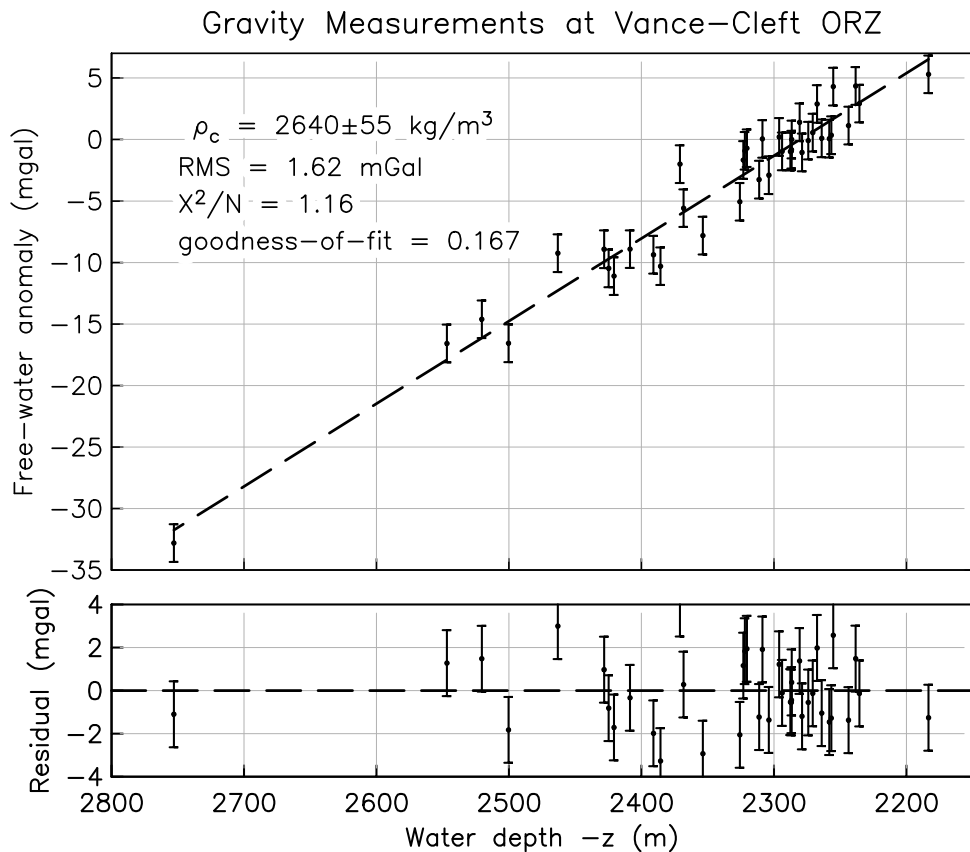


Figure C.8: Sea-floor gravity versus elevation, measured underwater above the Vance-Cleft Overlapping Rift Zone on the Juan de Fuca ridge ([Stevenson et al., 1994](#)). The data have been corrected for the earth's vertical gravity gradient and the presence of seawater. The top panel shows the data and a linear fit; the lower panel shows the residuals (data minus fit), which should always be plotted to highlight discrepancies.

which is read as, “the expected value of the random variable X_2 , given that $X_1 = x_1$ ”: if we imagine fixing X_1 to a particular value x_1 , this produces a slice of the joint pdf of X_1 and X_2 , $\phi(x_1, x_2)$, a univariate pdf since x_1 is fixed. The expected value is the first moment of this pdf from this slice, giving a function

$$b_2(x_1) = \mathcal{E}[X_1 | X_2 = x_2] \quad (\text{C.26})$$

The function $b_2(x_1)$ (note that there are no random variables in it or its argument) is called the **regression** of X_2 on X_1 .¹¹ Note that the situation is symmetric: we can also find $b_1(x_2) = \mathcal{E}[X_1 | X_2 = x_2]$, the regression of X_1 on X_2 . But these functions will almost always be different.

A special (but common) case of this is when we think there is, for theoretical reasons, a linear relationship between the variables, and also that only one variable needs to be modeled as random. Figure C.8 shows the gravity anomaly δg measured on the seafloor, plotted against the elevation z . For smooth terrain we expect the two to be related by

$$\delta g = 2\pi G \rho_R z + c \quad (\text{C.27})$$

where G is Newton’s gravitational constant and ρ_R is the local rock density. Finding density from the slope of the line is known as **Nettleton’s Method**. The gravity variable is much less accurately known than the water depth because of instrument shaking due to water currents; also, the rock density is not really constant, so the relation is not exact. Here the appropriate probability model is

$$G = \alpha z + \beta + X \quad (\text{C.28})$$

where X is a random variable that models uncontrollable variations and is assumed to have zero mean; the data δg become the random variable G . Given these data, we want to estimate the slope of the line, α , which by equation (C.27) gives ρ_R . We would also like to know the uncertainty of our estimate of α . Taking expected values, we get

$$\mathcal{E}[G] = \mathcal{E}[\alpha z + \beta + X] = \alpha z + \beta$$

since the expected value of an algebraic variable is just its value, and $\mathcal{E}[E] = 0$ by assumption.

This looks just like the regression equation (C.25) in the case where $b_2(x_1)$ is a linear function of x_1 : and indeed, in statistics this kind of function fitting is also called regression, in this case **linear regression**. But the assumptions of the two situations are different: in Figure C.6 both variables (for either case shown) are

¹¹“Regression” is probably the most unfortunate term in statistics, since none of its ordinary uses have anything obvious to do with expected values of bivariate distributions. Just treat it as a name.

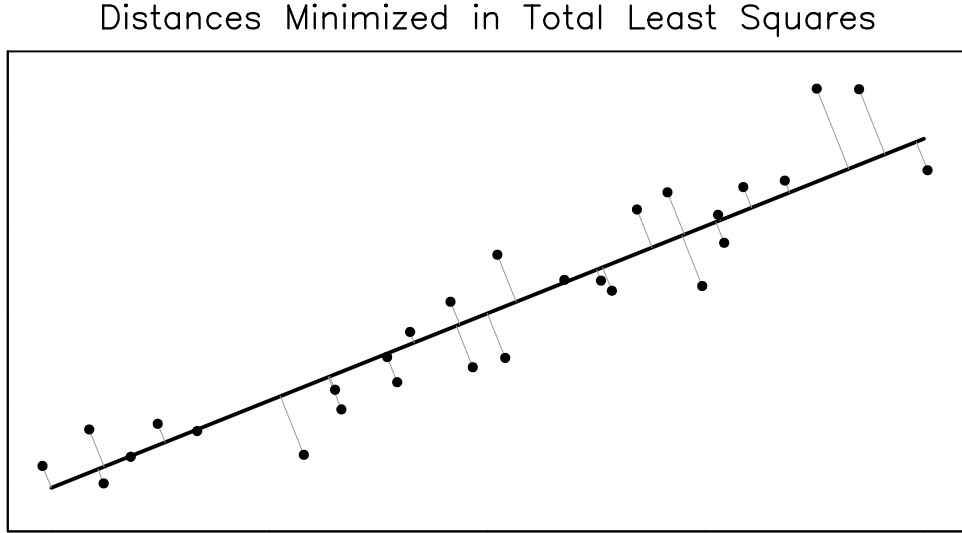


Figure C.9: Distances used in Total Least Squares fitting of a line.

best modeled as random variables, whereas in Figure C.8 one, the depth, can be adequately modeled as an algebraic variable.

If E is Gaussian, the best estimate of α is given by least squares:

$$\hat{\alpha} = \frac{\sum_j (x_j - \hat{x})(y_j - \hat{y})}{\sum_j (x_j - \hat{x})^2} = \hat{\rho}_{XY} \frac{\hat{\sigma}_Y}{\hat{\sigma}_X} \quad (\text{C.29})$$

If E is uncorrelated random variables, the estimate (C.29) has the least variance of all unbiased linear estimators (the Gauss-Markov Theorem; see Section C.4 for what “unbiased” means).

Notice that in (C.28) that *all* the randomness is attributed to the g variable: in this example, the gravity measurement. But what if both coordinates have random components? Then things get considerably more complicated, depending on what can be assumed about the noise. The least-square criterion will give a different estimate of the slope if we assume that the x_2 coordinate is not random while the x_1 is. That is, the linear form of $b_2(x_1)$ is not the same as the linear form of $b_1(x_2)$: we get two regression lines, as shown in Figure C.6.

A third case comes from assuming that both X_1 and X_2 are random “to the same extent”. This really only makes sense if X_1 and X_2 are measured in the same units; it is meaningless to say the water depth in meters has the same uncertainty as the gravity anomaly in ms^{-2} ! However, we can make the variability in X_1 and X_2 the same, and nondimensional, if we replace them by standardized variables, as we did in Figure C.6 by changing the axis labels.

In this special case we could fit a line using what is called a **total least squares** (TLS) estimate: we minimize the sum of squares of the Euclidean dis-

tances from the points in the plane to the line, as shown schematically in Figure C.9. This line may be said to give the “best relation” between the two variables, but note that it is not the relationship to use if the aim is to predict x_2 from x_1 or vice versa.

If the straight line is $x_2 = \alpha x_1 + \beta$, the TLS estimator for the intercept is

$$\hat{\beta} = \frac{1}{N} \sum_j \frac{Y_j - \hat{\alpha}}{N \sum_j X_j} = \hat{X} - \hat{\alpha} \hat{Y}$$

where $\hat{\alpha}$ is the slope estimate, which is given by the solution of this quadratic equation:

$$\begin{aligned} 0 &= -c_2 + c_1 \hat{\alpha} + c_2 \hat{\alpha}^2 \\ c_2 &= \sum_j (X_j - \hat{X})(Y_j - \hat{Y}) \\ c_1 &= \sum_j [(X_j - \hat{X})^2 - (Y_j - \hat{Y})^2] \end{aligned}$$

Of course, a quadratic equation usually has two solutions: in this case, one corresponds to the best fit, and the other to the worst.

APPENDIX D

TIMES AND DATES

from Strachius I imbibed the elements of chronology: the Tables of Helvicus and Anderson, the Annals of Usher and Prideaux, distinguished the connection of events, and engraved the multitude of names and dates in a clear and indelible series the Dynasties of Assyria and Egypt were my top and cricket-ball; and my sleep has been disturbed by the difficulty of reconciling the Septuagint with the Hebrew computation.

Edward Gibbon, *Memoirs of My Life and Writings*

D.1 Introduction

This Appendix provides basic information about time scales and ways of describing particular times. Some of this should seem very familiar, but probably not all of it will be.¹ We also suggest what systems of time-reckoning and description you should use, and avoid, in working with or presenting data.

D.2 Time

The usual and familiar smaller units of time are the second, the minute (60 s), the hour (60 min) and the day (24 h, 1 d); these symbols are SI-compliant. Originally the last was what defined time, through the rotation of the Earth; “one day” then depended on what this rotation was referenced to: the stars, the actual Sun, or the mean Sun, the last being used to define “mean time”. Since 1967 the base unit of time has been the second, defined as a certain number of oscillations produced by a quantum-mechanical effect in cesium atoms: the other units are then defined by the multiples given above. Two conversion factors to remember are that one day is 86400 s (10^5 is a rough approximation), or 1440 minutes.

The familiar longer units are based, like the day, on astronomical phenomena. The mean tropical year (defined by the mean Sun’s celestial longitude increasing by 360°) is 365 d 5 h 48 min 45.2 s: or, (some useful conversion factors),

¹For much, much more on these topics, see McCarthy and Seidelmann (2018) and Richards (1998).

365.24218967 days, 8765.81 hr, or 31556925.2 seconds, the last being very well approximated by the easily-remembered $\pi \times 10^7$. The year matters because it is the repeat time of the patterns of insolation that drive weather and climate. The other unit related to astronomy is the month. Again, there are various lengths, depending on what is being referred to; the mean interval between the Moon having the same phase is called the **synodic month** and is 29.530587981 days (29 days 12 hours, 44 minutes, and 2.8 seconds): or, 708.734 h or 2551442.8 s. There are 12.368 synodic months in a tropical year; 12 synodic months is 354.367056 days (354 d 8 h 48 min 33.6 s). Except for tidal effects few geophysical phenomena depend on the month.

D.3 Dates

The units of time just discussed allow us to describe the difference in time between two events; a system of dates allows us to specify the time of a single event. Such a system needs two elements:

1. An **epoch** at which time is taken to be some specified value, often but not always zero; dates are simply time intervals from, or up to, this epoch. Since the time of (say) noon depends on longitude, we also need to specify the location used.
2. Some pattern of one or more of the time units described in the last section, used to describe the interval between the epoch and the time of whatever it is we wish to assign a date to. If this pattern is used to specify days it is called a **calendar**, and the year of the epoch is called an **era**.

Most calendars are in units that are compromises between being an integer number of days and a match to the period of the year or month. These units are calendar years and calendar months, which almost always² have differing numbers of days chosen to produce a long-term average value that approximates one or more astronomical periods. For the year one approximation (the Julian calendar) adds one day (a **leap** or **intercalary** day) to every fourth year, giving a year length of $365 + \frac{1}{4} = 365.25$ days,³ which, relative to the tropical year, errs by one day after 128 years. A better approximation is the Gregorian calendar, which omits three Julian leap days in every 400 years, to give a year length of $365 + \frac{1}{4} - \frac{3}{400} = 365.2425$ days, leading to a one-day error in 3225 years. Trying to have an integer number

²Almost always because some calendars have units with fixed lengths. The ancient Egyptian calendar (in use, one way or another, for over 4000 years) defined the year to have 365 days: 12 months of 30 days each and 5 extra days.

³This approximation is called the **Julian year**, and is still used in a number of astronomical applications.

of months in a year, each month with an integer number of days, leads to much more complicated patterns along with even more complicated rules for converting calendar-month dates to fractions of a synodic month.⁴

In the sciences, as in many other areas, dates are most often given in the year/month/day system of the Gregorian calendar. While conventional, this calendar has exactly the kind of complicated pattern that makes it difficult to determine the amount of time between two dates. Numerical forms for the dates also differ by country: 12/01/12 in the United States is 324 days later than 12/01/12 in most of the rest of the world. This ambiguity, and many of the complications, can and should be avoided by using a count of days from the start of the year, running from 1 through 365 (or 366 in leap years). The location of a day-number in the year can be understood quickly by thinking of it as an angle in degrees.⁵ In this format the two versions of 12/01/12 become 2012:012 and 2012:334.

However, this still leaves the complication of leap years—somewhat simplified, for now, by the convenient happenstance that in the Gregorian calendar all years from 1901 through 2099 and divisible by 4 are leap years. But a complete escape from this complication requires the use of a dating system in which the units are all the same; in the language of calendrics, there are no intercalations. Five such systems are

1. **Unix time:** the number of seconds since midnight, January 1, 1970 (that is, New Year).
2. **GPS week:** the number of 7-day periods since January 6, 1980, which is day 0 of week 0.⁶
3. **Julian date (JD):** The number of days and fractions of a day since January 1, 4713 BCE (in the Julian calendar, extended backwards), with day JD 0.000 beginning at noon on that date. The number of days is called the **Julian day number (JDN)**.
4. **Modified Julian date (MJD):** The Julian date minus 2400000.5, which means that MJD 0.000 is at midnight at the start of November 17, 1858.
5. **Radiocarbon years before present (BP):** The number of years before January 1, 1950. This epoch was initially used for radiocarbon years ([Currie, 2004](#)), which were measured assuming a particular value for the halflife of ^{14}C . But it seems reasonable to extend it to more general dating.

⁴Again, this is not always true: the Islamic religious calendar ignores the solar year completely and sets the length of each month by actual observation of the visibility of a New Moon.

⁵Day of year is sometimes incorrectly called the Julian Day.

⁶The 7-day week is one of a number of cycles, independent of astronomy, used to identify days. Its only geophysical application is that anything with a weekly period must have some human cause.

If precision at the day level or better is possible, the JD is the best way of tabulating a date for scientific purposes, since it is a completely uniform time scale, and the range of dates for which the JD is positive covers the period during which dating has had this level of precision. It is standard in astronomy and used in some branches of geodesy.

One final and unavoidable complication is that not all days have the same number of seconds; for complicated reasons⁷ a few have 86401 seconds. For such days a “leap second” is added and the last minute runs from 23:59:00 through 23:59:60 before changing to 24:00:00. This is a nuisance, especially because this does not happen at a regular interval. The GPS week, like GPS time, has omitted leap seconds for the times it covers (after 1980) in order to ensure a uniform time scale. Unix time was and is defined as though leap seconds did not exist.

D.4 Best Practices

In this section we set out a set of practices for time reckoning and stating and displaying time and dates.

Reckoning

In scientific timekeeping always use Universal Time (UT), which was invented for geophysical purposes: since 1972 UTC (Coordinated UT), and before that Universal Time and its predecessor, Greenwich Mean Time. Never use time in a local time zone,⁸ except as a supplementary value for use by the local public or when dealing with some phenomenon related to solar effects. Always designate hours by values from 0 through 23.

If creating your own set of programs for finding time differences, or relating series length and sample interval to start and stop times, using JD (if only internally) will simplify everything. As with the metric system, it is initially unfamiliar, but in the long run the inherent simplicity saves a lot of work. There are algorithms for converting between calendar dates (for many calendars) and JDN,

⁷The current definition of the second was designed to match an earlier definition that gave the second as a fraction of the tropical year for 1900, so this definition matches the average value of the second from about 1780 through 1890. But because of the slowing of the earth’s rotation by tidal friction and postglacial rebound, one current day (defined astronomically) is slightly less than 86400 defined seconds. Over time, the “slightly less” builds up to the point that noon as defined by the Earth’s rotation is out of step with noon defined by counting seconds by more than 0.5 s, so another second is needed to keep the timescale close to the Earth’s angular position. The Earth’s rotation rate fluctuates enough (owing to motions in the core) that, since leap seconds were introduced in 1972, the interval between them has varied from 0.5 to 7 years.

⁸Not least because local time zones may include changes from regular to Daylight Savings time, with rules that depend on location.

and once this is done everything else is easy. For example, the day of the week, counting Monday as 1, is $\text{JDN}_{\text{mod}7} + 1$.

Note that two 32-bit integers, one for JDN and one for seconds and fractions of a second within a day, can cover a range of almost 12 million years with a resolution of 25 microseconds.⁹ This will be sufficient unless your data include frequencies above 200 kHz, predate the Pliocene, or are collected more than six million years from now.

Stating

The simplest format for dates is a decimal number: either MJD (or JD for long time spans), or years in the Common Era. The former is the standard in astronomy, while the latter is well entrenched in geophysics.

The International Organization for Standardization (ISO) standard 8601 provides a number of formats for particular times (usually called “time and date” with the former being parts of a day and the latter the day designation). For example, 2021-04-26T06:43:54.12Z, where the punctuation must be as given, the T separates date (in the Gregorian calendar) from time, and the Z denotes Universal Time. This may also be written, unpunctuated, as 20210426T064354.12Z.

Since months complicate all calculation and are irrelevant to geophysics, we strongly suggest avoiding them and instead using what the ISO calls an ordinal date, using day of year. The same point in time would then be written as 2021-116T06:43:54.12Z.

If referring to a time interval (such as time since an earthquake), choose whatever unit seems best (preferably one that can be given as a number less than 1000) and decimalize it. That is, do not do what was done above in first stating the length of the year: 365.2422 days is much better than $365^{\text{d}}6^{\text{h}}8^{\text{m}}45.2^{\text{s}}$.¹⁰

Displaying

When producing a plot of a time series, how should a time axis be labelled? Figures 1.1, 1.2, 1.3, 1.4, 2.4, 7.7, and 10.6 show our preferences, which are the following:

1. Use an actual unit of time, not (say) numbers of samples. Choose a unit, if possible, that will give a range of numbers that are relatively small, but use

⁹ $2.5 \times 10^{-6} \times 2^{32} = 107374$ s, more than a day.

¹⁰This superscripting is sometimes used to parallel with the system of sexagesimal angles; entirely appropriate, since this division of the hour was introduced by the thirteenth century by Sacrobosco in deliberate parallel with angular measurement (Nothaft, 2018).

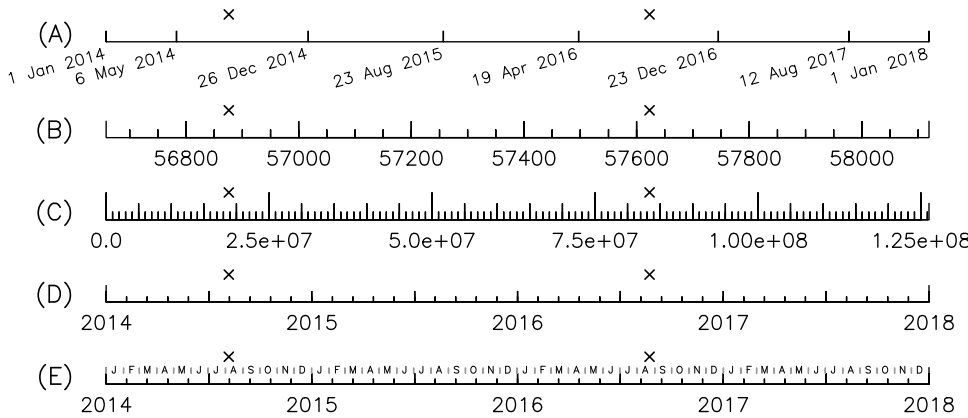


Figure D.1: Five ways of labelling the time axis on a plot of four years of data. A uses calendar dates at semiregular intervals; B uses Julian dates; C uses seconds from the start time; D uses fractional years: obtained, in this case, by $(MJD - 56658)/365.25 + 2014.00$, which is exact at the start of 2014 and makes all years the same length; and E is the same as D, with additional annotation to show the months.

only seconds, hours, days, or years. Do not use more than one unit, and if at all possible avoid months,¹¹ since the calendar month is not a time unit.

2. For observational data, include sufficient information to find the absolute time of any part of the time series shown, either by appropriate labeling or by giving the time of some obvious point within the time series, such as the start time or time of some event.
3. When providing dates, use the year and day of year.

Figure D.1 shows possible ways to label the time axis, all based on figures actually published.

The first example, labeled A, places day-month-year labels at nearly equal intervals along the time axis. We can only describe this procedure as sublimely idiotic, since it is impossible to estimate the time of any intermediate points, such as the two crosses shown on the plot. And, it requires knowledge of the English month names. This is such a poor labeling system that it could only occur by being standard within some plotting package, and unfortunately it is: the increasingly popular Python package matplotlib uses this as its default.

Examples B through D all use a uniform time unit. In B this is days, an appropriate unit; but since absolute time is given by using Modified Julian Day, un-

¹¹Unfortunately, for many long-term data sets this may not be possible because only monthly means are available, as with the sea level data shown in Figure 1.1. Cartwright (1983) discusses this now-obsolete practice.

familiar to many scientists, we would not recommend it unless you are an astronomer. In C the unit is seconds, given from the start time at the beginning of 2014: completely SI compliant, but not easy to understand without some mental arithmetic to convert to days or years. D, decimalized years, is our preferred labeling system: uniform, absolute, language-independent, and able to provide times anywhere along the series to within, probably, 0.02 year, which is 8 days. Example E shows how to annotate Example D to show months, if this is deemed important.

One final best practice for plots is not to make the plot bigger (in file size) than it needs to be. So if you have a year of data, and your time axis is 20 cm, remember that the resolution of the eye (not to mention the display system) is probably larger than 0.02 mm, so showing more than 10000 values is pointless. So in this case it would be appropriate to lowpass and decimate your data to hourly values.

APPENDIX E

ESTIMATING POWER SPECTRA: OTHER METHODS

Here are left out many things, whereof some be untrue, some uncertain, some vain and superstitious.

THOMAS CRANMER, *The Book of Common Prayer*, Preface (1549).

E.1 Introduction

As we indicated in Chapter 12, there are many methods of PSD estimation that are still in use, even though they involve overly restrictive assumptions or have worse statistical properties than the multitaper methods we described in Chapter 13. Here we summarize these methods, and briefly explain what the problems are with each one. We should say at the outset that some of these will provide a roughly valid power spectrum – it is just that they provide worse estimates than the multitaper methods. Others do not do even this: they give misleading or (in our view) meaningless results.

E.2 The Blackman-Tukey Method

In Chapter 12 we tried to create an estimation method by replacing a definition for the PSD with the equivalent expression applied to actual data. When the definition of the PSD is through the Fourier transform of the data, this results in the periodogram estimate – which, with significant modifications, is the basis for the multitaper methods. But we can also proceed from the autocovariance function: first, from the data x_n we estimate this function:

$$\hat{R}_X(n) = \frac{1}{N-n} \sum_{k=1}^{N-n} x_k x_{k+n} \quad \text{for } n = 0, 1, 2, \dots, N-1 \quad (\text{E.1})$$

and then take the DFT of this to find \hat{S}_X . This procedure, (known as the **Blackman-Tukey** method), was very popular in the early days of spectral analysis because it could be made computationally efficient: the method was to find \hat{R}_X up to some

smaller value of n (say, $n = 0, 1, 2, \dots, M$); it was then easy to compute the DFT of the resulting (short) \hat{R}_X . This was important when taking the DFT was thought to require M^2 operations, a rationale that disappeared with re-invention of the FFT in 1966. This procedure amounted to truncating the \hat{R}_X function defined in equation (E.1); a refinement of this was to taper the \hat{R}_X using some function that went from one to zero as n went from 0 to M . This taper was called a **lag window**; unlike the data tapers we have discussed, it could not be negative. [Jenkins and Watts \(1968\)](#), written just as the FFT was being introduced, has a full discussion.

This method turns out to be a very poor estimator, whether of R_X or of S_X . One problem is that the variance of the autocovariance estimate in (E.1) gets worse and worse as n increases, and these higher variances are then spread across the whole spectrum; there can easily be significant bias. It is also very difficult to find the uncertainties of these estimates. This method is almost never seen today – except in some parts of the paleoclimate literature!

E.3 Parametric Methods

Some estimation methods take the PSD to be a function that can be described by a few parameters. Spectrum estimation then becomes the task of somehow estimating these parameters, after which we declare the function described by them to be the spectrum. Procedures of this type work well if the stochastic process is indeed of the class they are designed to model, but poorly otherwise. Since you cannot know whether your process falls into the useful or useless category, we consider these methods to be unreliable. But they are popular, and often come with claims of being able to do things that the more general nonparametric methods cannot, so we discuss them here.

Many of these estimators derive from applying filter theory. Recall equation (11.22) from Chapter 11: if $X = g * Y$ then

$$S_X = |\tilde{g}|^2 S_Y$$

Suppose that you could somehow choose the filter g so that when Y is white noise, the filter output is the desired process X ; then

$$S_X(f) = c|\tilde{g}(f)|^2$$

where c is a constant. This idea is usually implemented by selecting g to be an IIR (autoregressive or AR) filter with M weights:

$$X_n = Y_n + a_1 X_{n-1} + a_2 X_{n-2} + \dots + a_M X_{n-M} \quad (\text{E.2})$$

where Y_n is a white noise. Multiplying by with X_j and taking the expectation produces the Yule-Walker equations for estimating a_j in terms of the estimated autocovariances.

We have, in Section 14.2, used just this procedure to develop the inverse, prewhitening filter that turns X into a whiter noise Y ; our aim there was to produce a series for which bias from spectral leakage will be much less of a problem in estimating the spectrum. But the aim here is somewhat different: we are also producing a filter – but then we claim that this filter response *is* the spectrum. Again, this might make sense if we knew that the spectrum came from a white-noise excitation of this kind of filter – but it is rare to know this. Even if we knew that an IIR filter was involved, we would still have to choose the order M . As we saw in Section 14.3, if the order is not correct the answer can be wrong; Figure 14.1 shows this, in particular the feature of producing peaks that are not really present. And there is no good theory to decide the correct value of M . Partly for this reason, it is very difficult to estimate the uncertainty of spectra found in this way.

There are alternatives to the Yule-Walker equations for finding the coefficients: for example, **Burg's method**, and the ever-popular but equally problematic **method of maximum entropy**. These all suffer from the same problems: the assumptions needed are too restrictive and there is no good basis for choosing the number of parameters.

E.4 Singular Spectrum Analysis

E.5 Least-squares Spectrum

APPENDIX F

COMPUTING THE DISCRETE FOURIER TRANSFORM

F.1 Introduction

As we noted in Chapter 5, the nominal form of the Discrete Fourier Transform (equation 5.20), which is

$$\tilde{x}_k = \sum_{n=0}^{N-1} x_n e^{-2\pi i n k / N} \quad \text{for } k = 0, \dots, N-1$$

does not well express how to actually perform the computation. First of all, as noted in that chapter, we would first compute the exponents using $e^{2\pi i n k / N} = e^{-2\pi i (nk)_{\text{mod}N}/N}$; then the formula above would imply doing N “operations” (additions and multiplications) to get a single \tilde{x}_k – and we would then do this N times to get all the DFT values, for a total of N^2 operations. The Fast Fourier Transform gives us the same result with many fewer operations.

F.2 The Basis of the Fast Fourier Transform

Gauss developed the first FFT algorithm in 1805, though it was only published posthumously in 1866, and not noticed even then (Heideman et al., 1985). It turns out to be the same as the first FFT widely used, the Cooley-Tukey algorithm, if it is updated to use complex exponentials.

The key to the FFT is that N , the series length, has to be a composite integer, so that we can write $N = N_1 N_2$, where N_1 and N_2 are both integers. We will show how to compute the DFT in fewer operations for this case; then we will assume that N_1 is also composite, apply the same procedure, and continue until we run out of factors. The simplest algorithm is for all the composite factors of N to be equal and as small as possible – which happens when N is a power of two.

We divide the N -length sequence of data x_n into N_2 sequences of length N_1 , and the N -length sequence of DFT values \tilde{x}_k into N_1 sequences of length N_2 . Then we re-index the subscripts for the two sequences as

$$n = N_2 n_1 + n_2 \quad \text{and} \quad k = k_1 + N_1 k_2 \\ \text{where } n_1, k_1 = 0, \dots, N_1 - 1 \quad \text{and} \quad n_2, k_2 = 0, \dots, N_2 - 1$$

We apply this indexing to the $e^{2\pi i n k / N}$ in the DFT expression:

$$e^{-2\pi i (k_1 n_1 N_2 + k_1 n_2) / N} e^{-2\pi i N_1 k_2 n_2 / N} e^{-2\pi i k_2 n_1}$$

and note that the last exponential is always one. Then the full DFT expression becomes

$$\tilde{x}_{k_1+N_1 k_2} = \sum_{n_2=0}^{N_2-1} \left[\sum_{n_1=0}^{N_1-1} x_n e^{-2\pi i (k_1 n_1 N_2 + k_1 n_2) / N} \right] e^{-2\pi i N_1 k_2 n_2 / N}$$

which we can write more compactly as

$$\tilde{x}_{k_1+N_1 k_2} = \sum_{n_2=0}^{N_2-1} S_{k_1 n_2} e^{-2\pi i N_1 k_2 n_2 / N}$$

where $S_{k_1 n_2}$ is the sum in brackets: we can view this as an N_1 by N_2 matrix, each of whose terms takes N_1 operations to compute.¹ Each of the columns of this matrix is just the result of performing a DFT on a sequence of length $N - 1$ to get $N - 1$ coefficients; So the total operations count to get all the elements of S is $N_1(N_1 N_2) = N_1^2 N_2$. Then to get the final result requires the second (outer) sum, multiplying the S matrix into the N_2 -length vector represented by the final exponential to get a second vector of length N_1 – which we have to do for N_2 values of k_2 . The operations count for each matrix multiplication is $N_1 N_2$; doing it N_2 times makes the total operations count for this step $N_1 N_2^2$. The total number of operations is the sum: $N_1^2 N_2 + N_2^2 N_1$; since $N = N_1 N_2$, this is

$$\frac{N^2}{N_2} + N \cdot N_2$$

which for N large and N_2 small would be less than N^2 ; for $N_2 = 2$ it would be $\frac{1}{2}N^2 + 2N$.

But now suppose that N_1 is composite, with $N_1 = N_2 N_3$, which means that $N = N_3 N_2^2$. then we can decompose each of the N_1 -length sequences in the same way, and use the same decomposition to compute each of the DFT's in S more efficiently. The total number of operations then becomes, replacing the N_1^2 term in the above,

$$N_2(N_3^2 N_2 + N_2^2 N_3) + N_2^2 N_1 = \frac{N^2}{N_2^2} + 2N_2 N$$

And finally, if $N = N_2^q$ we can do this decomposition q times, so that the total operations count is

$$\frac{N^2}{N_2^q} + q N_2 N = N(1 + q N_2)$$

Since $q = \log_{N_2} N$, the operations count scales as $N \log_{N_2} N$, or for $N_2 = 2$, $N \log_2 N$: a much smaller number than N^2 , even for N as small as 1024, 100 times smaller.

¹Actually $2N_1$ operations if we count both additions and multiplications as operations; but here and in the rest of the derivation we ignore expressions that do not depend on N .

F.3 Computing DFT's of Real Series

If we are computing the DFT of a real-valued series, we can always reduce the computation time, and storage requirements, by a factor of two. The standard definition of the DFT, which is followed by almost all FFT programs, assumes that the sequence x_n is complex. Transforming N real numbers then means transforming N complex numbers, all with imaginary parts equal to zero – and then half the output will be redundant, because the \tilde{x}_n 's will be Hermitian. While we could replace the DFT with a purely real transform, (such as the Hartley transform), this is not necessary. Instead, we represent our N real numbers as $N/2$ complex numbers, take an $N/2$ -length complex DFT, and rearrange the output to give the $N/2$ complex \tilde{x}_k 's that we want.

To do this, we combine adjacent pairs of real x_n 's to form our complex-valued sequence; we may not even have to do this explicitly, because in many computer languages (certainly FORTRAN), passing a real-valued sequence to a subroutine that expects complex numbers will automatically cause this reassignment to occur. The DFT is then

$$C_k = \sum_{n=0}^{N/2-1} (x_{2n} + ix_{2n+1})e^{-2\pi kn/M} \quad \text{for } k = 0, \dots, M-1$$

where $M = N/2$. To see what to do with the C_k 's, construct two complex-valued sequences A and B , defined by the sums

$$A_k = \sum_{n=0}^{M-1} x_{2n} e^{-2\pi ink/M} \quad B_k = \sum_{n=0}^{M-1} x_{2n+1} e^{-2\pi ink/M}$$

which means that $C_k = A_k + iB_k$. If we could find the A and B sequences, we can compute the X_k that we actually want, since

$$\begin{aligned} X_k &= \sum_{n=0}^{2M-1} x_n e^{-2\pi ink/2M} = \sum_{n=0}^{M-1} x_{2n} e^{-2\pi i2nk/2M} + \sum_{n=0}^{M-1} x_{2n+1} e^{-2\pi i(2n+1)k/2M} \\ &= A_k + e^{-\pi ik/N} B_k \quad \text{for } k = 0, \dots, N/2-1 \end{aligned}$$

To get the A 's and B 's from the C 's that we have computed with our DFT, consider

$$C_{N-k} + C_k = A_{n-k} + A_k + i(B_{N-k} + B_k)$$

Since A and B are both derived from real sequences, both are Hermitian, with $A_{N-k} = A_k^*$ and $B_{N-k} = B_k^*$. Therefore,

$$C_{N-k} + C_k = 2\Re[A_k] + 2i\Im[B_k]$$

which means that

$$\Re[A_k] = \frac{1}{2}\Re[C_{N-k} + C_k] \quad \Im[B_k] = \frac{1}{2}\Im[C_{N-k} + C_k]$$

and similarly,

$$\mathcal{I}[A_k] = \frac{1}{2}\mathcal{I}[C_k - C_{N-k}] \quad \mathcal{I}[B_k] = -\frac{1}{2}\mathcal{R}[C_k - C_{N-k}]$$

So, by computing first C then A and B , and finally X , we have achieved our aim. We can get slightly greater efficiency using DFT algorithms specifically designed to handle real sequences (or, for the inverse transform, Hermitian ones), though the improvements are not large enough to be important unless you plan to do a lot of transforms; [Sorensen et al. \(1987\)](#) give both algorithms and comparisons.

F.4 Computing the Fourier Transform for a Few Frequencies

Finally, suppose we want to compute, instead of the DFT coefficients, the transform $\tilde{x}(f)$ for arbitrary f :

$$\tilde{x}(f) = \sum_{n=0}^{N-1} x_n e^{-2\pi i f n} \tag{F.1}$$

Certainly you might imagine (correctly) that even for the DFT case, where $f = k/N$, that the FFT will not be the most efficient procedure if we only want a few values of f . But again, we do not need to do the sum as written; by using a recursive method known as the **Goertzel algorithm** we need to compute only one trigonometric function for each frequency.

We define a series of sums:

$$U_k(f) = \frac{1}{\sin 2\pi f} \sum_{n=k}^{N-1} x_n \sin 2\pi f [n - (N - k) + 1] \quad \text{for } k = 1, \dots, N$$

and set $U_0 = U_{-1} = 0$. Then the difference between the final sum and the penultimate one, multiplied by $e^{2\pi i f}$ turns out to be the Fourier transform we seek:

$$\begin{aligned} & U_N(f) - e^{2\pi i f} U_{N-1}(f) \\ &= \frac{1}{\sin 2\pi f} \left[\sum_{n=0}^{N-1} x_n \sin 2\pi(n+1)f - \cos 2\pi f \sum_{n=1}^{N-1} x_n \sin 2\pi n f \right] - i \sum_{n=1}^{N-1} x_n \sin 2\pi n f \\ &= x_0 + \frac{1}{\sin 2\pi f} \left[\sum_{n=1}^{N-1} x_n (\sin 2\pi n f \cos 2\pi f + \cos 2\pi n f \sin 2\pi f - \cos 2\pi f \sin 2\pi n f) \right] \\ &\quad - i \sum_{n=1}^{N-1} x_n \sin 2\pi n f \\ &= x_0 + \sum_{n=1}^{N-1} x_n (\cos 2\pi n f - i \sin 2\pi n f) = \sum_{n=1}^{N-1} x_n e^{-2\pi i n f} \end{aligned}$$

The point of all this is that we can compute the U_k 's recursively, and need to compute only one cosine, once, to do so. As above, we start with the answer and show that it gives the result we wish. Take

$$\begin{aligned} & x_{N-k} + 2U_{k-1} \cos[2\pi f - U_{k-2}] \\ &= x_{N-k} + \frac{1}{\sin 2\pi f} \sum_{N-k+1}^{N-1} x_n [2 \cos[2\pi f \sin 2\pi(n-N+k)f] \\ &\quad - \sin[2\pi(n-N+k-1)f]] \end{aligned}$$

A general expression for the trigonometric functions is

$$2 \cos u \sin[(m-1)u] - \sin[(m-2)u] = \sin^m u$$

which, applied to the sum in F.4, gives

$$\begin{aligned} & x_{N-k} + 2U_{k-1} \cos[2\pi f - U_{k-2}] \\ &= x_{N-k} + \frac{1}{\sin 2\pi f} \sum_{N-k+1}^{N-1} x_n \sin[2\pi(n-N+k+1)] \\ &= \frac{1}{\sin 2\pi f} \sum_{N-k}^{N-1} x_n \sin[2\pi(n-(N-k)+1)] \\ &= U_k \end{aligned}$$

a recursion that allows us to find $U_1, U_2 \dots U_N$ in N real multiplications and $2N$ real additions; and once we have the U_{N-1} and U_N , we can find $\tilde{x}(f)$.

One difficulty with this approach is that, for values of f near 0 or $\frac{1}{2}$, it can be inaccurate because of roundoff (Gentleman, 1969). For example, for $f = 0$, the recursion becomes

$$\begin{aligned} U_1 &= x_{N-1} \\ U_2 &= x_{N-2} + 2x_{N-1} \\ U_3 &= x_{N-3} + 2x_{N-2} + 3x_{N-1} \\ &\dots \end{aligned}$$

Finally, we would compute $\tilde{x}(0) = U_N - U_{N-1}$ by differencing two numbers that are potentially very large: this is a sure invitation to roundoff error. There is however a simple solution to this: define $\Delta U_k = U_k - U_{k-1}$. Then the recursion in terms of ΔU is

$$\begin{aligned} \Delta U_k &= U_k - U_{k-1} = x_{N-k} + 2(\cos 2\pi f - 1)U_{k-1} - U_{k-2} + U_{k-1} \\ &= x_{N-k} + 2(\cos 2\pi f - 1)U_{k-1} + \Delta U_{k-1} \end{aligned}$$

and the expression for $\tilde{x}(f)$ is

$$X(f) = \Delta U_N - (\cos 2\pi f - 1)U_{N-1} - i(\sin 2\pi f)U_{N-1}$$

Now, for f small, $\cos 2\pi f - 1$ becomes small, and the recursion and its final processing become numerically stable.

There is a similar problem with the original recursion for f close to $\frac{1}{2}$; for $f = \frac{1}{2}$ the original recursion is for which the original recursion gives

$$\begin{aligned} U_1 &= x_{N-1} \\ U_2 &= x_{N-2} - 2x_{N-1} \\ U_3 &= x_{N-3} - 2x_{N-2} - 3x_{N-1} \\ &\dots \end{aligned}$$

which again means (potentially) differencing large numbers. The cure is again to define a new quantity (for which we use the same notation):

$$\Delta U_k = U_k + U_{k-1}$$

in terms of which the recursion becomes

$$\Delta U_k = x_{N-k} + 2(\cos 2\pi f + 1)U_{k-1} - \Delta U_{k-1}$$

and the final step becomes

$$X(f) = \Delta U_N - (\cos 2\pi f + 1)U_{N-1} - (-i(\sin 2\pi f)U_{N-1})$$

The need for three recursions complicates the process somewhat, but not so much so as to render this method unattractive for special purposes.

APPENDIX G

TAPERS FOR SPECTRUM ESTIMATION: THE DETAILS

Tapered curves have gained such wide use that it is needless to dwell at length on their advantages.

LEE PERKINS The Railroad Taper (1915)

G.1 Slepian Tapers

As explained in Section 13.2, these tapers maximize the functional $\mathcal{N}[w]$ that expresses the concentration of the Fourier transform inside a given band; this concentration was defined by equation (13.1), which we repeat here for convenience:

$$\mathcal{N}[w] = \frac{\int_{-F}^F |\tilde{w}(f)|^2 df}{\int_{-\infty}^{\infty} |\tilde{w}(f)|^2 df} \quad L[w] = 1 - \mathcal{N}[w]$$

To remove the normalization of the total power, we simply set it to unity as a side condition. Then we introduce a Lagrange multiplier μ and look for stationary points of the functional

$$U[w] = \int_{-F}^F \tilde{w}(f) \tilde{w}(f)^* df - \mu \int_{-\infty}^{\infty} \tilde{w}(f) \tilde{w}(f)^* dt \quad (\text{G.1})$$

To solve this we need to introduce the parent function $w(t)$, whose Fourier transform is $\tilde{w}(f)$, along with the fact that w vanishes outside $(-T/2, T/2)$. We use Parseval's theorem for the second term in equation (G.1):

$$\int_{-\infty}^{\infty} \tilde{w}(f) \tilde{w}(f)^* df = \int_{-T/2}^{T/2} w(t)^2 dt \quad (\text{G.2})$$

Then we insert equation (G.2) and the definition of \tilde{w} , namely,

$$\tilde{w}(f) = \int_{-T/2}^{T/2} e^{-2\pi i f t} w(t) dt$$

into equation (G.1) and get:

$$\begin{aligned} U[w] &= \int_{-F}^F df \int_{-T/2}^{T/2} e^{-2\pi ift} w(t) dt \int_{-T/2}^{T/2} e^{2\pi ift'} w(t') dt' - \mu \int_{-T/2}^{T/2} w(t)^2 dt \\ &= \int_{-T/2}^{T/2} dt \int_{-T/2}^{T/2} dt' w(t) w(t') \int_{-F}^F e^{-2\pi if(t-t')} df - \mu \int_{-T/2}^{T/2} w(t)^2 dt \quad (\text{G.3}) \\ &= \int_{-T/2}^{T/2} \int_{-T/2}^{T/2} w(t) w(t') \frac{\sin 2\pi F(t-t')}{2\pi(t-t')} dt dt' - \mu \int_{-T/2}^{T/2} w(t)^2 dt \end{aligned}$$

This equation is a Hilbert-space equivalent of the one you have encountered for the principal axes of inertia, to maximize the moment of inertia, I . We can use a more abstract notation to write equation (G.3) as

$$U[w] = (w, \mathcal{K}w) - \mu(w, w) \quad (\text{G.4})$$

where the linear operator \mathcal{K} on $L_2(-T/2, T/2)$ is

$$(\mathcal{K}w)(t) = \int_{-T/2}^{T/2} \text{sinc}[2(t-t')]w(t')dt'$$

The stationary points of equation (G.4) are obtained by differentiating with respect to w .¹ The result for equation (G.4) is that we seek the solution to the eigenvalue equation:

$$\mathcal{K}w = \mu w$$

or, explicitly,

$$\int_{-T/2}^{T/2} \frac{\sin 2\pi F(t-t')}{2\pi(t-t')} u_n(t') dt' = \mu_n u_n(t), \quad \text{for } |t| \leq T/2, n = 0, 1, 2, \dots \quad (\text{G.5})$$

where the eigenvalues are μ_n and the corresponding eigenfunctions are $u_n(t)$. The eigenvalues of the system correspond to concentration factors \mathcal{N} in equation (13.1) for the appropriate eigenfunction. The largest eigenvalue, μ_0 , gives the largest concentration (lowest leakage); so the corresponding eigenfunction u_0 is the taper with the most concentrated Fourier transform for the specified values of F and T .

Before describing some of the remarkable properties of the solutions to equation (G.5), we make a change of variables to remove the apparent dependence on the two parameters T and F , so that we can parameterize the complete family of solutions with a single dimensionless number. We let $x = 2t/T$, $y = 2t'/T$, and $p = FT$; then equation (G.5) becomes

$$\int_{-1}^1 \frac{\sin \pi p(x-y)}{\pi(x-y)} \psi_n(y) dy = \mu_n \psi_n(x) \quad \text{for } |x| \leq 1 \quad (\text{G.6})$$

¹Such differentiation with respect to a function is called **Gateaux differentiation**.

with $u_n(t) = \psi_n(2t/T)$; this gives equation (13.2) in Section 13.2.²

Choosing the bandwidth F fixes p , which is called the **time-bandwidth product**. As we mentioned in Section 13.2 we cannot expect to get good concentration into a frequency band narrower than $1/T$, and in practice we always choose $p \geq 1$,

It can be proved there are infinitely many distinct, real, positive eigenvalues, with the property

$$1 > \mu_0 > \mu_1 > \mu_2 > \dots \quad (\text{G.7})$$

and as $n \rightarrow \infty$, $\mu_n \rightarrow 0$. Since the concentration function $\mathcal{N}[\psi_n] = \mu_n$, the first eigenfunction, ψ_0 is the taper whose Fourier transform is the most concentrated for whatever p we have chosen. A general property of a self-adjoint eigensystem like equation (13.2) is that the eigenfunctions are mutually orthogonal on $(-1, 1)$:

$$\int_{-1}^1 \psi_m(x)\psi_n(x)dx = 0 \quad \text{for } m \neq n$$

and so we may use the corresponding tapers to produce independent spectral estimates (Section 13.3).

A result that is not so general is that the values in equation (G.7) do not decrease uniformly as n increases. For values of n below a threshold that is proportional to p , the spectral concentration \mathcal{N} , which is the same as the eigenvalue μ_n , will be close to one, and the leakage $L = 1 - \mu_n$ will be small. Above this threshold the eigenvalues (and the concentration) all have very small values, so the leakage L will be large – so the taper would be useless for avoiding bias. Figure 13.3 shows how $m\mu_n$ depends on p for $0 \leq n \leq 12$ – though what we plot there is actually $1 - \mu_n$, on a log scale. As n increases, equation (G.7) states that μ_n will decrease, so $1 - \mu_n$ will increase – as it does. In this plot, for n below the threshold value, $1 - \mu_n$ is close to zero; for larger n , it is close to one (0 dB). The plot suggests that $n = 2p$ is an adequate approximation for this threshold – though as we discuss in Section 13.2, we will want to choose a lower value of n to reduce possible leakage.

One remarkable property of these tapers is that $\tilde{\psi}_0$, the Fourier transform of ψ_0 , is equal to a constant times $\psi_0(2\pi f/p)$, that is, a stretched version of the original function; when the argument of the stretched function is outside $(-1, +1)$, we simply use the left side of equation (13.2) to extend it! And the relationship is the same between ψ_n and $\tilde{\psi}_n$.

There are hosts of other properties – Percival and Walden (1993) list eight on pages 79-80, but they do not explain why the functions ψ_n are called the **prolate spheroidal wavefunctions**. The reason hardly obvious: the self-adjoint integral operator in equation (13.2) commutes with a second-order differential operator that describes wave motion in prolate spheroidal coordinates! Commuting operators share eigenfunctions, hence the name. And in fact, computation of ψ_n

²This is very nearly equation (33) of Percival and Walden (1993), but in a slightly more readable notation.

is greatly facilitated by this commutation. As noted in Section 13.2 we use the simpler name **Slepian functions**.

So far we have looked at the theory only for continuous time and -frequency – so all these results, including equation (13.1), which motivates the whole idea, are only approximations to the theory for a discrete time series of finite length. The exact theory for this case looks almost exactly like the results for continuous time, except that we need to introduce one more parameter, namely the number of points in the time domain. We would use this theory when we want the most exact results for an actual computation.

As you will appreciate by consulting [Percival and Walden \(1993\)](#) there is much that we have not covered, for example how to calculate the tapers. For the discrete-time case the solution of the matrix eigensystem can be formulated as a three-term recurrence scheme, like the one used for computing spherical harmonics. Then the computation time rises only as N , the number of points, not N^3 as a naive approach would give, which makes these tapers computable even for very large N . The Matlab Signal Processing Toolbox provides code for computing the Slepian functions; a Fortran package that includes them as part of a multitaper estimation package is [Prieto et al. \(2009\)](#), and they are included in Parker's spectral estimation program PSD.

APPENDIX H

THE DURBIN-LEVINSON ALGORITHM

As noted in Section 14.2, we find the weights of the filter used for prewhitening (the prediction-error filter) by solving the matrix equation (14.7). This can be done with the usual matrix methods, but because the matrix \mathbf{R} is Toeplitz there is a more efficient method available, the Durbin-Levinson algorithm; this proceeds iteratively, at each step using the weights for the prediction filter of one order to compute those for the next. For prewhitening filters, for which the order M is small, there is little gain in using this method compared to more general inversion procedures; if M is large, the Durbin-Levinson algorithm is preferable.

To show how it works, we assume that we have weights a_m^M which satisfy the matrix equation $\mathbf{R}^M = \mathbf{C}^M \mathbf{a}^M$ where \mathbf{R}^M , \mathbf{C}^M , and \mathbf{a}^M are as defined just after equation (14.7); introducing the vectors $\mathbf{S}^M = (R_M, R_{M-1}, \dots, R_1)^T$ (note the reverse order) and $\mathbf{a}^{M+1} = (a_1^{M+1}, a_2^{M+1}, \dots, a_M^{M+1})^T$, we can write the matrix equation for order $M+1$ in partitioned form as

$$\left(\begin{array}{c|c} \mathbf{C}^M & \mathbf{S}^M \\ \hline \mathbf{S}^M & R_0 \end{array} \right) \left(\begin{array}{c} \mathbf{a}^{M+1} \\ a_{M+1}^{M+1} \end{array} \right) = \left(\begin{array}{c} \mathbf{R}^M \\ R_{M+1} \end{array} \right) \quad (\text{H.1})$$

Next, we write the predictor weights for order $M+1$ as $a_m^{M+1} = a_m^M - a_{M+1}^{M+1} t_m$, where the t_m 's are for now undefined; if we write these as a vector, $\mathbf{T} = (t_1, t_2, \dots, t_M)^T$, equation (H.1) becomes

$$\left(\begin{array}{c|c} \mathbf{C}^M & \mathbf{S}^M \\ \hline \mathbf{S}^M & R_0 \end{array} \right) \left(\begin{array}{c} \mathbf{a}^M - a_{M+1}^{M+1} \mathbf{T} \\ a_{M+1}^{M+1} \end{array} \right) = \left(\begin{array}{c} \mathbf{R}^M \\ R_{M+1} \end{array} \right) \quad (\text{H.2})$$

The part of this that comes from the first M rows of \mathbf{C}^M gives:

$$\mathbf{C}^M \mathbf{a}^M - a_{M+1}^{M+1} \mathbf{C}^M \mathbf{T} + a_{M+1}^{M+1} \mathbf{S}^M = \mathbf{R}^M \quad (\text{H.3})$$

the first and last terms of which vanish because $\mathbf{C}^M \mathbf{a}^M = \mathbf{R}^M$; but then equation (H.3) becomes

$$\mathbf{C}^M \mathbf{T} = \mathbf{S}^M \quad (\text{H.4})$$

If $t_m = a_{M+1-m}^M$, then the Toeplitz form of \mathbf{C}^M means that (H.4) would be just a permutation of equation (14.7); we thus have \mathbf{T} , and can write all but the last of the prediction weights for order $M+1$ as

$$a_m^{M+1} = a_m^M - a_{M+1}^{M+1} a_{M+1-m}^M \quad (\text{H.5})$$

It now remains to find a_{M+1}^{M+1} . To do this we write the rest of the matrix equation (H.2) as:

$$\mathbf{S}^M(\mathbf{a}^M - a_{M+1}^{M+1}\mathbf{T}) + a_{M+1}^{M+1}R_0 = R_{M+1}$$

whence

$$a_{M+1}^{M+1} = \frac{R_{M+1} - \sum_{m=1}^M a_m^M R_{M+1-m}}{R_0 - \sum_{m=1}^M a_m^M R_m} = \frac{R_{M+1} - \sum_{m=1}^M a_m^M R_{M+1-m}}{P^M} \quad (\text{H.6})$$

where we have used equation (14.6). We use P^M in the denominator because we can form successive values of it without actually computing the sum in equation (14.6), which makes the procedure less affected by roundoff. We have

$$\begin{aligned} P^{M+1} &= R_0 - \sum_{m=1}^{M+1} a_m^{M+1} R_m \\ &= R_0 - \sum_{m=1}^M (a_m^M - a_{M+1}^{M+1} a_{M+1-m}^M) R_m - a_{M+1}^{M+1} R_{M+1} \\ &= R_0 - \sum_{m=1}^M a_m^M R_m - a_{M+1}^{M+1} \left(- \sum_{m=1}^M a_{M+1-m}^M R_m + R_{M+1} \right) \\ &= P^M - a_{M+1}^{M+1} (a_{M+1}^{M+1} P^M) = P^M \left[1 - (a_{M+1}^{M+1})^2 \right] \end{aligned} \quad (\text{H.7})$$

The Durbin-Levinson algorithm starts by setting $P^0 = R_0$, and $a_1^1 = R_1/R_0$; we then iterate, going from equation (H.7) to get the next value of P , to equation (H.6) to compute the next value of a_{M+1}^{M+1} , then using equation (H.5) to find the other prediction coefficients – and finally back to equation (H.7).

As noted in the main text, it is not true that the Durbin-Levinson algorithm has less numerical stability than other matrix inversion methods; Cybenko (1980) has shown that this algorithm is as numerically stable as most others – the problem is that, when computing prewhiteners, the Durbin-Levinson algorithm is often being applied to very ill-conditioned matrices.

APPENDIX I

OTHER READING

I.1 Introduction

There are many books that cover different aspects of this course, but none that provide the mix we think most useful. As might be expected from the origins of the field (Section 1.3), there is a disciplinary division: books for engineers focus on signal processing but pay less attention to estimation, and books by statisticians do the reverse. We list some of our favorites in both categories, some are textbooks and some reference monographs.

I.2 Linear Systems and Fourier Analysis

[Pippard \(1978\)](#) gives a particularly detailed and readable discussion of one class of linear system: the damped oscillator (or sets of oscillators), including a number of interesting ways of looking at the Fourier transform. Books on the Fourier transform differ substantially in their level of mathematical rigor. The two least rigorous are [James \(1995\)](#), and the much more complete [Bracewell \(1965\)](#), which is probably the best book on Fourier theory for non-mathematicians. We have followed its emphasis on getting a “feel” for transforms and being able to visualize the connection between the time and frequency domains; its lengthier discussion well illustrates the ubiquity of Fourier transforms in a wide range of topics, though most are from electrical engineering. There are several later editions, though the only changes are in a discussion of the Hartley transform, about which the author is, we think, overenthusiastic.

A more rigorous treatment is [Champeney \(1987\)](#), which describes the Fourier theorems with due attention to what kinds of functions they apply to and what the integrals really mean, though results are given rather than proved. [Korner \(1988\)](#) is a collection of anecdotes, theorems and applications, mostly to do with Fourier analysis; many of the essays can be read in isolation from the rest of the book. It provides an entertaining look at some mathematical culture. [Lighthill \(1958\)](#) is a brief, elegant, readable, and rigorous exposition of some of Fourier analysis and its connection with generalized functions; if you want to see the proofs done right, but readably, this is the place to look. For the mathematically inclined [Dym and McKean \(1972\)](#) treat the subject with modern notation, and full rigor but

in a lively style. They show lots and lots of unexpected applications ranging from differential equations to the Prime Number Theorem. They do not make any use of generalized functions.

I.3 Digital Signal Processing

Since digital signal processing is now used in devices ranging from satellites to washing machines, it has a huge literature; because this subject is a standard course for electrical engineers, many authors have tried their hands at textbooks. Perusal of the relevant classification number (TK5102.9) in the library catalog will reveal dozens of books, all with similar content, though at levels ranging from introductions for computer musicians to detailed treatments for graduate-level engineers. Many of these books address issues of finite word length and computational efficiency that, while of considerable engineering importance, are rarely relevant to data analysis. Most of these books also include a section on spectrum analysis, but rarely do justice to the statistical questions involved.

Two basic introductions, both of which avoid the common assumption that the reader is an electrical engineer, are [Scherbaum \(2001\)](#), aimed at seismologists but not very complete, and [Steiglitz \(1996\)](#), aimed at people doing computer music. An older, somewhat idiosyncratic, but still useful book is [Hamming \(1983\)](#), which provides a very readable discussion of common stumbling blocks, and shows how to view such operations as numerical integration as digital filters.

[Oppenheim and Schafer \(1989\)](#) is a standard introductory textbook, with probably all the information that you are likely to ever need, presented in a way that shows the authors' command of the subject and how to teach it. It is much more detailed than the books just mentioned; and does assume some familiarity with continuous-time theory and (in places) an electrical-engineering background. We have followed its notation as much as possible.

Signal processing in exploration geophysics has very different goals and standards from the rest of the field. [Robinson and Treitel \(1980\)](#), by two of the founders of the subject, begins at a very basic level, but can be quite advanced in the later chapters, which tend to focus on special topics the authors happen to be interested in.

I.4 Probability and Statistics

Statistics is even more ubiquitous in modern science than signal processing, so there are an even more enormous number of books on how to analyze data, for specialities from forestry to finance – and varying in mathematical level from the extremely elementary to the very advanced. We can only offer a few suggestions.

Dekking *et al.* (2005) is a relatively elementary introduction but covers a broad range of topics: its large number of problems with solutions make it useful for self-study. Hogg and Tanis (2000) is a good example of a relatively sophisticated introductory statistics textbook. the basic areas. We prefer Rice (1995) (now out of print; Rice (2006) is not, but is stunningly expensive); this takes a somewhat different viewpoint, perhaps more up-to-date. Sivia (1996) is a good introduction to statistical analysis with a different flavor than others, namely the Bayesian approach, which is becoming more and more popular. Evans *et al.* (2000) is a handy reference on univariate probability density functions, with plots, summary information, and instructions on how to generate random variates.

More of a reference work, though still containing exercises, and laid out fairly didactically, are the books by Stuart and Ord (1991, 1994), which are called *Kendall's Advanced Theory of Statistics* because they are descendants of *The Advanced Theory of Statistics*, by M. Kendall and Stuart. The treatment is not what modern mathematicians would call advanced, but it is very thorough: you can expect to find a discussion of almost any topic. The sections on inference are quite readable, though probably better read after you have had some experience than as an introduction.

Wall and Jenkins (2012) introduces a variety of statistical methods for astronomical data – many of which, because astronomy and geophysics are both observational sciences, are often useful for geophysicists. The focus of the second edition has moved much more towards Bayesian methods; though the book is quite well-written, it is aimed more at the practitioner who wants to learn methods than at students learning the subject for the first time.

I.5 Time Series and Spectral Estimation

Jenkins and Watts (1968) was an early and standard text in the field. The specific estimation methods they propose are out of date, but the theory described, both for univariate and multivariate methods, is still perfectly correct, and their chapter on statistical inference is still well worth reading. Priestley (1981) provides a careful but readable treatment of all the standard material with a nice balance between proof, discussion and illustration. This book focuses on the statistical issues, and includes some discussion of time-domain estimation. Bendat and Piersol (1986) has a strong emphasis on estimation, particularly of response functions for linear systems. The orientation is towards engineering, not statistics.

Percival and Walden (2020), an updated and expanded version of Percival and Walden (1993), is unquestionably the best single book on univariate spectral estimation. They cover stochastic processes, filtering, Fourier theory, and spectral estimation, with special emphasis on direct multitaper estimation techniques. They also cover harmonic analysis, along with the parametric spectral estimation methods we urge

you to avoid. Just about every issue gets discussed, especially in the “Comments and Extensions” that are present for many sections. The treatment is at a more mathematical level than ours, and is not always easy going; the authors have emulated the inventor of multitaper methods, Dave Thomson, in a lavish use of subscripts and superscripts. which tends to obscure the discussion.

I.6 History

As noted in Section 1.3, the subjects covered in this book come from a wide range of fields, so there is no unified history available – indeed, many topics have not been discussed by historians at all.

To start with Fourier methods, [Darrigol \(2007\)](#) provides a good description of the connections between Fourier’s work, earlier investigations into the vibrating-string problem, and the even earlier science of music. [Hewitt and Hewitt \(1979\)](#) give the the history of the most unusual result in Fourier analysis, Gibb’s phenomenon, along with some excellent simple derivations.

The engineering development of signal processing has not had much treatment. [Hoddeson \(1981\)](#) and [McGinn \(1983\)](#) describe how research was introduced into and supported by the Bell Telephone Laboratory; [Mindell \(2002\)](#), though mostly addressing the related field of control engineering, describes early work at Bell on improving signal transmission. For the later developments in digital signal processing, [Nebeker \(1998\)](#) provides a very broad overview. [Deakin \(1992\)](#) shows how the Laplace transform became the preferred approach for the analysis of linear systems. [Heideman et al. \(1985\)](#) describes the first (and uninfluential) discovery of an FFT algorithm by Gauss in 1805. How common, but un-noticed, the FFT could be is shown by its usage at SIO in the early 1960’s, when Walter Munk’s group, at IGPP, was computing a great many Fourier transforms in an inefficient way. But at the same time Philip Rudnick, at the Marine Physical Laboratory, had been using his own version of an FFT, though he appears not to have thought it important, and only published it ([Rudnick, 1966](#)) in response to Cooley and Tukey.

On the development of time series analysis as a branch of statistics, [Klein \(1997\)](#) covers the earliest era (up to about 1910) with particular focus on economic time series. [Mills \(2011\)](#) and [Mills \(2013\)](#) cover later developments, again with an emphasis on econometric methods – and a somewhat dismissive attitude towards spectral methods, as being of interest largely to physicists and engineers.

Bibliography

- Agnew, D. C. (2020), Time marks and clock corrections: A century of seismological timekeeping, *Seism. Res. Lett.*, **91**, 1417–1429, doi:10.1785/0220190284.
- Agnew, D. C., and K. M. Hodgkinson (2007), Designing compact causal digital filters for low-frequency strainmeter data, *Bull. Seismol. Soc. Am.*, **97**, 91–99.
- Alsop, L. E., and A. A. Nowroozi (1966), Faster Fourier analysis, *J. Geophys. Res.*, **71**, 5482–5483, doi:10.1029/JZ071i022p05482.
- Ardhuin, F., B. Chapron, and F. Collard (2009), Observation of swell dissipation across oceans, *Geophys. Res. Lett.*, **36**, L06,607, doi:10.1029/2008GL037030.
- Barber, N. F. (1961), *Experimental Correlograms and Fourier Transforms*, Pergamon Press, Oxford.
- Bendat, J. S., and A. G. Piersol (1986), *Random Data: Analysis and Measurement Procedures*, John Wiley, New York.
- Benjamin, D., J. M. Wahr, R. D. Ray, G. D. Egbert, and S. D. Desai (2006), Constraints on mantle anelasticity from geodetic observations, and implications for the j_2 anomaly, *Geophys. J. Int.*, **165**, 3–16, doi:10.1111/j.1365-246X.2006.02915.x.
- Bensen, G., M. Ritzwoller, M. Barmin, A. Levshin, F. Lin, M. Moschetti, N. Shapiro, and Y. Yang (2007), Processing seismic ambient noise data to obtain reliable broad-band surface wave dispersion measurements, *Geophys. J. Int.*, **169**, 1239–1260, doi:10.1111/j.1365-246X.2007.03374.x.
- Berger, J., D. C. Agnew, R. Parker, and W. Farrell (1979), Seismic system calibration: 2. Cross-spectral calibration using random binary signals, *Bull. Seismol. Soc. Am.*, **69**, 271–288.
- Bracewell, R. (1965), *The Fourier Transform and Its Applications*, 378 pp., McGraw-Hill, New York.
- Bracewell, R. (1986), *The Fourier Transform and its Applications*, McGraw-Hill, New York.
- Bracewell, R. N. (1956), Strip integration in radio astronomy, *Austral. J. Phys.*, **9**, 198–217.

- Brocher, T. M. (2005), Empirical relations between elastic wavespeeds and density in the earth's crust, *Bull. Seismol. Soc. Am.*, **95**, 2081–2092.
- Campbell, G. A. (1928), The practical application of the Fourier integral, *Bell Sys. Tech. J.*, **7**, 639–707, doi:10.1002/j.1538-7305.1928.tb00347.x.
- Cartwright, D. E. (1983), On the smoothing of climatological time series, with application to sea-level at Newlyn, *Geophys. J. Roy. Astron. Soc.*, **75**, 639–658, doi:10.1111/j.1365-246X.1983.tb05003.x.
- Champeney, D. C. (1987), *A Handbook of Fourier Theorems*, 184 pp., Cambridge University Press, New York.
- Clayton, A. (2021), *Bernoulli's Fallacy: Statistical Illogic and the Crisis of Modern Science*, 346 pp., Columbia University Press, New York.
- Cohen, M. B., R. K. Said, and U. S. Inan (2010), Mitigation of 50 and 60 Hz power line interference in geophysical data, *Radio Sci.*, **45**, 1–12, doi:10.1029/2010RS004420.
- Constable, C. G., and R. L. Parker (1988), Statistics of the geomagnetic secular variation for the past 5 m. y., *J. Geophys. Res.*, **93**, 11,569–11,581.
- Cooley, J. W., and J. W. Tukey (1965), An algorithm for the machine computation of complex Fourier series, *Math. Comput.*, **19**, 297–301, doi:10.2307/2003354.
- Currie, L. A. (2004), The remarkable metrological history of radiocarbon dating [III], *J. Res. Nat. Inst. Stand. Tech.*, **109**, 185–217, doi:10.6028/jres.109.013.
- Cybenko, G. (1980), The numerical stability of the Levinson-Durbin algorithm for Toeplitz systems of equations, *SIAM J. Sci. Stat. Comput.*, **1**, 303–319.
- Darrigol, O. (2007), The acoustic origins of harmonic analysis, *Arch. Hist. Exact Sci.*, **61**, 343–424, doi:10.1007/s00407-007-0003-9.
- Deakin, M. A. B. (1992), The ascendancy of the Laplace Transform and how it came about, *Arch. Hist. Exact Sci.*, **44**, 265–286.
- Dekking, F. M., C. Kraaijkamp, H. P. Lopuhaä, and L. E. Meester (2005), *A Modern Introduction to Probability and Statistics: Understanding Why and How*, Springer, London.
- Dym, H., and H. P. McKean (1972), *Fourier Series and Integrals*, Academic Press, New York.
- Egbert, G. D., and J. R. Booker (1986), Robust estimation of geomagnetic transfer functions, *Geophys. J. Roy. Astron. Soc.*, **87**, 173–194.

- Egbert, G. D., R. D. Ray, and B. G. Bills (2004), Numerical modeling of the global semidiurnal tide in the present day and in the last glacial maximum, *J. Geophys. Res.*, **109**(C3), C03003, doi:10.1029/2003JC001973.
- Evans, M., N. Hastings, and J. B. Peacock (2000), *Statistical Distributions*, Wiley, New York.
- Fox, C., and D. Hayes (1985), Quantitative methods for analyzing the roughness of the seafloor, *Rev. Geophys.*, **23**, 1–48, doi:10.1029/RG023i001p00001.
- Gamble, T. D., J. Clarke, and W. M. Goubau (1979), Magnetotellurics with a remote magnetic reference, *Geophys.*, **44**, 53–68.
- Gentleman, W. M. (1969), An error analysis of Goertzel's (Watt's) algorithm, *Comput. J.*, **12**, 160–165.
- Gross, R. S. (2015), Earth rotation variations: Long period, in *Treatise on Geophysics: Geodesy*, edited by T. A. Herring, pp. 215–261, Elsevier, New York, doi:10.1016/B978-0-444-53802-4.00059-2.
- Haigh, I. D., et al. (2020), The tides they are a-changin': A comprehensive review of past and future nonastronomical changes in tides, their driving mechanisms, and future implications, *Rev. Geophys.*, **58**, e2018RG000,636, doi: 10.1029/2018RG000636.
- Hamming, R. W. (1983), *Digital Filters*, Prentice-Hall, Englewood Cliffs.
- Harris, F. J. (1976), On the use of windows for harmonic analysis with the discrete Fourier transform, *Proc. IEEE*, **66**, 51–83.
- Heideman, M. T., D. H. Johnson, and C. S. Burrus (1985), Gauss and the history of the Fast Fourier Transform, *Arch. Hist. Exact Sci.*, **34**, 265–277.
- Hewitt, E., and R. Hewitt (1979), The Gibbs-Wilbraham phenomenon: an episode in Fourier analysis, *Arch. Hist. Exact Sci.*, **21**, 129–169.
- Hoddeson, L. (1981), The emergence of basic research in the Bell Telephone system, 1875–1915, *Tech. Cult.*, **22**, 512–544, doi:10.2307/3104388.
- Hogg, R. V., and E. A. Tanis (2000), *Probability and Statistical Inference*, Prentice-Hall, Upper Saddle River N.J.
- James, J. F. (1995), *A Student's Guide to Fourier Transforms: With Applications in Physics and Engineering*, 131 pp., Cambridge University Press, New York.
- Jenkins, G. M., and D. G. Watts (1968), *Spectral Analysis and its Applications*, 525 pp., Holden-Day, San Francisco.

- Kaiser, J. F., and W. A. Reed (1977), Data smoothing using low-pass digital filters, *Rev. Sci. Instrum.*, **48**, 1447–1454.
- Kaiser, J. F., and W. A. Reed (1978), Bandpass (bandstop) digital filter design routine, *Rev. Sci. Instrum.*, **49**, 1103–1106.
- Kass, R. E. (2011), Statistical inference: The big picture, *Statistical Science*, **26**, 1–9, doi:10.1214/10-STS337.
- Klein, J. L. (1997), *Statistical Visions in Time: A History of Time Series Analysis, 1662-1938*, 345 pp., Cambridge University Press, New York.
- Koen, C. (2006), The Nyquist frequency for irregularly spaced time-series: a calculation formula, *Mon. Not. Roy. Astron. Soc.*, **371**, 1390–1394, doi:10.1111/j.1365-2966.2006.10762.x.
- Korner, T. W. (1988), *Fourier Analysis*, Cambridge University Press, Cambridge.
- Lambeck, K. (1988), *Geophysical Geodesy*, Clarendon Press, Oxford.
- Langel, R., G. Ousley, J. Berbert, J. Murphy, and M. Settle (1982), The MAGSAT mission, *Geophys. Res. Lett.*, **9**, 243–245, doi:10.1029/GL009i004p00243.
- Lighthill, M. J. (1958), *Fourier Analysis and Generalized Functions*, 79 pp., Cambridge University Press, Cambridge.
- McCarthy, D. D., and P. K. Seidelmann (2018), *Time: From Earth Rotation to Atomic Physics*, Cambridge University Press, New York, doi:10.1017/9781108178365.
- McGinn, R. E. (1983), Stokowski and the Bell Telephone Laboratories: Collaboration in the development of high-fidelity sound reproduction, *Tech. Cult.*, **24**, 38–75, doi:10.2307/3104169.
- Menard, H. W. (1986), *The Ocean of Truth*, Princeton University Press, Princeton.
- Mills, T. C. (2011), *The Foundations of Modern Time Series Analysis*, 461 pp., Palgrave Macmillan, Basingstoke.
- Mills, T. C. (2013), *A Very British Affair: Six Britons and the Development of Time Series Analysis During the 20th Century*, 451 pp., Palgrave Macmillan, Basingstoke.
- Mindell, D. A. (2002), *Between Human and Machine: Feedback, Control, and Computing Before Cybernetics*, 439 pp., Johns Hopkins University Press, Baltimore.

- Nebeker, F. (1998), *Fifty Years of Signal Processing: The IEEE Signal Processing Society and its Technologies 1948-1998*, 58 pp., IEEE History Center, Hoboken, NJ.
- Nothaft, C. P. E. (2018), *Scandalous Error: Calendar Reform and Calendrical Astronomy in Medieval Europe*, 384 pp., Oxford University Press, Oxford.
- Oglesby, L. C. (2005), *The Salton Sea: Geology, History, Potential Problems, Politics, and Possible Futures of an Unnatural Desert Salt Lake*, Southern California Academy of Sciences, Los Angeles.
- Oppenheim, A. V., and R. W. Schafer (1989), *Discrete-time Signal Processing*, Prentice Hall, Englewood Cliffs, N.J.
- Orchard, H. J., and A. N. Willson (2003), On the computation of a minimum-phase spectral factor, *IEEE Trans. Circuits Systems I*, **50**, 365–375.
- Parker, P. R., M. A. Zumberge, and R. L. Parker (1995), A new method of fringe-signal processing in absolute gravity meters, *Manuscr. Geod.*, **20**, 173–181.
- Parker, R., and M. S. O'Brien (1997), Spectral analysis of vector magnetic field profiles, *J. Geophys. Res.*, **102**, 24,815–24,824, doi:10.1029/97JB02130.
- Percival, D. B., and A. T. Walden (1993), *Spectral Analysis for Physical Applications: Multitaper and Conventional Univariate Techniques*, 580 pp., Cambridge University Press, Cambridge.
- Percival, D. B., and A. T. Walden (2020), *Spectral Analysis for Univariate Time Series*, 686 pp., Cambridge University Press, Cambridge.
- Pippard, A. B. (1978), *The Physics of Vibration*, Cambridge University Press, New York.
- Priestley, M. B. (1981), *Spectral Analysis and Time Series*, 890 pp., Academic, Orlando, Fla.
- Prieto, G. A., R. L. Parker, D. J. Thomson, F. L. Vernon, and R. L. Graham (2007), Reducing the bias of multitaper spectrum estimates, *Geophys. J. Int.*, **171**, 1269–1281, doi:10.1111/j.1365-246X.2007.03592.x.
- Prieto, G. A., R. L. Parker, and F. L. Vernon (2009), A Fortran90 library for multitaper spectrum analysis, *Comput. Geosci.*, **35**, 1701–1710, doi:10.1016/j.cageo.2008.06.007.
- Rice, J. A. (1995), *Mathematical Statistics and Data Analysis*, Duxbury MA, Belmont.

- Rice, J. A. (2006), *Mathematical Statistics and Data Analysis*, third ed., Duxbury MA, Duxbury Press.
- Richards, E. G. (1998), *Mapping Time: The Calendar and its History*, 438 pp., Oxford University Press, Oxford.
- Riedel, K. S., and A. Sidorenko (1995), Minimum bias multiple taper spectral estimation, *IEEE Trans. Signal Proc.*, **43**, 188–195.
- Riedel, K. S., and A. Sidorenko (1996), Adaptive smoothing of the log-spectrum with multiple tapering, *IEEE Trans. Signal Proc.*, **44**, 1794–1800.
- Riedesel, M., D. C. Agnew, J. Berger, and F. Gilbert (1980), Stacking for the frequencies and Q's of $0s_o$ and $1s_o$, *Geophys. J. Roy. Astron. Soc.*, **62**, 457–471.
- Robinson, E. A., and S. Treitel (1980), *Geophysical Signal Analysis*, Prentice Hall, Englewood Cliffs, N.J.
- Rosat, S., S. Watada, and T. Sato (2007), Geographical variations of the zSz normal mode amplitude: predictions and observations after the Sumatra-Andaman earthquake, *Earth, Planets Space*, **59**, 307–311.
- Rudnick, P. (1966), Note on the calculation of Fourier series, *Math. Comp.*, **20**, 429–430, doi:10.1090/S0025-5718-66-99926-1.
- Scherbaum, F. (2001), *Of Poles and Zeros: Fundamentals of Digital Seismology*, Kluwer Academic Publishers, Boston.
- Scherbaum, F., and M.-P. Bouin (1997), FIR filter effects and nucleation phases, *Geophys. J. Int.*, **130**, 661–668.
- Scrope, G. P. (1827), *Memoir on the Geology of Central France, Including the Volcanic Formations of Auvergne, the Velay, and the Vivarais*, Longman, Rees, Orme, Brown, and Green, London.
- Silverman, B. W. (1986), *Density Estimation for Statistics and Data Analysis*, Chapman and Hall, New York.
- Simcoe, R. J. (2009), Evaluating commercial scanners for astronomical image digitization, in *Preserving Astronomy's Photographic Legacy: Current State and the Future of North American Astronomical Plates*, vol. 410, edited by W. Osborn and L. Robbins, pp. 111–127, Astronomical Society of the Pacific: ASP Conference Series, San Francisco.
- Singleton, R. C. (1969), An algorithm for computing the mixed radix fast Fourier transform, *IEEE Trans. Audio Electroac.*, **AU-17**, 93–103.

- Sivia, D. S. (1996), *Data Analysis: a Bayesian Tutorial*, Clarendon Press, Oxford.
- Slepian, D. (1976), On bandwidth, *Proc. IEEE*, **6**, 292–300.
- Smith, M. L., and F. A. Dahlen (1981), The period and Q of the Chandler wobble, *Geophys. J. Roy. Astron. Soc.*, **64**, 223–281.
- Snodgrass, F. E., G. W. Groves, K. F. Hasselmann, G. R. Miller, W. H. Munk, and W. H. Powers (1966), Propagation of ocean swell across the Pacific, *Phil. Trans. Roy. Soc. Ser. A*, **259**, 431–497.
- Sorensen, H., D. L. Jones, M. T. Heideman, and C. S. Burrus (1987), Real-valued Fast Fourier Transform algorithms, *IEEE Trans. Acoustics Speech Sign. Proc.*, **35**, 849–863.
- Steiglitz, K. (1996), *A DSP Primer: with Applications to Digital Audio and Computer Music*, Addison-Wesley, Menlo Park.
- Steiglitz, K., T. W. Parks, and J. F. Kaiser (1992), METEOR: A constraint-based FIR filter design program, *IEEE Trans. Signal Proc.*, **40**, 1901–1909, doi:10.1109/78.149993.
- Stevenson, J. M., J. A. Hildebrand, M. A. Zumberge, and C. G. Fox (1994), An ocean bottom gravity study of the southern Juan de Fuca Ridge, *J. Geophys. Res.*, **99**, 4875–4888.
- Stuart, A., and J. K. Ord (1991), *Kendall's Advanced Theory of Statistics: Distribution Theory*, Edward Arnold, London.
- Stuart, A., and J. K. Ord (1994), *Kendall's Advanced Theory of Statistics: Classical Inference and Relationship*, Edward Arnold, London.
- Thomson, D. J. (1982), Spectrum estimation and harmonic analysis, *Proc. IEEE*, **70**, 1055–1096.
- Wall, J. V., and C. R. Jenkins (2012), *Practical Statistics for Astronomers (2nd ed.)*, Cambridge University Press, New York.
- Watts, A. B. (2001), *Isostasy and Flexure of the Lithosphere*, Cambridge Univ. Press, Cambridge.
- Welch, P. D. (1967), The use of Fast Fourier transform for the estimation of power spectra: a method based on time averaging over short, modified periodograms, *IEEE Trans. Audio Electroac.*, **15**, 70–73.
- Wiener, N. (1949), *Extrapolation, Interpolation, and Smoothing of Stationary Time Series, with Engineering Applications*, MIT Press, Cambridge, Mass.

Index

- s*-plane, *see* Laplace transform
z-plane, *see* z-transform
- Abbott, Edwin A., 52
Abel transform, 57, 223
Acausal filter, *see* Finite Impulse Response filter
Algebraic variable, *see* Random variable, *see also* Random variable
Aliasing, *see* Nyquist frequency
Allpass filter, 130
Amplitude spectrum, 36, *see* Cross-spectrum
Analog system, 81
Analog-to-digital converter, *see* Datalogger
Analytic series, *see* Hilbert transform
Anti-aliasing filter, *see* Datalogger
AR, *see* Autoregressive system
Argand diagram, *see* Phasor diagram
Argument dimensions, 61
Argument of complex variable, *see* Complex variables
Argument types, 13
ARMA, *see* Autoregressive Moving Average system
Asymptotically unbiased, *see* Estimate
Autocorrelation, 140
Autocovariance, 137–140
 matrix, 140
 symmetry, 139
Autoregressive Moving Average system, 95
Autoregressive system, 95, 201
- Bandlimited function, *see* Function, bandlimited
Bandwidth
 of function, 86
Biased, *see* Estimate
Bilinear transformation, *see* Mappings of complex plane
Blackman-Tukey method, *see* Spectrum estimates
Bode plot, 109
Boxcar frequency, *see* sinc function
Brownian process, *see* Stochastic process
- Campbell, William, 31
- Carrier wave, 47
Chandler wobble, 109, 113
 dissipation in, 113
 simulating with recursive filter, 122–123
Chebyshev polynomials, *see* Orthogonal functions
- Circular convolution, *see* Convolution
Circular symmetry, 55
Circular time and frequency, 21–23, 73
 convolution theorem for, 73–75
 shift theorem for, 73
Coherence, *see* Cross-spectrum, *see also* Cross-spectrum
Complex conjugate, *see* Complex variables
Complex numbers
 for two-dimensional quantities, 236
Complex variables
 argument, 233
 Complex conjugate, 234
 magnitude, 233
Computation speed
 exponential time, 78
 linear time, 78
 polynomial time, 77
Concentration factor, 186
Conditional probability, 250
Confidence limits, 249
Consistent, *see* Estimate
Convergence, *see* Fourier series
Convolution
 circular, 74
 discrete-time, infinite, 60
Convolution theorem, Fourier, *see* Fourier transform
Convolving function, 180
Corner frequency, *see* sinc function
Correlation coefficient, 252
Cosepectrum, *see* Cross-spectrum
Cranmer, Thomas, 266
Cross-spectrum
 amplitude spectrum, 213
 autospectrum, 212
 coherence, 213
 cospectrum, 212
 defined using cross-covariance, 212
 phase spectrum, 213

- quadrature spectrum, 212
squared coherence, 211
- Cumulative distribution function, 243
- Dahlen, F. A., 150
- Datalogger
analog-to-digital converter, 81
anti-aliasing filter, 81
jitter, 83
quantization, *see* Quantization
sample and hold, 81
- Datalogger operation, 81–82
- Decibels, 8
- Decimation, 90–91
- Deconvolution, 96
- Deflation of a polynomial, 131
- Derivative theorem, *see* Fourier transform
- Deterministic behavior, 4, 137
- DFT, *see* Discrete Fourier Transform
- Differentiability, *see* Fourier transform
- Differentiation filter, *see* Finite Impulse Response filter, differentiation
- Digital system, 81
- Dimensional arguments
Argument types, 13
- Dirichlet conditions, *see* Fourier series
- Dirichlet kernel, 64–66
and sinc function, 66
plot of, 65
- Discrete Fourier Transform, 67–70
of real series, 270–272
of sinusoids, 71
Parseval's relation for, 76
shift theorem for, 72
- Discrete-time sequence
causal, 61
defined, 60
delta function, 60
Fourier transform, *see* Fourier transform
step function, 60
- Domains, 33
- Dot product of functions, *see* Orthogonal functions
- Dot product of vectors, *see* Vectors
- Durbin-Levinson algorithm, 201, 279
- Dynamic range, *see* Quantization
- East Pacific Rise
data, 146
- Empirical pdf, 243
- Ensemble, *see* Random variable
- Envelope, *see* sinc function
- Envelope function, *see* Hilbert transform
- Equiripple filters, *see* Finite Impulse Response filter, frequency fitting design methods, minimax fitting
- Ergodic, *see* Stochastic process
- Estimate
asymptotically unbiased, 248
biased, 248
consistent, 247
inconsistent, 248
unbiased, 247
- Estimator, 246
relative efficiency, 249
- even functions, 17
- Expectation operator, 242
- Exponential time, *see* Computation speed
- Fast Fourier Transform, 77–80
computational details, 269–270
Fastest Fourier Transform in the West, 78
for real-valued sequences, 79
history, 78
possible sequence lengths for, 78
speed increase from using, 77, 78
- Fechner's law, 8
- Fejér kernel, 66–67, 180
in power spectrum estimate, 178
- FFT, *see* Fast Fourier Transform
- FFTW, *see* Fast Fourier Transform
- Filter
analog, *see* RC filter
prediction-error, 200–204
recursive, 117–123
stability, *see* Stability criterion
recursive prediction-error, 200
- Filtered white noise, 142–145
- Finite Impulse Response filter
acausal, 98
differentiation, 124–126
for linear fit, 128
frequency fitting design methods, 102–104
least squares, 102
minimax fitting, 103
frequency selection, 96–106
Hilbert transform, 126
least squares equivalent to, 127–129
linear phase, 98
minimum-phase, 129–133
design by spectral factorization, 133

- roots, 129–131
- taper design methods, 99–102
- transition width, 102
- zero phase, 98
- FIR filters, *see* Finite Impulse Response filter
- Folding of frequency axis, *see* Nyquist frequency
- Fourier series, 18–23
 - convergence, 19–23
 - Dirichlet conditions, 20
 - pointwise, 20
 - uniform, 20
- Gibbs' phenomenon, 21
- Fourier transform
 - and differentiability, 43
 - as special case of Laplace transform, 111
 - as special case of z-transform, 115
 - convolution theorem, 44–45
 - derivative theorem, 41
 - discrete-time sequence, 61
 - modulation theorem, 46–50
 - moment theorems, 41
 - power theorem, 45
 - shift theorem, 36
 - similarity theorem, 35
 - symmetry relations, 40
- Fractal, *see* Power spectral density
- Frequency-averaging, *see* Periodogram
- Function
 - bandlimited, 35, 86
 - transient, 31
- Functional, 186
- Gateaux differentiation, 276
- Gaussian pdf
 - multivariate, 251
- Gaussian pdf, univariate, 242
- Gibbs' phenomenon, *see* Fourier series
- Goertzel algorithm, *see* Slow Fourier Transform
- Group delay, 48
 - minimum-phase filter, 131
- Hamming, Richard, 100
- Hankel transform, 57
 - for spectra, 222
- Hermite polynomials, *see* Orthogonal functions
- Hermitian function, 40
- Hilbert transform, 126–127
- IIR filter
 - see* Filter, recursive, 117
- Imputation, 83
- Inner product, *see* Orthogonal functions
- Innovations process, 201
- Inconsistent, *see* Estimate
- Instantaneous amplitude, *see* Hilbert transform
- Instantaneous phase, *see* Hilbert transform
- Interpolation of bandlimited functions, *see* Nyquist criterion
- Isostatic response, 219
- Isotropic Processes, 222
- Isotropy, 55
- Jitter, *see* Datalogger
- Joint pdf, *see* Probability density function
- Kaiser-Bessel taper, *see* Taper
- Kalman filter, 96
- Lag (definition), 138
- Lag window, 267
- Laplace transform, 110–114
 - s plane
 - poles and zeros, 112
 - transfer function, 112
- Leacock, Stephen, 12
- Leakage, *see* Periodogram, bias
- Leakage factor, 186
- Least count, *see* Quantization
- Least squares, *see* Regression
- Least-squares spectrum estimate, *see* Spectrum estimates
- Legendre polynomials, *see* Orthogonal functions
- Linear fit
 - frequency response of, 127–129
- Linear regression, *see* Regression
- Linear systems, 25
 - lumped-parameter, 107–110
 - time-invariant, 25
- Linear time, *see* Computation speed
- Linear-phase filter, *see* Finite Impulse Response filter
- MA, *see* Moving Average system
- Magnitude of complex variable, *see* Complex variables
- Magsat data, 146
- Main lobe, 101
- Mappings of complex plane
 - bilinear transformation, 119
 - sampling, 116

- Maximum entropy, *see* Spectrum estimates, parametric
Mean square error, 170, 248
Minimum-phase filter, *see* Finite Impulse Response filter
Modulation amplitude, 46
Modulo notation defined, 71
Moment and Fourier transform, 41
Moving Average system, 95
Multivariate pdf, *see* Probability density function

Negative frequencies, 236
Nettleton's method, 256
Nondimensional arguments Argument types, 13
Normal pdf, *see* Gaussian pdf
Northridge earthquake, 105
Nyquist criterion, 85 for sinusoid, 87 reconstruction of functions that satisfy, 87 safely violating, 91
Nyquist frequency aliasing, 87–90 minimizing the effect of, 89 definition, 86 folding of frequency axis, 89

odd functions, 17
Order, *see* Orthogonal functions
Order of prediction-error filter, 200
Orthogonal functions, 13–23 Chebyshev polynomials, 15 dot product, 13 weight function, 13 Hermite polynomials, 15 inner product, 13, 14 complex functions, 15 Legendre polynomials, 15 order, 15 orthonormal, 15 sinusoids, 16–23 two-norm, 14 Walsh functions, 16
Orthogonal vectors, *see* Vectors
Orthonormal Functions, *see* Orthogonal functions
Outliers

effect on spectrum, *see* Spectrum estimate, 179 highlighting with prediction-error filter, 204

Parametric spectrum estimation, *see* Spectrum estimates
Parks-McClellan algorithm, *see* Finite Impulse Response filter, frequency fitting design methods, minimax fitting
Parseval's relation for Discrete Fourier Transform, 76
Parseval's theorem, *see* Fourier transform, power theorem
pdf, *see* Probability density function, *see* Probability density function
Periodicity of transforms, *see* Circular time and frequency
Periodogram, 170–179 averaging for stability, 175–177 averaging in frequency, 176 bias, 179 bias reduction with single taper, 179 definition, 170 for nonwhite spectra, 177–179 for white noise, 172–174 inconsistency, 174 overly smooth, 179 symptoms of using, 171
Phase sign convention for, 236
Phase spectrum, 36, *see* Cross-spectrum
Phasor diagram, 235
Plancheral's theorem, *see* Fourier transform, power theorem
Point processes, 136
Pointwise convergence, *see* Fourier series
Poisson sum formula, 91
Polar motion, *see* Chandler wobble
Poles and zeros in s plane, *see* Laplace transform in z -plane, *see* z -transform
Polynomial deflation, 131
Polynomial time, *see* Computation speed
Power spectral density autocovariance definition, 154 by bandpass filtering, 152 dimensions, 152–153 Fourier transform definition, 153 fractal, 165

- normalization, 153, 161–162
- one-sided, 154
- power law, 165
- Power spectrum
 - spherical, 227
- Prediction-error filters, *see* Filters
- Prewhitenning data, 199–204
- Principle of superposition, 25
- Probability density function, 135, 239
 - joint, 249
 - multivariate, 251
- Probability plot, 243
- Project Magnet data
 - cross-spectra, 225–226
- Project Magnet profile
 - data, 146
 - spectra, 163–165
- Projection
 - of a function, 56
 - projection-slice theorem, 56
 - for spectra, 222
- Prolate spheroidal taper, *see* Taper, prolate spheroidal
- Quadratic multitaper estimation, *see* Spectrum estimate
- Quadrature spectrum, *see* Cross-spectrum
- Quadrature, defined, 235
- Quantization, 81–82, 92–93
 - as a stochastic process, 142
 - least count, 92
- Random variable, 134
 - definition and behavior, 134–135, 239–242
 - ensemble, 136
 - realization, 136
 - standardized, 242
 - use in models, 135–136
- Random walk, *see* Stochastic process
- rank of data, 244
- Rayleigh criterion, *see* Sinusoids, resolving
- Rayleigh's theorem, *see* Fourier transform, power theorem
- RC filter, 108
- Realization, *see* Random variable
- Regression, 256
 - linear, 256
- Relative efficiency, *see* Estimator
- Replication of sampled functions, *see* Nyquist frequency, aliasing
- Robinson, Enders, 115
- Root mean square (rms), 163
- S-plane
 - stability criterion for, *see* Stability criterion
- Salton Sea water level
 - data, 146
 - spectrum, 162
- Sample and hold, *see* Datalogger
- Sampled-data function, 62
 - Fourier transform, 62
- Scatterplot, 253
- Sea level
 - at SIO pier, 1
 - steric effect, 3
 - swell, 4
- Seiche, 146
- Seismometer, *see* Simple harmonic oscillator
- Shah function, 84
 - Fourier transform, 85
- Shakespeare, William, 31
- Sidelobes, 101
- Signal detection, 96
- Simons, F. J., 150
- Simple harmonic oscillator, 27, 109
 - critical damping, 28
- sinc function
 - corner frequency, 33
 - envelope, 33
- Singular spectrum analysis, *see* Spectrum estimates
- Sinusoid
 - sampled, *see* Nyquist criterion
- Sinusoids
 - resolving, 47
- Slepian function, *see* Taper, prolate spheroidal
- Slepian function or sequence, *see* Taper, prolate spheroidal
- Slice theorem, *see* Projection
- Slow Fourier Transform, 272–274
- Slow Fourier transform, 80
- Spectral concentration, measure for, 186
- Spectral factorization, *see* Finite Impulse Response filter
- Spectrum
 - of a transient, 152
 - of sinusoids, 152
- Spectrum estimate
 - Blackman-Tukey, 266–267
 - Least-squares, 268
 - local bias, 194–195

- outliers, effect of, 179
- overly smooth, 179
- parametric, 267–268
- periodogram, *see* Periodogram
- prolate spheroidal multitaper, 188–192
- quadratic multitaper, 198
- sine multitaper, 192–198
- Singular spectrum, 268
- summary recommendations, 204–206
- Welch's method, 181–183
- WOSA estimate, 181–183
- Spherical power spectrum, *see* Power spectrum
- Stability criterion
 - s plane, 113
 - for recursive filter, 119
 - in z -plane, 119
- Standard deviation, 242
- Standardized variable, *see* Random variable
- Stationary process, *see* Stochastic process
- Stationary processes, 136–137
 - on a sphere, 226–227
- Statistical estimation, 169–170
- Stochastic process, 134
 - Brownian process, 144
 - ergodic, 168
 - isotropic, 222–223
 - quantization noise, *see* Quantization
 - random binary, 24
 - random walk, 144
 - stationary process, 136
 - white noise, 140, 172
- Swell, propagation, 6
- Symmetry relations
 - for DFT, 76–77
- Symmetry relations of Fourier transform, *see* Fourier transform
- Systems, *see* Linear systems
- Taper
 - Kaiser-Bessel, 101, 125
 - minimum bias, 185–188, 275–277
 - prolate spheroidal
 - associated eigenvalues, 277
 - reason for name, 277
 - von Hann, 100
 - normalized for PSD, 181
 - reducing PSD bias, 181
- Taylor series, 12
- Time invariance, *see* Linear systems
- Toeplitz matrix, 140
 - inverting, *see* Durbin-Levinson algorithm
- Tolstoy, Leo, 12
- Total least squares, 257
- Transfer function, *see* Laplace transform
- Transient
 - spectrum of, 152
- Transient function, *see* Function, transient
- Transition width, *see* Finite Impulse Response filter
- Tukey, John W., ii
- Two-norm, *see* Orthogonal functions
- Unbiased, *see* Estimate
- Uniform convergence, *see* Fourier series
- Variable, *see* Random variable, *see* Random variable
- Variance operator, 242
- Vectors
 - dot product, 13
 - orthogonal, 13
- Vibration diagram, *see* Phasor diagram
- von Hann, Julius, 100
- Walsh functions, *see* Orthogonal functions
- Wave packet, 49
- Wavenumber, 52
- Wavenumber vector, 220
- Weight function, *see* Orthogonal functions
- Weighted Overlapping Section Averages, *see* Spectrum estimate
- Welch's method, *see* Spectrum estimate
- Wellington, A. M., 94
- White noise, *see* Stochastic process, 140–142
- Window, *see* Taper
- Windowing
 - incorrect view of, 70–73
- Wraparound effects, 74
- Yule-Walker equations, 201
- z -transform, 114–117
 - definition, 114
 - different forms of, 115
 - stability criterion for, *see* Stability criterion
- Zero-phase filter, *see* Finite Impulse Response filter